Natural Ester Oils as Liquid Insulation in HVDC Converter Transformers

A Thesis

Submitted in Partial Fulfillment of the Requirements for the Award of the Degree of

Doctor of Philosophy (PhD)

By

Kanumuri Deepak

Department of Electronics and Electrical Engineering
Indian Institute of Technology Guwahati
Guwahati, Assam-781039, India

March, 2025

Dedicated

To

my Supervisor

Prof. Sisir Kumar Nayak

for his guidance and support

My Parents

Prasad Kanumuri *and* ***Padmaja Kallepalli***

and ***my brother Dileep Kanumuri***

for their Support and Love

Declaration

I hereby certify that the work presented in this thesis entitled "**Natural Ester Oils as Liquid Insulation in HVDC Converter Transformers"** is entirely my own account of research performed under the guidance of Prof. Sisir Kumar Nayak. Any part of this work has not earlier been submitted for the award of any degree, diploma, associate-ship, fellowship or its equivalent to any University or Institution.

Date: 17.03.2025

(Kanumuri Deepak)
Registration No. 196102006
Department of Electronics and Electrical Engineering
Indian Institute of Technology Guwahati
Guwahati – 781039, India

Department of Electronics and Electrical Engineering
Indian Institute of Technology Guwahati
Guwahati – 781039, India

Certificate

This is to certify that the thesis entitled "***Natural Ester Oils as Liquid Insulation in HVDC Converter Transformers***", submitted by ***Kanumuri Deepak*** (196102006), a research scholar in the Department of Electronics and Electrical Engineering, Indian Institute of Technology Guwahati, for the award of the degree of Doctor of Philosophy, is a record of an original research work carried out by him under my supervision and guidance. The thesis has fulfilled all the requirements as per the regulations of the institute and in my opinion has reached the standard needed for submission. The results embodied in this thesis have not been submitted to any other University or Institute for the award of any degree or diploma.

Date: 17.03.2025

Place: Guwahati

Prof. Sisir Kumar Nayak
Professor
Dept. of EEE
IIT Guwahati
Guwahati - 781 039,
Assam, India.

Acknowledgements

The first and foremost gratitude goes to my supervisor **Prof. Sisir Kumar Nayak** for his valuable guidance throughout the research work. I thank him for his encouragement, patience towards research and support, which enabled me to develop a better understanding of the subject leading to the presentation of this thesis. I would like to thank him for spending his precious time to discuss thoroughly on the topic and make me what I am today. I would also like to acknowledge my sincere gratitude to my doctoral committee members, **Prof. Harshal B. Nemade, Dr. Praveen Tripathi, Dr. Sanjib Ganguly and Prof. Praveen Kumar** for their advice and suggestions throughout my research work.

I also like to extend my gratitude towards the members of the Regional Testing Laboratory (RTL), Central Power Research Institute (CPRI) Guwahati especially Mr. Manas Chakraborty for the support in availing the testing facility. I also like to acknowledge Mr. Das and the members of Power Maker, EPIP, Amingaon, Guwahati Assam for providing us the raw material for the experimental analysis.

I am grateful to my research group members Dr. Niharika Baruah, Dr. Rohith Sangineni, Mr. Ambuj Kumar, Mr. Subhendu Sekhar Sahu and Mr. Satyajeet Anandh, for their co-operative assistance and suggestions in performing experiments. I am thankful to my friends and lab mates Mr. Abhishek Paikray, Dr. Shashank Kulkarni, Mr. Anurag Lambor, Mr. Vivek Kumar, Ms. Chandrima Saha, Mr. Amarnath Kumar and Ms. Chayanika Baishya for their encouragement. I would also like to thank to the most important support system during my research, my friends Dr. Nikhil Rahul Dhongde, Dr. Gunnola Nagendra Prasad, Mr. Imran Hussain, Mr. Siddharth Kumar Sahu and Dr. Rammohan Draksarapu for their support and motivation outside the lab activities and inside hostel.

I would like to thank all the faculty members, and staffs of Electronics and Electrical Engineering Department for rendering their whole-hearted cooperation and support in the entire course of work. I would like to thank my parents, Mrs. Padmaja Kallepalli, Mr. Prasad Kanumuri and my brother Mr. Dileep Kanumuri for all their love, support and encouragement. I would also like to thank Dr. Baby Nasrin Siddiqua, Dr. Sukriti Tiwari, Mr. D. Ramesh Kumar, Mr. M. Sridhar Bhatlu, Mr. Sandeep Rangala, Mr. Ramavath Dhakeswar Naik, Mr. Yamalakonda Venu Gopal, Mr. K. Sai Kumar and Mr. Dinesh Kumar Addala, for understanding my work schedule and encouraging me throughout the PhD journey and

bearing with me during my phases of breakdown. I feel proud of their patience in times when I was unable to spend much time at a stretch with them during the last few years.

Lastly, I am and will always be thankful to God for guiding me through this testing period of my life. I will be grateful to him who has destined my life to be a part of Indian Institute of Technology Guwahati.

(Kanumuri Deepak)
Registration No. 196102006
Department of Electronics and Electrical Engineering
Indian Institute of Technology Guwahati
Guwahati – 781039, India

Abstract

The ongoing shift towards sustainable and environmentally friendly technologies has brought significant attention to the development of biodegradable dielectric fluids for power transformers. Traditional petroleum-based transformer oils, despite their widespread use, suffer from drawbacks such as low biodegradability, limited fire resistance, and environmental concerns due to resource depletion and potential spillage. Natural ester oils (NEOs), derived from renewable resources like sunflower and soybean etc., have emerged as promising alternatives. Major companies like Hitachi Energy-ABB and Siemens are already integrating NEO-based dielectric fluids into their transformer designs, reflecting a clear industry trend towards greener solutions. While the benefits of NEOs in HVAC transformers are well-documented, their application in HVDC transformers is relatively new and less explored. The unique operational stresses of HVDC systems, including high direct currents and associated electrical phenomena, necessitate a thorough understanding of how NEOs perform under these conditions. Existing research highlights the potential of NEOs to provide superior insulation performance, enhanced breakdown strength, and better conductivity than traditional mineral oils (MOs). However, these findings primarily focus on HVAC applications, leaving a significant knowledge gap in HVDC context. The primary motivation for this thesis is to bridge this gap by extensively investigating the dielectric performance of NEOs in HVDC transformer insulation systems. This research aims to provide a comprehensive evaluation of the DC breakdown voltage (DCBDV) and DC conductivity of NEOs under various operational conditions, including thermal and oxidative ageing. The objectives of this thesis include studying the effects of oxidative ageing on the DCBDV of NEOs and comparing these results with MOs, and also analyzing the effects of accelerated thermal ageing, investigating the geometric effects on dielectric breakdown strength measurements, and evaluating the degradation of solid insulation materials aged in NEOs and MOs. It also involves developing a new experimental setup for studying pre-breakdown phenomena and analyzing streamer formation in both liquid and solid insulation materials. This thesis is organized into six chapters, covering the introduction, effects of ageing on DC conductivity and DCBDV of natural ester oils, impact of electrode geometry, effects of ageing on pressboard insulation, design of experimental apparatus for pre-breakdown studies, and the conclusion with future research suggestions. By enhancing the understanding of NEOs in HVDC applications, this thesis aims to contribute to the development of more

sustainable transformer technologies, promoting the reliable and widespread adoption of environmentally friendly dielectric fluids in the power industry.

Table of Contents

List of Figure xiii

List of Table xvii

List of Acronyms xix

List of Symbols xxi

1 Introduction **1**

1.1 Introduction. 2

1.2 HVDC Converter Transformer. 3

1.2.1 Components of HVDC converter transformer. 3

1.3 Insulation in Transformers…..... 5

1.3.1 Solid-liquid insulation materials of a transformer. 5

1.3.2 HVDC converter transformer insulation. 6

1.3.3 Insulation degradation…… 9

1.3.4 Breakdown and pre-breakdown strength of an insulation……. 10

1.3.5 Geometric effects on breakdown voltage measurement of an Insulation……. 11

1.4 Literature survey…… 12

1.4.1 Alternative dielectric liquids. 12

1.4.2 Dielectric properties of HVDC transformer insulation. 15

1.5 Motivation. 20

1.6 Objective of the thesis. 21

1.7 Contribution of the thesis. 22

1.8 Organization of the thesis. 23

2 Effects of ageing on DC conductivity and DCBDV of natural ester oils **28**

2.1 Introduction. 29

2.2 Sample preparation. 32

2.2.1 Oxidative ageing experimental setup 32

2.2.2 Accelerated thermal ageing setup. 33

2.2.3	Viscosity and moisture content of the samples.	35
2.3	Experimental configuration and methodology.	36
2.4	Measurement of DC conductivity from frequency domain analysis (FDS) and Cole-Cole plots.	38
2.5	Statistical analysis of DCBDV experimental results.	43
2.5.1	Conformity of DCBDV experimental data to a distribution through Anderson-Darling test.	43
2.5.2	Goodness of fit.	44
2.5.3	Normal distribution.	44
2.5.4	Skewness and kurtosis.	44
2.5.5	Two parameter and three parameter Weibull distribution.	45
2.6	Experimental Results of DC Breakdown Voltage of Fresh and Oxidatively Aged Samples.	46
2.6.1	Statistical analysis of DCBDV experimental results…….	49
2.7	Experimental Results of DCBDV for Fresh and Thermally Aged Samples.	55
2.7.1	Statistical analysis of DCBDV experimental results.	57
2.8	Comparison of Dielectric Strength in Thermally Aged and Oxidatively Aged NEOs under DC Voltage Stresses.	63
2.9	DC Conductivity of Natural Ester Oils and its Influence on Dielectric strength.	64
2.9.1	DC conductivity of thermally aged samples.	64
2.9.2	DC conductivity of oxidatively aged samples.	67
2.9.3	Fitting discrepancies for the imaginary part of complex permittivity. .	70
2.9.4	Influence on DC conductivity by energization time and field strength.	71
2.10	Summary of the chapter.	71
3	**Geometric effects on DC breakdown strength measurement of natural ester oils**	**75**
3.1	Introduction.	76
3.2	Methodology and experimental setup.	78
3.2.1	Effect of effective electrode area on breakdown strength using Weibull analysis.	78
3.2.2	Materials and experimental setup.	80

3.3 Results and discussion. 82
3.3.1 Experimental results of DC breakdown voltage of MO and FR3 in positive and negative polarities for different electrode shapes. 82
3.3.2 Effect of Electrode Stressed Area on DCBDV of MO and NEO-FR3 in both polarities. 85
3.3.3 Comparison of the Influence of Electrode Area on the Breakdown Strength of MO and NEO-FR3 under DC Voltage Stresses with a 1mm Gap versus ACBDV Results. 91
3.4 Summary of the chapter. 91

4 Study of oxidative ageing and thermal ageing effects on natural ester oil immersed solid insulation **94**
4.1 Introduction. 95
4.2 Materials and Methodology. 98
4.2.1 Sample preparation. 98
4.2.2 Experimental methodology. 100
4.3 Results and Discussion. 104
4.3.1 Experimental Results of TGA Analysis of Oil Immersed Pressboard. 104
4.3.2 Experimental Results of FTIR of Oil Immersed Pressboard. 107
4.3.3 Tensile Strength of Oil Immersed Pressboard. 112
4.3.4 AC and DC Breakdown Voltage. 115
4.4 Summary of the chapter. 117

5 Design of experimental setup for pre-breakdown phenomena in liquid and solid dielectrics **121**
5.1 Introduction. 122
5.2 Design of experimental setup for studying pre-breakdown phenomena in liquid dielectrics. 123
5.3 Design of experimental setup to study the streamers along the surface of solid dielectrics immersed in liquid insulation.. 132
5.4 Summary of the chapter. 138

6 Conclusion and future work **141**
6.1 Summary of the present work. 142

6.2 Contribution of the thesis. 143
6.3 Suggestions for future research work. 144

List of Publications 147
Bibliography 150
Appendices 167

List of Figures

1.1 Energy loss with respect to transmission distance in HVAC and HVDC systems. 2

1.2 HVDC converter station. 3

1.3 HVDC converter transformer core and winding structures. 4

1.4 Evolution of transformer liquid insulation. 6

1.5 Stress distributions applied on outer winding with DC voltage (left side) and AC voltage (right)…… 7

1.6 Stress pattern in a composite of oil and pressboard between two electrodes. (a) Steady state; (b) Capacitive distribution of voltage -U after the start up; (c) Capacitive distribution immediately after polarity reversal from -U to +U…….. 8

1.7 Degradation and ageing of oil paper insulation……. 9

1.8 Breakdown phenomena of oil insulation with test cell……. 10

1.9 Pre-breakdown phenomena of oil insulation……. 11

1.10 Triglyceride structure…… 13

1.11 Basic hydrocarbon structures in mineral oil……. 14

1.12 Generic molecular structure of Envirotemp FR3……... 14

2.1 (a) Open beaker oxidative aging (OBOA) chamber; (b) Samples placed inside oxidative aging chamber……... 33

2.2 a) Open beaker oxidative aged samples of MO@ 0, 90, 200- and 500-hours b) Open beaker oxidative aged samples of FR3@ 0, 90, 200 and 500 hours…… 33

2.3 Accelerated thermal ageing setup (a) Hermetically sealed tube (b) Temperature controller (c) Band heater with thermocouple……... 34

2.4 a) Thermally Aged MO Samples at 0, 90, 200, and 500 hours b) Thermally Aged FR3 Samples at 0, 90, 200, and 500 hours…… 34

2.5 Viscosity of samples with the change in temperature for (a) fresh and thermally aged MO (b) fresh and oxidatively aged MO (c) fresh and thermally aged FR3 (d) fresh and oxidatively aged FR3…….. 36

2.6 Schematic diagram of DCBDV experimental setup…….. 37

2.7 FDS setup with dielectric interface and test cell…… 40

2.8 Cole-Cole plots……..…….. 42

2.9 DCBDV of fresh and oxidatively aged samples for positive polarity with breakdown series…….. 47

2.10 DCBDV of fresh and oxidatively aged samples for negative polarity with 48

breakdown series……..

2.11 Average positive and negative DCBDV for fresh and oxidatively aged oils…… 48

2.12 Normal probability plot for oxidatively ages samples for (a) positive DCBDV results; (b) negative DCBDV results……. 49

2.13 Two parameter Weibull distribution of oxidatively aged samples for (a) positive DCBDV results; (b) negative DCBDV results……. 52

2.14 Three parameter Weibull distribution of oxidatively ages samples for (a) positive DCBDV results; (b) negative DCBDV results…… 53

2.15 DCBDV of fresh and thermally aged samples across breakdown series for (a) positive polarity (b) negative polarity…….. 56

2.16 Average DCBDV of fresh and thermally aged oil samples under positive and negative polarity with error bars…….. 57

2.17 Normal probability plot for thermally aged samples for (a) positive DCBDV results; (b) negative DCBDV results……. 58

2.18 Two parameter Weibull distribution of thermally aged samples for (a) positive DCBDV results; (b) negative DCBDV results……. 60

2.19 Three parameter Weibull distribution of thermally aged samples for (a) positive DCBDV results; (b) negative DCBDV results……. 61

2.20 Imaginary part of relative permittivity imaginary part with respect to frequency for fresh and thermally aged (a) MO (b) FR3…… 65

2.21 Curve fitting for imaginary part of complex permittivity for fresh and thermally aged MO and FR3……. 67

2.22 Imaginary part of relative permittivity imaginary part with respect to frequency for fresh and oxidatively aged (a) MO (b) FR3…… 68

2.23 Curve fitting for imaginary part of complex permittivity for fresh and oxidatively aged MO and FR3…… 69

3.1 Parallel breakdown probability model for area effect…… 80

3.2 Experimental setup to test DCBDV of (a) MO and FR3 (b) solid insulation immersed in MO and FR3……. 81

3.3 (a) Positive DCBDV (kV) with respect to breakdown series (b)Negative DCBDV (kV) with respect to breakdown series…… 83

3.4 Average Positive and Negative DCBDV (kV) with error bar for various electrode shapes…… 84

3.5 DCBDV (kV) for solid insulation in MO and FR3 under various electrode shapes…… 85

3.6 Weibull distribution plot for (a) Positive DCBDV (b) Negative DCBDV of MO 87

and FR3…….

3.7 Electrode configurations and EESA; a) VDE Electrodes (Total diameter: 35mm, stressed diameter: 8.8mm); b) Plane electrode (Total diameter: 25mm, stressed diameter: 25mm); c) Sphere electrode (Total diameter: 12.5mm, stressed diameter: 5.66mm)…… 88

3.8 Correlation plot of Scale parameter (α) and EESA (mm^2) in logarithmic scale for various samples…… 88

4.1 Chemical structure of cellulose polymer……... 96

4.2 a) Open beaker oxidative ageing setup b) open beakers with samples are placed in the oven c) 300 ml beaker with 20:1:1 base oil to solid to copper samples….. 99

4.3 Accelerated thermal ageing setup (a) Hermatically sealed tube (b) Temperature Controller (c) Band heater with thermocouple……. 100

4.4 Thermogravimetric analyser (Model No.: TG 209 F1 Libra; Make: M/s Netzsch, Germany)…….. 101

4.5 FTIR Spectrophotometer (Make: PerkinElmer, Model: Spectrum Two)…….. 101

4.6 250 KN Servo Hydraulic Universal Testing Machine (Make: BISS, Model: MEDIAN 250) with pressboard sample…… 102

4.7 a) Test cup arrangement for solid insulation breakdown with VDE electrodes; b) Experimental setup for ACBDV of solid insulation samples; c) Experimental setup for DCBDV of solid insulation samples…….. 103

4.8 Mass (%) vs Temperature (℃) of oxidatively aged of (a) MO immersed pressboard samples; b) FR3 immersed pressboard samples……. 105

4.9 Mass (%) vs Temperature (℃) of thermally aged (a) MO immersed pressboard samples; b) FR3 immersed pressboard samples…… 107

4.10 Percentage transmittance (%T) vs wavenumber (cm^{-1}) of (a) MO immersed pressboard samples; b) FR3 immersed pressboard samples…….. 108

4.11 Absorbance (a.u.) vs wavenumber (cm^{-1}) of (a) MO immersed pressboard samples; b) FR3 immersed pressboard samples…… 109

4.12 Absorbance (a.u.) vs wavenumber (cm^{-1}) of (a) MO immersed pressboard samples at a range of 2800-3000 cm^{-1}; b) FR3 immersed pressboard samples at a range of 2800-3000 cm^{-1}…… 109

4.13 Absorbance (a.u.) vs wavenumber (cm^{-1}) of (a) MO immersed pressboard samples at 1700 cm^{-1}; b) FR3 immersed pressboard samples at 1700 cm^{-1}…….. 110

4.14 Absorbance (a.u.) vs wavenumber (cm^{-1}) of (a) MO immersed pressboard samples at a range of 900-1500cm^{-1}; b) FR3 immersed pressboard samples at a range of 900-1500cm^{-1}…….. 110

4.15 Percentage transmittance (%T) vs wavenumber (cm^{-1}) for thermally aged (a) 111

MO immersed pressboard samples; b) FR3 immersed pressboard samples……

4.16 a) Tensile strength (MPa) and the Load (kN) of pressboard samples for oxidatively aged b) Tensile Strength (MPa) vs Ageing Time (Hours) of oxidatively aged pressboard samples…… 113

4.17 a) Tensile strength (MPa) and the Load (kN) of pressboard samples for thermal ageing b) Tensile Strength (MPa) vs Ageing Time (Hours) of thermally aged pressboard samples for thermal ageing……. 114

4.18 a) ACBDV vs Ageing time (Hours) of oxidatively aged pressboard samples; b) Positive DCBDV vs Ageing time (Hours) of oxidatively aged pressboard samples; c) Negative DCBDV vs Ageing time (Hours) of oxidatively aged pressboard samples…… 116

4.19 a) ACBDV vs Ageing time (Hours) of thermally aged pressboard samples; b) Positive DCBDV vs Ageing time (Hours) of thermally aged pressboard samples; c) Negative DCBDV vs Ageing time (Hours) of thermally aged pressboard samples……. 117

5.1 Exemplary profile of an apparatus for analyzing breakdown and pre-breakdown phenomena in liquid-dielectrics…….. 124

5.2 Schematic of test chamber…….. 124

5.3 Inner view of test chamber……. 126

5.4 Different electrodes shapes that are placed inside a test chamber…….. 127

5.5 Filtering and degassing system with temperature controller…….. 127

5.6 Shadow graphic and photon detection system…… 128

5.7 Inner view of test chamber (Top view)…… 132

5.8 Side view/cross-sectional view of high voltage electrodes with solid insulation sample holder that are placed inside a test chamber…… 133

5.9 Schematic of solid insulation sample holder……... 133

5.10 Schematic of needle plane electrode configuration and alignment of xenon lamp and high-speed camera……. 134

List of Tables

2.1	Basic properties of insulating oils.	32
2.2	Moisture content of the fresh and aged samples……..	36
2.3	Conformity to normal distribution of average DCBDV for fresh and oxidatively aged samples……	50
2.4	Failure probabilities of normal distribution for fresh and oxidatively aged samples…….	50
2.5	Statistical parameters of normal distribution for fresh and oxidatively aged samples……	51
2.6	Failure probabilities and goodness of fit data for DCBDV under positive polarity for fresh and oxidatively aged samples……..	54
2.7	Failure probabilities and goodness of fit data of DCBDV under negative polarity for fresh and oxidatively aged samples…….	54
2.8	Conformity to Weibull distribution of average positive DCBDV for fresh and oxidatively aged samples…….	54
2.9	Conformity to Weibull distribution of average negative DCBDV for fresh and oxidatively aged samples…….	54
2.10	Conformity of average DCBDV to normal distribution for fresh and thermally aged oil samples…….	59
2.11	Failure probabilities of oil samples obtained from normal distribution in (kV) for fresh and thermally aged oil samples…….	59
2.12	Statistical parameters of normal distribution for fresh and thermally aged oil samples…….	59
2.13	Goodness of fit coefficients and failure probabilities for DCBDV data under positive polarity for fresh and thermally aged oil samples……..	61
2.14	Goodness of fit coefficients and failure probabilities for DCBDV data under negative polarity for fresh and thermally aged oil samples…….	62
2.15	Conformity of average DCBDV to 2-parameter Weibull distribution for fresh and thermally aged oil samples……	62
2.16	Conformity of average DCBDV to 3-parameter Weibull distribution for fresh and thermally aged oil samples……	62
2.17	Average DCBDV of fresh and aged samples……..	63
2.18	DC conductivity estimated from Cole-Cole relaxation model for fresh and thermally aged oils……..	66

2.19 DC Conductivity Estimated from Cole-Cole Relaxation Model for Fresh and oxidatively Aged Oils…….. 68

3.1 Parameters of Weibull Distribution for Positive DCBDV……. 87

3.2 Parameters of Weibull Distribution for Negative DCBDV……. 87

3.3 Configurations of electrodes used for DCBDV tests…… 88

3.4 Coefficients of Scale Parameters Calculated from linear fit curves…… 89

3.5 Average Values, standard deviation and 90% Confidence Interval of Shape Parameter…….. 89

3.6 Calculated Average DCBDV Values at 10% and 1% Probability…….. 90

List of Acronyms

HVDC	High voltage direct current
LCC	line-commutated converter
VSC	voltage source converter
HV	high-voltage
MO	Mineral oil
NEO	Natural ester oil
OIP	Oil Impregnated Paper
GTL	Gas to Liquid
FDS	Frequency Domain Spectroscopy
ACBDV	AC Breakdown Voltage
DCBDV	DC Breakdown Voltage
XRD	X-Ray Diffraction Analysis
SEM	Scanning Electron Microscope
FTIR	Fourier Transform Infrared Spectroscopy
ATR	Attenuated Total Reflection
TGA	Thermogravimetric Analysis
DTG	Derivative Thermogravimetric Analysis
DP	Degree of Polymerization
HVDC	High Voltage Direct Current
ASTM	American Society for Testing and Materials
IEC	International Electrotechnical Commission
IEEE	Institute of Electrical and Electronics Engineers
TO	Transformer oils
VO	Vegetable oils

NP	nanoparticles
JMEO	Jatropha methyl ester oil
EESA	effective electrode-stressed area
VDE	Verband Deutscher Elektrotechniker
LIBDV	Lightning impulse BDV
NFs	Nanofluids
TAA	Thermal accelerated ageing
OBOA	Open beaker oxidative ageing
AD	Anderson-Darling

List of Symbols

ε_0	*Permittivity of free space*
ε_r	*Relative permittivity*
ε'_r	*Real part of relative permittivity*
ε''_r	*Imaginary part of relative permittivity*
ω	*Angular frequency*
$\tan\delta$	*Dielectric dissipation factor*
V	*Voltage*
f	*Frequency*
ε_∞	*High frequency permittivity*
$\Delta\varepsilon_1$	*Relaxation amplitude of first relaxation*
$\Delta\varepsilon_2$	*Relaxation amplitude of second relaxation*
τ_1	*Time constant of first relaxation*
τ_2	*Time constant of second relaxation*
α_1	*Spread of first relaxation*
α_2	*Spread of second relaxation*
σ_{dc}	*DC conductivity*
σ_0	*Conductivity constant*
y_i	*Data values in Shapiro-Wilk equation*
H_o	*Null hypothesis*
H_A	*Alternate hypothesis*
AD	*Anderson-Darling test statistic*
x_i	*i^{th} value in a dataset*
N	*Number of sample size*
$F(x)$	*Cumulative distribution function*
S	*Skewness*
K	*Kurtosis*
$\bar{x}$	*Average value*
s	*Sample standard deviation*
α	*Scale parameter in Weibull distribution*
β	*Shape parameter in Weibull distribution*

γ	*Location parameter in Weibull distribution*
ρ	*Correlation coefficient*
μ	*Mean*
σ	*standard deviation*
σ^2	*variance*
+ve	*Positive polarity*
- ve	*Negative polarity*

1

Introduction

Contents

1.1	Introduction…….…….	2
1.2	HVDC Converter Transformer…….……..	3
1.3	Insulation in HVDC converter transformers…….	5
1.4	Literature survey ……..…...	12
1.5	Motivation…….	20
1.6	Objective of the thesis……..	21
1.7	Contribution of the thesis…….	22
1.8	Organization of the thesis……	23

1.1 Introduction

Over the past century, AC voltage transmission has dominated electrical power systems due to its safety and efficiency. However, recent advancements in high-power, high-voltage conversion techniques have enabled higher capacity and more efficient HVDC transmission, which offers several notable advantages. HVDC transmission is particularly beneficial for long-distance power transfer due to its lower losses, resulting from fewer transmission lines, the absence of reactive power components, and no skin effect. Additionally, HVDC systems eliminate phase angles, thus avoiding stability issues found in AC systems. They also have a larger short-circuit capacity, enhancing reliability and efficiency. Despite the higher initial costs of conversion technology compared to AC generation, HVDC systems are more cost-efficient over long distances due to the reduced number of required transmission lines, significantly lowering net operational costs and energy losses as shown in Figure 1.1. These factors make HVDC a compelling choice for modern power systems, as highlighted in a study presented by ABB [1]. Currently, two types of HVDC techniques are used for power transmission: line-commutated converter (LCC-HVDC) and voltage source converter (VSC-HVDC). LCC technology is primarily utilized for long-distance bulk power transmission, while VSC technology is employed for offshore wind generation and connecting to remote areas [2].

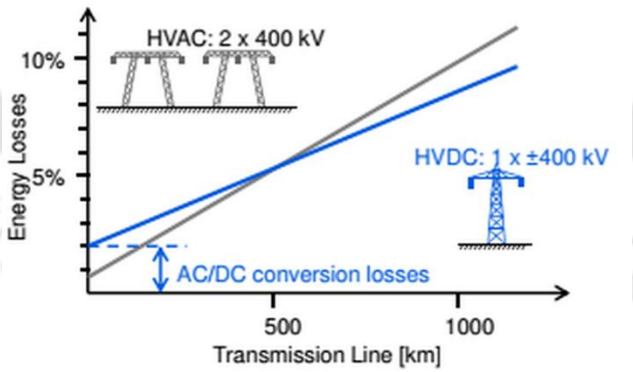

Fig. 1.1. Energy loss with respect to transmission distance in HVAC and HVDC systems [1].

In the LCC technique, converter transformers play a crucial role in connecting the AC network to the converter circuit. As illustrated in Figure 1.2, an HVDC converter station can be divided into two main sections: the AC and the DC sides. On the AC side, various techniques are employed before the voltage is converted to DC. Harmonic filters are used to remove the harmonics generated during the conversion process, and capacitor banks provide the necessary reactive power to the converter transformer, which consumes a significant

amount of reactive power during operation [3-4]. On the DC side, smoothing reactors and filters are connected to the DC line to eliminate ripples from the converted waveforms. The AC and DC sides are equipped with control and protection units (such as switchgear). As shown in Figure 1.2, the AC and DC sides are connected by converter transformers and a valve hall, facilitating the AC-DC conversion process.

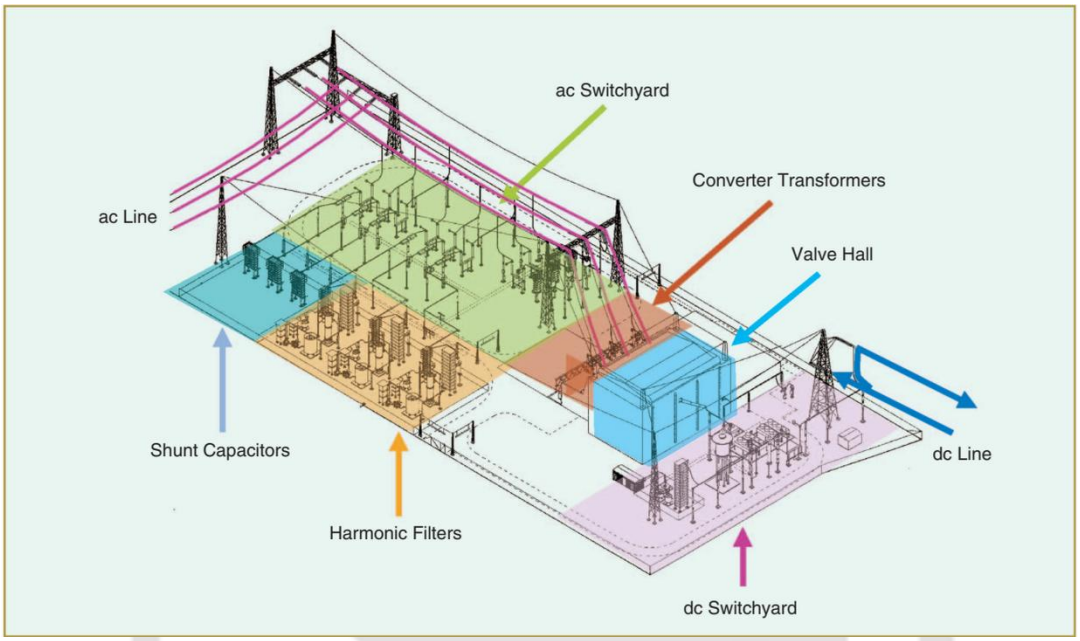

Fig. 1.2. HVDC converter station [3].

1.2 HVDC Converter Transformer

The growth of the HVDC power transmission market has led to a continuous increase in the voltage levels and capacities of HVDC systems. Notably, Siemens manufactured a converter transformer with a voltage level of 1100 kV and a capacity of 587 MW, which was designed for the Changji-Guquan 1100 kV HVDC project in China [5]. In the LCC-HVDC technique, converter transformers connect three-phase AC networks to converter valves. These transformers play a crucial role in HVDC systems by transferring power between the AC network and converter valves, supporting voltage levels during conversion, providing galvanic isolation between AC and DC systems, offering short-circuit impedance to minimize fault currents, and supplying a 30-degree phase shift to the converter valves using 12-pulse bridge is two three-phase voltages with a 30-degree phase shift – one to the upper part and one to the lower. Further details on these functions are discussed in the following sections.

1.2.1 Components of HVDC converter transformer

The main components of converter transformer are given below

- **Core and Windings**: The operation of a converter transformer relies on magnetic flux, making the core and winding essential components. Typically, core-type laminated steel is used in these transformers. Figure 1.3 illustrates the core and winding structures of a single-phase three-winding converter transformer. The valve winding, closest to the core, is surrounded by the line winding, with the tap winding forming the outer layer. In the figure, the valve winding of left limb is in a star-connection for the upper converter bridge, while the valve winding on the right limb is in a delta-connection for the lower bridge. Converter transformers adopt traditional AC transformer insulation methods, using oil and cellulose.

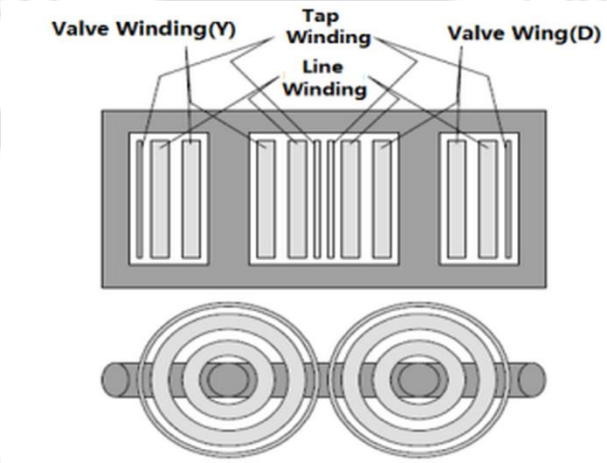

Fig. 1.3. HVDC converter transformer core and winding structures [6].

Conductors are wrapped in cellulose paper for turn-to-turn insulation, and cellulose boards provide mechanical support and act as barriers to enhance insulation performance. The entire winding assembly and the cellulose insulation are immersed in insulating oil. This oil insulates the high voltage and dissipates heat generated within the transformer through natural or forced flow.

- **Bushing**: As prominent components on a converter transformer, Bushings facilitate the transfer of substantial power into and out of the transformer. The line side bushings are designed using AC technology, while the HVDC bushings on the valve side are crucial in the LCC-HVDC technique. Currently, the HVDC bushing technology primarily employs oil-impregnated and resin-impregnated paper insulation methods [7].
- **Cooling system**: The cooling system of a converter transformer, similar to that of a large power transformer, includes components such as oil ducts, pipes, and radiators to manage heat dissipation.

- **Oil tank**: The internal high-voltage components of the converter transformer are enclosed in a grounded oil tank. In addition to the primary components, converter transformers are equipped with tap changers, protection units, and monitoring devices to ensure efficient and safe operation.

All these components are immersed in liquid insulation and are covered with solid insulation to provide protection and cooling to the transformer, ensuring long-term, reliable operation. Therefore, it is crucial to study the HVDC transformer insulation, as it is one of the critical functional components of this equipment. This thesis discusses the insulating properties and limitations of the converter transformer insulation.

1.3 Insulation in Transformers

A transformer is a critical high-voltage (HV) apparatus in a power system network, and its reliability is crucial for the continuity of the power supply. Among its various functional systems, the insulation system is the weakest. Throughout its operational lifetime, the insulation system is subjected to multiple stresses simultaneously, including electrical, mechanical, chemical, and thermal stresses.

1.3.1 Solid-liquid insulation materials of a transformer

Transformer is comprised of solid and liquid insulation which is susceptible to degradation due to hot spots, moisture, partial discharges, arcing, and electromechanical forces on the winding. Repairing or replacing insulation system often necessitates a transformer shutdown, which is undesirable as it causes significant disruptions to the power supply. Therefore, efforts must focus on identifying the factors that cause insulation ageing and implementing corrective actions proactively to minimize the need for shutdowns.

Solid insulation, primarily composed of cellulose, ages rapidly in the presence of heat and moisture. Liquid insulation, mainly consisting of mineral oil (MO), serves as a coolant, impregnant, and insulant, playing a crucial role in the overall functionality of the transformer. The thermal conductivity of the oil is vital; higher conductivity results in a lower temperature rise in the cellulose. Being hygroscopic, cellulose retains significantly more water than oil. Therefore, maintaining moisture equilibrium between oil and cellulose is essential. During temperature rise, the oil should absorb more moisture from the cellulose, thereby reducing the rate of cellulose aging [9]. Degradation of the oil not only diminishes its insulating properties

but also affects the insulation strength of the cellulose. When MO-impregnated cellulose Kraft paper is exposed to heat over time, it generates ageing byproducts such as acids, oxides, and peroxides. These byproducts form sludge and solid wax, which can be deposited on the windings and at the bottom of the transformer tank, leading to undesirable operational issues and reducing dielectric properties.

MO traditionally used as an insulating liquid in transformers, has several drawbacks, including a low flash point, poor biodegradability, and lower breakdown strength. Additionally, MO has limited moisture retention capacity, making it challenging to keep the solid insulation dry, as it cannot capture much moisture from the solid insulation. To address these issues, there is a need for an alternative insulating fluid with improved thermal conductivity, moisture absorption from cellulose, higher dielectric strength, and a higher flash point. Natural ester oil (NEO) is emerging as a significant alternative due to its many advantages, such as higher biodegradability, higher flash point, and greater breakdown voltage [10,11,12]. Research is being conducted on using vegetable seed-based NEOs, which are environment friendly and have enhanced dielectric properties. Studies have shown that the thermal, physicochemical, and electrical properties of MO-based transformer oils are inferior to those of other alternatives [13-15]. Therefore, developing oils with a higher flash point and breakdown voltage is crucial to preventing accidental fires or electrical breakdowns. This has led researchers to focus on advancing the use of NEO in high-voltage apparatus. The timeline of the evolution of transformer insulating fluids is illustrated in Figure 1.4.

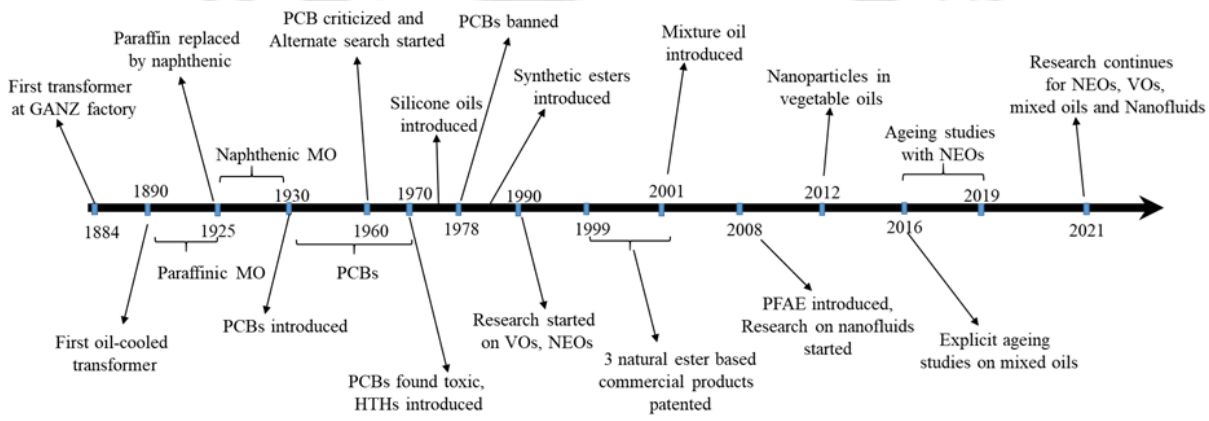

Fig. 1.4. Evolution of transformer liquid insulation.

1.3.2 HVDC converter transformer insulation

As discussed in the introduction and section 1.2.1 of this chapter, HVDC transformers are crucial for power transmission and consist of both solid and liquid insulation. However, the DC potentials present in HVDC transformer valve windings introduce additional stress beyond the normal AC stresses. In steady-state conditions, DC stresses are primarily influenced by the resistivities of the individual insulation materials. This contrasts with AC stresses, which are determined by the capacitive distribution based on the relative permittivity of the insulation materials. Conventional insulation materials, such as cellulose-based paper and pressboard, combined with MO, have also proven effective for converter transformers [8]. The insulation arrangement typically involves paper-covered conductors and barrier systems of pressboard sheets oriented perpendicular to the field stress. The actual properties of insulation materials lead to significantly different stress distributions under AC and steady-state DC conditions. In 1985, EHV-Weidmann Industries, Inc., Saint Johnsbury, Vermont, and H. Weidmann Ltd., Rapperswil/SG, Switzerland, developed a novel oil-impregnated cellulose-based insulation board specifically for use in HVDC converter transformers. At that time, naphthenic transformer oil was used as the insulation oil for these HVDC transformers [16]. This innovative insulation material incorporated small amounts of commercial-grade sodium silicate, making it more compatible with the DC electric fields in HVDC transformers than conventional electrical-grade boards. The modified material significantly reduced DC volume resistivity (VR), enhancing its performance under HVDC conditions. The resistivity ratio of cellulose to oil can vary widely, from 10 to 500, depending on factors like moisture content, quality, ageing, and temperature. In contrast, the relative permittivity ratio between oil and cellulose is much smaller, approximately two [8].

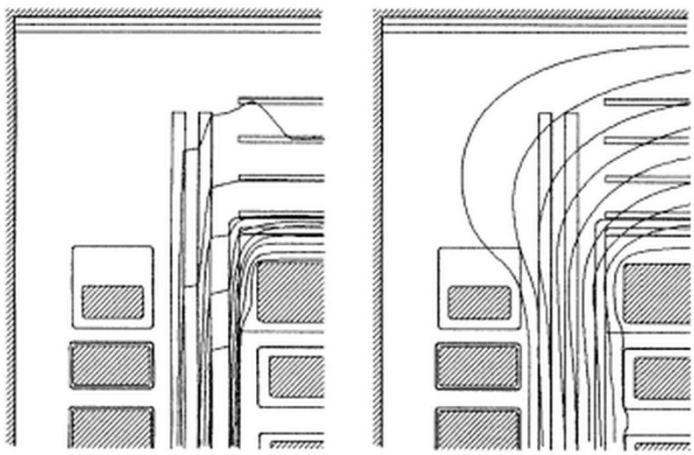

Fig. 1.5. Stress distributions applied on outer winding with DC voltage (left side) and AC voltage (right). [8]

Consequently, under steady-state conditions with a resistive voltage distribution, almost all stress is across the solid insulation. Conversely, AC and transient DC voltages create a capacitive voltage distribution, resulting in roughly double the stress across the oil compared to the solid insulation. These stress patterns for DC and AC voltages are illustrated in Figure 1.5. DC voltages result in resistive distributions, while AC voltages create capacitive distributions, leading to different stress patterns that must be considered in insulation system design. The withstand strength of cellulose is significantly higher than that of oil, which influences insulation arrangements. In AC systems, a minimal amount of solid insulation is used to avoid exposing metal surfaces to oil. Excessive solid insulation increases oil stress, which is undesirable. In contrast, DC systems require more solid insulation to handle steady-state stress, increasing the number and thickness of barriers and adding paper covering to valve side windings and bushings.

In addition to the stress patterns caused by steady-state DC and normal AC voltages, two transient phenomena must be considered for DC voltage. First, full DC potentials from the bridges develop almost instantaneously during the startup of the converter. Second, polarity reversal occurs when the power direction changes in an HVDC system in an LCC HVDC system; the current direction remains the same, but the voltage polarity reverses. After a sudden change in DC voltage its distribution will be capacitive and it will by time change into a resistive distribution. The time constant for the transition from a capacitive to a resistive distribution is about an hour after the application of step voltage. Voltage patterns for steady-state, immediate post-application and polarity reversal are shown in Figure 1.6. All these properties depend on the stresses that are well established for the MO and cellulose paper used in HVDC transformers.

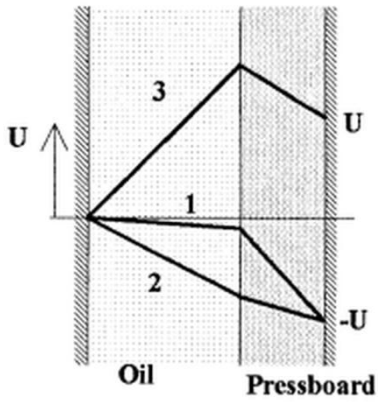

Fig. 1.6. Stress pattern in a composite of oil and pressboard between two electrodes. (1)

Steady state; (2) Capacitive distribution of voltage -U after the start up; (3) Capacitive distribution immediately after polarity reversal from -U to +U. [8]

1.3.3 Insulation degradation

During service, oil-paper insulation in transformers is subjected to electrical, thermal, and mechanical stresses, leading to material degradation. The rate of this degradation largely determines the lifespan of the transformer. The detailed mechanisms behind this degradation are complex [17], but the basic process is illustrated in Figure 1.7. Oxygen and moisture primarily degrade oil and cellulose in transformers through oxidation and hydrolytic reactions. This leads to oil ageing and the breaking of cellulose chains. The by-products of oil degradation, such as water and acids, further age the cellulose, while the by-products of cellulose degradation, including carbon monoxide and carbon dioxide, accelerate oil degradation. Assessing the degradation level is crucial for transformer maintenance. Oil degradation is evaluated through colour, breakdown voltage, water content, acidity, and dissipation factor [18]. Cellulose insulation is assessed by the degree of polymerization (DP) and tensile strength, often measured indirectly through oil samples or conditional monitoring techniques like Frequency Domain Spectroscopy [19].

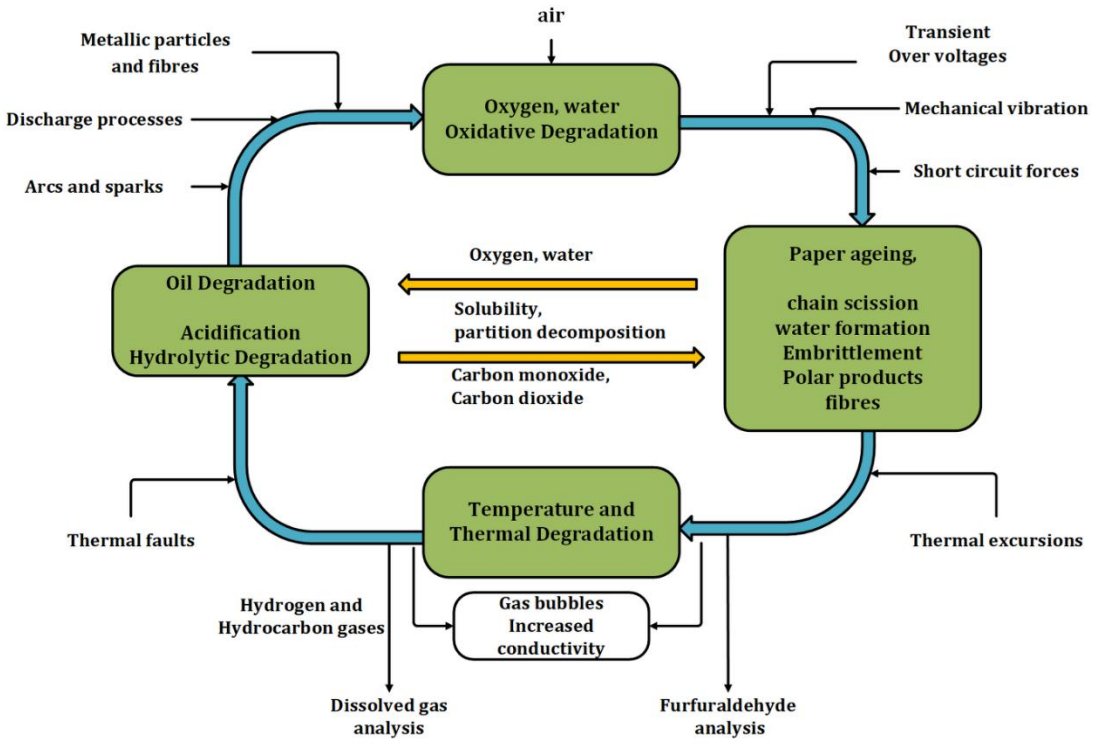

Fig. 1.7. Degradation and ageing of oil paper insulation

1.3.4 Breakdown and pre-breakdown strength of an insulation

Liquid-insulated power equipment, especially power transformers, are crucial and costly components of an electricity transmission network. Their reliable operation is essential, prompting utilities and operators to closely monitor transformer conditions, particularly the dielectric liquids used for insulation and thermal management. Their insulating performance degrades over time due to oxidation and contamination with moisture, cellulose matter, temperature and dissolved gases. If these contaminants compromise the performance of the oil, it must be replaced to prevent electrical breakdown. Insulation failure in transformers can cause severe damage, operational disruptions, and significant financial loss. Consequently, scientists and engineers have long studied transformer oils to understand electrical breakdown, reduce its likelihood, and mitigate damage. The dielectric strength is a critical parameter when selecting oils for use in oil-filled equipment like power transformers. The chosen oil must provide effective electrical insulation and ensure proper impregnation of solid insulating components such as paper, polymer, pressboard, and wood. Proper impregnation eliminates air or other gases, preventing partial discharges. The dielectric strength of oils is compared using their breakdown voltage (BDV), which measures the efficiency of the oil as an insulator. BDV is highly sensitive to oil quality and is affected by contaminants like particles, moisture, water droplets, and gases. When an insulating material is inserted between two electrodes and is subjected to an applied electric field, that material will be polarized. The bounded charges will be displaced by a certain length proportional to the field. When the applied electric field exceeds the dielectric strength of the material, the charges within the dipoles will be pulled apart and thus becoming free charges.

Fig. 1.8. Breakdown phenomena of oil insulation with test cell

This will cause the material to become conductive and a dielectric breakdown occurs as shown in Figure 1.8. This maximum electric field intensity before a dielectric breakdown is

known as a dielectric strength of the material. Testing the breakdown voltages of insulating liquids in quasi-uniform configurations is commonly done to aid in insulation design or assess the quality of the liquids. To ensure consistency and accuracy in these tests, specific standards such as IEC 60156, ASTM D1816, and ASTM D877 [20-22] have established specific procedures for conducting breakdown voltage tests. The electrical breakdown of a dielectric liquid is the final stage in the breakdown process, preceded by several pre-breakdown stages. Breakdown occurs when an arc forms, creating a short circuit through the liquid and allowing large currents to flow between terminals. Before an arc forms, electrical streamers which are highly conductive structures appear in the liquid as shown in Figure 1.9. These streamers initiate at an electrode if the electric field intensity exceeds a certain threshold (typically 1 x 10^8 to 1 x 10^9 V/m for MO). Streamers propagate towards a grounding point or an electrode of opposite polarity. However, streamer initiation does not always lead to arc formation and electrical breakdown; if the initiating excitation falls below a certain level, the streamer will collapse, resulting in a partial discharge. The characteristics of streamer propagation depend on several factors, including the polarity and amplitude of the initiating excitation. Monitoring and understanding these pre-breakdown activities are essential for early detection and prevention of breakdown events.

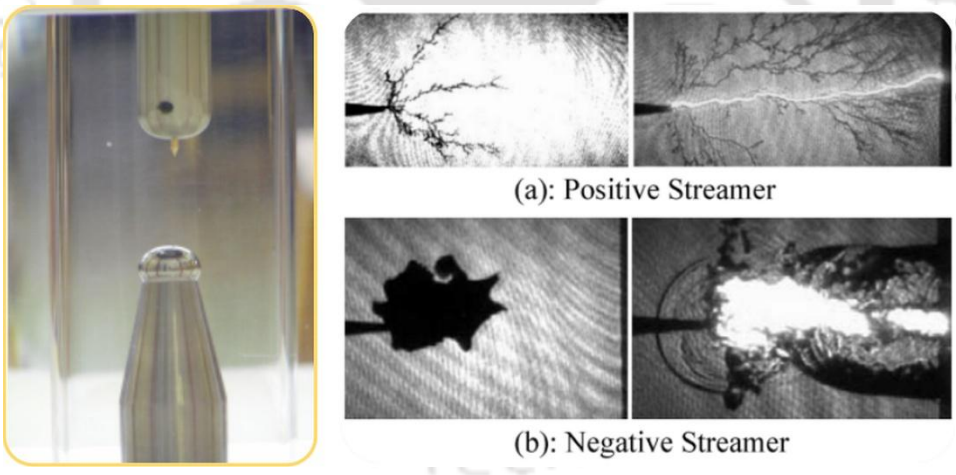

Fig. 1.9. Pre-breakdown phenomena of oil insulation [23]

1.3.5 Geometric effects on breakdown voltage measurement of an insulation

As discussed in section 1.3.4, to ensure consistency and accuracy in breakdown voltage tests, specific standards such as IEC 60156, ASTM D1816, and ASTM D877 [20-22] have been established. The measurement of breakdown voltage (BDV) in insulating liquids is influenced by various factors, including electrode configurations, which can lead to variations

in BDV values as observed in different ASTM and IEC standards. These variations create inconsistencies in BDV measurements under voltage stress, making direct comparisons across different test setups unreliable. Addressing this issue requires a standardized approach that accounts for geometric effects, ensuring that BDV values reflect the actual dielectric strength of the insulating liquid rather than artifacts of the test configuration. Therefore, a new measurement technique is necessary to normalize these differences by deriving an analytical expression that compensates for geometric variations. This will enhance the reliability and consistency of BDV assessments, ultimately improving the accuracy of evaluating insulation performance in high-voltage applications. This concept is explained in more detail in Chapter 3 of this thesis.

1.4 Literature survey

With the growing emphasis on environmental safety and the need for sustainable and eco-friendly alternatives, the search for biodegradable dielectric fluids with superior heat transfer, fire resistance, and insulating properties has intensified. Among these, NEOs like BIOTEMP from sunflower and ENVIROTEMP from soybean have shown promise as substitutes. Companies like ABB and Siemens have already adopted NEO based dielectric fluids in transformers, signaling a shift towards greener solutions. While NEOs have been extensively researched in HVAC transformers, with well-established literature on breakdown and pre-breakdown strength, dielectric properties, fire resistance, and mechanical, physicochemical, and thermal properties, their application in HVDC transformers is a more recent development gaining significance. This literature review delves into the current advancements and ongoing research, highlighting the properties, benefits, and challenges of using NEOs in HVDC transformer insulation systems.

1.4.1 Alternative dielectric liquids

Companies like ABB and Siemens have already implemented VO-based dielectric fluids in transformers [24-26]. Their AC breakdown voltage (ACBDV) and fire resistance properties, physicochemical properties and thermal conductivity are well-studied [27-31]. VOs primarily consist of triacylglycerols, comprising 98% of the total content, with the remainder including free fatty acids, diglycerol, tocopherols, and sterols. The triacylglycerol structure, formed by the condensation of three fatty acids with glycerol, is shown in Figure 1.10.

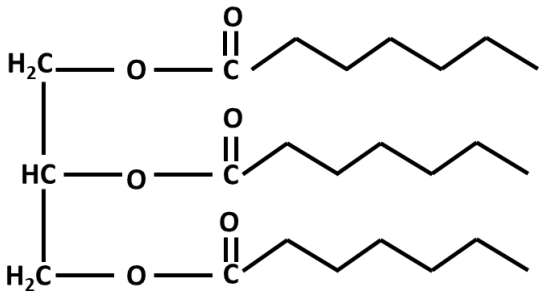

Fig. 1.10. Triglyceride structure.

The triglyceride structure of VOs contributes to their high viscosity due to their large molecular weight. VOs contain three types of fatty acids: saturated, mono-unsaturated, and poly-unsaturated. Saturated fatty acids have only single bonds between carbon atoms, whereas unsaturated fatty acids contain one or more C=C double bonds, making them prone to oxidation. This oxidation, which can be accelerated by contaminants and temperature, is a critical factor in the stability of VOs. Typically, higher percentages of unsaturated fatty acids in NEOs make them more susceptible to oxidation and contribute to their viscous nature [32]. VOs can be sourced from rapeseed, palm kernel, sunflower, and soybean plants. Processing crude VO yields suitable NEOs, potential candidates for transformer oil. However, using edible crops for oil production may lead to food shortages [33]. Therefore, investigating non-food crop oils as dielectric fluids for transformers is essential.

Researchers have compared NEO and MO, finding that NEOs are fire-safe with a high fire point ("K" class liquid) and can hold more water due to their hygroscopic nature, which extends the life of solid insulation. NEOs also exhibit better breakdown strength than MOs for smaller gaps but lower breakdown voltage for larger gaps [34]. Breakdown strength analysis of different MOs, synthetic esters, and natural esters showed that ester oils have a slightly better dielectric withstand capacity under AC, homogeneous field, and small gap conditions [35]. Experiments with BN nanoparticles in VO improved thermal conductivity, dissipation factor, and electrical conductivity [36]. Jatropha curcas methyl ester oil has been identified as a potential substitute for MO, showing similar streamer characteristics and stopping lengths [37]. Further comparison revealed longer stopping lengths and higher conductivity in ester oils compared to MOs, especially when the point is negative [38]. Despite some studies on the thermophysical and electrical properties of VO-based TO, the applicability of non-edible VO as an insulant and coolant needs more attention. Limited research has been conducted on non-food seed oils like jatropha curcas, neem, mahua, and

pongamia for transformer applications, focusing on BDV and streamer propagation but not on heat transfer and other properties [33,37].

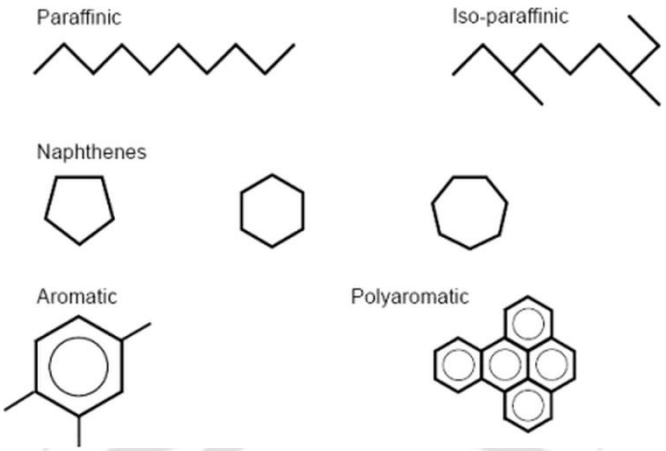

Fig. 1.11. Basic hydrocarbon structures in mineral oil [39].

The oils investigated in this thesis are MO and Envirotemp FR3. Here is some introduction of the oils. MO comprises various hydrocarbons, primarily paraffins, naphthene, aromatics, and polyaromatics [39]. As a refined blend from crude oil, the structure of MO is often reported as percentages of paraffinic, naphthenic, and aromatic compounds as illustrated in Figure 1.11. The transformer industry favours naphthenic oils for their superior low-temperature performance and lower likelihood of wax formation. While aromatics enhance the dielectric strength of MOs, they can oxidize and precipitate as sludge, reducing stability. Sulfur compounds, which remain from refining, can act as mild antioxidants but may also react corrosively with copper, risking insulation failure. The refining process aims to eliminate olefins, as their reactive double bonds can form sludge and acids [40]. FR3 is a refined vegetable oil-based dielectric fluid, primarily made from soybean oil and consists of saturated and unsaturated fatty acids with up to 22 carbon atoms and 1 to 3 double bonds as shown in Figure 1.12.

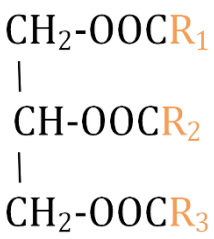

Fig. 1.12. Generic molecular structure of Envirotemp FR3 [41].

The base oil can be sourced from various VOs, including soybean, sunflower, rapeseed, cottonseed, olive, safflower, jojoba, lesquerella, and verona [41]. The structure of the ester

affects its properties: higher bond saturation increases oxidative stability but also raises viscosity. Manufacturers balance viscosity and stability by selecting esters with 1 to 3 unsaturated bonds and adding antioxidants and pour point suppressants.

1.4.2 Dielectric properties of HVDC transformer insulation

The transition from MO to NEOs in HVDC transformers has gained momentum due to their environmental benefits and performance potential. The development and application of natural ester insulating oils in AC transformers have been extensively studied due to their environmental and performance benefits. The advancement of HVDC converter transformers and their insulating materials has become a critical area of research due to the complexities of handling AC and DC stresses. Ab Ghani et al. [42] provide a comprehensive review of methods to improve the workability of natural ester insulating oils, highlighting advancements in pour point depression, chemical modifications, and additive enhancements. They emphasize the importance of addressing issues like low oxidation stability and high viscosity to make NEO oils more viable for high-voltage applications. Fofana [43] presents the development of insulating liquids over the past 50 years, noting the shift towards esters for their biodegradability and fire safety. The review underscores that while MOs remain widely used, esters offer significant advantages for future applications. Piovan [44] studied current insulation systems in HVDC transformers, emphasizing the need for better characterization of insulating materials and improved testing methods for oil conductivity. Cigre [45] analyzed the performance of HVDC Thyristor Converter Transformers, emphasizing operational reliability and performance metrics. Moreover, the Joint Working Group A2-B4 [46] from CIGRÉ reviewed design, test procedures, ageing evaluation, and service reliability of HVDC converter transformers.

Effects of Nanoparticles in DC voltages

Khaled and Beroual [47] explore the effects of nanoparticles (NPs) on the DC breakdown voltage (DC-BDV) of natural esters, noting that Fe_3O_4 and Al_2O_3 nanoparticles enhance DC-BDV significantly, whereas SiO_2 does not. They point out the practical challenges of nanoparticle application, such as high costs and sedimentation. Oparanti et al. [48] investigate the effects of SiO_2 nanoparticles on the dielectric properties of neem ester, finding that the addition of nanoparticles enhances breakdown strength, making it a viable alternative to MO for transformer insulation. Mahidhar et al. [49] and Swati et al. [50] investigated the performance of nanoparticle-dispersed synthetic ester oils and titania nanoparticles in

transformer oils, respectively. Both studies concluded that the addition of nanoparticles improved corona inception voltage and breakdown strength, with titania nanoparticles offering enhanced performance under AC and DC voltages.

Dielectric properties of natural esters and mineral oils

Hao et al. [51] compare cellulosic particle accumulation and conductivity characteristics of NEO and MO, finding that natural esters exhibit better insulation properties under DC fields, which could lead to improved transformer performance. Li et al. [53] studied the migration behaviour of cellulose particles under DC electric fields and concluded that a complete cellulose particle bridge forms more easily in mineral oil than in natural ester. Under identical electric field conditions, contaminated mineral oil exhibits a higher stable saturated conduction current than contaminated natural ester, indicating that natural ester performs better in this regard. Another study by Hao et al. [52] supports this finding, showing that natural esters result in lower leakage currents and better particle accumulation control under DC electric fields, indicating superior dielectric performance.

Vahidi et al. [54] compare MO and NEOs electrical conductivity, revealing that NEO offers more stable conductivity, particularly as HVDC equipment ages. Zhao et al. [55] studied the bridging effect of cellulose particles in natural ester oil under DC voltage, finding that controlling particle concentration is critical to maintaining insulation performance. Cheng et al. [56] examine the impact of fibre and copper particles on the conductivity and breakdown characteristics of natural ester and mineral oil under DC voltage. Their findings reveal copper particles move faster than fibre particles, forming impurity bridges in mineral oil but not natural ester. This leads to higher current density in mineral oil than natural ester, suggesting that natural ester could better resist particle contamination and provide superior insulation properties.

Zou et al. [57] investigate the DC breakdown characteristics and charge accumulation behaviour of thermally upgraded paper aged in NE versus MO. They report that natural ester-immersed paper has higher volume resistivity and DC breakdown voltage than MO-immersed paper due to the larger deep trap density in NEO. This makes the combination of thermally upgraded paper and natural ester a promising alternative for HVDC applications. Yoon, Chen, and Hosier [58] studied the impact of thermal ageing on the dielectric properties of natural ester oil-impregnated paper compared to mineral oil-impregnated paper. Despite higher acid formation in natural ester during ageing, leading to more charge accumulation, NEO-

impregnated paper shows higher DC breakdown voltage. This indicates natural ester's potential as an environment friendly alternative to MO in HVDC transformers, given with proper moisture management.

Nadarajah et al. [59] investigate olive oil as an alternative insulating liquid, demonstrating its superior AC and DC breakdown voltages at higher temperatures compared to unused transformer oil, thus suggesting its potential as a sustainable option for transformer insulation. Rumpelt and Jenau [60] examine ester-based insulation fluids in HVDC systems, finding comparable conductivities to mineral oils when using pressboard barriers, thus validating esters suitability for HVDC applications. Schober [61] investigates the electrical conductivity of pressboards in HVDC systems, concluding that oil-impregnated pressboards significantly enhance conductivity, emphasizing the importance of understanding and optimizing these properties for better insulation design. Zainuddin et al. [62] study the bridging phenomenon in ester oils, indicating that particle size and oil viscosity significantly influence the formation of cellulose bridges and breakdown behaviour. Beroual et al. [63] conducted a comparative study on the BDV of mineral, synthetic, and natural oils, showing that mixtures containing natural or synthetic esters significantly enhance the dielectric strength of MO, suggesting potential for transformer re-filling practices. Hao et al. [64] analyze the impact of moisture on particle accumulation and oil breakdown characteristics, concluding that NEOs exhibit better resistance to particle pollution and superior insulation properties compared to MOs. Liao et al. [65] compare the effects of oil ageing on the motion of cellulose particles and conductivity in mineral oil and natural ester under a non-uniform DC electric field. Their results show that while wet conditions accelerate particle accumulation and impurity bridge formation in both oils, natural ester demonstrates better resistance to particle pollution and superior insulation properties than MO.

HVDC transformer insulation design

Fabian et al. [66] highlight the challenges in designing HVDC converter transformers, emphasizing the significant differences in the conductivities of oil and insulating boards and the need for detailed studies on conductivity changes under operational stresses. Jing et al. [67] compare the DC breakdown voltage and mobility characteristics of different insulating liquids, noting that natural ester fluids exhibit higher breakdown voltages than synthetic esters and mineral oils under positive polarity. In a comparative study, Jing et al. [68] explore the dielectric properties of synthetic ester, mineral oil, and natural ester, revealing that synthetic

esters have higher AC breakdown voltages, but NEOs demonstrate more stable performance under DC stress.

Muscio et al. [69] examine the effects of strong DC electric fields on the flow properties of insulating liquids, finding that natural ester oils show a significant increase in viscosity under high electric fields, which could inform better transformer designs. Rumpelt and Jenau [70] discuss the challenges posed by the combined alternating and direct voltage stresses in HVDC systems, emphasizing the need for detailed investigations into the conductivity of ester-based insulating liquids compared to traditional MOs. Their study highlights the influence of these fluids on DC conductivity in insulation barrier systems, providing a reference for future HVDC insulation designs. Xiang et al. [71] compare streamer characteristics and breakdown in mineral oil and synthetic ester liquids under DC voltage. Their study shows synthetic esters exhibit longer streamer stopping lengths and lower 50% breakdown voltages than MOs under both polarities. This indicates the need to consider liquid dielectric properties in HVDC applications carefully.

Alshehawy et al. [72] study the space charge behaviours of ester liquid and Kraft paper double-layer insulation systems under polarity reversal. They observe that ester-Kraft paper samples show faster space charge redistribution after polarity reversal, reducing the duration of electric field distortion compared to mineral oil samples, which is beneficial for HVDC converter transformers. Atalar, Ersoy, and Rozga [73] investigate the dielectric strength of mineral oil, natural ester, and synthetic ester under different high-voltage conditions. Their study finds that synthetic ester exhibits the highest dielectric strength under AC and negative DC stress, but mineral oil proves most resistant under lightning impulse voltages. These results underscore the necessity of a multifaceted evaluation when selecting liquid dielectrics for transformers.

Space Charge Behaviour and Partial Discharges

Bo Huang [74] delves into the space charge behaviour in thick oil and pressboard under temperature gradients in HVDC converter transformers. The research, facilitated by a pulsed electroacoustic (PEA) system, highlights the significant impact of temperature gradients and multilayer insulation structures on space charge dynamics, providing valuable insights for the design and operation of HVDC transformers. A similar focus on space charge behaviour is seen in Zhou Mu [75], which studies mineral oil and ester liquid-impregnated cellulose paper under DC stress. Their work reveals that ester liquids, despite causing stronger homo-charge

injection and faster charge dissipation than mineral oil, offer better insulation performance when properly managed, making them suitable for HVDC applications.

Yoon and Chen [76] examine the space charge characteristics of natural ester oil-impregnated paper with different moisture contents. They reveal that due to its hydrophilic nature, natural ester oil forms hetero charges more slowly than mineral oil, which has significant implications for insulation ageing and electric field distortion under DC conditions. Azcarraga [77], in his PhD dissertation, investigates partial discharge phenomena in converter and traction transformers. He identifies the critical factors affecting partial discharge behaviour under DC voltage and highlights the importance of understanding these phenomena to improve the reliability and lifespan of HVDC transformers. Trnka et al. [78] explore partial discharges under DC voltage in a paper-oil insulating system. They find that space charge formation and electric field deformation are significant under DC stress, emphasizing the need for specialized diagnostic techniques to monitor and manage partial discharges in HVDC systems.

Design Optimization and Environmental Considerations

Wang et al. [79] analyze the insulation performance of natural esters under DC voltages, emphasizing their potential as sustainable alternatives to mineral oils. Their findings highlight the need for further research into esters long-term performance and ageing characteristics to ensure their viability in HVDC applications.

Shuai et al. [80] address major insulation design considerations for converter transformers, focusing on the complex interaction between various electrical stresses. Their study provides insights into the design parameters that need to be optimized to ensure effective insulation performance under the demanding conditions of HVDC applications.

Liang et al. [81] investigate the ion mobility of vegetable insulation oil under different influencing factors, such as voltage amplitude and temperature. Their findings indicate that ion mobility increases with temperature, following the Arrhenius relationship, and is influenced by moisture content, which is critical for optimizing the performance of vegetable oils in HVDC applications. Sitorus et al. [82] conducted a statistical analysis of breakdown voltages for Jatropha methyl ester oil (JMEO) and mineral oil under AC and DC voltages. They observed that JMEO exhibited higher AC breakdown voltages than mineral oil, while their DC breakdown voltages were similar.

Streamer Characteristics and Breakdown

Nadarajah et al. [59] investigate natural ester liquids' dielectric performance under high-voltage DC conditions, finding that esters offer comparable or superior insulation performance to MOs, particularly in terms of breakdown strength and conductivity. Yea et al. [83] delve into the design optimization for the insulation of HVDC converter transformers under composite electric stresses. Their research underscores the critical role of optimizing insulation design to manage AC and DC stresses, emphasizing the need for advanced materials and innovative engineering solutions to enhance transformer performance.

These studies collectively highlight the promising potential of natural esters as environment friendly and effective insulating fluids for HVDC applications. They demonstrate that NEOs can offer superior insulation performance, better breakdown strength, and improved conductivity compared to traditional mineral oils. Despite these advantages, further research is necessary to optimize the performance of NEOs under various operational conditions. In particular, it is critical to extensively investigate the DC breakdown voltage (DCBDV) across different ageing conditions and their effects and geometric levels to ensure the reliability and longevity of NEOs in HVDC insulation systems. Addressing these gaps will be essential for the widespread adoption and application of NEOs in HVDC transformers.

1.5 Motivation

The ongoing shift towards sustainable and environment friendly technologies has brought significant attention to the development of biodegradable dielectric fluids for power transformers. Despite their widespread use, traditional petroleum-based transformer oils face numerous drawbacks, including low biodegradability, limited fire resistance, and environmental concerns due to resource depletion and potential spillage. In response to these challenges, NEOs derived from renewable resources such as sunflower and soybean etc. have emerged as promising alternatives. Major companies like ABB and Siemens have already started integrating NEO-based dielectric fluids into their transformer designs, demonstrating a clear industry trend towards greener solutions.

While the benefits of NEOs in HVAC transformers are well-documented, their application in HVDC transformers is relatively new and less explored. The unique operational stresses of HVDC systems, including handling high direct currents and associated electrical phenomena,

necessitate a thorough understanding of how NEOs perform under these conditions. Existing research literature has highlighted the potential of NEOs to provide superior insulation performance, enhanced breakdown strength, and better conductivity than traditional MOs. However, these findings primarily focus on HVAC applications, leaving a significant knowledge gap in HVDC contexts.

The primary motivation for this thesis is to bridge this gap by extensively investigating the dielectric performance of NEOs in HVDC transformer insulation systems. This research aims to provide a comprehensive evaluation of the DC breakdown voltage (DCBDV) and DC conductivity of NEOs, considering various operational conditions, including thermal and oxidative ageing. Furthermore, it will explore the geometric effects on DCBDV measurements and assess the dielectric strength of solid insulation materials impregnated with NEOs.

This thesis seeks to enhance the understanding of NEOs in HVDC applications by addressing these critical aspects, ultimately contributing to their reliable and widespread adoption. The outcomes of this research will support the development of more sustainable transformer technologies and ensure their operational efficacy and longevity, thereby advancing both environmental and technological goals in the power industry. This thesis also focuses on designing and developing an experimental setup specifically for studying and analyzing pre-breakdown and breakdown phenomena in NEOs under HVDC conditions. This setup will facilitate detailed how this equipment gets observations and measurements of critical parameters, providing valuable insights into the behaviour and performance of NEOs in real-world HVDC applications.

1.6 Objective of the thesis

The objectives of the thesis are described as follows:

- To study and determine the effects of oxidative ageing of NEOs on DC breakdown voltage (DCBDV) and compare these results with MO. Additionally, to establish a pattern and theory on how oxidative ageing influences breakdown strength, test the results reliability and repeatability through statistical hypothesis testing, and obtain DC conductivity values for different ageing states.

- To analyze the effects of accelerated thermal ageing on the DC conductivity and DCBDV of NEOs and compare the results of thermal ageing with oxidative ageing effects on the DCBDV of NEOs.

- To study the geometric effects on dielectric breakdown strength measurements in natural ester oils (NEOs) under DC voltage stresses and to develop an analytical equation to normalize these effects for more accurate results.

- To study the degradation of solid insulation materials that are oxidatively and thermally aged and immersed in NEOs and MO. This includes testing the solid insulation for AC and DCBDV, as well as conducting thermal, chemical, and mechanical degradation studies using Fourier Transform Infrared Spectroscopy (FTIR), Thermogravimetric Analysis (TGA), and tensile strength measurements.

- To develop a new experimental setup for studying pre-breakdown phenomena and analyzing streamer formation in both liquid and solid insulation materials.

1.7 Contribution of the thesis

The major contributions of the thesis for the application of NEOs in HVDC converter transformers are given as follows. This thesis

- A new test cell is developed by modifying the existing test cell according to ASTM D1816, to test DCBDV measurements of the liquid insulation as a huge amount of force is exerted between the electrodes which literally reduces the mechanical integrity just after a very few tests. The new designed test cell can withstand long tests runs and heavy forces exerted during BDV in the test cell.

- DCBDV of NEOs is obtained, establishing patterns and theories on how oxidative ageing influences breakdown strength. Offers comparative analysis between NEOs and traditional MO, enhancing understanding of their relative performance. Obtains DC conductivity values for NEOs under different ageing conditions, contributing valuable data for future research.

- Analyzes the impact of accelerated thermal ageing on the DC conductivity and DCBDV of NEOs. Comparison of effects of thermal and oxidative ageing on DCBDV, offering a holistic view of ageing impacts on NEOs under DC voltage stresses.

- Studies the geometric effects on dielectric breakdown strength measurements in NEOs under DC voltage stresses. Development of an analytical equation to normalize these geometric effects, ensuring more accurate and reliable dielectric breakdown strength measurements.

- Investigates the degradation of solid insulation materials that are oxidatively and thermally aged and immersed in NEO-FR3 and MO. Tests the solid insulation for AC and DCBDV, comprehensively evaluating their dielectric performance. Conducts thermal, chemical, and mechanical degradation studies using advanced techniques such as Fourier Transform Infrared Spectroscopy (FTIR), Thermogravimetric Analysis (TGA), and tensile strength measurements, contributing valuable insights into the degradation mechanisms of solid insulation.

- Provides a design and development of a new experimental setup for studying and analyzing pre-breakdown and breakdown phenomena in NEOs under HVDC conditions. Facilitates detailed how this equipment can be used for observations and measurements of critical parameters, enhancing the understanding of streamer formation and propagation in liquid and solid insulation materials.

These contributions collectively advance the knowledge and application of NEOs in HVDC transformer insulation systems, supporting the development of more sustainable and efficient transformer technologies. The findings and methodologies presented in this thesis will be valuable for academic research and industrial practices, promoting the reliable and widespread adoption of environment friendly dielectric fluids in the power industry.

1.8 Organization of the thesis

This thesis is organized into six chapters as follows:

Chapter 2 details the comprehensive experimental methodology used to investigate the statistical behaviour of DCBDV of NEO-FR3 and MO subjected to thermal and oxidative

ageing over prolonged ageing periods of 90, 200, and 500 hours. This chapter describes about the materials employed and sample preparation procedures, highlighting the importance of maintaining uniform ageing conditions to ensure reliable and consistent results. It then elaborates the experimental setup, including the high-voltage DC power supply, test cell, and measurement instruments used to apply controlled DC voltage stresses and measure breakdown voltages. The thermal ageing process, emphasizing the controlled temperature conditions and oxidative ageing environment designed to simulate real-life operational scenarios is explained. Finally, the chapter discusses the statistical analysis methods employed, focusing on the application of normal, two-parameter Weibull, and three-parameter Weibull distributions to model the experimental data and verify the results using the Anderson-Darling test and goodness-of-fit tests. Additionally, this chapter provides a detailed explanation of theory to obtain DC conductivity of oils from FDS results and Cole-Cole plots. The statistical analysis of breakdown strength of NEO-FR3 and MO under DC voltage stresses after oxidative and thermal ageing obtained experimentally are studied. From the statistical hypothesis testing it is employed that, the majority of the experimental data conform to normal and Weibull distributions, ensuring the reliability of the results. The breakdown strength of FR3 is found to be higher than that of MO under both polarities after oxidative and thermal ageing. However, both the oils exhibit a reduction in breakdown strength with increased ageing duration. This chapter further explores the differences in ageing characteristics between MO and NEO-FR3, noting the DC conductivity of FR3 significantly rises over time maintaining a relatively stable breakdown voltage. Additionally, the chapter investigates DC conductivity through frequency domain spectroscopy (FDS), providing insights into the effects of oxidative and thermal ageing on the dielectric strength of both the oils and highlighting the distinct degradation patterns.

Chapter 3 further delves into the impact of the effective electrode-stressed area (EESA) on the dielectric breakdown strength of MO and NEO-FR3 when subjected to DC voltage stresses. The investigation evaluates the effect of different electrode shapes on the measurement of DCBDV of these insulating oils. Three types of electrodes are employed in this study such as: Verband Deutscher Elektrotechniker (VDE) electrodes, plane electrodes, and sphere-sphere electrodes. These electrodes are chosen from standard testing methods to provide a diverse range of stress distributions and to assess their influence on the breakdown characteristics of the oils. The measurement of DCBDV for both MO and FR3 is conducted with a 1mm gap distance between the electrodes, adhering to the ASTM D1816 standard,

which specifies the test methods for evaluating the dielectric strength of insulating oils. The experimental setup ensures precise control and repeatability of the voltage application and breakdown measurements. After obtaining the DCBDV data, the results are analyzed using Weibull analysis, which involves calculating the scale and shape parameters to model the statistical distribution of breakdown voltages. This analysis helps to understand the dielectric strength variability and reliability under different conditions. The study further incorporates the weakest-link theory and the parallel breakdown probability model to explore the relationship between the effective electrode-stressed area and the DCBDV of the insulating oils. By considering these theoretical models, the research investigates how the size and shape of the electrode area influence the likelihood of dielectric breakdown. The chapter discusses the observed differences in the breakdown behaviour of MO and FR3 when tested with various electrode configurations, providing insights into the fundamental mechanisms governing the dielectric breakdown measurements in these oils.

Chapter 4 explains the oxidative and thermal ageing effects on pressboard insulation performance within MO and NEO. It comprehensively evaluates both oxidative and thermal aged pressboard samples of non-immersed pressboard, fresh MO-immersed, and fresh NEO-immersed pressboard, alongside their oxidatively aged counterparts post 90, 200, and 500 hours, across various parameters. The assessment includes thermogravimetric analysis for thermal stability, Fourier transform infrared spectroscopy for changes in chemical composition, and tests for tensile and dielectric strengths to evaluate mechanical and electrical properties. The study thoroughly investigates the impact of ageing on electrical properties, specifically AC and DC breakdown voltages, for both fresh and aged pressboard samples in MO and NEO environments. This insight is pivotal for advancing transformer technology, focusing on sustainable and eco-friendly insulating materials.

Chapter 5 presents the specialized experimental apparatus and procedure designed to examine the processes leading to and causing breakdown in oil-immersed solid insulation systems commonly used in oil-filled power equipment. The apparatus and its accompanying method investigate the initiation and development of both positive and negative streamers within solid insulation submerged in liquid insulation systems. The primary goal is to better understand the pre-breakdown phenomena by measuring and analyzing the conditions and factors contributing to these events in mixed or heterogeneous insulation systems (combining solid and liquid insulation) within power apparatuses. To achieve this, the device is equipped with advanced shadowgraph and photodetection systems, which enable detailed visualization

and analysis of streamer initiation and propagation. Additionally, it features filtering and degassing systems to ensure the purity and consistency of the insulating liquids, as well as a heating rod that simulates the operational conditions of transformers or other oil-filled equipment. This heating rod enhances the accuracy of pre-breakdown testing by replicating real-world conditions. By studying the behaviour of liquid-immersed solid insulation under various stress factors and operational conditions, this apparatus provides valuable insights into the mechanisms of breakdown and pre-breakdown phenomena, thereby contributing to developing more reliable and efficient power equipment.

In Chapter 6, the conclusion of the thesis and the suggestions for the extension of this research work are presented.

2

Effects of ageing on DC conductivity and DCBDV of natural ester oils

Contents

2.1	Introduction ……..……	29
2.2	Sample preparation……..……..……	32
2.3	Experimental configuration and methodology….....	36
2.4	Measurement of DC conductivity from frequency domain spectroscopy (FDS) and Cole-Cole plot…….	38
2.5	Statistical analysis of DCBDV experimental results…….……..……	43
2.6	Experimental results of DC breakdown voltage of fresh and oxidatively aged samples……	46
2.7	Experimental results of DCBDV for fresh and thermally aged samples….	55
2.8	Comparison of dielectric strength in thermally aged and oxidatively aged NEOs under DC voltage stresses …….…….....	63
2.9	DC conductivity of natural ester oils and its influence on dielectric strength.……	64
2.10	Summary of the chapter ...…….....	71

2.1. Introduction

Electrical utilities and researchers are attempting to develop an eco-friendly, dependable, and economically viable insulating oil for the cooling and insulation of electrical equipment. Natural ester oil (NEO) demonstrates environment friendly and outstanding dielectric properties. Due to its better performance compared to mineral oil (MO), NEO has the potential to be used as an alternative liquid insulation in power apparatus. Thus, certain NEOs employed in high voltage applications are currently available in the market, such as Biotemp, Envirotemp FR3, MIDEL 1204, and MIDEL 1215 [84-86], among others. In addition to being biodegradable, NEOs have a higher flash and fire point than MO, ensuring fire safety, and these oils can be used to insulate extremely high voltage (EHV) installations without the need for additional protective systems [87]. As the world transitions to renewable energies in an effort to combat climate change, one of the greatest problems is transporting electrical energy over greater distances with minimal losses using HVDC systems. HV transformers and HV converter transformers are two critical components of HVDC transport systems. Typically, MO is used for insulation and cooling [47]; however, the new technology adapts NEOs as an alternative and sustainable material, so it is vital to test the limitations of NEOs for DC voltage stresses and verify that their fundamental properties are compatible with equipment.

Over time, chemical reactions will degrade any insulating oil. So, it is necessary to know the factors for oil deterioration and their likely impact on its dielectric strengths. It is well-known that temperature has the greatest impact on the ageing of these insulating oils and, consequently, the lifespan of a power equipment [88]. There are often two areas of concern if an insulating oil degrades [89]: one is due to a rise in the quantity of water content the dielectric performance of oil as an insulator degrades, and other is due to ageing by-products impacting the overall insulation of the transformer. Despite their inherent advantages, these insulating oils experience a slow and irreversible loss of physical properties, often resulting from structural changes at the macromolecular level. Water and oxygen are significant factors that accelerate transformer oil deterioration and ageing. It is well-established that cellulose paper, commonly used in transformers, can retain water, while oil can dissolve oxygen. Furthermore, elevated temperature and electrical field intensity are crucial in expediting the ageing process. This investigation of thermal and oxidative ageing phenomena in insulating materials serves two primary objectives. Firstly, it aims to determine the expected service life under thermal stress. Secondly, it investigates the relationship between the ageing

phenomenon and the specific stress factors responsible for its occurrence. Studying insulating oils dielectric strength (primarily Breakdown strength) becomes crucial when examining the effects of ageing. Before delving into the research findings on the breakdown strength and DC conductivity of insulating liquid dielectrics with ageing, it is essential to review the available literature on the ageing of NEO-FR3, BDV, and DC conductivity. The following discussion provides a comprehensive overview of the research done in these topics.

Envirotemp FR3, obtained from Cargill India Pvt. Ltd., is the primary insulating material utilized as NEO in this study. The insulating oil FR3 is widely available and is used in several transformers around the world. Oommen and Lewand discovered that FR3 gels when subjected to the ASTM D2440 testing standard, with Oommen proposing that FR3 may be oxidizable [10]. According to Lewand, NEO cannot be directly correlated with MO because their chemistries are so different; he continued to explain that although oxidation is the primary mechanism underlying the breakdown of MO, hydrolysis, and oxidation are the primary mechanisms behind the breakdown of NEO [41]. D. Martin [90] examined MO, synthetic and NEOs (FR3) for ACBDV, LIBDV (lightning impulse BDV), acidity, and dielectric dissipation factor over 28 days at 115°C in the presence of oxygen. The ageing is done in open containers with copper and glass-coated steel immersed in the oil. Pressboard was not used for the ageing phenomena in this study. It has been reported that oxidation and hydrolysis did not influence the breakdown strength of the oil appreciably in their research since the ester BDVs remained constant during heating. For their study, H. M. Wilhelm [91] utilized ABB Biotemp and Envirotemp FR3. Samples of Envirotemp FR3, in the presence and absence of dried Kraft paper, with oxygen flow rate of 1 L/h, were aged in a thermo-stabilized bath at 70℃, 95℃, and 110℃ and for specified periods of time as per ASTM D924. From the results of the experiment, it has been reported that the hydrolysis of NEOs can result in an increase of acidity, while their oxidation can result in an increase of viscosity. S. Tenbohlen [92] compared the electrical and physical performance and ageing characteristics of three NEOs, one of which is FR3, against those of one synthetic and one standard MO. The ACBDV of fresh NEO is higher than 80 kV, which is greater than that of MO, according to this research. In the presence of oxygen, vegetable oils undergo oxidation, resulting in a considerable increase in viscosity.

N. Baruah et al. examined the various dielectric properties to determine the condition of the NEO (FR3) and natural ester oil based nanofluids (NEO-NF) in both fresh and aged

circumstances. An oxidative open beaker ageing (OBOA) test setup is utilized to age these oil samples. By evaluating the AC breakdown data of the oils, it is discovered that the NEO-NF has a higher breakdown voltage than the NEO due to the nanoparticles (NPs) electron-scavenging property [93]. Similarly, N. Baruah et al. investigated the dielectric behaviour of insulating liquids. After verifying the null hypothesis, a statistical analysis is conducted to evaluate the ACBDV of the oil samples which match a specific probability distribution. Further they analyzed the experimental data and failure probabilities of 50%,10% and 5%, are studied for the Weibull and normal distribution functions [94]. In addition to the above studies various researchers have studied the DC BDV of FR3 under various conditions, such as the effect including the presence of the cellulose particles on dielectric strength [55, 95-96]. The AC and DC BDV of fresh as well as aged FR3 and its blending (MO+FR3) are investigated in [63].

Apart from these analyses, as mentioned above, understanding the field strength distribution within the installed components is crucial in evaluating the condition of insulation systems in HVDC transformers beyond the breakdown strength. This necessitates a comprehensive understanding of the conductivity behavior of electrical insulating oils [97]. HVDC transformers insulation design differs from conventional transformers, as they must withstand AC voltage with a DC offset. While the permittivity plays a decisive role in the insulation construction under AC voltages, the conductivity becomes crucial for the DC layout. HVDC equipment, subjected to AC and DC stress, relies on understanding DC conductivity for optimizing field distribution in insulation systems. Rumpelt et al. [97] emphasize the significance of DC conductivity in lower temperatures and present simulation approaches to anticipate its behaviour. Additionally, Matharage et al. [98] evaluate coconut oil as an alternative transformer liquid insulation, demonstrating its suitability despite certain limitations. Furthermore, Liu et al. [99] investigate the dielectric frequency response of oil-paper composite insulation modified by nanoparticles, highlighting the enhanced insulation properties and introducing a new low-frequency relaxation phenomenon.

Since oxidative ageing and thermal ageing are two primary mechanisms significantly affecting insulating oils, it is imperative to investigate both phenomena thoroughly. By doing so, researchers can identify potential limitations in implementing NEOs in HVDC applications. Although some studies have examined the dielectric strength of NEOs under DC voltage stresses under various conditions, the long-term applicability of NEOs for HVDC

equipment remains underexplored.

This chapter comprehensively discusses the experimental methodology and sample preparation. It covers the preparation of MO and NEO undergoing oxidative and accelerated thermal ageing. The pretreatment of samples before ageing is also discussed. The samples are tested for viscosity and moisture content after the ageing process to verify proper ageing. The impact of moisture on the tests conducted is also discussed. Additionally, the chapter briefly addresses the storage of the prepared samples. The experimental methodology and setup for DCBDV testing, including testing conditions and standards, are thoroughly discussed. The statistical behaviour of DCBDV in NEO-FR3 and MO subjected to thermal and oxidative stresses over prolonged ageing periods of 90, 200, and 500 hours is analyzed. This chapter also details the statistical analysis methods employed, focusing on applying normal, two-parameter Weibull, and three-parameter Weibull distributions to model the experimental data. The results are verified using the Anderson-Darling test and goodness-of-fit tests. The DC conductivity is calculated using frequency domain spectroscopy (FDS) and Cole-Cole plots, and the underlying theory of these methods is briefly discussed in the chapter. The results obtained from these methods are discussed in Chapter 3.

2.2. Sample preparation

The two primary base insulating oils such as MO (TRANSOL) and Envirotemp FR3 are obtained from Savita Industries and Cargill India Pvt. Ltd., respectively to carry out this study. The fundamental properties of these oils are listed in Table. 2.1.

Table 2.1: Basic properties of insulating oils [94]

Characteristics	Unit	MO	FR3
Tan Delta	**at 90℃**	0.0089	0.00863
Interfacial Tension at 27℃	**N/m**	0.047	0.0206
Kinematic Viscosity at 27℃	**cSt**	11.25	59.00
Density of oil	**kg/m^3**	0.825	0.910
Flash Point	**℃**	140	268
Dielectric constant	**at 90℃**	2.01	2.83

2.2.1. Oxidative ageing experimental setup

Figure. 2.1 illustrates oxidative open beaker ageing (OBOA) chamber developed in the laboratory to age the samples oxidatively. The Kraft paper and the oils are vacuum dried at 80℃ for 24 hours and 60℃ for 48 hours to remove the residual moisture before ageing.

(a) (b)

Fig. 2.1. (a) Open beaker oxidative aging (OBOA) chamber; (b) Samples placed inside oxidative aging chamber

A 300 ml open beaker is filled with oil, pressboard and copper of weight ratio 20:1:1 [93-94] are used for the oxidative ageing. A spiral copper conductor is put into oil as a catalyst for faster deterioration. The oxidative ageing process used in this study adheres to the ASTM D1934 standard [100]. Pressboard and copper are used to create more accurate conditions for the ageing of oils as all the materials coexist in a transformers that lead to ageing of oil. These materials also act as catalysts for the ageing process. These 300 ml open beakers containing the samples are put inside the oven on a platform. According to the standard, the temperature within the oven is maintained at 115°C ±1°C. MO and NEO (FR3), both the oils undergo oxidative ageing for 90, 200, and 500 hours. Each sample is collected after the specified time period and is stored in an air tight reagent bottle as it is shown in Figure. 2.2.

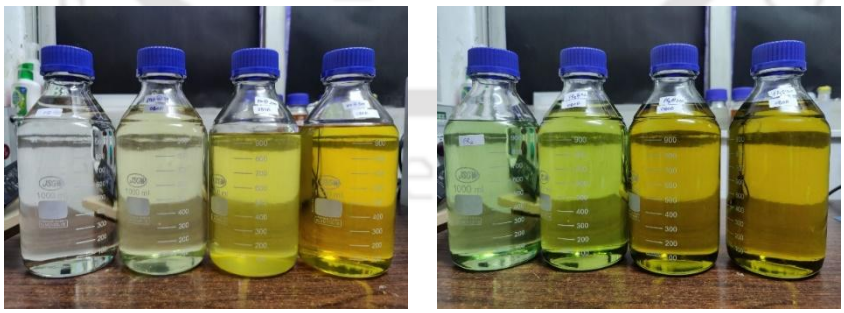

(a) (b)

Fig. 2.2. a) Open beaker oxidative aged samples of MO@ 0, 90, 200- and 500-hours b) Open beaker oxidative aged samples of FR3@ 0, 90, 200 and 500 hours

2.2.2. Accelerated thermal ageing setup

2. Effects of ageing on DC conductivity and DCBDV of natural ester oils

Before thermally ageing the samples, Kraft paper and oils undergo vacuum drying at 80℃ for 24 hours, followed by 60℃ for 48 hours, to eliminate residual moisture. The ageing takes place within a dedicated hermetically sealed chamber with a capacity of 1.5 litres to prevent air exchange as shown in Figure. 2.3. Accelerated thermal ageing employs a composite mixture of oil, pressboard, and copper in a weight ratio 20:1:1 [94]. A copper spiral conductor is introduced into the oil as a catalyst to expedite degradation.

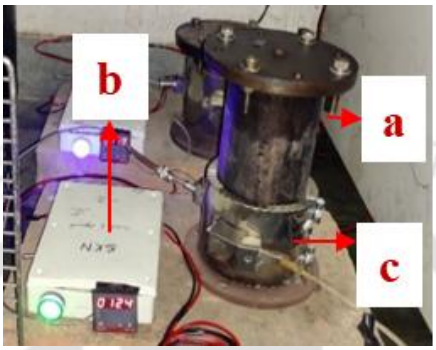

Fig. 2.3. Accelerated thermal ageing setup (a) Hermetically sealed tube (b) Temperature controller (c) Band heater with thermocouple.

The accelerated thermal ageing process follows the guidelines of IEEE C57.100-1999 [101] standard. As per this standard, the temperature inside the chamber is carefully maintained at 125℃±2℃.

(a) (b)

Fig. 2.4. a) Thermally Aged MO Samples at 0, 90, 200, and 500 hours b) Thermally Aged FR3 Samples at 0, 90, 200, and 500 hours.

Since MO is one of the samples in this investigation and its flash point is approximately 140℃, this temperature is chosen for the thermal ageing of the MO and FR3 to ensure a fair comparison. The oil samples undergo accelerated thermal ageing for specific durations of 90, 200, and 500 hours. After each specified time, samples are collected, as illustrated in Figure

2.4. The collected specimens are subsequently utilized to investigate the impact of accelerated thermal ageing on dielectric strength under both positive and negative DC voltage stresses.

2.2.3. Viscosity and moisture content of the samples

The mere colour of these samples collected after ageing is insufficient to characterize the accelerated ageing and oxidative ageing conditions of MO and FR3 fully. Therefore, the viscosity of these oils is measured across a temperature range of 30℃ to 80℃ using an Anton Paar MCR 301 Rheometer. The data presented in Figures 2.5a, 2.5b, 2.5c and 2.5d indicate accelerated thermal ageing and oxidative ageing effect on the samples and as the oils aged, their viscosity increases with ageing time, which is a definitive indicator of the ageing state of these samples. In the case of FR3, the fresh and FR3@90_TAA have almost the same viscosity, so they overlap in thermally aged samples as shown in Figure 2.5a. From Figure 2.5b it is observed that for OBOA the viscosity for MO@200hrs samples is greater below 50℃ than MO@500hrs. One possible reason for this observation is that during the early stages of ageing (i.e. 200 hours), the formation of oxidation by-products, such as sludge and acids, increases the oils viscosity. However, as ageing progresses (i.e. 500 hours), these by-products might undergo further chemical reactions, breaking down into smaller, less viscous compounds.

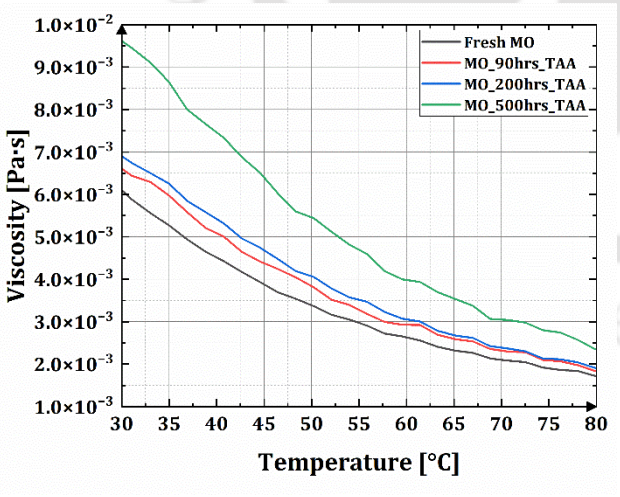

(a)

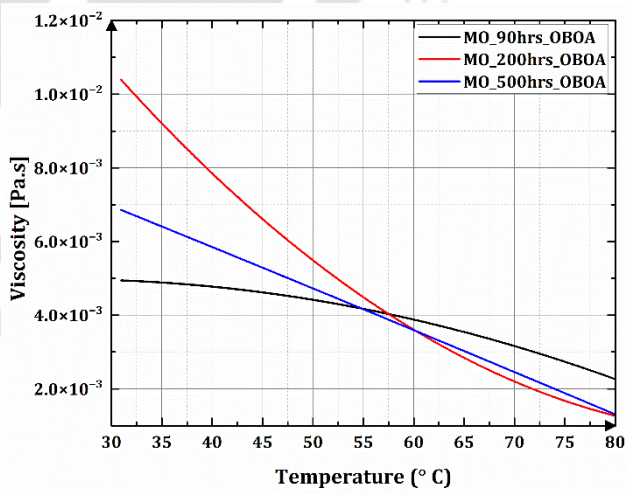

(b)

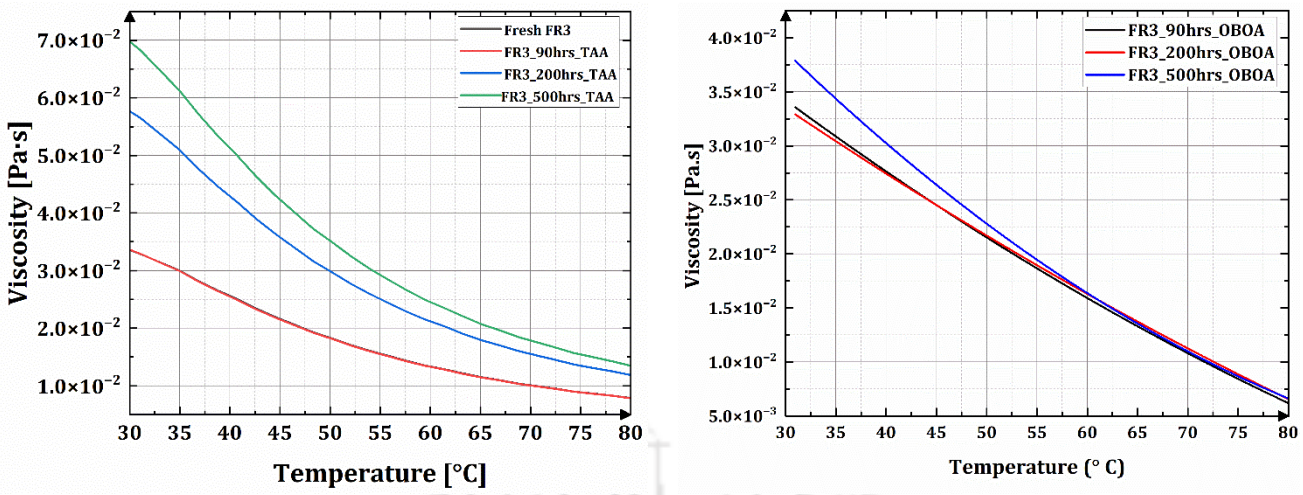

(c) (d)

Fig. 2.5. Viscosity of samples with the change in temperature for (a) fresh and thermally aged MO (b) fresh and oxidatively aged MO (c) fresh and thermally aged FR3 (d) fresh and oxidatively aged FR3

Additionally, the thermal and oxidative stress over an extended period can lead to the degradation of these by-products, reducing their overall impact on the viscosity of the oil. Thus, the initially higher viscosity at 200 hours decreases at 500 hours. In addition to viscosity measurements, the moisture content of the samples is determined using a Metrohm 899 KF Coulometer. To ensure consistency across measurements, each sample is measured with a weight of 0.5 to 0.6 grams. The results of these measurements are presented in Table 2.2. The data presented in the table clearly indicate that the moisture content in NEO-FR3 is significantly higher than in MO, which can be attributed to the inherent high-water retention capacity of natural esters. Despite the elevated moisture levels in NEO, the average DCBDV is minimally affected compared to MO in both the aged samples.

Table 2.2: Moisture content of the fresh and aged samples

Moisture content (ppm)				
	Themally aged samples		Oxidatively aged samples	
Ageing hours	**FR3**	**MO**	**FR3**	**MO**
0 hrs	839.7	189.7	839.7	189.7
90 hrs	588	53.7	374.0	148.0
200 hrs	1017.6	79.1	995.2	113.0
500 hrs	1461.2	159.6	1021.7	108.5

2.3. Experimental configuration and methodology

Using spherically-capped brass electrodes with a 1 mm gap are placed in a testing cup and

a WSTS high voltage generation unit with a DC generating capacity of 140 kV is used for measuring breakdown voltages of samples under DC voltage stresses in accordance with ASTM D1816 [21]. The schematic of complete experimental setup is depicted in Figure 2.6. As there is no specific standard for DC breakdown voltage for insulating liquids, the abovementioned standard is applied to obtain the DC breakdown voltage of the oil samples. The voltage rise rate is 2 kV/step. The initial standing time of 5 minutes is given before voltage application to allow the bubbles formed to settle. Each breakdown is followed by a one-minute pause.

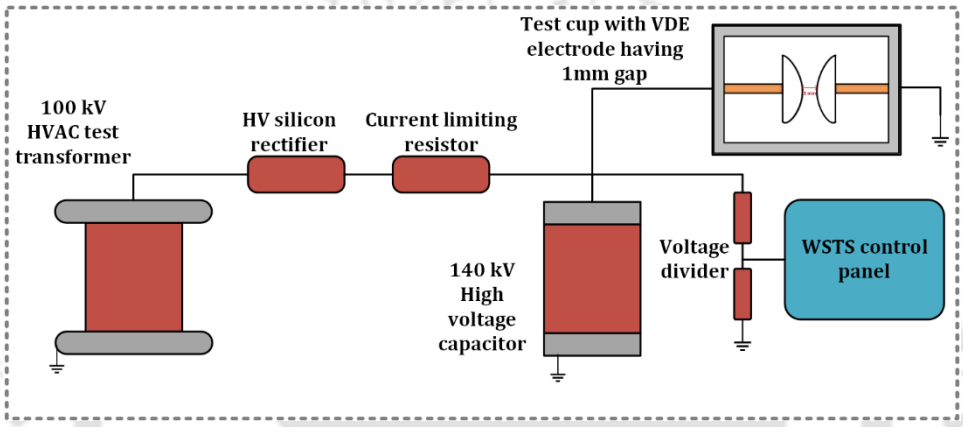

Fig. 2.6. Schematic diagram of DCBDV experimental setup

All experiments are performed at room temperature. In industrial applications, the breakdown voltage (BDV) of insulating liquids is a critical parameter for ensuring the reliable operation of high-voltage equipment such as transformers and circuit breakers. While the mean BDV provides an overall indication of the dielectric strength of a liquid, it does not fully capture the risk of early failures that could lead to catastrophic equipment breakdowns. In practical scenarios, insulation failure is often determined by extreme cases rather than average performance. In industrial applications, the breakdown voltage (BDV) of insulating liquids is a critical parameter for ensuring the reliable operation of high-voltage equipment such as transformers and circuit breakers. While the mean BDV provides an overall indication of the dielectric strength of a liquid, it does not fully capture the risk of early failures that could lead to catastrophic equipment breakdowns. In practical scenarios, insulation failure is often determined by extreme cases rather than average performance. Therefore, industry standards emphasize BDV values with a low probability of breakdown (e.g., lower percentile values from statistical distributions) to account for worst-case scenarios. Since the six breakdowns mentioned in ASTM D1816 are insufficient for this purpose four sets of six breakdowns are done on each sample to overcome this limitation. In

total, 24 breakdowns are done on each sample. The pause period between each set is 5 minutes for MO and 15 minutes for NEO [21, 63]. In this gap, the oil is swirled using a glass rod. The identical methods are employed for negative DC polarity, and all experimental findings are then assessed statistically to check the randomness of the obtained data.

2.4. Measurement of DC conductivity from frequency domain analysis (FDS) and Cole-Cole plots

Apart from the DCBDV the DC conductivity is calculated using frequency domain analysis (FDS) and Cole-Cole plots. A frequency response analyzer (Solartron 1260A) is employed in conjunction with a dielectric interface (Solartron 1296A), as depicted in Figure 2.7. An alternating voltage is applied to the oil sample using a two-electrode configuration upon applying an external field; the capacitance stores a portion of energy, while another part is dissipated due to resistance effects. The frequency range considered for this analysis spans from 10^{-3} to 10^{4} Hz. Typically, a three-electrode setup is used for measurements, with a guard electrode to improve accuracy, especially when the measured current is low. However, this study uses a frequency response analyzer (Solartron 1260A) with a dielectric interface (Solartron 1296A). For this particular equipment, noise in the signal applied to the analyzer can be eliminated by a technique known as signal integration through dielectric interface. This procedure averages the signal over a large number of cycles, narrowing the measuring bandwidth and thereby increasing the signal-to-noise ratio. The more a signal is averaged, the longer it takes to obtain a result. Here, averaging is done over multiple measurement cycles of the applied signal. Each cycle contributes combined data points to reduce random noise, thereby improving accuracy. The iterations refer to the number of times the measurement cycle is repeated to compute an averaged response. This process addresses the issue of signal noise, which can interfere with low-current conductivity measurements. By averaging the signal over multiple cycles, the system narrows the measuring bandwidth, enhancing the signal-to-noise ratio (SNR). However, this comes at the cost of increased measurement time, as more cycles must be recorded and processed before obtaining a final value. The trade-off is between higher accuracy (more averaging) and faster measurement speed (less averaging). Hence, there is a trade-off between the required accuracy and measuring speed. The measurement setup defaults to a fixed Integration Period, with auto integration turned off [102]. Based on this explanation, it is evident that incorporating the dielectric interface improves measurement accuracy and reliability. Each experiment is carried out through three

iterations, and the resultant data represents the average of these three runs to ensure greater accuracy in the obtained values. Data recording is carried out through the utilization of the SMaRT software.

The relative permittivity of all the oil samples are achieved by performing the FDS analysis. The complex permittivity of any dielectric material defines the dielectric properties, i.e. the ability of the material to accumulate electrical energy, on the application of an external electric field and also indicates the losses. Under the effect of a voltage, the dielectric material will polarize. The extent of polarization varies for different materials at different frequencies. This process depends on the integrity of the material, like, what quantity of polar contaminants is present, ageing of the dielectric, moisture, temperature and their relaxation mechanisms. It has also been observed by many researchers that real dielectrics do not follow the standard Debye model which gives a semicircular arc with its centre on the x-axis. K. S. Cole and R. H. Cole developed a method to correlate the dielectric response of real materials with idealized Debye behaviour [103,104]. They obtained a plot between real and imaginary components of complex permittivity (ε_r' and ε_r'') from the FDS over the entire range of frequency. It is found that during experimental observations on real dielectrics, the plot often formed only an arc of a circle, rather than a full semicircle, while its centre lying below the $\varepsilon_r'' = 0$ axis, which is a deviation from Debye model [103,104]. Such deviation in the Cole–Cole plot is attributed to the distributed nature of relaxation process taking place in the complex dielectric material. These plots have been used by researchers for characterizing different materials and composites [105, 106]. Researchers have investigated the dielectric response measurement results of transformer oil insulation with Cole–Cole model and highlighted the fact that real dielectrics have more than one relaxation frequency and the intermolecular interactions should be considered while interpreting their dielectric response. Thus, to ascertain the number of relaxations in the oil samples, Cole-Cole plots between ε_r' (x-axis) and ε_r'' (y-axis) are plotted from the values obtained from the FDS measurement. Figure 2.8 shows the presence of more than one semicircle in all oil samples, each corresponding to a dominant relaxation mechanism in a specific frequency range [107]. Notably, the plots exhibit a combination of two or more semicircles in the lower frequency region, with overlapping semicircles distorting the Cole–Cole plot shape. This distortion occurs when multiple relaxation mechanisms coexist with comparable time constants.

The presence of multiple relaxation times in the Cole-Cole plots indicates that different

polarization mechanisms contribute to the dielectric response of the oil samples. One key mechanism is dipolar relaxation, which occurs due to the reorientation of polar molecules under an applied electric field. This effect is more pronounced in natural ester oils like FR3, which contain a higher concentration of polar contaminants. Another significant mechanism is interfacial (Maxwell-Wagner) relaxation, where charge accumulation at the interfaces of different dielectric phases, such as oil impurities or oxidation by products, leads to additional relaxation processes, typically dominating at intermediate frequencies [186]. At lower frequencies, ion conduction and space charge effects become significant, as indicated by the tail in the Cole-Cole plot, which corresponds to DC conductivity. This is primarily due to the migration of free charge carriers, which increases with oil ageing as more degradation products and contaminants accumulate. The deviation from a perfect semicircle in real dielectric materials, as predicted by the Debye model, is attributed to the broad distribution of relaxation times caused by complex intermolecular interactions and impurities in the oil. The presence of multiple semicircles in the Cole-Cole plot suggests that the dielectric response is governed by a spectrum of relaxation behaviours rather than a single, well-defined relaxation time.

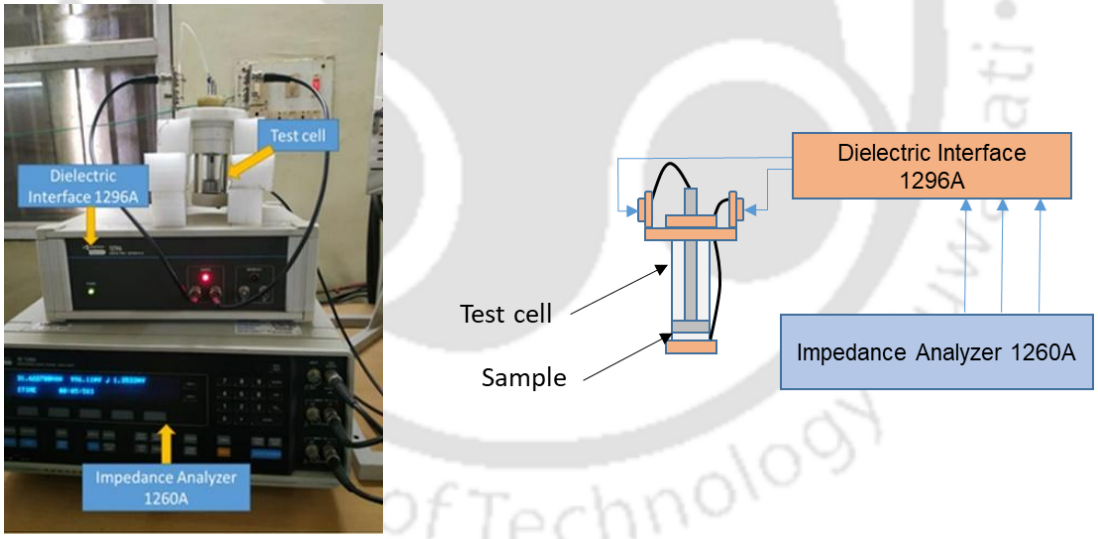

Fig. 2.7. FDS setup with dielectric interface and test cell.

This data is then used to obtain the DC conductivity values of the oil samples. To ascertain the number of relaxations in oil samples, Cole–Cole plots between ε′ (x-axis) and ε″ (y-axis) are constructed based on FDS measurements.

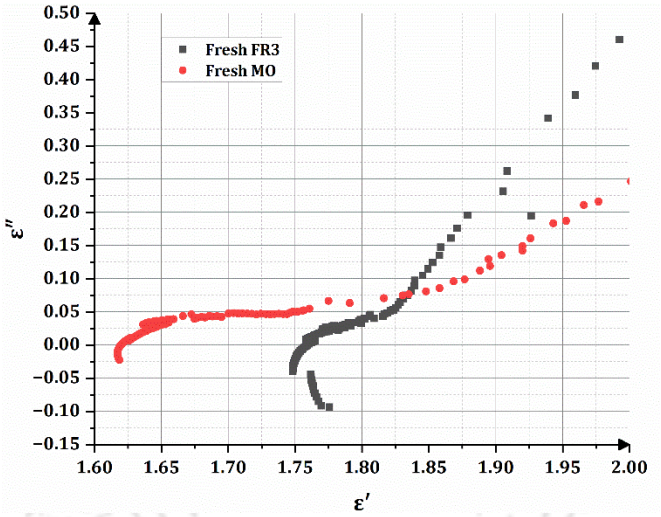

(a)

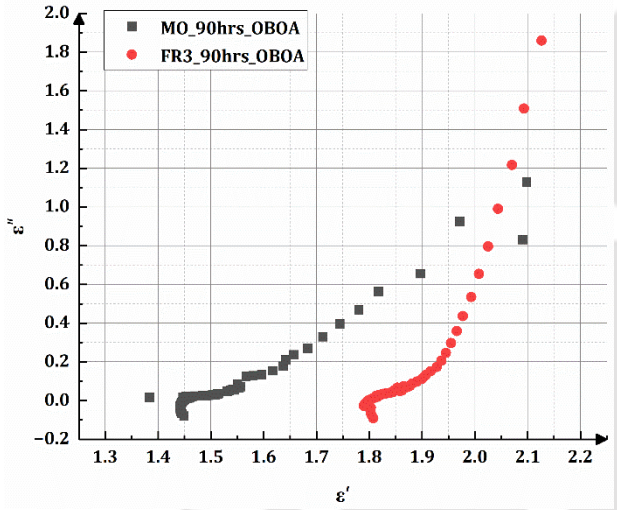

(b)

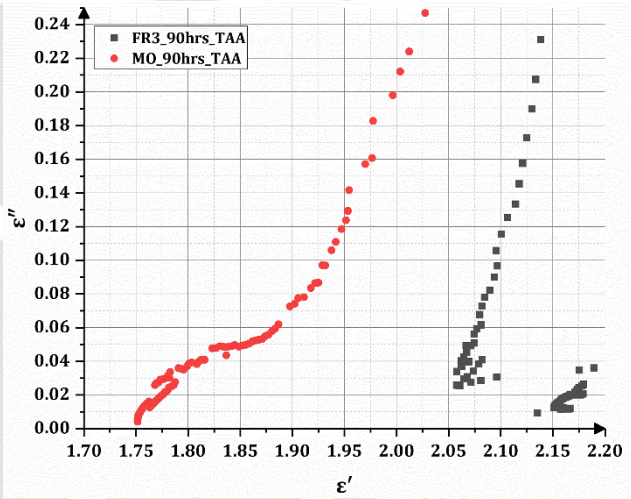

(c)

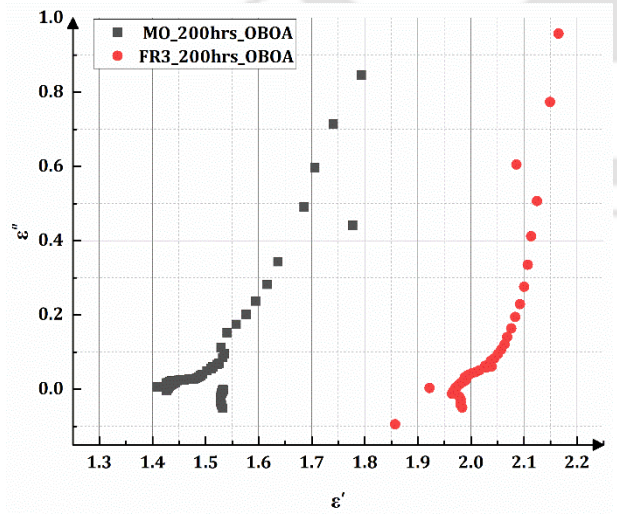

(d)

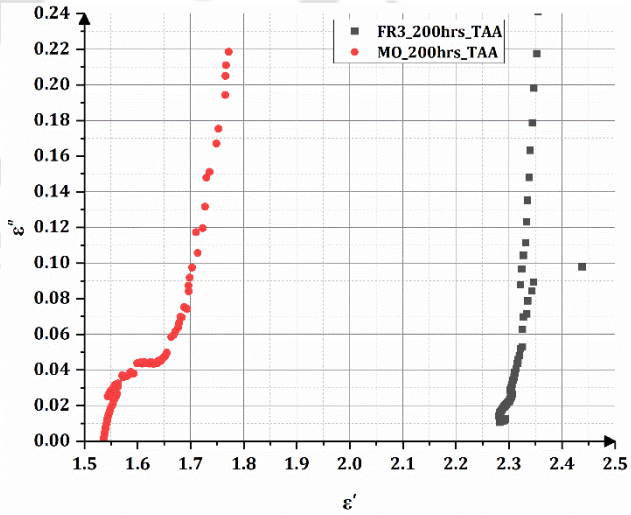

(e)

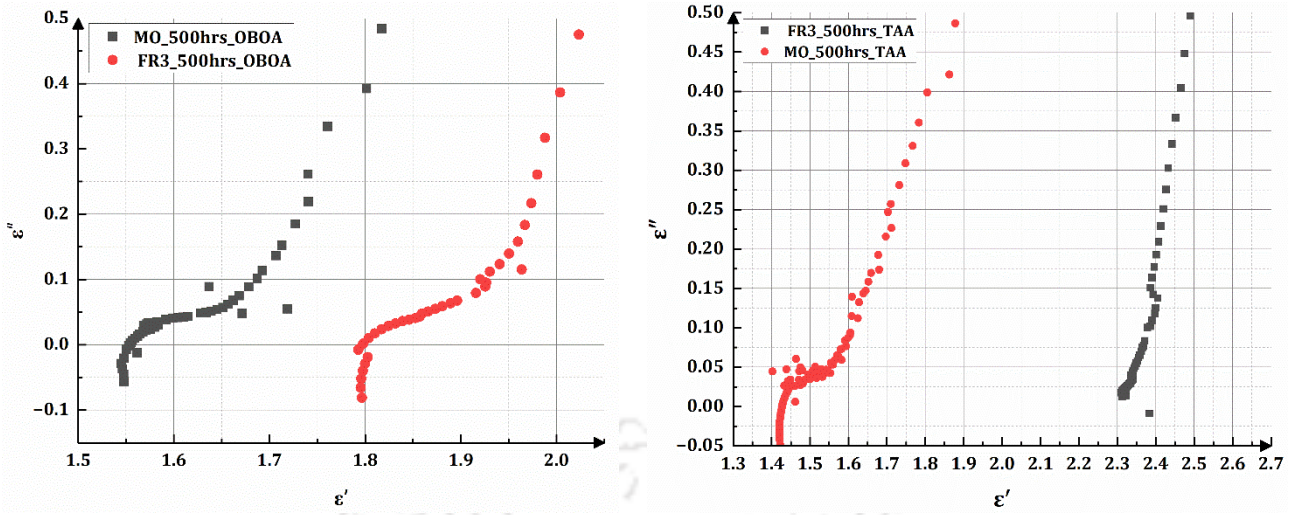

(f) **(g)**

Fig. 2.8. Cole Cole plots

Figure 2.8 displays Cole-Cole plots showcasing the behaviour of Fresh and aged MO and FR3 samples. The tail in the lower frequency region corresponds to DC conductivity. Considering all these factors, the Cole–Cole double relaxation model is employed for in-depth analysis of the oil samples and comparing DC conductivity. The model parameters such as (A, n, $\Delta\varepsilon_1$, τ_1, α_1, $\Delta\varepsilon_2$, τ_2, α_2, σ_{dc}) [98, 99] are obtained by curve fitting of oil sample data of ε' and ε'' with frequency by employing equation (2.1) and (2.2).

$$\varepsilon' = \varepsilon_\infty + \mathrm{A}\omega^{-\mathrm{n}} + \mathrm{Re}\left[\frac{\Delta\varepsilon_1}{1+\left(\mathrm{j}\omega\tau_1\right)^{(1-\alpha_1)}} + \frac{\Delta\varepsilon_2}{1+\left(\mathrm{j}\omega\tau_2\right)^{(1-\alpha_2)}}\right] \tag{2.1}$$

$$\varepsilon'' = \frac{\sigma_{\mathrm{dc}}}{\varepsilon_0\omega} + \mathrm{A}\omega^{-\mathrm{n}}\cot\left[(1-\mathrm{n})\frac{\pi}{2}\right] + \mathrm{Im}\left[\frac{\Delta\varepsilon_1}{1+\left(\mathrm{j}\omega\tau_1\right)^{(1-\alpha_1)}} + \frac{\Delta\varepsilon_2}{1+\left(\mathrm{j}\omega\tau_2\right)^{(1-\alpha_2)}}\right] \tag{2.2}$$

The observed decrease in permittivity at low frequencies is captured by $A\omega^{-n}$ expression, reflecting an inverse power dependence on frequency. Concurrently, the remainder of the data is modeled using the Cole–Cole expression with two relaxation times. The parameters $\Delta\varepsilon_1$, τ_1, and α_1 characterize the relaxation amplitude, time constant, and spread of the first relaxation, while $\Delta\varepsilon_2$, τ_2, and α_2 represent the corresponding attributes for the second relaxation. Additionally, σ_{dc} accounts for the DC conductivity within the system [98, 99]. In this study, emphasis is placed on DC conductivity, and thus, only the imaginary part of

complex permittivity with respect to the frequency is considered. Equation (2.2) is employed to derive this parameter, a topic that will be elaborated upon in chapter 3 of this thesis.

2.5. Statistical analysis of DCBDV experimental results

To assess the repeatability of the DCBDV experimental data and determine whether they follow a specific distribution, statistical hypothesis testing is performed using normal, two parameter and three parameter Weibull distribution analysis. This analysis involves plotting the statistical distribution graphs generated using the Minitab data analysis tool. The conformity of DCBDV experimental data to a distribution is assessed through the Goodness of fit and Anderson Darling test [108]. In determining the distribution followed by DCBDV data, the p-value is computed. If the calculated p-value exceeds the predetermined significance level (α=0.05), the null hypothesis is accepted, signifying that the sample data adheres to a statistical distribution [109, 110]. An essential observation is that the Weibull distributions utilized in this study are generally continuous function distributions. Nevertheless, the nature of the data for DCBDV is not definitively established as continuous functions. In addressing this uncertainty, implementing these distributions to the data becomes a consideration. T. Nakagawa and S. Osaki conducted a study [111] providing mathematical explanations that support the use of discrete Weibull distribution as a viable approximation for failure analysis. This study suggests that even if the data is not distinctly categorized as continuous or discrete, both Weibull distributions can be applied effectively for analyzing the failure of the samples. All the parameters used to test the experimental data using statistical analysis are briefly discussed below.

2.5.1. Conformity of DCBDV experimental data to a distribution through Anderson-Darling test

The Anderson-Darling (AD) test is used to figure out the p-value and AD-value [112] and see how well a set of data fits the distribution. In this statistical study, a significance level test at the 5% (α= 0.05) level is looked at. If the p-value is higher than the significance threshold (α= 0.05), then the null hypothesis is accepted. If the p-value is lower than the significance threshold, then the null hypothesis is rejected. This method uses an AD-value to figure out if a random sample, x_1, x_2..., x_n, comes from a certain distribution. The AD-value was found by using the following equation (2.3)

$$AD = -N - \frac{1}{N}\sum_{i=1}^{n}(2i-1)\left[\ln F(X_i) + \ln\left(1 - F(X_{n-i+1})\right)\right] \quad (2.3)$$

where N is the sample size, X_i denotes the data values and $F(X)$ is the cumulative distribution function for any specified distribution. The alternate hypothesis (H_A) represents the data that does not follow a specified distribution and null hypothesis (H_O) represents the data that follows a specified distribution for the AD test.

2.5.2. Goodness of fit

The values of the correlation coefficient (ρ) show how closely a set of data follows a distribution and when the model fits close to the dataset, ρ is 1. The ρ values for each distribution are shown given in chapter 3 for positive and negative polarity datasets respectively. The coefficient is given by:

$$\rho = \frac{\sum_{i=1}^{n}\left(x_i - \bar{x}\right)\left(y_i - \bar{y}\right)}{(n-1)S_x S_y} \quad (2.4)$$

where, ρ is correlation coefficient, $\bar{x}$ is the sample mean for the first variable x_i, S_x is the sample standard deviation for the first variable, $\bar{y}$ is the sample mean for the second variable y_i, S_y is the sample standard deviation for the second variable, n is the number of rows with no missing data for the pair of variables.

2.5.3. Normal distribution

The normal distribution is calculated using equation (2.5).

$$f(x) = \frac{1}{\sigma\sqrt{2\pi}} e^{\frac{-(x-\mu)^2}{2\sigma^2}} \quad (2.5)$$

where $f(x)$ represents probability, x is value of the data, μ represents mean, σ represents standard deviation and σ^2 represents variance.

2.5.4. Skewness and kurtosis

The skewness and kurtosis data also govern whether a distribution data set is normal. In a perfectly normal distribution, the values of skew and kurtosis are zero. These values specify the deviance from normality. If the skewness value is positive, it is called positive skewed

and it indicates that the values of the distribution are grouped at the lower end. Similarly, if the skewness value is negative, it is called negatively skewed and it indicates that the mean values of the distribution are grouped at the higher end. The skewness (*S*) is given as equation (2.6),

$$S = \frac{N}{(N-1)(N-2)} \sum_{i=1}^{N} \frac{(x_i - \bar{x})}{s^3} \tag{2.6}$$

where N is the sample size, x_i is the i^{th} value of the dataset, $\bar{x}$ is the average and s is the sample standard deviation.

The kurtosis value signifies the degree to which the values of the dataset cluster at the tails or at the peak of a distribution. The positive kurtosis signifies that the distribution has a sharper peak and heavier tails compared to a perfectly normal distribution. Whereas, distributions having negative kurtosis means that the distributions have a flatter peak and thinner tails compared to a perfectly normal distribution. The kurtosis (*K*) is given as equation (2.7),

$$K = \left\{ \frac{N(N+1)}{(N-1)(N-2)(N-3)} \sum_{i=1}^{N} \frac{(x_i - \bar{x})^4}{s^4} \right\} - \frac{3(N-1)^2}{(N-2)(N-3)} \tag{2.7}$$

where N is the sample size, x_i is the i^{th} value of the dataset, $\bar{x}$ is the average and s is the sample standard deviation.

2.5.5. Two parameter and three parameter Weibull distribution

To understand the behaviour of the breakdown voltages, both 2- and 3-parameter Weibull statistical analyses are considered. Weibull statistical analysis is a highly effective tool for determining the probability of failure for all the oil samples. Equation 2.8 shows the Weibull distribution with two parameters and a 95% confidence interval.

$$F(x:\alpha,\beta) = 1 - \exp\left(-\left(\frac{x}{\alpha} \right)^{\beta} \right); x > 0 \tag{2.8}$$

where x represents the DCBDV, $F(x)$ represents the cumulative density function, α represents the scale parameter, and β represents the shape parameter.

The 3-parameter Weibull distribution with 95% confidence interval as given in equation 2.9 [113] is also applied to DCBDV dataset by adding the threshold parameter to 2-

parameter Weibull distribution to analyze the breakdown characteristics of fresh and aged MO and FR3.

$$F\left(x:\alpha,\beta,\gamma\right)=1-\exp\left(-\left(\frac{x-\gamma}{\alpha}\right)^{\beta}\right);x\geq\gamma \tag{2.9}$$

Where *F(x)* indicates the proportion of specimens initially tested which will fail by time *x* (voltage is applied at t=0). x is the random variable, usually time to breakdown or the electric field required to puncture the dielectric where the electric field increases linearly with time. The scale parameter (α) represents the time required for reaching 63.2 percentage of the tested units to fail. The shape parameter (β), is a measure of dispersion of the failure times from $t=\alpha$ or defines the failure mechanism and data dispersion. The parameter γ indicated the time from voltage application in which the failure of any unit is not possible or can also be written as the threshold parameter (γ) denotes the minimum possible breakdown voltage, below which failure is inevitable. The units of α and γ are time (or electric field when this is the random variable), while β is dimensionless [185]. These parameters collectively help assess material reliability and performance in high-voltage applications.

2.6. Experimental Results of DC Breakdown Voltage of Fresh and Oxidatively Aged Samples

Figure .2.9 and Figure. 2.10 represent the positive and negative polarity DCBDV results obtained experimentally from four series of six consecutive measurements. Figure .2.11 depicts all the mean DC breakdown voltages for several oil samples with error bars. From these data, it is evident that the negative DCBDV of all fresh and aged oils of both MO and FR3 is greater than the positive DCBDV except for cases of fresh FR3, FR3@90 hrs and FR3 @200 hrs does not follow this trend of negative DCBDV greater than positive DCBDV. Another observation is there is a polarity difference in a homogeneous (symmetric) field situation and seems to be more for mineral oil than FR3. This is because MO exhibits a larger polarity difference due to its non-polar nature and ageing-induced effects. Under negative polarity, oxidation byproducts such as acids and sludge form an insulating layer on the cathode, hindering electron injection and increasing negative DCBDV. Additionally, the absence of polar molecules weakens charge stabilization, amplifying asymmetry in electron and ion transport. Ageing introduces ionic impurities that enhance leakage currents under positive polarity, lowering positive DCBDV. In contrast, FR3 shows a smaller polarity

difference due to its polar molecular structure, which enables dipole alignment, stabilizing the electric field. In solid insulation, such as pressboards, polarity effects are negligible due to the absence of interfacial ageing layers. Charge transport relies on bulk conduction, ensuring symmetric breakdown behaviour under both polarities, irrespective of immersion in MO or FR3.

The positive mean DCBDV for fresh MO is 27.01 kV, whereas for fresh FR3 it is 38.06 kV at a 1mm gap. It represents an increase of 29.03% in DC breakdown voltage from standard MO to FR3 (NEO) for the same 1mm gap length. Similarly, the negative mean DCBDV for fresh MO and FR3 is -31.82 kV and -33.31 kV, respectively. There is no significant difference between BDV of MO and FR3, as the negative mean BDV of FR3 is only 4% more than that of MO for negative polarity. Consequently, at short gaps (1mm), the BDV is closely correlated with the initial voltage of the streamer, and these voltages for various insulating oils are similar [114]. According to [71], NEO has a faster streamer velocity than MO and a shorter streamer stopping length, which might be a significant reason why NEO DCBDV is 4% higher than BDV of MO at this gap distance. The results in [26] demonstrate a similar pattern in experimental results at a 1mm gap for negative DC polarity, supporting the current study. As these samples undergo oxidative aging, the positive mean DCBDV decreases drastically by 34.3%, 35.6%, and 49.34% for MO@90hrs, 200hrs, and 500hrs, with respect to fresh MO.

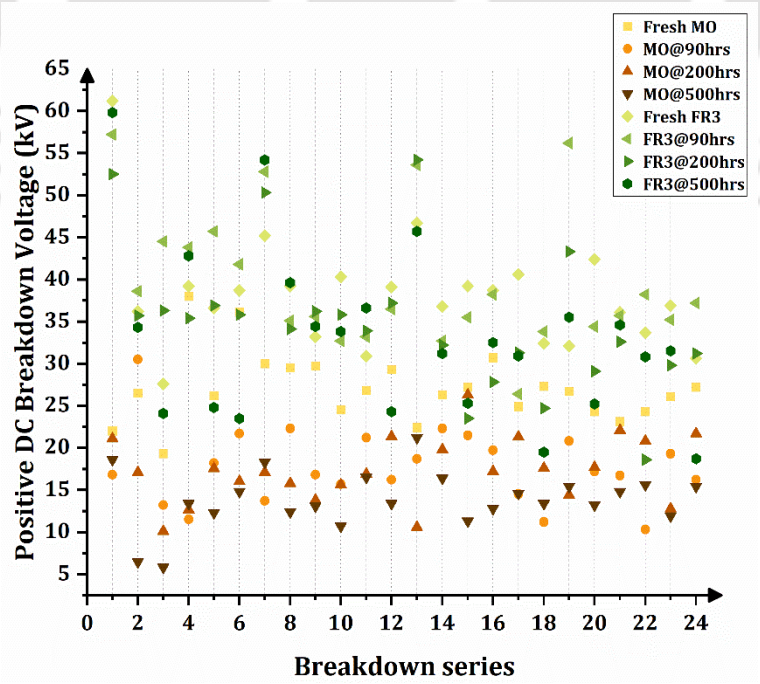

Fig. 2.9. DCBDV of fresh and oxidatively aged samples for positive polarity with breakdown series

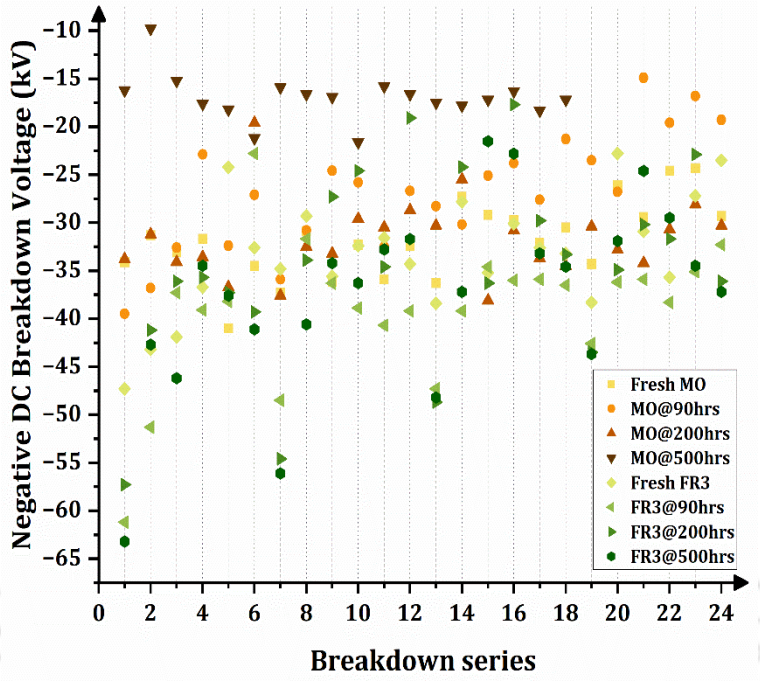

Fig. 2.10. DCBDV of fresh and oxidatively aged samples for negative polarity with breakdown series

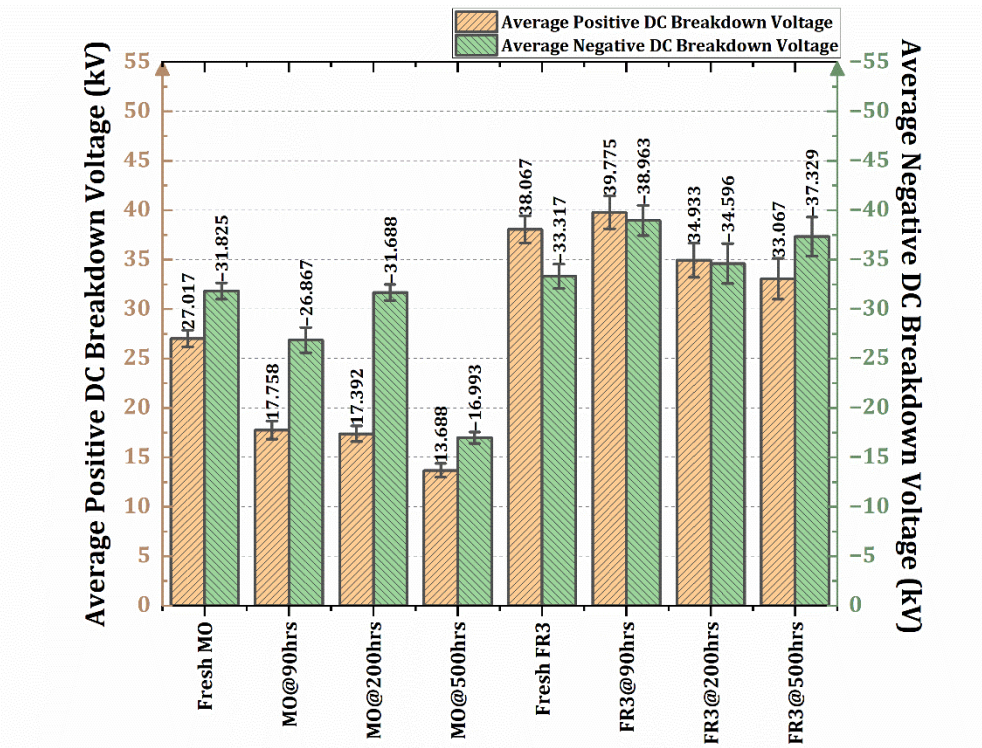

Fig. 2.11. Average positive and negative DCBDV for fresh and oxidatively aged oils

For FR3, as ageing time increases, the mean DCBDV increases by 4.47 % for FR3@90hrs and decreases by 8.24 %, 13.13 % for FR3@200hrs and 500hrs as compared with fresh FR3.

Negative mean DCBDV experimental results of oxidatively aged oils suggest that the dielectric strength of MO decreases by 22.8%, 9%, and 51.2% as the aging period increases from MO@90hrs, 200hrs and 500hrs, compared to fresh MO. Similarly, as the ageing time for FR3 increases, the negative DCBDV increased at a very low rate of 16.9%, 4.0%, and 12.0% for FR3@90hrs, 200hrs and 500hrs, with respect to fresh FR3. The increase in negative DC breakdown voltage (DCBDV) with ageing, as shown in Fig. 2.11, can be attributed to the formation of ageing by-products such as polar compounds, moisture, and solid particles. These by-products act as electron traps, reducing the mobility of free electrons and inhibiting the formation of electron avalanches. As a result, a higher electric field is required to initiate breakdown, leading to an increase in negative DCBDV.

2.6.1. Statistical analysis of DCBDV experimental results

2.6.1.1. Normal distribution of experimental DCBDV results

Figure. 2.12a and Figure. 2.12b illustrate the cumulative probabilities of positive and negative DCBDV results for each of the eight oil samples.

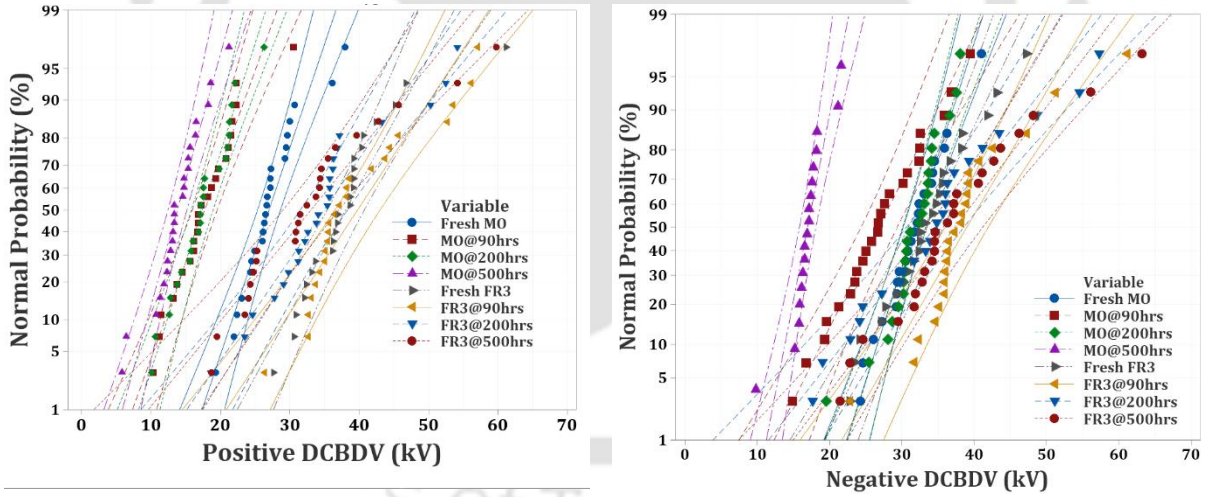

(a) (b)

Fig. 2.12. Normal probability plot for oxidatively aged samples for (a) positive DCBDV results; (b) negative DCBDV results

The reference points to which the values should be close are the straight lines. The proximity of the predicted values and reference lines on the probability plot implies that most of the frequency distributions of DCBDV data are normal. Since most of p-values are greater than the 0.05 significance level, the data cannot be rejected for the null hypothesis therefore it

is concluded that most of the dataset follows a normal distribution. However, some samples, notably fresh FR3, FR3@90, and FR3@200, do not adhere to the normal distribution for positive DCBDV. Similarly, the p value for negative DCBDV does not correspond to MO@500 and FR3@90hrs. Table 2.3 shows the conformity of the experimental data to normal distribution. Table 2.4 lists the probabilities of the occurrence of DCBDV at 5%, 10%, and 50%. To verify the compliance of DCBDV data with the normal distribution frequency, the skewness and kurtosis values are computed from histograms and are mentioned in Table 2.5.

Table 2.3: Conformity to normal distribution of average DCBDV for fresh and oxidatively aged samples

Oil Samples	DCBDV (*+ve*)			DCBDV (*- ve*)		
	p-value	AD-value	Conformity to normal distribution	p-value	AD-value	Conformity to normal distribution
Fresh MO	0.081	1.2	Confirmed	0.947	0.667	Confirmed
MO@90	0.524	0.851	Confirmed	0.981	0.637	Confirmed
MO@200	0.532	0.809	Confirmed	0.118	1.046	Confirmed
MO@500	0.189	1.007	Confirmed	0.007	1.661	Not confirmed
Fresh FR3	0.021	1.413	Not confirmed	0.867	0.719	Confirmed
FR3@90	< 0.005	1.821	Not confirmed	<0.005	1.830	Not confirmed
FR3@200	0.021	1.416	Not confirmed	0.335	0.925	Confirmed
FR3@500	0.071	1.196	Confirmed	0.147	1.082	Confirmed

From the skewness values it is noticed that the distribution of DCBDV data in both positive and negative polarities is more or less asymmetrical. The DCBDV is annotated in the Tables 2.3, 2.4, 2.5, 2.8 and 2.9 using the symbol (*+ve*) for positive polarity and (*-ve*) for negative polarity. In case of positive DCBDV data the skewness is positive in all the cases except for MO@500hrs and in case of negative DCBDV data the skewness is positive in all the cases except for MO@200 and 500 hrs. In these three cases the skewness is negative where the data is towards the left side of the mean value [110]. Similarly, in case of kurtosis the values indicate that almost all the values are lower than 3 except for the value of FR3 fresh oil in positive DCBDV data and value of MO@500hrs in negative DCBDV data. According to p-value, skewness, and kurtosis values, there are some deviations from normal distribution in the experimental data. In order to validate the data further, the Weibull distribution is employed for analysis in the following section.

Table 2.4: Failure probabilities of normal distribution for fresh and oxidatively aged samples

Oil Samples	DCBDV (*+ve*)(kV)	DCBDV (*-ve*)(kV)

	5%	10%	50%	5%	10%	50%
Fresh MO	20.181	21.6908	27.0167	24.876	26.411	31.825
MO@90	10.2817	11.9330	17.7583	16.143	18.512	26.866
MO@200	10.7091	12.1851	17.3917	25.225	26.652	31.687
MO@500	8.1196	9.379	13.821	13.121	13.976	16.992
Fresh FR3	27.4494	29.7944	38.0667	22.993	25.273	33.316
FR3@90	26.612	21.519	39.775	27.128	29.742	38.962
FR3@200	20.937	24.028	34.933	17.888	21.578	34.595
FR3@500	16.469	20.134	33.0667	21.296	24.837	37.329

Table 2.5: Statistical parameters of normal distribution for fresh and oxidatively aged samples

Oil Samples	Skewness		Kurtosis		Standard Deviation	
	+ve	*-ve*	*+ve*	*-ve*	*+ve*	*-ve*
Fresh MO	0.92812	0.0574	1.72531	0.0362	4.137	4.061
MO@90	0.68667	0.0976	1.54747	-0.324	4.470	6.241
MO@200	0.099899	-1.099	-0.0845	2.8504	3.929	3.940
MO@500	-0.39208	-0.92	1.27961	4.383	3.409	2.454
Fresh FR3	1.71881	0.274	5.35704	0.185	6.712	6.049
FR3@90	0.949515	1.064	0.1355	3.159	8.123	7.425
FR3@200	0.70318	0.527	0.89833	0.437	8.485	9.895
FR3@500	1.0494	0.863	1.28034	1.401	10.062	9.626

2.6.1.2. Two parameter Weibull distribution of experimental DCBDV results

Weibull statistical analysis is also used to understand the change in the failure of breakdown voltages over time. Figure. 2.13a and Figure. 2.13b show the DCBDV data for fresh and aged MO and NEO (FR3) for both positive and negative polarities using 2-parameter Weibull model [113]. Equation 2.10 shows the Weibull distribution with two parameters and a 95% confidence interval.

$$F\left(x:\alpha,\beta\right)=1-\exp\left(-\left(\frac{x}{\alpha}\right)^{\beta}\right);x>0 \tag{2.10}$$

where x represents the DCBDV, $F(x)$ represents the cumulative density function, α represents the scale parameter, and β represents the shape parameter. The hypothesis test revealed that the p-values are more than 0.05, indicating that only MO@90, 200 and 500 hrs data adhere to the 2-parameter Weibull distribution; all other samples are inconclusive for DCBDV. In the case of a negative DCBDV test, only MO@500 and FR3@90 are not confirmed. Similarly, for aged FR3 when compared to fresh FR3 at 50% failure probability the values are decreased by 4.3%, 8.3% and 13.8%; at 10% failure probability by 0.09%, 19.8%, and 29.7%; and at 5% failure probability by 1.7%, 23.8%, and 34.7%, respectively for 90, 200 and 500 hours.

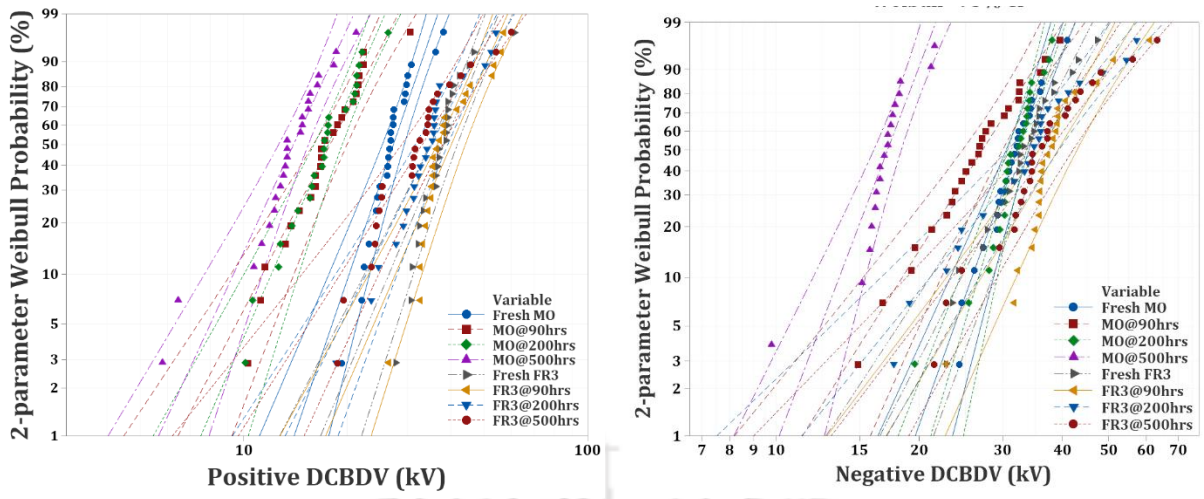

(a) (b)

Fig. 2.13. Two parameter Weibull distribution of oxidatively aged samples for (a) positive DCBDV results; (b) negative DCBDV results

At 50% failure probability for negative DCBDV the values are increased by 16.6%, 3%, 11.4%; at 10% failure probability the value is increased by 18.5% for 90 hours, decreased by 13.12% for 200 hours, and is increased by 0.6% for 500 hours; and at 5% failure probability the value is increased by 19.2% for 90 hours and are decreased by 18.6%, 3% with respect to aged FR3 for 200 and 500 hours. As the number of unconfirmed cases in 2-parameter distribution is high in both positive and negative polarities compared to a normal distribution, a 3-parameter Weibull analysis is performed on the data in the next section.

2.6.1.3. Three parameter Weibull distribution of experimental DCBDV results

The 3-parameter Weibull distribution with 95% confidence interval as given in equation 2.11 [113] is also applied to DCBDV dataset by adding the threshold parameter to 2-parameter Weibull distribution to analyze the breakdown characteristics of fresh and aged MO and FR3. The results obtained using 3-parameter Weibull distribution are depicted in Figure. 2.14a and Figure. 2.14b. The failure probabilities and conformity to distribution of the dataset are provided in Table 2.6, Table 2.7, Table 2.8 and Table 2.9.

$$F\left(x:\alpha,\beta,\gamma\right)=1-\exp\left(-\left(\frac{x-\gamma}{\alpha}\right)^{\beta}\right);x\geq\gamma \tag{2.11}$$

Where x represents DCBDV, $F(x)$ represents the cumulative density function, α represents the scale parameter, β represents the shape parameter, and γ represents the threshold parameter. The hypothesis test revealed that the p-values are greater than 0.05, therefore all

oil samples, with the exception of FR3@90 and FR3@200 for positive polarity and MO@500 and FR3@90 for negative polarity, adhere to the 3-parameter Weibull distribution.

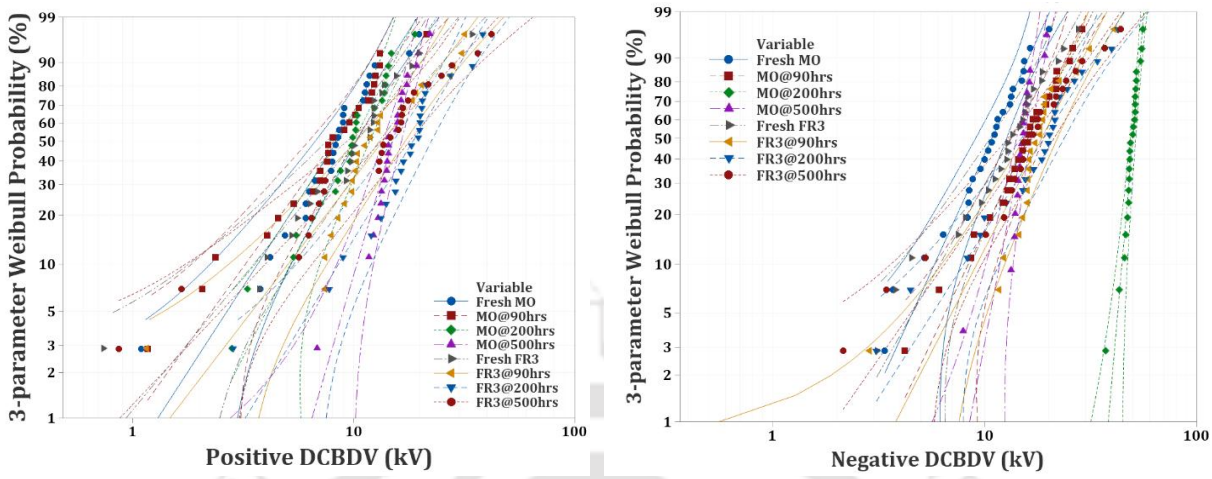

(a) (b)

Fig. 2.14. Three parameter Weibull distribution of oxidatively ages samples for (a) positive DCBDV results; (b) negative DCBDV results

Based on the figures and tables mentioned above, it is evident that the DCBDV decreases for aged MO when compared to fresh MO at 50% failure probability by 35%, 35.3%, and 47.2%; at 10% failure probability by 44.7%, 44.6%, and 58.5%, and at 5% failure probability by 47.19%, 48%, and 64.6%, respectively for 90, 200 and 500 hours. Consequently, at 50%, failure probability for negative DCBDV the value is decreased by 15.7% at 90 hours, increased by 1.15% at 200 hours, and is decreased by 45.6% at 500 hours; at 10% failure probability the values are decreased by 29.9%, 0.6%, 47.2%; and at 5% failure probability the values are decreased by 34.3%, 3.8%, 50.3% for 90, 200 and 500 hours.

Similarly, the DCBDV decreases for aged FR3 compared to fresh FR3; at 50% failure probability the value is increased by 4% for 90 hours and are decreased by 7.3% and 15.4% for 200 and 500 hours; at 10% failure probability the value is increased by 0.09% for 90 hours and are decreased by 20.6% and 29.5% for 200 and 500 hours, and at 5% failure probability the values are decreased by 1.4%, 25.7%, and 32.5%, respectively for 90, 200 and 500hrs. At 50% failure probability for negative DCBDV the values are increased by 17.7%, 2.6%, and 10.6%. At 10%, failure probabilities the value is increased by 18.1% for 90 hours, is reduced by 13.3% for 200 hours, and is increased by 0.5% for 500 hours. At 5% failure probability, the value increases by 14.29% for 90hrs and decreases by 17.89% and 1.8% for 200 and 500 hrs. respectively.

Table 2.6: Failure probabilities and goodness of fit data for DCBDV under positive polarity for fresh and oxidatively aged samples

Oil Samples	Failure probabilities of oil samples (kV)						Goodness of fit coefficients		
	2-parameter Weibull distribution			3-parameter Weibull distribution			Normal	2-parameter Weibull	3-parameter Weibull
	50%	10%	5%	50%	10%	5%	ρ	ρ	ρ
Fresh MO	27.313	21.8351	20.045	26.915	21.910	20.6615	0.958	0.949	0.974
MO@90	17.897	12.088	10.4057	17.479	12.1027	10.915	0.970	0.977	0.987
MO@200	17.567	12.122	10.5201	17.391	12.1205	10.749	0.986	0.986	0.988
MO@500	13.9204	8.954	7.5648	14.208	9.096	7.3092	0.970	0.956	0.970
Fresh FR3	38.439	30.297	27.663	37.534	30.523	29.022	0.917	0.920	0.975
FR3@90	40.1211	30.266	27.1760	39.169	30.5501	28.6029	0.939	0.914	0.947
FR3@200	35.2162	24.277	21.060	34.7907	24.2383	21.5537	0.956	0.963	0.970
FR3@500	33.114	21.297	17.991	31.7345	21.5144	19.6609	0.956	0.955	0.983

Table 2.7: Failure probabilities and goodness of fit data of DCBDV under negative polarity for fresh and oxidatively aged samples

Oil Samples	Failure probabilities of oil samples (kV)						Goodness of fit coefficients		
	2-parameter Weibull distribution			3-parameter Weibull distribution			Normal	2-parameter Weibull	3-parameter Weibull
	50%	10%	5%	50%	10%	5%	ρ	ρ	ρ
Fresh MO	32.1985	26.288	24.328	31.908	26.335	24.805	0.992	0.984	0.99
MO@90	27.133	18.466	15.941	26.864	18.467	16.297	0.996	0.994	0.996
MO@200	32.063	26.021	24.026	32.277	26.173	23.841	0.951	0.9560	0.973
MO@500	17.171	13.573	12.406	17.330	13.7	12.313	0.904	0.8950	0.915
Fresh FR3	33.711	25.2905	22.660	33.215	25.356	23.392	0.989	0.981	0.988
FR3@90	39.33	29.98	27.026	39.097	29.944	27.295	0.924	0.918	0.923
FR3@200	34.743	21.977	18.448	34.087	21.966	19.207	0.979	0.982	0.988
FR3@500	37.587	25.464	21.944	36.761	25.508	22.970	0.965	0.966	0.979

Table 2.8: Conformity to Weibull distribution of average positive DCBDV for fresh and oxidatively aged samples

Oil Samples	DCBDV (+ve)					
	2-parameter Weibull			3-parameter Weibull		
	p-value	AD-value	Conformity to Weibull	p-value	AD-value	Conformity to Weibull
Fresh MO	<0.010	2.260	Not confirmed	0.163	1.246	Confirmed
MO@90	>0.250	1.102	Confirmed	0.483	0.840	Confirmed
MO@200	>0.250	0.913	Confirmed	0.478	0.827	Confirmed
MO@500	0.217	1.067	Confirmed	0.157	1.137	Confirmed
Fresh FR3	<0.010	3.264	Not confirmed	0.122	1.222	Confirmed
FR3@90	<0.010	3.475	Not confirmed	0.034	1.807	Not confirmed
FR3@200	<0.010	1.956	Not confirmed	0.039	1.496	Not confirmed
FR3@500	0.047	1.741	Not confirmed	0.397	0.913	Confirmed

Table 2.9: Conformity to Weibull distribution of average negative DCBDV for fresh and oxidatively aged samples

Oil Samples	DCBDV (-ve)					
	2-parameter Weibull			3-parameter Weibull		
	p-value	AD-value	Conformity to Weibull	p-value	AD-value	Conformity to Weibull
Fresh MO	>0.250	0.871	Confirmed	>0.500	0.697	Confirmed
MO@90	>0.250	0.735	Confirmed	>0.500	0.650	Confirmed
MO@200	>0.250	0.977	Confirmed	0.222	1.011	Confirmed
MO@500	<0.010	1.806	Not confirmed	<0.005	2.206	Not confirmed
Fresh FR3	>0.250	0.980	Confirmed	>0.500	0.747	Confirmed
FR3@90	<0.010	2.926	Not confirmed	<0.005	2.377	Not confirmed
FR3@200	0.231	1.115	Confirmed	0.446	0.890	Confirmed
FR3@500	0.056	1.515	Confirmed	0.274	1.019	Confirmed

2.7. Experimental Results of DCBDV for Fresh and Thermally Aged Samples

Figures 2.15a and 2.15b depict the results obtained from experiments conducted under positive and negative polarity for DCBDV, involving four sets of six consecutive measurements. Figure 2.16 showcases the average DCBDV values for distinct oil samples, complemented by error bars. Notably, the negative DCBDV values of fresh and aged oils, specifically MO and FR3, exhibit higher magnitudes than the positive DCBDV values. MO registers an average positive DCBDV of 27.01 kV for fresh oils, while FR3 records 38.06 kV, both using a 1 mm electrode gap. The data showcases a remarkable increase of 29.03% in DCBDV when transitioning from MO to FR3 (NEO) while keeping the electrode gap consistent. Similarly, the average negative DCBDV values for fresh MO and FR3 are -31.825 kV and -33.31 kV, respectively. This demonstrates a minor difference of just 4.47% for the negative polarity. FR3 shows higher DCBDV in both polarities than in MO for fresh oils. Upon subjecting these samples to accelerated thermal ageing, the positive mean DCBDV experiences a drop of 38.59%, 23.96%, and 47.93% for MO aged at 90 hours, 200 hours, and 500 hours, compared to fresh MO. As ageing time increases, the mean DCBDV reduces by 20.67%, 22.48%, and 22.38% for FR3 aged at 90 hours, 200 hours, and 500 hours, compared to fresh FR3.The experimental results for the negative mean DCBDV of thermally accelerated aged oils indicate that the dielectric strength of MO decreases significantly as the ageing period increases. Specifically, for MO aged at 90 hours, 200 hours, and 500 hours, the negative DCBDV drops by 39.59%, 17.94%, and 61.90%, compared to fresh MO. In contrast, for FR3, the negative DCBDV decreases at a much lower rate as the ageing time increases. The reductions in the negative DCBDV for FR3 aged at 90 hours, 200 hours, and 500 hours are 8.68%, 7.07%, and 17.19%, compared to fresh FR3.

These results indicate that MO experiences a more significant reduction in dielectric strength with increasing ageing time compared to FR3, which shows a relatively slower decline in its DCBDV under similar thermal ageing conditions.

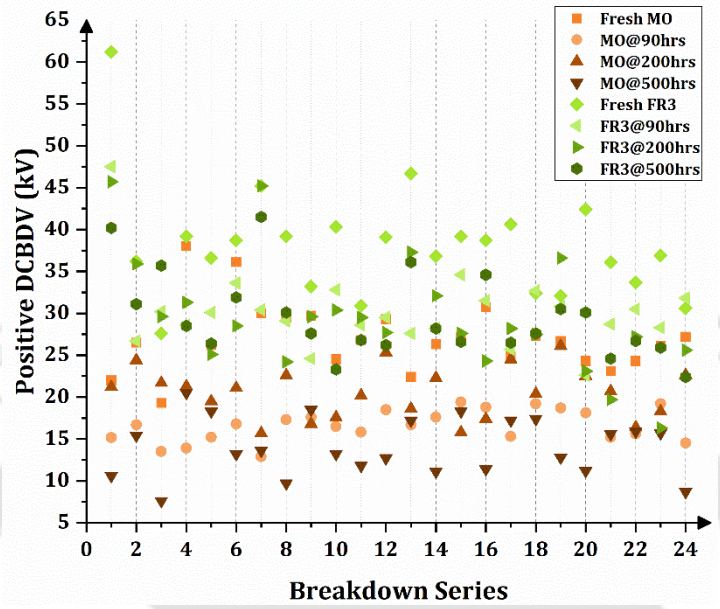

(a)

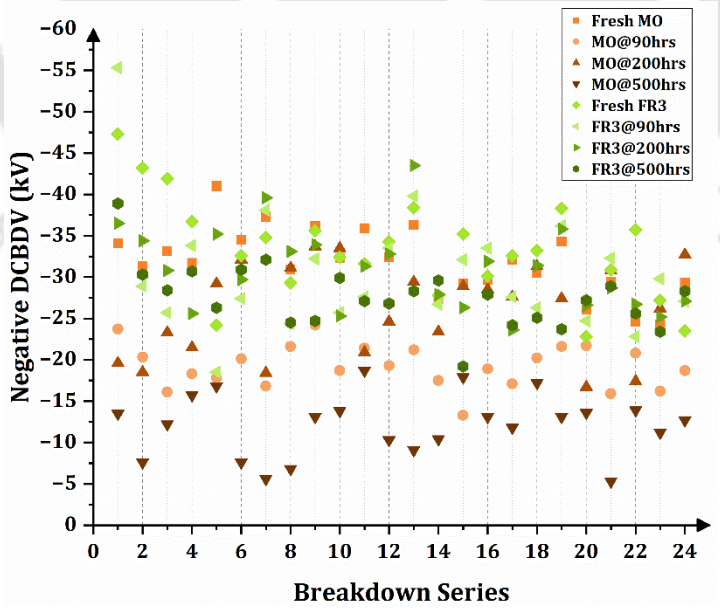

(b)

Fig. 2.15. DCBDV of fresh and thermally aged samples across breakdown series for (a) positive polarity (b) negative polarity

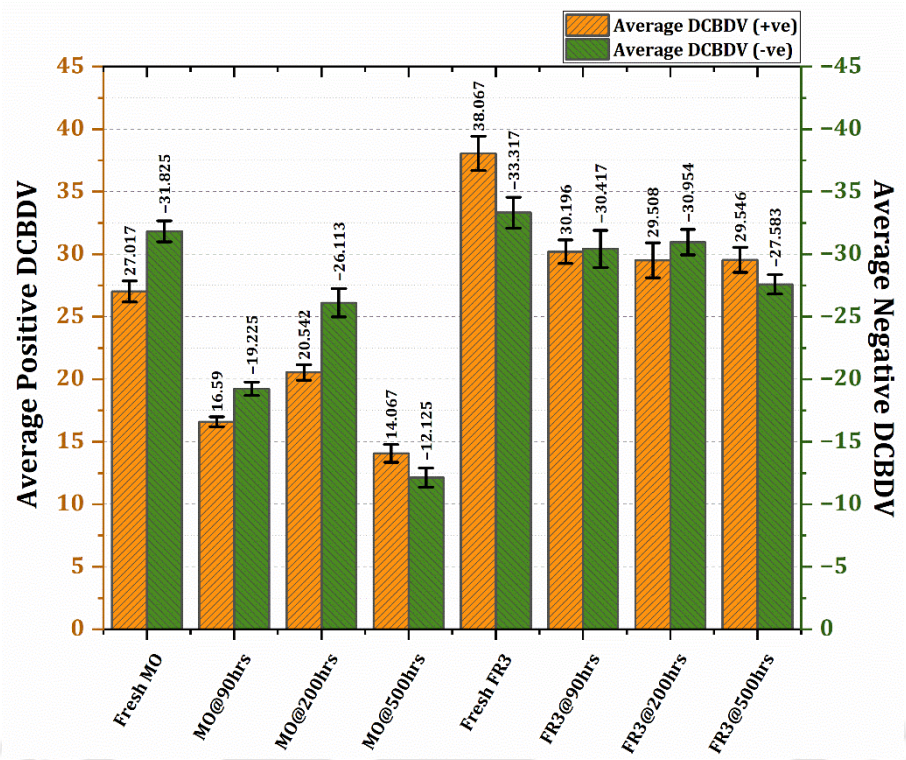

Fig. 2.16. Average DCBDV of fresh and thermally aged oil samples under positive and negative polarity with error bars

2.7.1. Statistical analysis of DCBDV experimental results

2.7.1.1. Fitting of experimental DCBDV results to a normal distribution

Figures 2.17a and 2.17b illustrate the cumulative probability of DCBDV results in positive and negative polarity for fresh and thermally aged oil samples. The statistical analysis using p-values at 0.05 significance level, reveals that for most of the dataset, the null hypothesis follows a normal distribution. Hence, most of the DCBDV data adheres to a normal distribution. However, some samples, specifically fresh FR3, FR3@ 90hrs and 500hrs, deviate from the normal distribution for positive DCBDV. Similarly, the data for FR3@90hrs does not align with the normal distribution for negative DCBDV. Table 2.10 provides detailed information on the conformity of the experimental data to the normal distribution which is calculated using equation (2.12)

$$f(x) = \frac{1}{\sigma\sqrt{2\pi}} e^{\frac{-(x-\mu)^2}{2\sigma^2}} \tag{2.12}$$

In probability theory, the function *f(x)* is commonly used to denote the probability associated with a specific value *x* of a given dataset. The symbol μ is conventionally employed to represent the mean of the dataset, while σ is used to denote the standard deviation. Additionally, the symbol σ^2 is utilized to indicate the variance of the dataset. Table 2.11 presents the probability associated with the incidence of DCBDV at 50%, 10%, and 5%. In order to assess the conformity of the DCBDV data to a normal distribution, the skewness and kurtosis values are computed based on the histograms and this is shown in Table 2.12. Upon examination of the skewness values, it can be observed that the distribution of DCBDV data exhibits a general lack of symmetry in both positive and negative polarities. Specifically, for positive DCBDV data, the skewness is positive, except for MO@90hrs and 500hrs. This indicates that the data tends to be skewed towards higher DCBDV values for most samples. The kurtosis values, on the other hand, help assess the sharpness of the peak in the distribution. For most samples, the kurtosis values are higher than 3, indicating a relatively higher peak or heavier tails than a normal distribution. Overall, the analysis of skewness and kurtosis values suggests that while the DCBDV data may not perfectly align with a normal distribution, it still provides valuable insights into the breakdown voltage characteristics of the oil samples under different conditions.

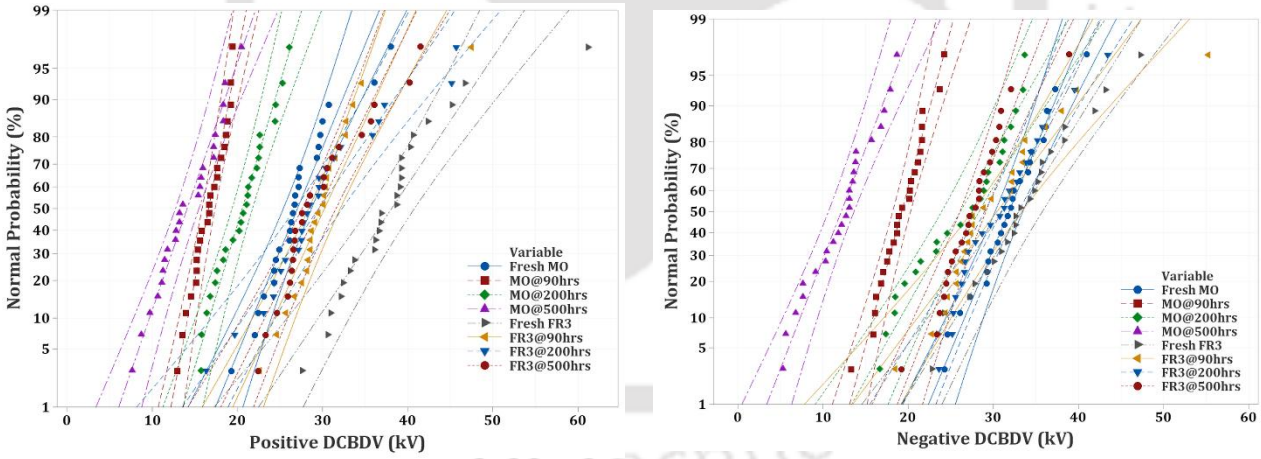

(a) (b)

Fig. 2.17: Normal probability plot for thermally aged samples for (a) positive DCBDV results; (b) negative DCBDV results

Regarding negative DCBDV data, positive skewness value is prevalent, except for instances such as MO@90hrs, 200 hours, and 500 hours, where negative skewness suggests data concentration towards the left of the mean [110]. Kurtosis values generally fall below 3,

except for FR3 fresh oil and FR3@90hrs in positive DCBDV data and FR3@90hrs in negative DCBDV data.

Table 2.10: Conformity of average DCBDV to normal distribution for fresh and thermally aged oil samples

Samples	Positive DCBDV			Negative DCBDV		
	AD-value	p-value	Conformity to Normal Distribution	AD-value	p-value	Conformity to Normal Distribution
Fresh FR3	0.871	0.021	NC	0.201	0.867	CNF
FR3@90h	1.214	<0.005	NC	0.878	0.021	NC
FR3@200h	0.683	0.065	CNF	0.339	0.47	CNF
FR3@500h	0.874	0.021	NC	0.39	0.356	CNF
Fresh MO	0.645	0.081	CNF	0.156	0.947	CNF
MO@90h	0.296	0.565	CNF	0.189	0.89	CNF
MO@200h	0.248	0.721	CNF	0.55	0.14	CNF
MO@500h	0.296	0.565	CNF	0.33	0.495	CNF

*** NC- Not Confirmed; CNF- Confirmed; h represents hours**

Table 2.11: Failure probabilities of oil samples obtained from normal distribution in (kV) for fresh and thermally aged oil samples

Samples	Positive DCBDV			Negative DCBDV		
	50%	10%	5%	50%	10%	5%
Fresh FR3	38.066	29.794	27.449	33.316	25.273	22.993
FR3@90h	30.195	24.715	23.161	30.416	21.413	18.861
FR3@200h	29.508	20.595	18.069	30.954	24.406	22.55
FR3@500h	29.545	23.193	21.392	27.583	22.662	21.267
Fresh MO	27.0167	21.690	20.181	31.825	26.411	24.876
MO@90h	16.59	14.066	13.35	19.225	15.733	14.743
MO@200h	20.541	16.543	15.41	26.112	18.923	16.884
MO@500h	14.066	9.474	8.172	12.125	7.139	5.725

Table 2.12: Statistical parameters of normal distribution for fresh and thermally aged oil samples

Samples	Statistical Parameters					
	Kurtosis		Skewness		SD	
	Positive DCBDV	Negative DCBDV	Positive DCBDV	Negative DCBDV	Positive DCBDV	Negative DCBDV
Fresh FR3	5.357	0.185	1.718	0.274	6.712	36.595
FR3@90h	8.266	5.034	2.176	1.715	4.630	53.154
FR3@200h	1.098	0.202	0.759	0.682	6.890	24.852
FR3@500h	0.558	2.697	1.0187	0.696	4.957	14.539
Fresh MO	1.725	0.0362	0.928	0.0574	4.137	16.491
MO@90h	-0.926	-0.134	-0.202	-0.148	1.904	6.877
MO@200h	-0.837	-1.24	0.0209	-0.327	3.006	30.139
MO@500h	-0.8877	-0.595	-0.0184	-0.176	3.451	14.133

***SD- standard Deviation**

The combination of skewness, p-values, and kurtosis reveals deviations from normality in the experimental results, indicating that while most data follow a normal distribution, some

variations are present. Using alternative statistical distributions can provide a more comprehensive understanding of the breakdown voltage characteristics and their conformity with different models. So, the Weibull distribution is employed for analysis to validate the data further.

2.7.1.2. Fitting of Experimental DCBDV Results to a 2-Parameter Weibull Distribution

Figures 2.18a and 2.18b illustrate the DCBDV data pertaining to the initial and aged states of MO and FR3 under both positive and negative polarities. This analysis employs a 2-parameter Weibull model. The Weibull distribution, characterized by two parameters and a 95% confidence interval, is defined by Equation 2.10. The hypothesis test results indicate that the p-values are greater than 0.05, suggesting that only the data for MO@90hrs, 200hrs, and 500hrs adhere to the 2-parameter Weibull distribution under positive polarity. For all other samples, the results are inconclusive for DCBDV.

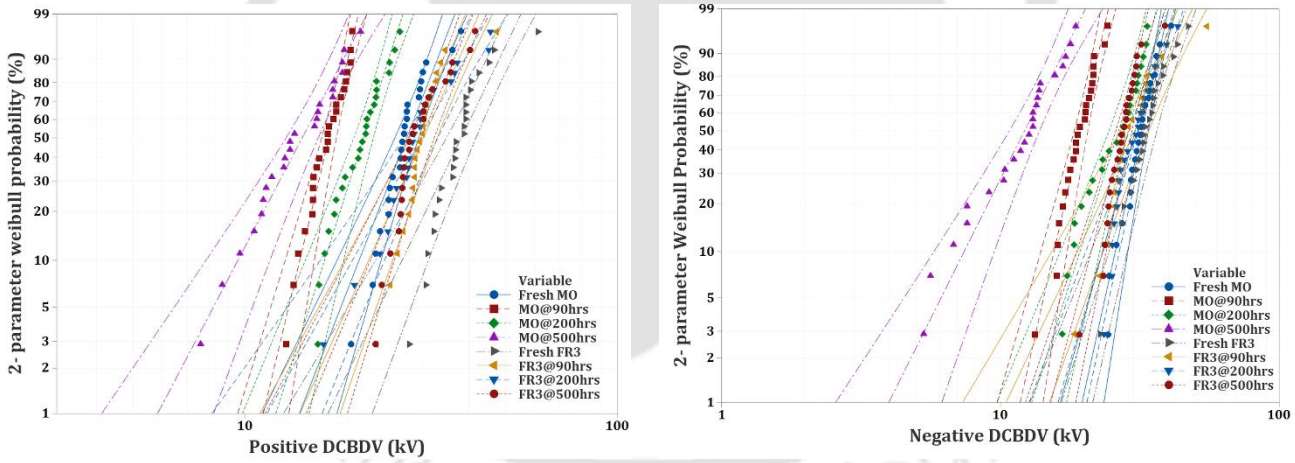

(a) **(b)**

Fig. 2.18. Two parameter Weibull distribution of thermally aged samples for (a) positive DCBDV results; (b) negative DCBDV results

Similarly, for negative DCBDV data, only FR3@90hrs and 500hrs do not conform to the 2-parameter Weibull distribution. Tables 2.13 and 2.14 present the failure probabilities at 50%, 10%, and 5% for the positive and negative polarities based on the 2-parameter Weibull distribution. Tables 2.15 and 2.16 provides details on the conformity of the experimental data to the 2-parameter Weibull distribution for positive and negative polarity. Since many cases

remain unconfirmed in the 2-parameter distribution for both positive and negative polarities, the subsequent section of the study employs a 3-parameter Weibull analysis on the data.

2.7.1.3. Fitting of Experimental DCBDV Results to a 3-Parameter Weibull Distribution

In addition to the 2-parameter Weibull, the 3-parameter Weibull distribution is applied to the DCBDV dataset by incorporating the threshold parameter as shown in equation 2.11. The results obtained using the 3-parameter Weibull distribution are represented in Figure 2.19a and Figure 2.19b. Tables 2.13, 2.14, 2.15 and 2.16 provide the failure probabilities and information on the conformity of the dataset to the distribution for both positive and negative polarities. The hypothesis test results suggest that the p-values, which are greater than 0.05, provide evidence supporting the conformity of all oil samples to the 3-parameter Weibull distribution. However, an exception is observed for FR3@90hrs under positive polarity. In contrast, the data from all cases exhibit conformity to the 3-parameter Weibull distribution when considering negative polarity.

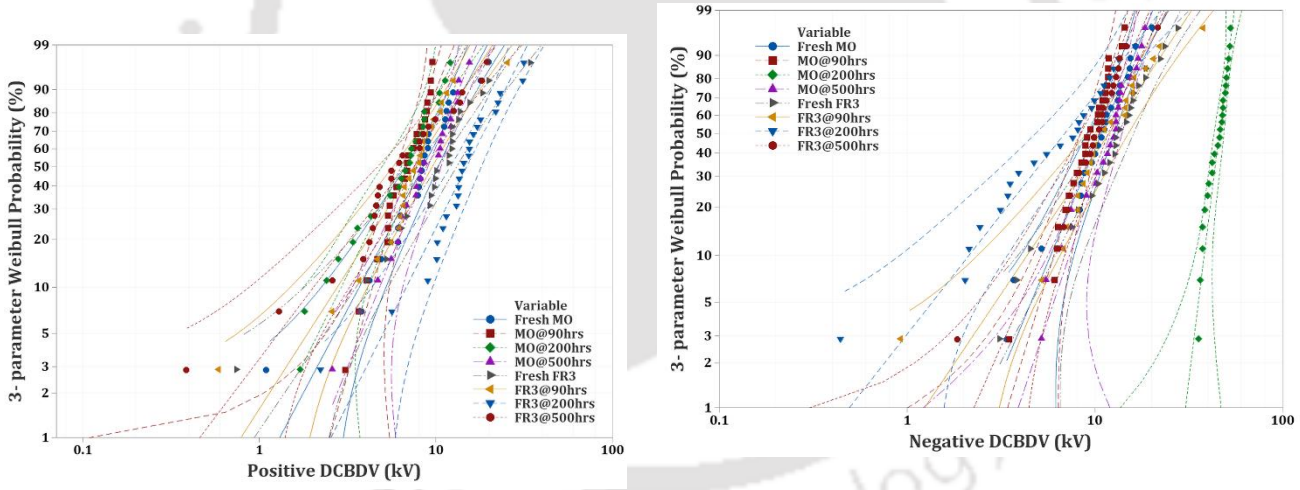

(a) (b)

Fig. 2.19. Three parameter Weibull distribution of thermally aged samples for (a) positive DCBDV results; (b) negative DCBDV results

Table 2.13: Goodness of fit coefficients and failure probabilities for DCBDV data under positive polarity for fresh and thermally aged oil samples

Samples	Failure Probabilities (kV)						Goodness of Fit coefficients for various distributions		
	2-parameter Weibull			3-parameter Weibull			Normal	2-parameter Weibull	3-parameter Weibull
	50%	10%	5%	50%	10%	5%	ρ	ρ	ρ

Fresh FR3	38.439	30.297	27.663	37.534	30.523	29.022	0.917	0.920	0.975
FR3@90h	30.478	25.007	23.187	29.946	25.097	23.959	0.881	0.893	0.956
FR3@200h	29.768	20.874	18.227	29.406	20.866	18.680	0.962	0.964	0.972
FR3@500h	29.843	23.621	21.603	28.901	23.969	23.062	0.953	0.922	0.981
Fresh MO	27.313	21.835	20.045	26.915	21.910	20.661	0.958	0.949	0.974
MO@90h	16.778	13.9599	13.012	16.595	13.977	13.295	0.986	0.986	0.992
MO@200h	20.786	16.501	15.107	20.311	16.582	15.788	0.989	0.976	0.986
MO@500h	14.118	9.431	8.069	13.979	9.429	8.327	0.990	0.990	0.994

Table 2.14: Goodness of fit coefficients and failure probabilities for DCBDV data under negative polarity for fresh and thermally aged oil samples

Samples	**Failure Probabilities (kV)**						**Goodness of Fit coefficients for various distributions**		
	2-parameter Weibull			**3-parameter Weibull**			**Normal**	**2-parameter Weibull**	**3-parameter Weibull**
	50%	**10%**	**5%**	**50%**	**10%**	**5%**	**ρ**	**ρ**	**ρ**
Fresh FR3	33.711	25.290	22.660	33.215	25.356	23.392	0.989	0.981	0.988
FR3@90h	30.636	22.173	19.596	29.981	22.298	20.522	0.919	0.929	0.961
FR3@200h	31.294	24.694	22.557	30.209	25.046	25.1603	0.977	0.949	0.991
FR3@500h	27.894	22.635	20.899	27.709	22.643	21.175	0.960	0.959	0.967
Fresh MO	32.198	26.288	24.328	31.908	26.335	24.805	0.992	0.984	0.990
MO@90h	19.459	15.597	14.333	19.392	15.602	14.442	0.991	0.989	0.990
MO@200h	26.390	18.642	16.323	25.688	18.620	17.115	0.974	0.976	0.979
MO@500h	12.117	6.984	5.658	12.188	6.991	5.579	0.987	0.986	0.986

Table 2.15: Conformity of average DCBDV to 2-parameter Weibull distribution for fresh and thermally aged oil samples

Samples	**2-parameter Weibull**					
	Positive DCBDV			**Negative DCBDV**		
	AD-value	**p-value**	**Conformity to Weibull**	**AD-value**	**p-value**	**Conformity to Weibull**
Fresh FR3	1.544	<0.010	NC	0.337	>0.250	CNF
FR3@90h	2.198	<0.010	NC	1.283	<0.010	NC
FR3@200h	0.903	0.019	NC	0.528	0.18	CNF
FR3@500h	1.168	<0.010	NC	0.878	0.022	NC
Fresh MO	1.118	<0.010	NC	0.253	>0.250	CNF
MO@90h	0.354	>0.250	CNF	0.239	>0.250	CNF
MO@200h	0.27	>0.250	CNF	0.518	0.19	CNF
MO@500h	0.316	>0.250	CNF	0.336	>0.250	CNF

*** NC- Not Confirmed; CNF- Confirmed**

Table 2.16: Conformity of average DCBDV to 3-parameter Weibull distribution for fresh and thermally aged oil samples

Samples	**3-parameter Weibull**					
	Positive DCBDV			**Negative DCBDV**		
	AD-value	**p-value**	**Conformity to Weibull**	**AD-value**	**p-value**	**Conformity to Weibull**
Fresh FR3	0.603	0.122	CNF	0.253	>0.500	CNF
FR3@90h	0.991	0.015	NC	0.612	0.117	CNF
FR3@200h	0.583	0.116	CNF	0.214	>0.500	CNF
FR3@500h	0.384	0.419	CNF	0.48	0.199	CNF

Fresh MO	0.534	0.163	CNF	0.191	>0.500	CNF
MO@90h	0.321	0.47	CNF	0.194	>0.500	CNF
MO@200h	0.336	0.486	CNF	0.468	0.16	CNF
MO@500h	0.298	>0.500	CNF	0.338	0.44	CNF

*** NC- Not Confirmed; CNF- Confirmed**

2.8. Comparison of Dielectric Strength in Thermally Aged and Oxidatively Aged NEOs under DC Voltage Stresses

Given that NEOs are intended for implementation in HVDC equipment, studying and comprehending the effects of the ageing mechanisms, which replicate long-term operations, becomes crucial. The study in this chapter investigates the DCBDV of fresh and oxidatively aged NEOs (FR3) for 90, 200, and 500 hours in both polarities and compares them with MO. The average DCBDV values of these studies are provided in Table 2.17. Some significant points observed and identified with this study are Fresh FR3 (NEO) exhibits higher DCBDV values compared to MO in both positive and negative polarities, indicating better dielectric strength of FR3 at the initial stage. After 90 hours of oxidative ageing, the DCBDV of FR3 shows an increase in both polarities, whereas MO experiences a significant decrease.

Table 2.17: Average DCBDV of fresh and aged samples

Ageing Time (hrs)		FR3 (+ve)	MO (+ve)	FR3 (-ve)	MO (-ve)
OA	90	39.78	17.76	-38.97	-26.87
	200	34.94	17.39	-34.60	-31.69
	500	33.07	13.69	-37.33	-16.99
TA	90	30.20	16.59	-30.42	-19.23
	200	29.51	20.54	-30.95	-26.11
	500	29.55	14.07	-27.58	-12.13

*__OA__- Oxidatively aged, **TA**- Thermally aged , **+ve** and **-ve** represents polarity of DCBDV

This suggests that FR3 performs better under oxidative ageing conditions. During thermal ageing for 90, 200, and 500 hours, FR3 shows a gradual decline in DCBDV, while MO also experiences a reduction, albeit to a lesser extent. The comparison between aged FR3 and MO shows that the deterioration effect is less severe in FR3. Additionally, when comparing the effects of oxidative ageing (OA) and thermal ageing (TA), it is evident that OA leads to a more significant decrease in DCBDV for both oils. Across both fresh and aged samples, the negative DCBDV values are consistently lower than the positive DCBDV values, indicating greater vulnerability to voltage breakdown in the negative polarity for both oils. The study highlights the superior dielectric strength of fresh FR3 compared to MO and emphasizes the

influence of ageing on the breakdown voltage. Notably, the oxidation process substantially impacts the dielectric strength of both oils compared to thermal ageing. These findings are crucial for comprehending the behaviour of NEOs and MO in HVDC applications over the long term.

2.9. DC Conductivity of Natural Ester Oils and its Influence on Dielectric strength.

2.9.1. DC conductivity of thermally aged samples

The relative permittivity of the imaginary part with respect to frequency is represented for both fresh and thermally aged oil samples of MO and FR3 in Figure 2.20. The parameters are estimated using the least square technique to achieve the optimal fit for the measured ε'', as plotted in Figure 2.21. A strong alignment is observed between the measured data and the fitted response, based on the Cole-Cole expression featuring two relaxation times. The relative permittivity of the imaginary part for FR3 shows a strong fit when employing the least square technique, as depicted in Figure 2.21.

The DC conductivity parameter obtained through the least square method for dielectric responses of various oil samples using equation (2.2) as discussed and all the results obtained are summarized in Table 2.18. It is observed from Figure 2.20b that as the frequency increases, there is a decrease in the ε″ values of all the oil samples. Figures 2.20a and 2.20b highlight that the ε'' parameter, indicative of losses [99], rises with ageing for FR3. Conversely, in the case of MO, the trend shows a decrease with ageing, where MO samples aged for 90 and 200 hours exhibit higher values, while those aged for 500 hours have values lower than fresh MO samples. Furthermore, it is notable that the permittivity values exhibit minimal dependence on frequency beyond 10 kHz. At lower frequencies, charge carriers exhibit faster reactions to applied electric fields, consequently enhancing the permittivity values. Conversely, the rapid variations in the electric field at higher frequencies do not allow sufficient time for charge carrier dipoles to respond, leading to lower permittivity values. Despite a significant increase in conductivity, the relative stability of DCBDV values of FR3 in both positive and negative polarity suggests that FR3 possesses inherent properties that protect it against the degradation of dielectric properties under increased ionic conductivity.

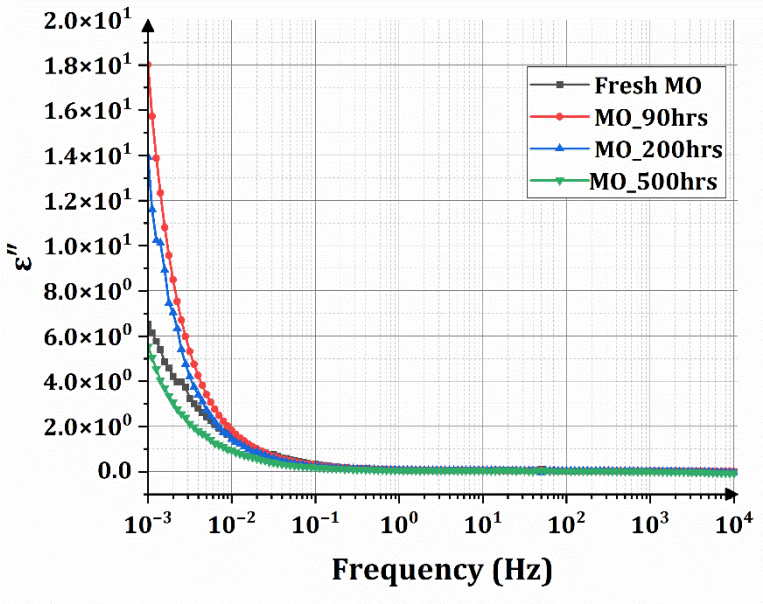

(a)

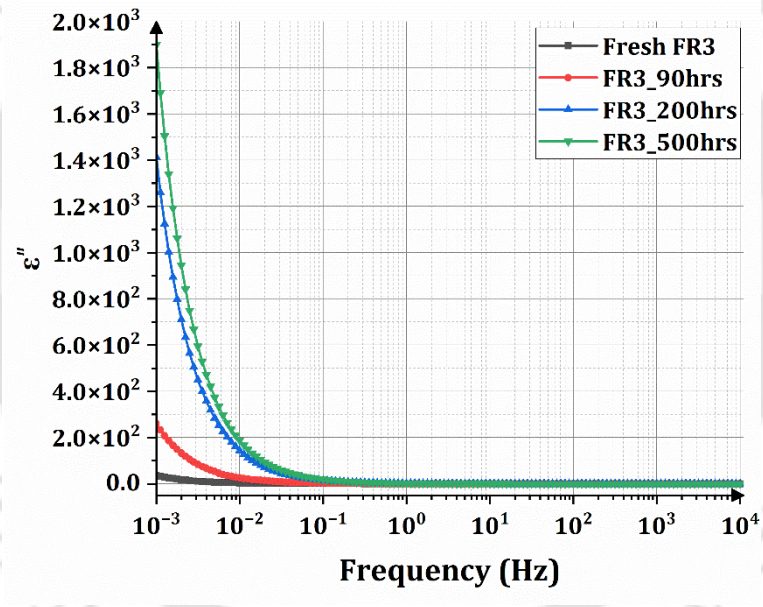

(b)

Fig. 2.20. Imaginary part of relative permittivity imaginary part with respect to frequency for fresh and thermally aged (a) MO (b) FR3

On the other hand, MO shows a decline in DCBDV, which does not correspond to significant changes in conductivity. This disparity may indicate the presence of ageing by-products or degradation mechanisms that impair the insulation capacity of the oil more than its conductivity. The comparative analysis reveals that FR3 undergoes more substantial chemical changes, likely due to oxidation or hydrolysis processes more prevalent in NEOs than in MO. The variability in conductivity values may arise from the influence of pressboard

and copper used in the ageing process, coupled with temperature, resulting in uneven distributions, a phenomenon also noted in previous studies [98-99,115]. These DC conductivity values play a crucial role in delineating field distributions in oils, ultimately contributing to the understanding of DC breakdown strengths.

Table 2.18: DC conductivity estimated from Cole-Cole relaxation model for fresh and thermally aged oils

Ageing Time	DC conductivity (S/m)	
	FR3	MO
0 hours	3.24×10^{-12}	2.14×10^{-12}
90 hours	1.61×10^{-11}	2.63×10^{-12}
200 hours	8.06×10^{-11}	2.15×10^{-12}
500 hours	1.05×10^{-10}	1.82×10^{-12}

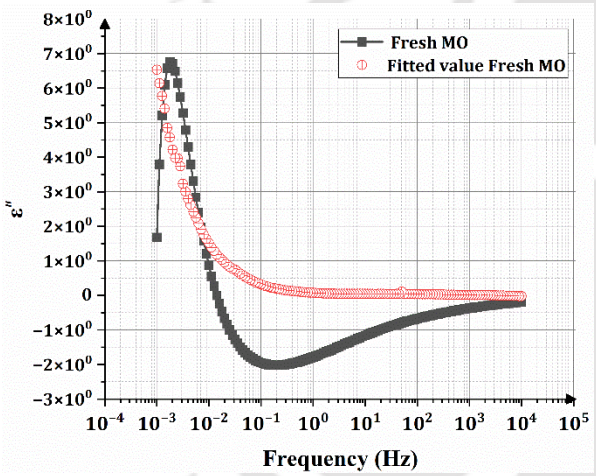

(a)

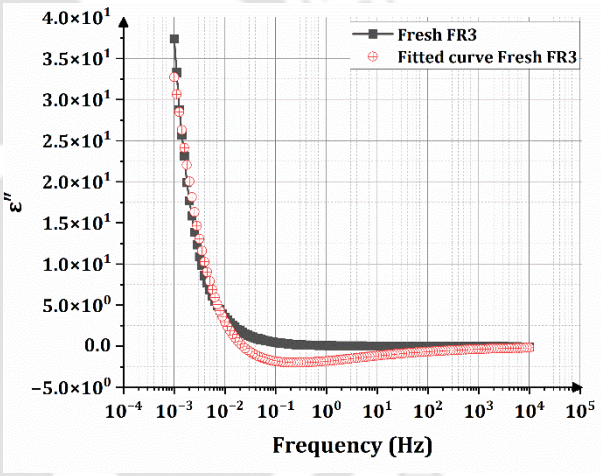

(b)

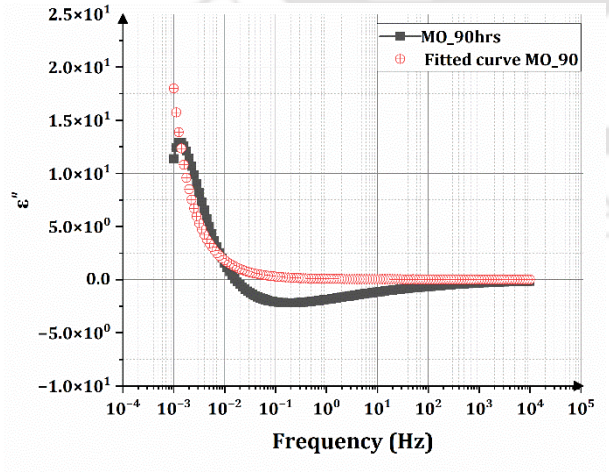

(c)

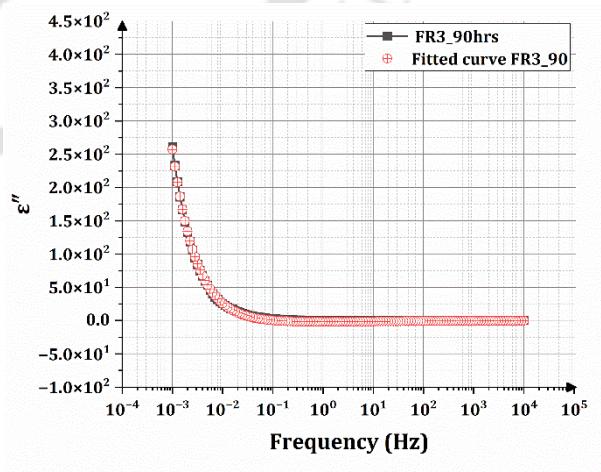

(d)

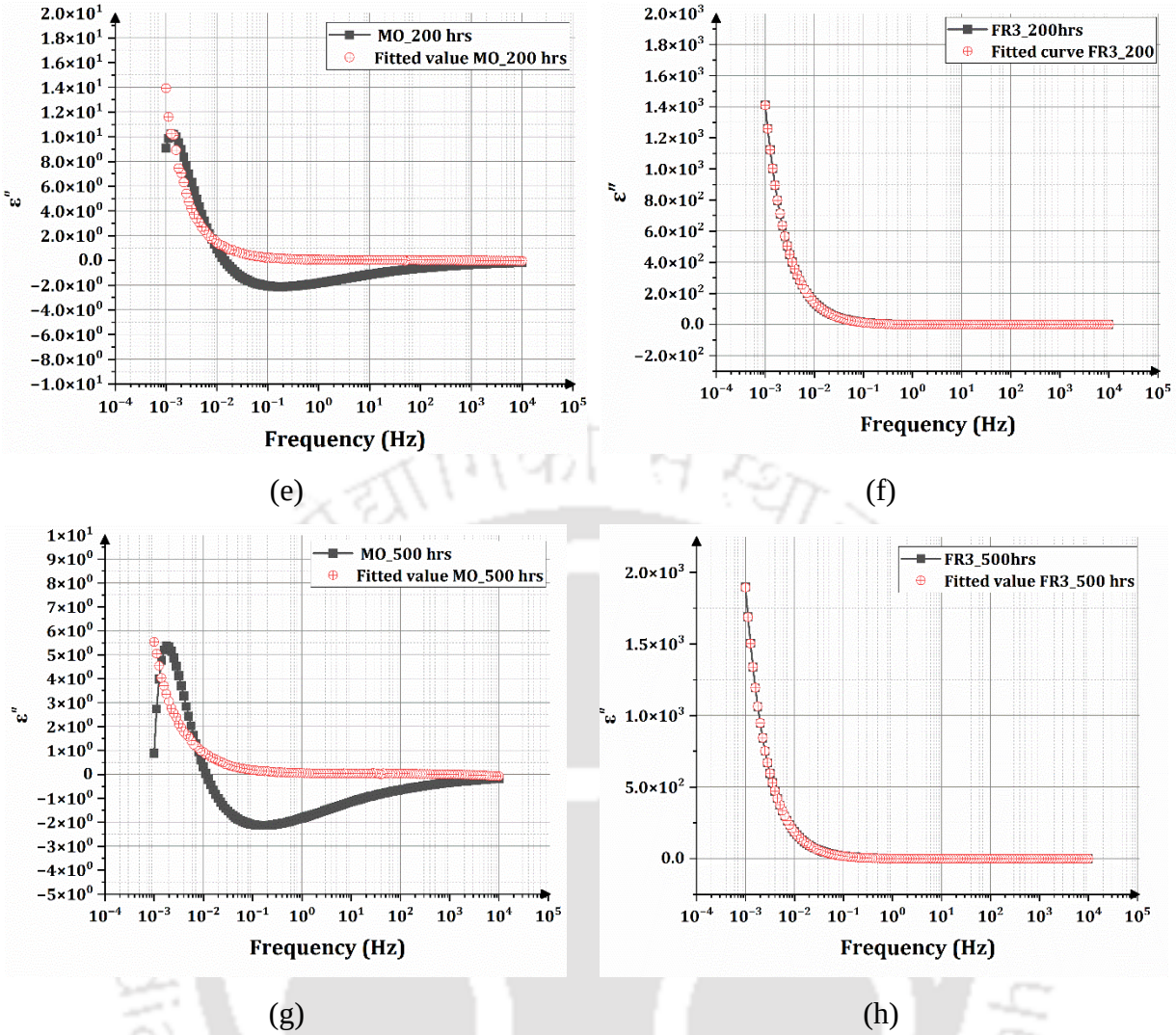

Fig. 2.21. Curve fitting for imaginary part of complex permittivity for fresh and thermally aged MO and FR3.

2.9.2. DC conductivity of oxidatively aged samples

The relative permittivity of the imaginary part with respect to frequency is represented for both fresh and oxidatively aged oil samples of MO and FR3 in Figure 2.22. Table 2.19 provides data on the DC conductivity of oxidatively aged samples of FR3 and MO over different ageing periods at 0 hours, 90 hours, 200 hours, and 500 hours. FR3 exhibits higher conductivity (3.241×10^{-12} S/m) than MO (2.142×10^{-12} S/m), indicating a greater inherent ability to conduct electricity. After 90 hours of ageing, conductivity of FR3 significantly increases to 1.04×10^{-11} S/m, while MOs conductivity decreases to 3.42×10^{-13} S/m, suggesting a reduction in its electrical conductivity. By 200 hours, conductivity of FR3 continues to rise to 1.70×10^{-11} S/m, whereas MO shows an increase to 8.06×10^{-13} S/m, indicating that prolonged ageing starts to affect MOs conductivity more significantly.

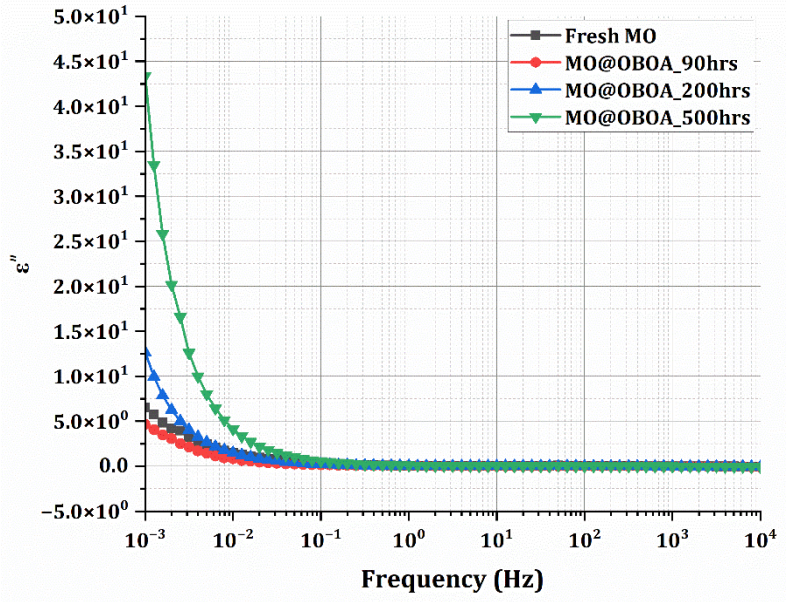

(a)

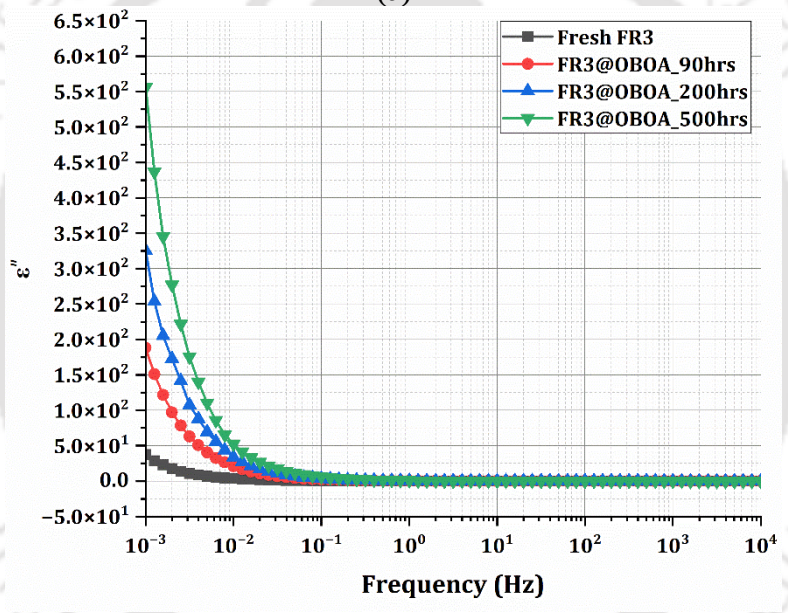

(b)

Fig. 2.22. Imaginary part of relative permittivity imaginary part with respect to frequency for fresh and oxidatively aged (a) MO (b) FR3

Table 2.19: DC Conductivity Estimated from Cole-Cole Relaxation Model for Fresh and oxidatively Aged Oils

Ageing Time	DC conductivity (S/m)	
	FR3	MO
0 hours	3.24×10^{-12}	2.14×10^{-12}
90 hours	1.04×10^{-11}	3.42×10^{-13}
200 hours	1.70×10^{-11}	8.06×10^{-13}
500 hours	3.34×10^{-11}	3.82×10^{-12}

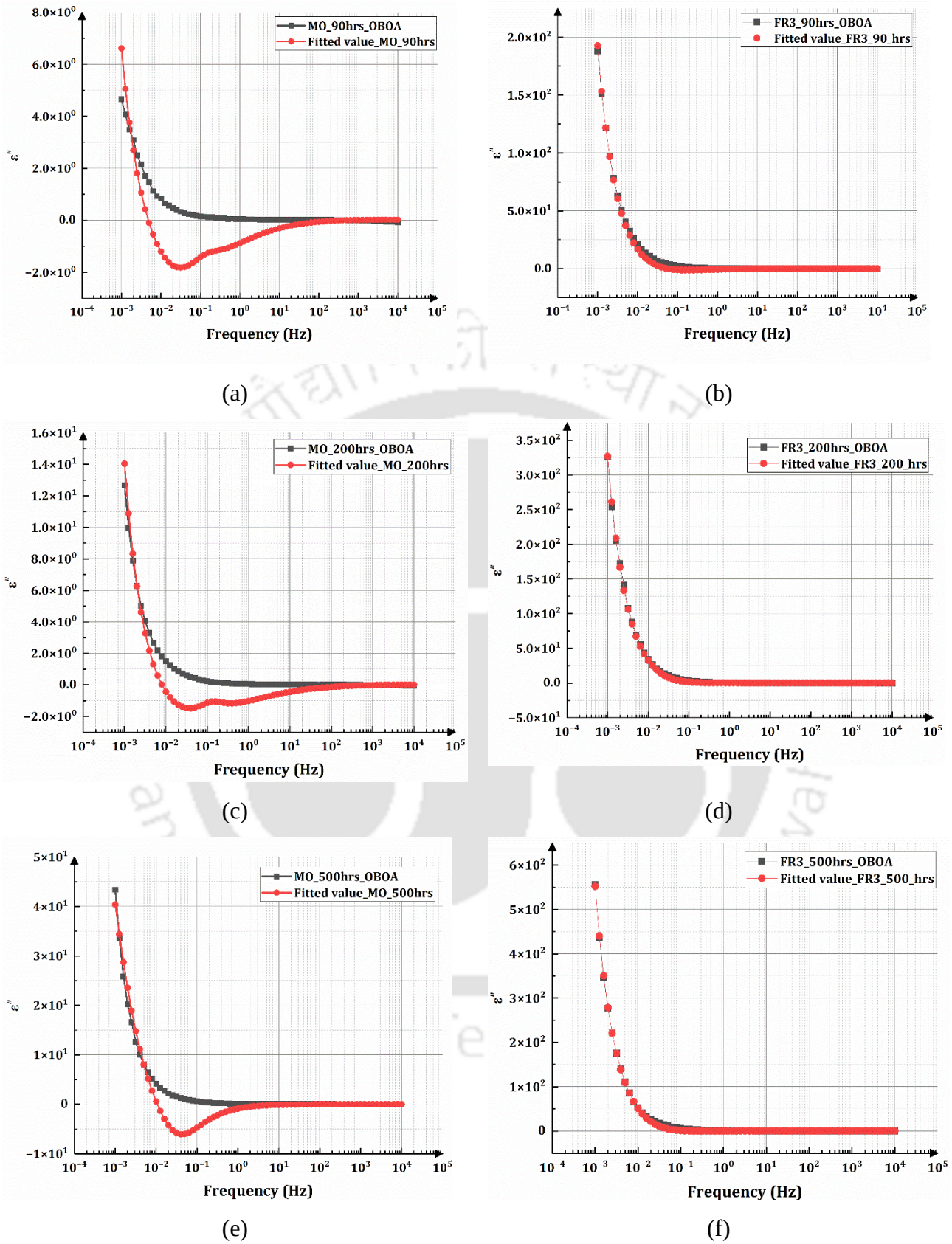

Fig. 2.23. Curve fitting for imaginary part of complex permittivity for fresh and oxidatively aged MO and FR3.

After 500 hours, conductivity of FR3 markedly increases to 3.34×10^{-11} S/m, reflecting significant degradation due to oxidative ageing. On the other hand, MO shows a substantial increase in conductivity to 3.82×10^{-12} S/m, indicating that long-term oxidative ageing eventually leads to higher electrical conductivity in MO as well. The consistent rise in conductivity of FR3 suggests a continuous degradation process, and the insulating material is affected by oxidation. Conversely, MO exhibits a delayed but substantial increase in conductivity, implying its degradation under oxidative ageing accelerates after a certain period.

2.9.3. Fitting discrepancies for the imaginary part of complex permittivity

The relative permittivity of the imaginary part for FR3 shows a strong fit when employing the least square technique, as depicted in Figure .2.21 and Figure 2.23. However, the fitting for the imaginary part of complex permittivity for fresh MO and aged MO is not as satisfactory, particularly at low frequencies. MO displays a notable "hump" phenomenon in the imaginary part of its relative permittivity inside the low-frequency region. The presence of this hump is caused by interfacial polarization, which is affected by parameters such as the oil pressboard ratio and insulation geometry [116]. The presence of this peak around 10^{-3} Hz highlights the importance of interfacial polarization in influencing the dielectric behavior of MO. Unlike FR3, where the impact of insulation geometry is insignificant, MO exhibits a more noticeable influence of interfacial polarization. The discrepancy is apparent in the shape of the observed curve, especially when seen on a logarithmic scale, as there are fewer data points that perfectly match the curve being fitted. As a result, the fit may not precisely represent the subtle differences in the experimental values, resulting in variations from the expected form of the curve. Although there are difficulties in accurately fitting the intricate permittivity curve for MO, the resulting DC conductivity value agrees with other experimental findings, confirming the reliability of the conductivity estimation. More precisely, the present findings are consistent with a DC conductivity value of 2.6×10^{-13} S/m at 20℃, as measured using a Keithley 6430 Pico ammeter [117]. This alignment emphasizes the dependability of the conductivity measurement methods and strengthens the importance of precise conductivity estimations for HVDC transformer applications.

One reason for negative ranges in Figures 2.8 and 2.21 might be the assumption of ground and guard electrodes as a single point [188]. However, there is an interesting observation that is in both thermal and oxidative ageing the negative values in lower frequency range only

MO has the negative range. However, FR3 does not have negative values. The negative dielectric loss factor (ε″) observed at low frequencies (<50 Hz) in mineral oil (MO), but not in FR3, is a measurement artefact primarily caused by electrode polarization and interfacial effects [187]. At low frequencies, MO exhibits higher charge accumulation at the electrode interface due to its non-polar nature and the presence of aging byproducts, which can lead to erroneous shifts in the impedance measurement. This results in an apparent negative ε″ value.

2.9.4. Influence on DC conductivity by energization time and field strength

For DC applications, the conductivity of insulating materials is crucial for determining electric field distributions. In the case of insulating liquids like MO used in HVDC converter transformers, their conductivity is not constant. Instead, it varies depending on different parameters and combinations. Short-term conductivities can be significantly higher (one to two orders of magnitude) than steady-state values relevant for testing and operation [118]. Temperature variations (following the Arrhenius law) and field strength changes (illustrated by the bathtub curve) also play a significant role. There is no direct correlation between short-term and long-term conductivities, making mathematical extrapolation unfeasible. Measurement methods complying with standards, which involve short energization times and low field strengths, fail to reflect the stresses encountered during HVDC transformer operation and testing. However, the energization time and low electric field for the samples in this study is around 7-8 hours for three iterations, as mentioned, section 2.4, for accuracy. Moreover, in [118], it is mentioned that once the energization time changes from minutes to hours, the conduction tends to enter steady state conduction, supporting the present calculated results. However, conductivity is not only time-dependent but varies, with temperature, electrical field strength, water content, impurities and ageing conditions.

2.10. Summary of the chapter

This chapter provides a presents the experimental methodology and sample preparation for investigating the dielectric insulating properties of MO and FR3 under oxidative and thermal ageing, the two primary mechanisms significantly affecting insulating oils. Understanding these phenomena is crucial for identifying potential limitations in implementing NEOs in HVDC applications, as long-term applicability remains underexplored despite some research on dielectric strength under DC voltage stresses. The chapter details the preparation of oxidatively and thermally aged MO and NEO samples, including pretreatment before ageing,

to ensure consistent results. Post-ageing tests for viscosity and moisture content verify proper ageing, and the impact of moisture on tests is also examined. Storage conditions of the prepared samples are briefly addressed to maintain integrity of the samples before testing. The experimental methodology and setup for DCBDV testing are discussed briefly, including testing conditions and standards. Statistical analysis of DCBDV data in NEO-FR3 and MO subjected to thermal and oxidative stresses over 90, 200, and 500 hours, using the normal distribution, two-parameter Weibull, and three-parameter Weibull distributions to model data is tested and these distributions are validated by Anderson-Darling and goodness-of-fit tests. The chapter also discusses DC conductivity measurement using Frequency domain analysis (FDS) and Cole-Cole plots, briefly explaining the underlying theory. Then a detailed examination of the DCBDV results for MO and FR3 under oxidative and thermal ageing conditions. The findings reveal that fresh FR3 exhibits a significantly higher DCBDV than MO under positive polarity, with a substantial 29.03% increase. However, this difference diminishes under negative polarity, with fresh FR3 showing only a marginal 4% increase over MO. For oxidative ageing as the oils age oxidatively, their DCBDV declines due to oxidation and sludge accumulation, with FR3 experiencing less severe deterioration than MO. The Anderson-Darling (AD) test confirms that the majority of samples conform to normal, 2-parameter, and 3-parameter distributions, with some alterations noted in fresh FR3 data under positive polarity in the 3-parameter Weibull distribution. Furthermore, the goodness of fit (CC) test indicates adherence to normal and Weibull distributions under both polarities. The study also investigates DC conductivity, revealing that FR3 exhibits higher conductivity than MO, with FR3's conductivity increasing significantly over time, suggesting continuous degradation.

For thermal ageing the decline in DCBDV during ageing is evident, with aged FR3 exhibiting less severe degradation effects than aged MO. Most data adhere to the 3-parameter Weibull distribution under both polarities, reinforcing the reliability of statistical models. The research underscores the advantageous properties of natural esters like FR3 in maintaining electrical insulation performance over time, compared to MO, which exhibits less increase in conductivity with age but shows more vulnerability in its breakdown voltage, especially under negative polarities. From the results obtained the correlation between increased DC conductivity and ageing in FR3, which does not correspond to a similar decrease in DCBDV, underscores the advantageous properties of natural esters like FR3 in maintaining electrical insulation performance over time. The observation that increased DC conductivity in aged

FR3 does not correspond to a significant decrease in DCBDV suggests that other mechanisms are compensating for the conductivity increase. One possible explanation is that FR3 has strong oxidative stability and high moisture tolerance compared to MO, which helps maintain its dielectric strength despite ageing. Additionally, the presence of natural antioxidants and higher molecular polarity in FR3 may contribute to forming stable charge carriers that suppress streamer propagation, preventing a drastic reduction in breakdown voltage. The increase in viscosity due to ageing may also slow down streamer development, counteracting the impact of increased conductivity on breakdown strength. These factors collectively contribute to the sustained DCBDV of FR3 despite an increase in conductivity. In contrast, MO exhibits less increase in conductivity with age but shows more vulnerability in its breakdown voltage, especially under negative polarities, indicating different ageing behaviors and degradation pathways that affect its performance as an insulating fluid.

This study employs the VDE electrode configuration to measure the DCBDV of fresh insulating liquids. However, it is noted that different electrode configurations can lead to variations in the measured BDV values with respect to various standards from ASTM and IEC. To address this issue, the next chapter further investigates the results obtained in this research by considering the geometric effects of different electrode configurations on the measurement of DCBDV. The goal is to derive an analytical expression that normalizes these differences, allowing for a more accurate comparison of BDV values obtained under various DC voltage stresses. This normalization process will help improve the reliability and consistency of BDV measurements, ensuring that the results are more representative of the actual dielectric strength of the tested insulating liquids.

***Note**: This entire work is published as mentioned below,*

1. **D. Kanumuri**, N. Baruah, A. Kumar and S. K. Nayak, “Effects of Oxidative Aging on Dielectric Strength of Natural Ester Oil Under DC Voltage Stresses,” has been published in ***IEEE Transactions on Dielectrics and Electrical Insulation***, vol. 30, no. 4, pp. 1517-1524, Aug. 2023.

2. **D. Kanumuri**, A. Kumar, N. Baruah and S. K. Nayak, "Influence of Thermal Aging on DC Conductivity and Breakdown Strength of Natural Ester Oils for HVDC Applications," in ***IEEE Transactions on Dielectrics and Electrical Insulation***, vol. 31, no. 6, pp. 3444-3452, Dec. 2024.

3

Geometric effects on DC breakdown strength measurement of natural ester oils

Contents

3.1	Introduction ……...……..	76
3.2	Methodology and experimental setup ……..……..	78
3.3	Results and discussion……..…….……...	82
3.4	Summary of the chapter…..……..	91

3.1. Introduction

In the context of the worlds transition to renewable energies to combat climate change, HVDC transmission systems play a crucial role in the power system network. One critical component of these systems is HV converter transformers, which are typically oil-filled apparatuses using MO as the primary insulating medium [47]. However, there has been a shift towards using NEOs instead of MOs in oil filled electrical equipment due to their superior biodegradable, electrical, and thermal properties. Therefore, it is necessary to examine the compatibility of NEOs with these HVDC power apparatuses. To ensure the effectiveness of these alternative insulating liquids, it is essential to investigate the electrical, chemical, thermophysical and mechanical properties under DC stresses.

A significant challenge associated with these parameters lies in the measurement and data processing, particularly in the context of electrical and thermophysical properties. To effectively assess the condition of a converter transformer, it is crucial to monitor the insulation system, which encompasses both solid and liquid components. Numerous researchers have explored various measurement techniques aimed at evaluating insulation conditions. These techniques include assessment of partial discharges (PD), polarization-depolarization (PDC), frequency-domain spectroscopy (FDS), and moisture analysis [119-125]. These methods are not used in isolation; instead, they complement traditional measurement techniques by enhancing and introducing additional real-time parameters to ensure precise and accurate measurements. In this present study, testing the breakdown strength of NEO under DC voltage stresses is explored. To achieve more precise results, the geometry effects have been incorporated to measured data to refine the DCBDV measurements.

One of the primary and most significant property to be explored for any new insulating oil to be compatible is breakdown voltage (BDV). In power transformers, the insulation structure often contains uniform or quasi-uniform field configurations. These configurations can be found in areas such as the oil gaps between windings or between windings and the tank. The dielectric strengths of the insulating liquids used in these configurations are heavily influenced by the quality of the liquid, particularly the presence of water, solid particles, and gas bubbles [126]. As a result, testing the breakdown voltages of insulating liquids in quasi-uniform configurations is commonly done to aid in insulation design or assess the quality of the liquids. To ensure consistency and accuracy in these tests, specific standards such as IEC

60156, ASTM D1816, and ASTM D877 [21-23] have established specific procedures for conducting breakdown voltage tests.

In the field of insulation design for power transformers, it is widely recognized that the breakdown strength decreases as the electrode area and gap distance between electrodes increase. This phenomenon, known as the scale effect or volume effect, is crucial in determining the breakdown voltage of transformer liquid under a uniform or quasi uniform field in the full-scale transformer [127]. To estimate this breakdown voltage accurately, it is a common practice to extrapolate from small-scale tests using the parallel or series breakdown probability models.

The area and volume effect on MO and NEOs have been well established in the literature under ACBDV [127-135, 31]. To be brief in their research, Weber and Endicott [127] aimed to present an extensive data for oil breakdown under specific conditions, analyze the impact of electrode size on oil breakdown in uniform fields, and determine the theoretical distribution fitting the data. Furthermore, they explored [128] the dependence of the 60-cycle breakdown strength of high-quality transformer oil on electrode size, emphasizing the extremal nature of the breakdown distribution. W. R. Wilson [129] proposed that the primary determinant of the unit dielectric strength in commercial oil around varied electrode geometries is the volume of stressed oil, attributing this to statistical reasons. Kawaguchi et al. [130] systematically examined the relationship between breakdown voltage and stressed oil volume across different electrode types. They found that the distribution type of breakdown probability is influenced by the quantity of stressed oil volume, with lesser quantities approaching a Gaussian distribution. Kato et al. [131] introduced an optimization technique to determine the best electrode contour for insulation performance, emphasizing the importance of considering dielectric breakdown characteristics over electric field distribution. Del Vecchio [132] proposed a Townsend-like breakdown process for transformer oil, highlighting the significance of the breakdown mechanism over localized field enhancement. X. Wang et al. [133] elucidated the electrode area effect on transformer liquids, noting that esters are more sensitive to this effect than mineral oil. In another study, X. Wang and Z. D. Wang [134] compared the AC dielectric strengths of synthetic ester, natural ester, and mineral oil, revealing that esters, when filtered and dehydrated, have comparable breakdown voltages to mineral oil but are more affected by contaminants and electrode area.

Limited research on this study makes it crucial to explore the electrode stressed area effect on DCBDV in NEOs. A thorough DCBDV analysis is done for both MO and NEO-FR3 for different electrodes with 1mm gap and results are analyzed on the variation of breakdown strength. This involves a thorough examination of effective electrode-stressed area (EESA) on DCBDV for both positive and negative polarities in MO and NEOs. It is also essential to test the application of existing theory to DCBDV under both polarities. This study delves into the area effect on MO and FR3, presenting the findings and discussions.

3.2. Methodology and experimental setup

3.2.1. Effect of effective electrode area on breakdown strength using Weibull analysis

The breakdown voltage distributions of insulating oils are found to be well-fit by the Weibull distribution [31]. To extrapolate the breakdown strengths of transformer oil at large electrodes, a Weibull distribution can be used to model the area effect. It is widely established that the breakdowns observed in transformer liquids under uniform electric fields are attributed to the presence of "weakest links," which can be found within both the bulk oil and on the surfaces of the electrodes [135].

As the electrode area expands, the count of these "weakest links" is expected to increase in direct proportion. Let H be the EESA of an electrode, and the BDV of insulating oil stressed between the electrode gap should follow the Weibull distribution as shown in equation (3.1).

$$R(E) = 1 - e^{-\left(\frac{E}{\alpha}\right)^{\beta}} \tag{3.1}$$

R(E) is the failure rate of the sample at applied voltage E. α and β are scale and shape parameters. From the parallel breakdown probability model and weakest link theory [136] as shown in Figure. 3.1, H can be regarded as n pieces of basic elements (H_0) connected in parallel. The BDV of oils stressed under electrode area of each element H_0 should also follow Weibull distributions as shown in equation (3.2)

$$R_i(E) = 1 - e^{-\left(\frac{E}{\alpha_i}\right)^{\beta_i}} \tag{3.2}$$

Where n pieces of basic elements H_0 are connected in parallel, the breakdown probability of R and R_i follows equations (3.3) and (3.4)

$$1-\mathrm{R}=\prod_{\mathrm{i}}^{\mathrm{n}}\left(1-\mathrm{R}_{\mathrm{i}}\right) \tag{3.3}$$

$$\ln\left(1-\mathrm{R}\right)=\sum_{\mathrm{i}}^{\mathrm{n}}\ln\left(1-\mathrm{R}_{\mathrm{i}}\right) \tag{3.4}$$

H_0 is the basic element of electrode H, and the applied voltage on each basic element is equal. Equation (3.4) can also be written as

$$\left(\frac{\mathrm{E}}{\alpha}\right)^{\beta}=\sum_{\mathrm{i}}^{\mathrm{n}}\left(\frac{\mathrm{E}}{\alpha_{\mathrm{i}}}\right)^{\beta_{\mathrm{i}}}=\frac{\mathrm{H}}{\mathrm{H}_0}\left(\frac{\mathrm{E}}{\alpha_{\mathrm{i}}}\right)^{\beta_{\mathrm{i}}} \tag{3.5}$$

By solving this equation (3.5) where H/H_0 represents the number of weak points on the electrode surface; Equation (3.6) is an assumption which indicates that the shape parameter β of the Weibull distribution is independent of the ESA of the electrode. It simplifies the analysis by assuming that all basic elements have the same shape parameter (β_i). This assumption implies that each element fails in a statistically similar manner, which simplifies the summation in equation (3.5) by eliminating the need to consider different failure distributions for each element.

$$\beta=\beta_{\mathrm{i}} \tag{3.6}$$

From equation (3.5) and equation (3.6); equation (3.7) is obtained

$$\left(\frac{\mathrm{E}}{\alpha}\right)^{\beta}=\sum_{\mathrm{i}}^{\mathrm{n}}\left(\frac{\mathrm{E}}{\alpha_{\mathrm{i}}}\right)^{\beta_{\mathrm{i}}}=\frac{\mathrm{H}}{\mathrm{H}_0}\left(\frac{\mathrm{E}}{\alpha_{\mathrm{i}}}\right)^{\beta_{\mathrm{i}}}$$

$$\left(\frac{\mathrm{E}}{\alpha}\right)^{\beta}=\frac{\mathrm{H}}{\mathrm{H}_0}\left(\frac{\mathrm{E}}{\alpha_{\mathrm{i}}}\right)^{\beta_{\mathrm{i}}};\text{where},\beta=\beta_{\mathrm{i}}$$

$$\left(\frac{\mathrm{E}}{\alpha}\right)=\left(\frac{\mathrm{H}}{\mathrm{H}_0}\right)^{\frac{1}{\beta}}\left(\frac{\mathrm{E}}{\alpha_{\mathrm{i}}}\right)^{\frac{\beta_{\mathrm{i}}}{\beta}}\rightarrow\left(\frac{1}{\alpha}\right)=\left(\frac{\mathrm{H}}{\mathrm{H}_0}\right)^{\frac{1}{\beta}}\left(\frac{1}{\alpha_{\mathrm{i}}}\right)$$

$$\alpha=\frac{\alpha_{\mathrm{i}}}{\left(\frac{\mathrm{H}}{\mathrm{H}_0}\right)^{\frac{1}{\beta}}}$$

simplifying the above equation

$$\alpha=\alpha_{\mathrm{i}}\left(\frac{\mathrm{H}}{\mathrm{H}_0}\right)^{-\left(\frac{1}{\beta}\right)} \tag{3.7}$$

Thus, it is a constant determined by the liquid type. equation (3.7) can be further expressed as

$$\log(\alpha) = -\frac{1}{\beta}\log(\mathrm{H}) + \left(\frac{1}{\beta}\log(\mathrm{H}_0) + \log(\alpha_\mathrm{i})\right) \tag{3.8}$$

Where H_0, α_i and β are area, scale and shape parameter of basic element in an electrode that can be considered as constants. Thus (3.8) can be rewritten as (3.9) where α, β are scale and shape parameters of BDV distributions under electrode H and second term of right-hand side of (3.8) can be defined as constant k which is determined by the type of oil used.

$$\log(\alpha) = -\frac{1}{\beta}\log(\mathrm{H}) + \mathrm{k} \tag{3.9}$$

$$\log(\alpha) = \mathrm{a} - \mathrm{b}\log(\mathrm{H}) \tag{3.10}$$

Equation (3.9) can be further reduced as (3.10) in which a and b are constants derived from type of insulating liquid, α is the BDV value of sample at 63% failure rate. Equation (3.10) gives the area effect on BDV of an insulating oil.

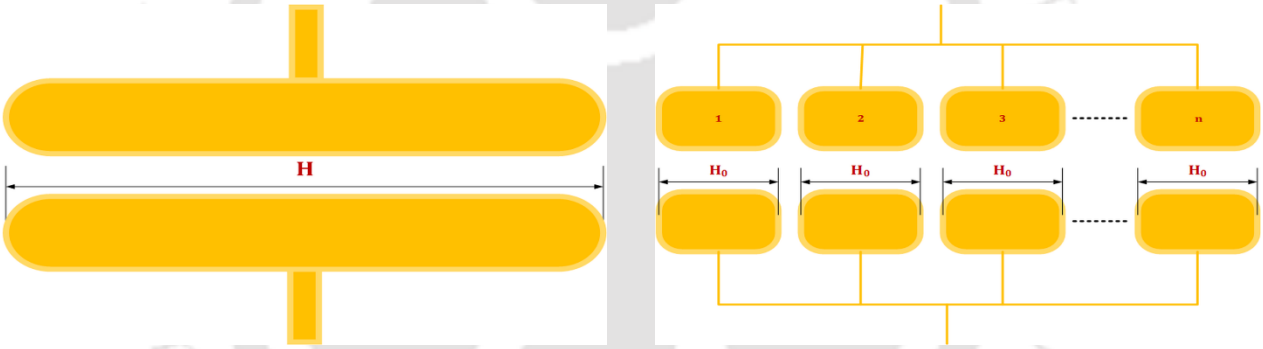

Fig. 3.1. Parallel breakdown probability model for area effect

3.2.2. Materials and experimental setup

Two base oils, MO and FR3 procured from Savita Industries and Cargill India Pvt. Ltd respectively. The pressboard used in the present investigation, which has a 1.5 mm thickness, was procured from the power maker, Guwahati. Before testing the samples, the Kraft pressboard is dried for 24 hours in a vacuum oven at 80°C. Similarly, oil samples are kept for 48 hours at 65°C in a vacuum oven [119] to remove the residual moisture present in these samples. Using the testing equipment shown in Figure. 3.2, these samples are tested for DCBDV under positive and negative polarity for both liquid and solid insulation under various electrode geometries. In this study, three types of electrodes, namely VDE (Verband Deutscher Elektrotechniker), plane, and sphere-shaped electrodes from [21-23] with a 1 mm electrode gap, are utilized for liquid insulation. These brass electrodes are placed within a

testing cup. To measure the breakdown voltages (BDV) of the samples under DC voltage stresses, the ASTM D1816 [21] standard is followed, as there is no specific testing standard for insulating liquids under DC voltage. The gap distance of 1mm is used across all electrode shapes to maintain the uniform testing conditions. A WSTS high voltage generation unit equipped with a 100kV AC test transformer was used with a high voltage silicone rectifier and a 140kV capacitor with a capacitance of 10^5 pF. A voltage divider connected to the control panel enabled voltage measurements, while the capacitor was linked to the test cup, applying stress to the electrodes with a DC voltage source. The polarity of the system is changed by changing the direction of the HV rectifier. The voltage applied to the test cup was incrementally increased at a rate of 2 kV per step.

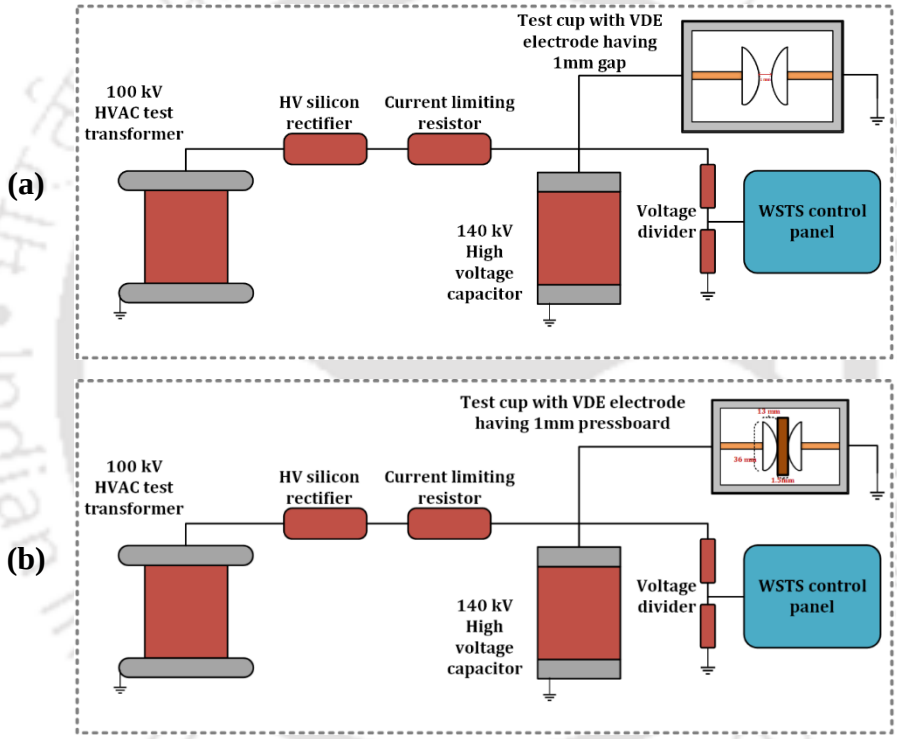

Fig. 3.2. Experimental setup to test DCBDV of (a) MO and FR3 (b) solid insulation immersed in MO and FR3

Before applying voltage, a 5-minute resting period is provided to allow any formed bubbles to settle, followed by a one-minute pause after each breakdown. All experiments are conducted at room temperature. In addition, considering the significance of low breakdown probability, according to industry design requirements, overcoming the limited number of breakdowns specified in ASTM D1816 is necessary. To address this, each sample underwent four sets of six breakdowns for each electrode configuration, resulting in 24 breakdowns per configuration per sample. For MO, the pause time between each set is 5 minutes, while for

NEO, it is extended to 15 minutes [63]. During this time, the oil was gently swirled using a glass rod. The same methods are applied for the negative DC polarity experiments.

In the case of solid insulation, the experimental setup depicted in Figure 3.2b is utilized to determine the DCBDV of solid insulation. The setup included a 1.5 mm thick pressboard positioned between VDE, sphere, and plane electrodes, with tests conducted in a cup filled with fresh MO or FR3. This arrangement effectively compared DC breakdown strengths under both positive and negative polarities. The voltage was applied in increments of 2 kV per step until a breakdown or puncture occurred in the solid insulation. This procedure is repeated for all electrode configurations across both polarities.

3.3. Results and discussion

3.3.1. Experimental results of DC breakdown voltage of MO and FR3 in positive and negative polarities for different electrode shapes

Figures 3.3a and 3.3b show the positive and negative DCBDV in relation to the breakdown series for MO and FR3 with different electrode configurations. Figure 3.4 depicts the average positive and negative DCBDV across all electrode configurations. From these figures, it is observed that for all the configurations, the BDV of MO is much less than FR3 in both positive and negative polarity. The positive mean DCBDV of MO for VDE, Plane, and sphere electrodes are 27.017 kV, 26.304 kV, and 29.042 kV at 1mm gap. There is a 2.63 % decrease in the breakdown strength of plane electrodes and a 6.97% increase in sphere electrodes compared to VDE. In the case of comparison between the plane and sphere electrode configuration, the dielectric strength of MO is increased by 9.42%. Electrode configuration with a sphere shape has the highest BDV for MO. For FR3, the DCBDV is 38.067 kV, 45.413 kV, and 51.225 kV for VDE (mushroom), plane, and sphere-shaped configurations at a 1mm gap. In FR3, the sphere-electrode configuration displays the highest positive DCBDV. Compared to MO, FR3's dielectric strength is increased by 29.02%, 42.07%, and 43.3% for VDE, plane, and sphere electrode configurations.

Similarly, in case of negative mean DCBDV of MO for VDE, plane, and sphere electrodes are -31.825 kV, -27.788 kV, and -33.283 kV at 1 mm gap. There is a 12.68% decrease in the breakdown strength of plane electrodes and a 16.5% increase in sphere electrodes compared to VDE. In the case of comparison between the plane and sphere electrode configuration, the dielectric strength of MO is increased by 4.38%. Electrode configuration with a sphere shape

has the highest negative DCBDV for MO. For FR3, the DCBDV is -33.317 kV, -50.144 kV, and -49.054 kV for VDE, plane, and sphere configurations at a 1mm gap. Compared to MO, FR3's dielectric strength is increased by 4.47%, 44.58%, and 32.15% for VDE, plane, and sphere electrode configurations.

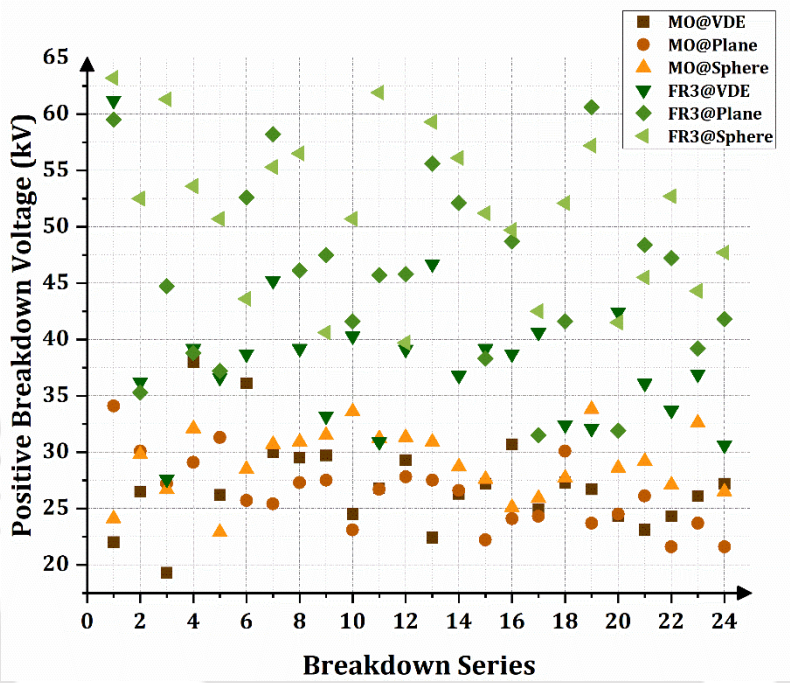

(a)

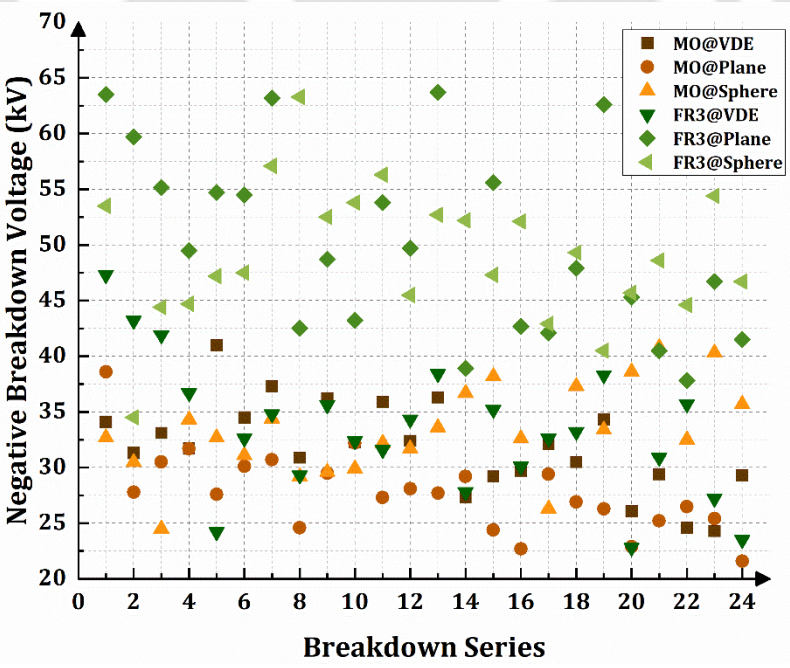

(b)

Fig. 3.3. (a) Positive DCBDV (kV) with respect to breakdown series (b)Negative DCBDV (kV) with respect to breakdown series

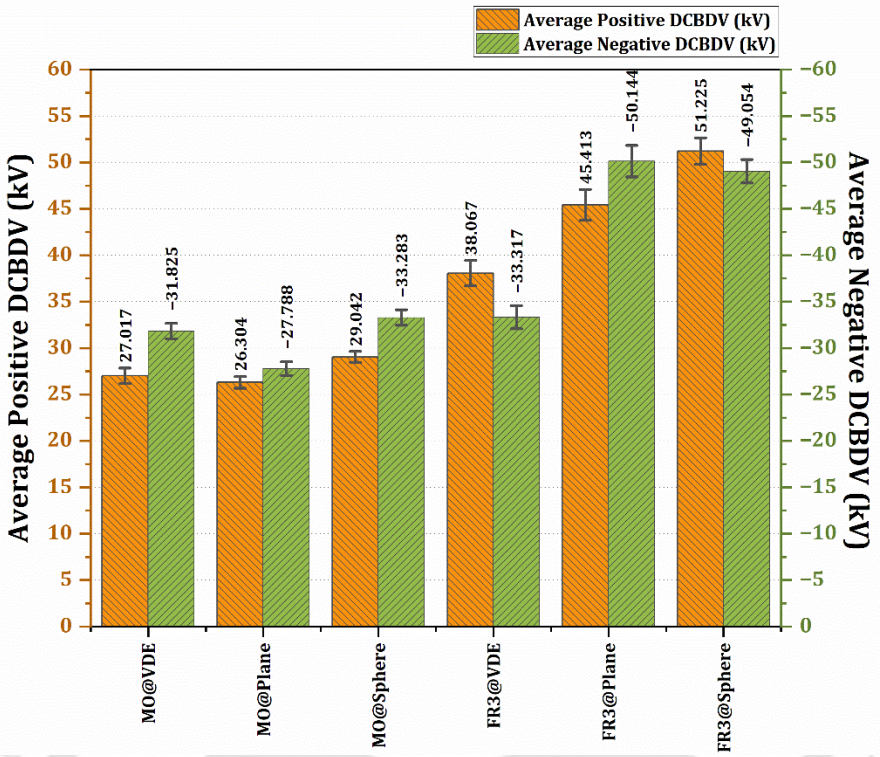

Fig. 3.4. Average Positive and Negative DCBDV (kV) with error bar for various electrode shapes

The DCBDV for solid insulation immersed in MO and FR3, as illustrated in Figure. 3.5, provides valuable insights into the behaviour and performance of solid insulation immersed in various liquids under DC electrical stress. In MO immersed solid insulation shows high breakdown voltages with the VDE configuration reaching up to 56.1 kV, higher than the liquid insulation for the same configuration under positive DCBDV. The sphere and plane configurations display lower voltages at 36.3 kV and 38.7 kV, respectively. Under negative polarity, the VDE configuration drops significantly to -53.1 kV, whereas the sphere and plane configurations show similar levels at around -36.5 kV and -36.8 kV. For FR3 under positive polarity, the VDE configuration demonstrates superior performance with a DCBDV of 50.7 kV, significantly higher than the plane (37.9 kV) and sphere (32.19 kV). In the case of negative polarity, VDE maintains high BDV at -53.2 kV, with plane and sphere configurations showing lesser but improved voltages under negative polarity at -39.8 kV and -33.9 kV. Comparing these results with the DCBDV of liquid insulation, a notable observation for MO is that all three electrode configurations (VDE, Sphere, and Plane) show increased DCBDV in solid insulation compared to liquid, with a particularly significant increase in the VDE configuration. For FR3), the DCBDV of solid insulation in the VDE

configuration is higher than that in liquid insulation. However, the breakdown voltages for the sphere and plane configurations are lower for solid insulation than for liquid.

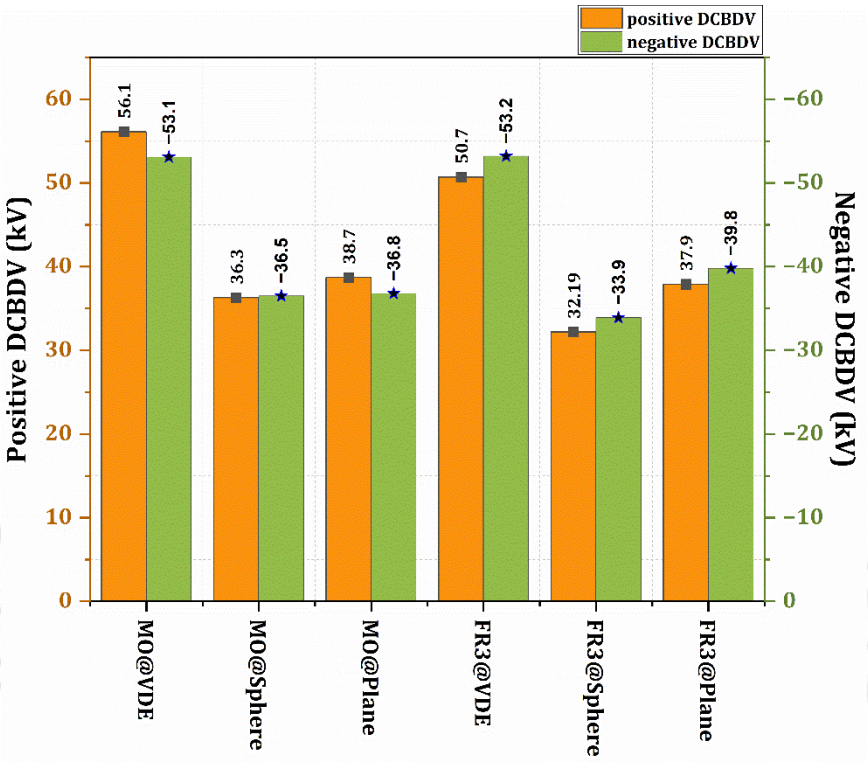

Fig. 3.5. DCBDV (kV) for solid insulation in MO and FR3 under various electrode shapes

3.3.2. Effect of Electrode Stressed Area on DCBDV of MO and NEO-FR3 in both polarities

Breakdown strength is analyzed mostly using the normal and Weibull distributions [47, 63, 108], but the Weibull distribution is particularly favoured for examining the area effect. The choice between Weibull analysis and normal distribution when analyzing the effect of effective electrode area depends on the nature of the data and the specific application. Weibull distribution is particularly suited for analyzing life data, especially "time-to-failure" or "stress-to-failure" scenarios, making it a popular choice in reliability engineering and materials science. Its versatility allows it to model various data shapes, from exponential to normal to skewed distributions. The parameters of the Weibull distribution, such as the shape and scale parameters, often have physical interpretations that can provide insights into underlying failure mechanisms. Additionally, Weibull analysis can effectively handle censored data with unknown failure times [137]. On the other hand, the normal distribution assumes symmetric and bell-shaped data. If the data related to the effective electrode area

effect is skewed or has a different shape, then the normal distribution might not be the best fit. For this study, the Weibull analysis is employed to assess the influence of the electrode area on the DC breakdown strength of MO and NEO, considering both positive and negative polarities. Figures 3.6a and 3.6b depict the Weibull probability plots of positive and negative DCBDV data of MO and FR3 for different electrode configurations. These graphs are plotted using a 2-parameter Weibull analysis [132]. The Weibull distribution, characterized by two parameters and a 95% confidence interval, is defined by equation (3.11).

$$F\left(x:\alpha,\beta\right)=1-\exp\left(-\left(\frac{x}{\alpha}\right)^{\beta}\right);x>0 \tag{3.11}$$

Where x signifies the DCBDV data, the function $F(x)$ corresponds to the cumulative density function, and the variables α and β represent the scale and shape parameters for this particular distribution. Tables 3.1 and 3.2 show scale (α) and shape (β) parameters obtained from Weibull probability plots of positive and negative DCBDV for various electrode shapes. Figure 3.7 depicts the electrodes that are used in this study. The dots on the electrode surface represent the specific region that experiences stress when subjected to an electric field exceeding 90% of the maximum electric field. Two dimensions are measured: one is the entire diameter of the electrode, and the other is the effective stressed diameter formed due to the application of DC voltages.

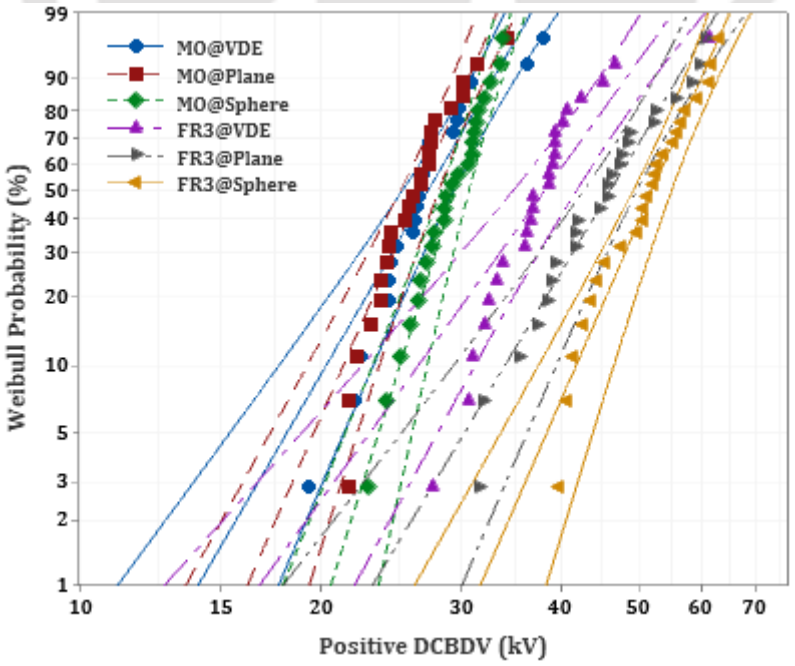

(a)

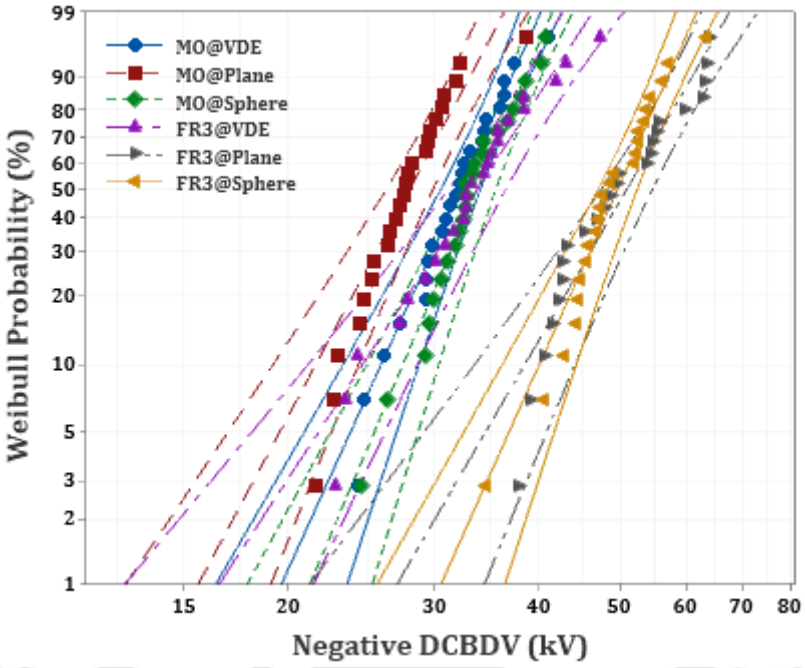

(b)

Fig. 3.6. Weibull distribution plot for (a) Positive DCBDV (b) Negative DCBDV of MO and FR3

The results from Tables 3.1 and 3.2 indicate that for MO in positive and negative DCBDV, the scale parameter (α) values are decreased with the increase in electrode stressed area; this shows the electrode area effect on dielectric strength of liquid insulation.

Table 3.1: Parameters of Weibull Distribution for Positive DCBDV

Electrode Shapes	MO		FR3	
	Scale Parameter (α)	Shape Parameter (β)	Scale Parameter (α)	Shape Parameter (β)
Sphere Electrodes	30.33	11.79	54.21	8.52
VDE	28.82	6.37	40.92	5.14
Plane Electrodes	27.71	8.51	48.81	6.17

Table 3.2: Parameters of Weibull Distribution for Negative DCBDV

Electrode Shapes	MO		FR3	
	Scale Parameter (α)	Shape Parameter (β)	Scale Parameter (α)	Shape Parameter (β)
Sphere Electrodes	35.05	9.17	51.69	8.70
VDE	33.58	8.57	35.81	5.95
Plane Electrodes	29.41	7.27	53.69	6.69

This trend is also observed in case of MO and FR3 under ACBDV for the same electrode configurations [133]. However, in positive and negative DCBDV of FR3 the scale parameters

of sphere and VDE electrodes follow the trend whereas in case of plane electrode the scale parameter is increased even though the effective area is increased from other two combinations. Table 3.3 shows the effective electrode stress area for various configurations of electrodes used in DCBDV tests.

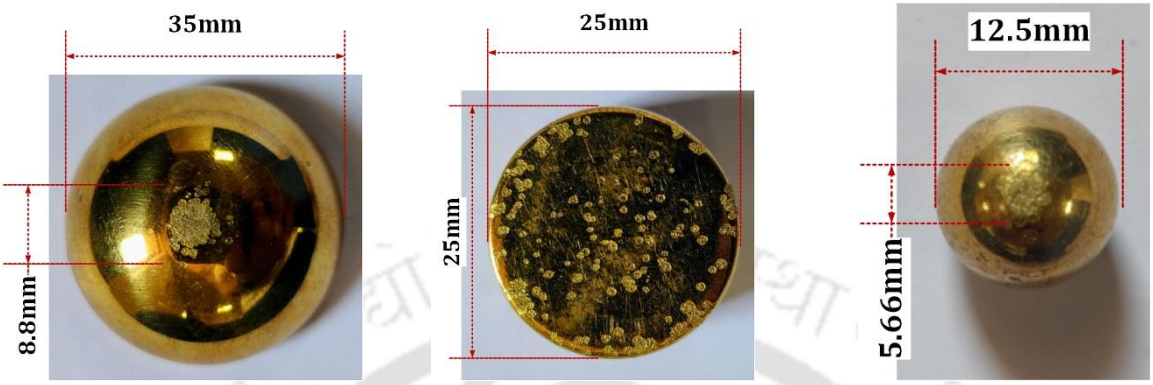

(a) (b) (c)

Fig. 3.7. Electrode configurations and EESA; a) VDE Electrodes (Total diameter: 35mm, stressed diameter: 8.8mm); b) Plane electrode (Total diameter: 25mm, stressed diameter: 25mm); c) Sphere electrode (Total diameter: 12.5mm, stressed diameter: 5.66mm)

Table 3.3: Configurations of electrodes used for DCBDV tests

	Sphere electrodes	VDE	Plane electrodes
Diameter of electrodes (mm)	12.5	35	25
Effective electrode stressed area (EESA) (mm^2)	2.55	6.16	490.87

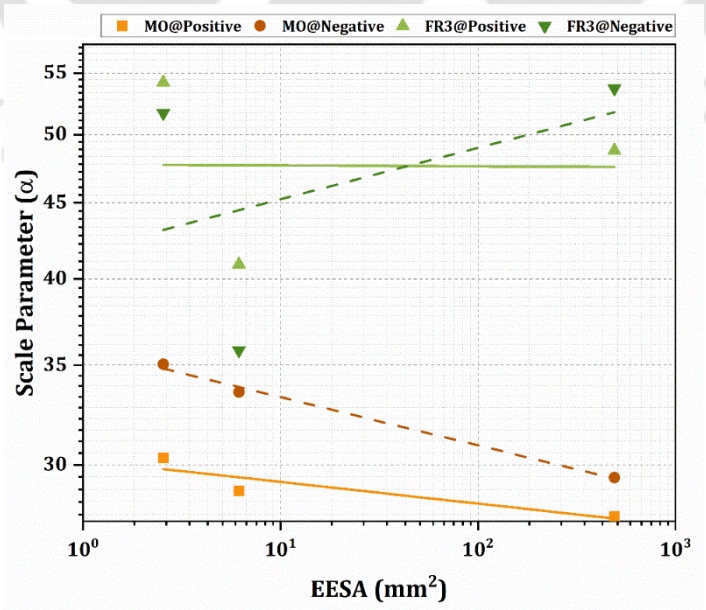

Fig. 3.8. Correlation plot of Scale parameter (α) and EESA (mm2) in logarithmic scale for various samples

Figure 3.8 showcases the relationship between the scale parameter (α) and the effective electrode stressed area (EESA), highlighting the impact of the electrode area. In most scenarios, the scale parameter (α) diminishes as the stressed area expands, signifying a distinct correlation. However, this trend is not observed for the negative DCBDV of FR3. The underlying reasons for these inconsistent results are elaborated upon in the following section. The graph employs a linear curve fitting method to represent the association between the scale parameter and EESA on a logarithmic scale. From these curves, area effect equations are formulated for each sample. The coefficients of scale parameters *a* and *b*, as presented in equation (3.12), are extracted from these equations and documented in Table 3.4.

$$\begin{cases} \log\left(\alpha_{\text{MO@Positive}}\right) = 1.4802 - 0.0145 \times \log(\text{H}) \\ \log\left(\alpha_{\text{MO@Negative}}\right) = 1.5550 - 0.0324 \times \log(\text{H}) \\ \log\left(\alpha_{\text{FR3@Positive}}\right) = 1.6789 - 0.0006 \times \log(\text{H}) \\ \log\left(\alpha_{\text{FR3@Negative}}\right) = 1.6209 + 0.0346 \times \log(\text{H}) \end{cases} \tag{3.12}$$

Table 3.4: Coefficients of Scale Parameters Calculated from linear fit curves

	a	b
MO@Positive	1.4802 ± 0.0112	0.0145 ± 0.0069
FR3@Positive	1.6789 ± 0.0825	0.0006 ± 0.0505
MO@Negative	1.5550 ± 0.0042	0.0324 ± 0.0026
FR3@Negative	1.6209 ± 0.1169	-0.0346 ± 0.0715

It is observed that the parameters as mentioned in Tables 3.1 and 2.2 of MO are larger than that of FR3 in both the polarities, and this trend of results is also observed in ACBDV data of MO and NEO [133]. These results indicate that the BDV of MO distributes narrower than FR3. From [133], [134] in the case of ACBDV, the scale and shape parameters of MO are larger than NEOs, wherein this study in DCBDV, the FR3 shows larger values in scale parameters, and MO shows larger values of shape parameters than FR3 in both polarities.

Table 3.5: Average Values, standard deviation and 90% Confidence Interval of Shape Parameter

Samples	β		
	Average	Std dev	90% Confidence Interval
MO@Positive	8.89	2.73	[2.116, 15.669]

FR3@Positive	6.61	1.74	[2.294, 10.922]
MO@Negative	8.34	0.97	[5.921, 10.751]
FR3@Negative	7.11	1.42	[3.582, 10.751]

Table 3.5 shows the samples average, standard deviation and 90% confidence interval of β. The DCBDV distribution of oil samples can be derived by placing the extrapolated scale parameter from Equation (3.12) and the mean shape parameter from Table 3.5 in Equation (3.1). The DCBDV distribution of MO and FR3 when stressed under electrode H is given by equation (3.13).

$$\begin{cases} R_{MO@Positive}(E) = 1 - \exp\left(-H^{0.13}\left(\frac{E}{30.2}\right)^{8.9}\right) \\ R_{MO@Negative}(E) = 1 - \exp\left(-H^{0.27}\left(\frac{E}{35.9}\right)^{8.3}\right) \\ R_{FR3@Positive}(E) = 1 - \exp\left(-H^{0.004}\left(\frac{E}{47.7}\right)^{6.6}\right) \\ R_{FR3@Negative}(E) = 1 - \exp\left(-\left(\frac{E}{40.08 + H^{0.0346}}\right)^{7.1}\right) \end{cases} \quad (3.13)$$

Electrode stressed area H has a unit of mm^2, and the applied voltage unit is kV/mm. Assuming a large electrode with a 1 m^2 effective electrode area, the average DCBDV at low probabilities (1% and 10%) is calculated using equation (3.12) and noted in Table 3.6. Also, to verify the results obtained from experiments, 490 mm^2 is assumed. From the Table 3.6, it can be observed that the DCBDV at lower probabilities for NEO is more than the MO in both polarities for larger and smaller electrode areas. In positive polarity the DCBDV of the MO and NEOs are significantly reduced with the increase in electrode effective stressed area and also it is observed that the positive BDV is greater than that of negative polarity. The calculated values are less than the experimental values as there might be the effect of moisture and contaminants in the oils.

Table 3.6: Calculated DCBDV Values at 10% and 1% Probability

Samples	DCBDV at 10% probability	DCBDV at 1% probability	DCBDV at 10% probability	DCBDV at 1% probability
	1 m^2 EESA		490 mm^2 EESA	
MO@Positive	19.167	14.720	21.424	16.453
FR3@Positive	33.636	23.560	33.792	23.669
MO@Negative	17.465	13.159	22.379	16.861
FR3@Negative	30.368	21.811	30.095	21.616

3.3.3. Comparison of the Influence of Electrode Area on the Breakdown Strength of MO and NEO-FR3 under DC Voltage Stresses with a 1mm Gap versus ACBDV Results.

Numerous studies, such as [133,134,138,139], have highlighted that AC breakdown strength of MO, NEOs, and synthetic ester oils decreases as the electrode surface area or the volume of liquid exposed to high electric field stresses increases. A crucial observation regarding the effect of area on breakdown strength is noted from [134], it is noticed that there are no visible variations in ACBDV for both MO and FR3 at a 1mm gap (i.e. almost the same voltage levels are maintained). However, a significant difference is evident between the two oils when considering DCBDV, with FR3 displaying a much higher breakdown strength. From the correlation plot between scale parameter and EESA shown in Figure 3.7, it is evident that MO consistently exhibits decreasing behavior under both positive and negative polarity. Figure 4.4 shows that the average DCBDV for MO, in both positive and negative polarities, follows the sequence: $DCBDV_{Sphere} > DCBDV_{VDE} > DCBDV_{Plane.}$ It is same as observed in case of ACBDV at 1mm gap with the increase in EESA [133]. In case of FR3, the scale parameter remains relatively stable across increasing area, indicating a minimal change in positive DCBDV. However, for negative DCBDV, the scale parameter increases with the increase of stressed electrode area. The positive DCBDV of FR3 decreases in the order of $DCBDV_{Sphere} > DCBDV_{Plane} > DCBDV_{VDE}$, while for negative polarity it is $DCBDV_{Plane} > DCBDV_{Sphere} > DCBDV_{VDE}$.

3.4. Summary of the chapter

In this chapter, the effects of EESA on the dielectric strength of NEOs under DC stresses are investigated. A thorough experimental investigation revealed that the electrode-stressed area has a substantial effect on the dielectric strength of the oils. The larger stressed area permitted a more uniform distribution of electrical stress within the oils, enabling a greater number of load-bearing elements (i.e. oil molecules, suspended particles, and any additives) to withstand failure. Contributing to the advancement of high-voltage applications, these findings offer important insights for the design and optimization of insulation systems utilizing natural ester oils. Some of the significant conclusions drawn from this study are as follows:

a) From experimental results, it is observed that the average DCBDV of both MO and FR3 for positive polarity sphere electrode configuration at a 1 mm gap is higher, followed by plane and VDE configurations for positive polarity and in case of negative polarity the same pattern is followed for MO where in for FR3 the plane electrode configurations show a larger average DCBDV followed by sphere and VDE.

b) The findings of this study indicate that the scale parameter (α) values of MO and FR3 are observed in the following patterns: For MO Positive and negative polarities $DCBDV_{Sphere}$ > $DCBDV_{VDE}$ > $DCBDV_{Plane}$; For FR3 positive it is $DCBDV_{Sphere}$ > $DCBDV_{Plane}$ > $DCBDV_{VDE,}$ wherein for negative polarity the pattern observed is $DCBDV_{Plane}$ > $DCBDV_{Sphere}$ > $DCBDV_{VDE}$.

c) Observations from calculated average DCBDV at 10% and 1% failure probability include higher DCBDV probabilities for NEO compared to MO at smaller and larger electrode areas.

These findings highlight the significance of electrode-stressed areas for comprehending the dielectric behaviour of natural ester oils in DC voltage stresses.

This chapter delves into the geometric effects impacting the breakdown strength to enhance the accuracy of BDV measurements in both fresh oils and oil immersed pressboards with various electrode type and shapes. However, while Chapter 2 highlighted the significance of ageing in the long-term reliability of MO and FR3, it did not explore the effects of ageing on solid insulation, which is equally crucial. Thus, the next chapter will delve into the effects of ageing on solid insulation, considering that solid insulation plays a pivotal role alongside liquid insulation. The chapter will investigate the DCBDV of solid insulation in conjunction with its thermal stability, chemical changes, and mechanical changes over time.

Note: *This work is submitted to*

D. Kanumuri, A. Kumar, N. Baruah and S. K. Nayak, " Effects of Electrode Geometry on Dielectric Breakdown Strength of Natural Ester Oils for HVDC Applications," is submitted in ***IEEE Transactions on Dielectrics and Electrical Insulation,*** Jan. 2025. [**Under Review**]

4

Study of oxidative ageing and thermal ageing effects on natural ester oil immersed solid insulation

Contents

4.1	Introduction ……...……...	95
4.2	Materials and methodology…...……..…...……	98
4.3	Results and Discussion.....……....…….....	104
4.4	Summary of the chapter …..……	117

4.1. Introduction

Mineral oil (MO) is extracted from petroleum, a non-renewable resource that may run out in the future [10]. Currently, utilities and other industries are interested in using natural ester-based insulating oils (NEOs) as alternatives to MO. It is primarily because of the presence of corrosive sulphur in MO, environmental concerns and the longevity of solid insulation lifetime in NEOs compared to MO. Studies have shown that the condition of oil–paper insulation significantly impacts the in-service power transformers reliability [140-142]. In the current economic context, examining the state of the oil-impregnated paper (OIP) primarily utilized as transformer insulation is essential. With increasing age, the likelihood of incurring significant monetary losses due to increase of unanticipated breakdowns and outages. Hence, the fundamental purpose is to achieve the longest possible service life with the lowest possible lifetime operational costs and to provide appropriate routine maintenance for transformer inspection, repairs, and replacement.

In the area of sustainable and renewable energy solutions, significant progress has been made in the development and application of natural ester oils in electrical transformers. The utility of NEOs as a greener alternative to traditional mineral oils has been extensively reviewed and researched in various studies. Wani et al. [143] and Rafiq et al. [144] delve into the advances in transformer condition monitoring and the use of vegetable oils, respectively, highlighting the shift towards more sustainable practices. Further, the work of Shanmugasundram et al. [145] provides a comprehensive classification of dielectric composites, essential for understanding the role of different insulating materials in transformer technology. Karatas and Bicen [146] explore the potential of nanoparticles in next-generation transformer insulating fluids, opening doors to innovative approaches in transformer technology. In a similar vein, the studies by de Faria Jr et al. [147] and Christina et al. [148] review various monitoring methods and diagnostic techniques for transformers, emphasizing the importance of predictive maintenance and failure analysis. Mariprasath and Kirubakaran [149] provide a critical review of alternating liquid dielectrics, including an interesting feasibility study on pongamia pinnata oil. The evolution of transformer health indices has been meticulously documented by Azmi et al. [150], offering valuable insights into the mathematical aspects of transformer health monitoring. Shen et al. [151] provide a critical review of plant-based insulating fluids, marking a 30-year development in this field and underscoring the shift towards more eco-friendly options. Finally, Das et al. [152] discuss

the use of coconut oil for utility transformers, presenting an intriguing perspective on environmental safety and sustainability.

Building on the foundation established by above studies, there is an emerging need to focus the research on solid insulation within transformers, particularly in the context of NEOs. This aspect of transformer technology is crucial as solid insulation plays a pivotal role in the overall performance and longevity of transformers. The interaction between solid insulation and NEOs in a transformer, especially under varying operational and environmental conditions, remains a vital area of study. This chapter aims to bridge this gap by specifically addressing the performance and characteristics of solid insulation in HVDC transformers when immersed in NEOs. Through, it seeks to enhance our understanding of the compatibility, efficiency, and reliability of solid insulation materials in harmony with sustainable and renewable insulating fluids. Transformer solid insulation is an insulation of electrical grade, also known as Kraft paper, cellulose, transformer board, and pressboard. Generally, unbleached sulphate cellulose is used to construct this product. As shown in Figure 4.1, they are composed of cross-linked cellulose fibre, with glucose as the monomer. In its dry state, the cellulose insulation has air pockets or spaces. When impregnated with an insulating oil, the air spaces become saturated with the oil enhancing the dielectric characteristics of the insulation made from cellulose. Consequently, insulating oil considerably affects the durability and longevity of the cellulose insulation. Oil degradation enhances cellulose deterioration by producing acids and other corrosive compounds. The oils ability of the insulating oil to retain moisture considerably impacts durability of cellulose [153]. Power transformers use insulating oil for two main reasons: (1) to dissipate heat generated by hotspots in windings during operating conditions and (2) to improve the dielectric properties of solid insulation by impregnation. The deterioration or ageing of insulating oil is typically connected with oxidation in a hostile environment. Electrical stress, heat, moisture, and catalysts, such as oxygen from air and copper, lead to oxidation of insulating oil, creating free radicals, acids, and sludge [154].

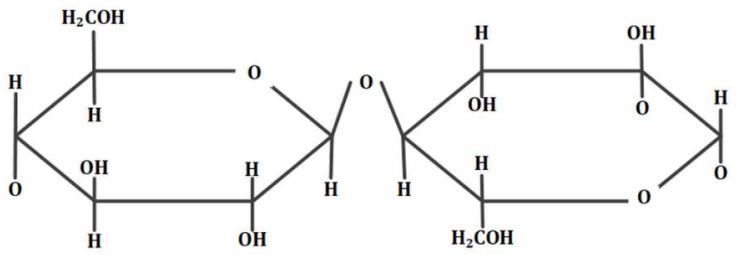

Fig. 4.1. Chemical structure of cellulose polymer

As the transformer ages in service, the oil becomes increasingly contaminated. Contaminants include particulate debris resulting from thermal, electrical, or oxidative deterioration of oil or fibres, solid insulation, and moisture, among others. The final phase of liquid degradation is characterized by acid content and sludge in sufficient quantities to compromise its heat transmission and dielectric properties. The large surface area of the paper absorbs colloidal suspensions and acids. They attack the cellulose fibre and metals, forming metallic lacquers, soaps, aldehydes, ketones, and alcohols, which are drawn to the windings by the strong electromagnetic field of the core and form a heavy, tarry, acidic sludge on the solid insulation [155-158]. These chemically reactive mediators are more concentrated in the windings than at the tank-bottom due to electromagnetic attraction. The degradation of solid insulation is closely related to its mechanical integrity.

Researchers have conducted some research on the degradation of solid insulation worldwide. Using FTIR and EDS analysis, Munajad A [159] examine the effects of accelerated thermal ageing at 120°C and 150°C for 336 hrs, 672 hrs, and 1008 hrs on insulating paper immersed in natural ester oil. Nasrat Loai S [160] examined the AC breakdown voltage, tensile strength, and water content of insulation papers immersed in mineral oil for various time periods such as 48, 72, and 96 hours at a confined temperature of 110°C to 170°C. Using TGA, SEM, and XRD techniques, Suwarno [161] investigated the deterioration of Kraft paper immersed in mineral oil and gas-to-liquid (GTL) dielectrics during accelerated ageing at 120°C and 150°C for up to 1344 hours in the controlled oven. Similarly, FTIR, DP, and XRD are used to study the influence of gelling in natural esters and insulating paper during open-beaker accelerated thermal aging [162]. In each of these studies, the deterioration of insulating paper in MO, NEOs, and GTL is investigated using various characterization techniques. In addition to cellulose Kraft paper, transformers contain pressboard insulation, which provides mechanical strength. Pressboard insulation with natural ester and mineral oil is analyzed for its physicochemical, dielectric, and thermal properties using moisture and acid content, ACBDV, and TGA [163]. Fofana I. et.al. [164] performed a study on the characterization of ageing of transformer mineral oil-pressboard insulation using common chemical diagnostics such as acidity tests and new chemical techniques such as spectrophotometry, turbidimetry, FTIR and polarisation-depolarisation current, recovery voltage measurement, and FDS measurements.

However, as the effects of oxidative and accelerated thermal ageing on transformer pressboard have yet to be extensively explored. This research will provide a detailed evaluation of cellulose pressboard as it run through an extended period of operation and the effect of degradation on DCBDV of solid insulation for HVDC transformers. Consequently, it is essential to evaluate the degradation of solid insulation in the presence of oxygen and heat. This work used an open-beaker oxidative ageing apparatus to age cellulose Kraft pressboard, a key aspect for providing transformers with insulation and mechanical robustness. In addition, these samples of pressboard are aged for 90, 200, and 500 hours in traditional MO and NEO before being collected and processed for further examination. These Kraft pressboard samples are evaluated for oxidative ageing effects on solid insulation following the ageing process. Utilizing Fourier transform infrared spectroscopy (FTIR) and Thermogravimetric analysis (TGA), the degradation of the pressboard is investigated. As a result of this deterioration, tensile strength testing is also carried out to assess the impact on mechanical strength. In addition, the AC and DC breakdown voltages of pressboards are utilized to investigate the impact of degradation on electrical strength of pressboards. Although extensive research has been conducted on thermally aged solid insulation for comparison this study focuses on preparing thermally aged samples under the same conditions as oxidatively aged samples, specifically for 90, 200, and 500 hours.

4.2. Materials and Methodology

4.2.1. Sample preparation

MO and FR3 (NEO) insulating base oils used for the present study are obtained from Savita Industries and Cargill India Pvt. Ltd. respectively. The pressboard of 1.5 mm thickness which is used in the present investigation are procured from Power Maker Pvt Ltd, Guwahati.

4.2.1.1. Preparation of oxidatively aged pressboard samples

These samples are aged using an in-house built open beaker oxidative ageing setup (OBOA) as per ASTM D1934 [100]. Before ageing the samples, the Kraft pressboard is dried for 24 hours in a vacuum oven at 80°C. Similarly, oil samples are kept for 48 hours at 65°C in a vacuum oven [89] to remove moisture present in these samples. In addition to the aged samples, non-immersed pressboards and pressboards immersed in Fresh MO and FR3 oil are prepared for comparison. All these fresh oil impregnated samples are prepared by placing them in a 300 ml open beaker filled with fresh base oils, pressboard and copper catalyst in 20:1:1 ratio [93,119]. Fresh oil-pressboard samples are placed in a vacuum oven at 560

mmHg at room temperature (i.e., 26°C) for 48 hours [165] to impregnate, and the collected samples are sealed in an airtight plastic bag.

(a) (b) (c)

Fig. 4.2. a) Open beaker oxidative ageing setup b) open beakers with samples are placed in the oven c) 300 ml beaker with 20:1:1 base oil to solid to copper samples

As depicted in Figure 4.2, the oxidative ageing effect on MO and FR3 samples is obtained using an OBOA apparatus following ASTM D1934. This ageing oven consists of a platform on which open beakers with a 300 mL capacity are positioned. In order to simulate the conditions of a real-time transformer, the oil samples are mixed with a ratio of 20:1:1 [93,119] of oil to solid insulation and a copper catalyst. The oven temperature is maintained at 115±1°C, and ageing is performed at a steady temperature for 90, 200, and 500 hours. Upon completion of the ageing period, aged MO and FR3 immersed pressboard samples are collected and stored in an airtight bag.

4.2.1.2. Preparation of thermally aged pressboard samples

The thermal ageing process for both the oil samples involves vacuum drying and the elimination of dissolved gases. The experiment takes place within a dedicated hermetically sealed chamber with a capacity of 1.5 litres to prevent air exchange as depicted in Figure 4.3. Before ageing, the kraft paper and oils undergo vacuum drying at 80°C for 24 hours, and 60°C for 48 hours respectively to eliminate the residual moisture. Accelerated thermal ageing employs a composite mixture of oil, pressboard, and copper in a weight ratio 20:1:1 [93,119]. A copper spiral conductor is introduced into the oil as a catalyst to expedite the degradation. The accelerated thermal ageing process follows the guidelines of IEEE C57.100-1999 [101] standard. As per this standard, the temperature inside the chamber is carefully maintained at 125°C±2°C. Since MO is one of the samples in this investigation and its flash point is

approximately 140℃, the temperature of 125°C±2℃ is chosen for the thermal ageing of the MO and FR3 to ensure a fair comparison. The oil samples undergo accelerated thermal ageing for specific durations of 90, 200, and 500 hours. After each specified time, thermally aged pressboard samples are collected and placed in air tight bag.

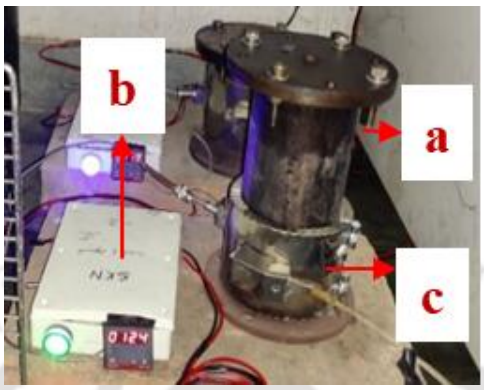

Fig. 4.3. Accelerated thermal ageing setup (a) hermatically sealed tube (b) temperature controller (c) band heater with thermocouple.

4.2.2. Experimental methodology

4.2.2.1. TGA analysis

Thermogravimetric (TG) and derivative thermogravimetric (DTG) studies are used to measure the amount and frequency of the weight variation of samples vs. temperature and time in a controlled atmosphere (e.g., nitrogen gas, helium, etc.) [166]. TG and DTG are primarily used to examine the thermal stability (the strength of the material at a particular temperature), oxidative stabilities (the oxygen absorption rate on the material), and compositional features (e.g., polymer resin, fillers, solvents) of samples. Also, the weight gain or loss of the samples is caused by different factors. Most of the time, adsorption or oxidation is the reason for weight gain, while decomposition, dehydration, desorption, volatilization, or desolvation are the reasons for weight loss [167–168]. As illustrated in Figure 4.4, cellulose pressboard thermal degradation properties are analysed using a thermogravimetric analyser. A computer is utilised to monitor and control the temperature and heat flow. After oil separation, 9.5 mg of pressboard samples are inserted into a TG analyser. The sample is heated in a high-temperature furnace with a heating temperature range between 30-900°C and a heating rate of 20°C per minute. The measurement is conducted in a contained environment of helium gas.

Fig. 4.4. Thermogravimetric analyser (Model No.: TG 209 F1 Libra; Make: M/s Netzsch, Germany)

4.2.2.2. Fourier Transform Infrared Spectroscopy (FTIR)

Electromagnetic radiation absorbed, reflected, transmitted, and dispersed offers information about molecular structure and energy level transition of a substance. Positioned in the path of an infrared beam, pressboard samples absorb and transmit light, which then passes through the sample to the detector. The detector detects the intensity of the radiation entering and transmitting through a sample. Figure 4.5 illustrates the FTIR spectrophotometer, whose output as a function of time is transformed by a computer using the Fourier transform method [35] into a plot of absorption vs wavenumber. In this work, FTIR uses attenuated total reflection (ATR) to explore the structural changes in cellulose pressboard caused by ageing. This measurement required just small batches of transformer pressboard samples, and each sample is examined twice to ensure accurate infrared spectra. The observed spectra represent the absorbance of various pressboard samples versus the range of wavenumbers from 4000–400cm^{-1}.

Fig. 4.5. FTIR Spectrophotometer (Make: PerkinElmer, Model: Spectrum Two)

4.2.2.3. Tensile strength measurement

Kraft pressboard primarily consists of cellulose fibres of a polymeric chain of cellulose synthesized from d-glucose monomers. The breakage of the cellulose polymer causes a

decrease in mechanical strength by water, oxygen, temperature, and, most likely, acids. The degree of polymerization (DP) refers to the number of d-glucose monomers in the cellulose fibre. Typically, the cellulose polymer of newly impregnated pressboard contains 1,000 and 1,100 monomers [170].

Fig. 4.6. 250 KN Servo Hydraulic Universal Testing Machine (Make: BISS, Model: MEDIAN 250) with pressboard sample

There is a relationship between mechanical strength and DP, and the degradation of the pressboard samples is affected mainly by moisture, ageing time, and ageing temperature [171]. Therefore, it is essential to examine the tensile strength to determine the degree of pressboard degradation owing to oxidative and thermal ageing. As illustrated in Figure 5.6, the tensile strength was measured using a 250 KN Servo Hydraulic Universal Testing Machine. All the samples are maintained with dimensions of 50 mm×35 mm (length × width), gauge length of 30 mm, and a thickness of 1.5 mm. A load of 50 KN is applied at a rate of 5 mm/min at room temperature.

4.2.2.4. Dielectric strength testing on oil immersed pressboards

In high-voltage transformers, both the liquid and solid insulation deteriorate over time. This study investigates the deterioration of solid pressboard due to ageing. Solid insulation

loses its mechanical and electrical properties as deterioration advances. Electrical strength is the most essential and critical characteristic to consider. This section evaluates the electrical breakdown strength of oxidatively and thermally aged pressboard samples immersed in MO and FR3. ACBDV and DCBDV are investigated on freshly immersed and oxidatively aged pressboard in both MO and FR3 oils. Figures 4.7b and 4.7c demonstrate the AC and DC breakdown voltage experimental setup, respectively. Figure 4.7a depicts the test cell used for the solid insulation breakdown study, corresponding to the standard ASTM D1816 – 12 [38].

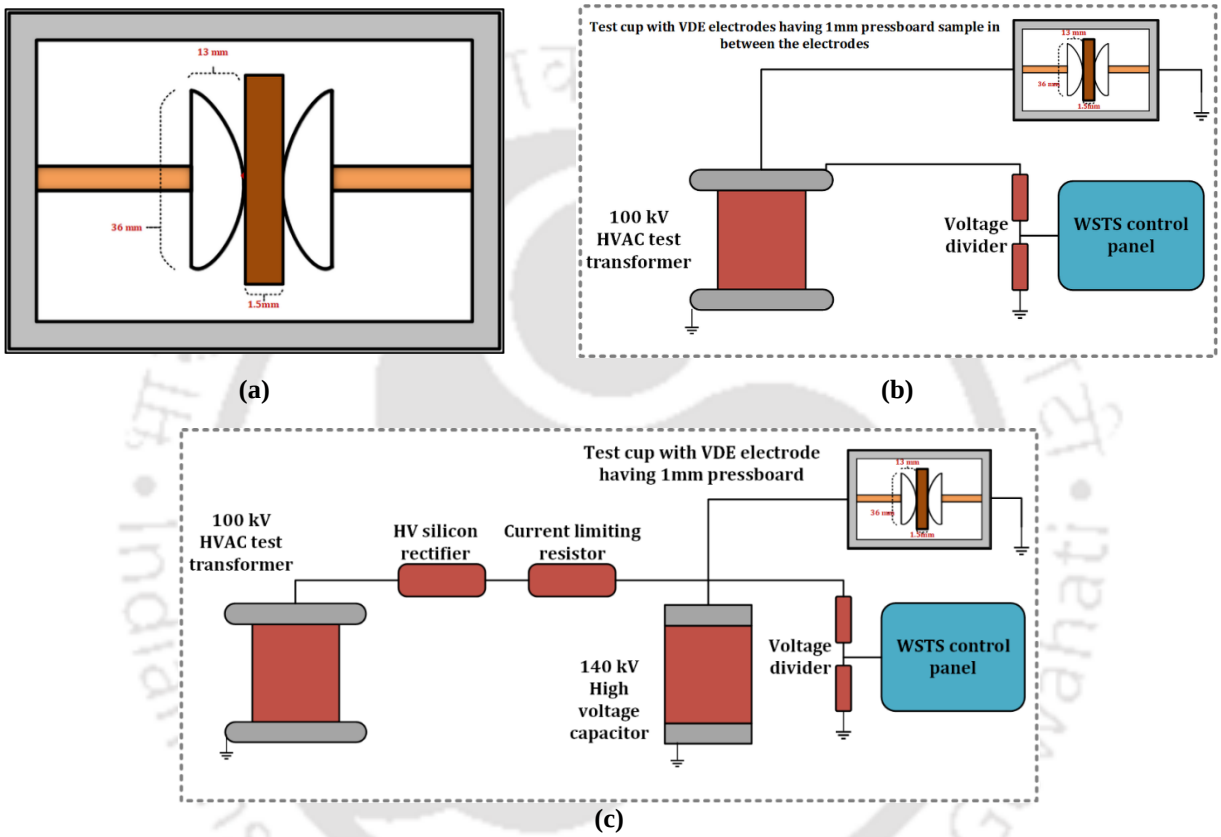

Fig. 4.7. a) Test cup arrangement for solid insulation breakdown with VDE electrodes; b) Experimental setup for ACBDV of solid insulation samples; c) Experimental setup for DCBDV of solid insulation samples

A pressboard with a thickness of 1.5 mm is positioned between two VDE electrodes in this study. Since the breakdown strength of the aged pressboard alone must be assessed, the test cup is filled with fresh MO and FR3 oil which is beneficial for comparing the breakdown strength of aged pressboards. All the MO-impregnated aged pressboards are immersed in the MO-filled test cell, while the FR3-impregnated aged pressboards are immersed in the FR3-filled test cell. Once the samples have been placed in the test cell, it is attached to a WSTS high voltage generation setup with 100kV AC and 140kV DC generation capacities. Positive and negative polarity effects on aged pressboard are determined for DCBDV. These data are

utilised to analyse the influence of oxidative ageing on pressboard degradation, which ultimately leads to the failure of electrical properties.

4.3. Results and Discussion

4.3.1. Experimental Results of TGA Analysis of Oil Immersed Pressboard

Figures 4.8 presents the comparison results of TGA conducted on non-immersed kraft pressboard, with the samples aged in MO and FR3 oils, respectively. The horizontal axis represents temperature in ℃ and the vertical axis represents the percentage of weight loss. The thermogravimetric method is utilized to assess various aspects such as polymer residue, moisture content, oxidation levels, vaporization, and thermal stability of the materials [172]. The TGA curve specifically shows the percentage of mass loss as it varies with temperature. Based on the degradation process of Kraft pressboard, as depicted by the TGA and DTG curves, is classified into three distinct stages. Stage I, ranging from 30°C to 100°C, exhibits minimal mass loss in non-immersed pressboard. Between 100°C and 300°C, there is a nearly constant rate of mass loss, about 90%, marking the completion of the first stage. Stage II is observed between 300°C and 400°C, where the mass loss drops from 90% to 15%. Stage III occurs between 400°C and 900°C, during which the rate of mass loss slows down, decreasing from 15% to almost zero for non-immersed pressboard. Throughout these stages, different components of the pressboard undergo decomposition. In the initial stage (i.e. Stage I), from 30°C to 300°C, water loss is noted around 100°C, signifying the start of thermal breakdown with the vaporization of water. In this stage, hemicellulose, which typically decomposes at temperatures ranging from 150℃ to 350℃, is primarily responsible for most of the degradation. This is in contrast to cellulose, which begins to decompose at temperatures between 250℃ and 300℃. The second stage (i.e. Stage II) involves the further deterioration of cellulose, occurring between 300℃ and 400℃. Lastly, in stage III, which spans from 400℃ to 900℃, degradation occurs primarily due to the decomposition of lignin [161]. Figures 4.8a and 4.8b display the temperature-induced mass loss of Kraft pressboard immersed and aged in MO and FR3 oil, respectively. Figure 4.8a clearly shows that the MO-immersed pressboard samples exhibit lower thermal stability throughout the temperature range compared to non-immersed samples. For the non-immersed pressboard, the mass loss remains steady at 90% from 100 to 300°C. In contrast, for MO-immersed samples with different aging durations, the mass loss starts at 150°C and reaches 70% before progressing to stage II. During stage I, non-aged samples show a slight advantage in mass loss compared to

those aged for longer periods. In stage II, all samples, regardless of their aging status, undergo the same level of mass reduction. Stage III is characterized by a very slow mass loss for all samples, with those aged for 500 hours and 200 hours showing a slower mass loss rate compared to the fresh and 90-hour aged samples. A similar analysis is conducted for pressboard samples immersed in FR3 and subjected to oxidative aging.

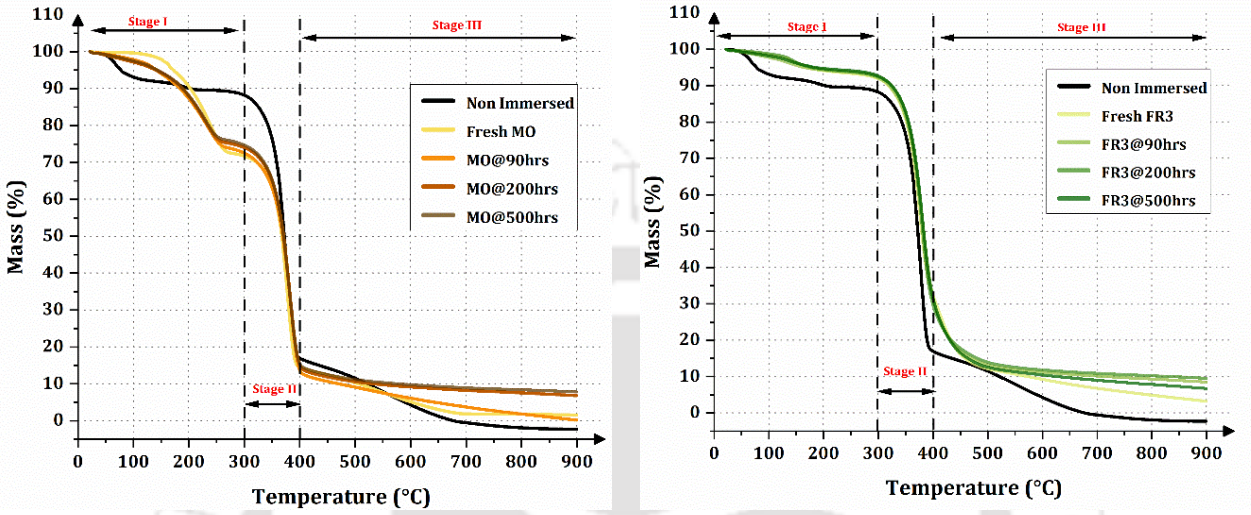

Fig. 4.8. Mass (%) vs Temperature (°C) of oxidatively aged of (a) MO immersed pressboard samples; b) FR3 immersed pressboard samples

Pressboard samples immersed and aged in FR3 oil demonstrate a comparatively lower percentage of mass loss across the temperature spectrum when compared to those non-immersed, fresh oil immersed and aged pressboards in MO. Each FR3 immersed sample, regardless of aging duration, shows a consistent mass loss pattern. In Stage I, the mass loss in FR3 immersed pressboard samples is notably higher than the pressboard immersed in MO samples, remaining above 90% up to 300°C. Moving into stage II, there is a reduction in mass from 90% to 30% from 300-400°C, with FR3 immersed pressboard displaying enhanced thermal stability conditions of the pressboard by 50°C to 20% when compared to MO immersed pressboard samples. Stage III reveals properties similar to those observed in MO-immersed pressboards. The enhanced thermal stability in FR3-impregnated and aged pressboard samples is likely due to FR3's capacity to retain moisture, thereby mitigating the aging effects on the pressboards. Nevertheless, the peak temperature for non-immersed pressboard is higher than that for the aged oils in both cases. Moreover, when compared with oxidatively aged cellulose papers, pressboards display greater thermal stability [173].

Similarly, for thermally aged pressboard samples, same testing conditions as OBOA samples are used. The TGA graphs of MO and FR3 with thermally accelerated ageing reveal

their thermal stability and decomposition behaviour under different conditions such as non-immersed, fresh, and aged for 90, 200, and 500 hours as illustrated in Figure 4.9. For MO, in Stage I (0-300°C), there is mass loss for fresh and aged samples is approximately 30% (i.e from 100% to 70% of mass reduction), attributed to the evaporation of moisture and light volatile components, indicating low volatile content. In Stage II (300-400°C), significant mass loss occurs with fresh MO decomposing rapidly around 300°C. The aged samples follow a similar trend with slight variations in onset and extent, suggesting primary decomposition of MO components and the presence of oxidation products due to ageing. In Stage III (400-900°C), the mass loss rate decreases, with all samples continuing to decompose and stabilizing around 600°C, with aged samples retaining slightly more mass, indicating the formation of thermally stable residues.

For FR3 immersed pressboard, Stage I (0-300°C) shows minimal mass loss of only 10%. In Stage II (300-400°C), significant mass loss is observed with fresh FR3 starting to decompose around 300°C and aged samples exhibiting earlier decomposition due to ageing-induced chemical changes from 90% to 30%. In Stage III (400-900°C), the mass loss rate decreases, with decomposition stabilizing around 600°C and aged samples retaining higher mass same as MO.

FR3 shows superior properties compared to MO in these TGA. This is evident as FR3 exhibits a more gradual and less pronounced mass loss in Stage II (300-400°C) compared to MO, indicating better thermal stability and slower decomposition. Additionally, in Stage III (400-900°C), FR3 retains a higher mass than MO, particularly in aged samples, suggesting that FR3 forms more thermally stable residues during ageing. These properties make FR3 more resistant to thermal degradation and better suited for applications requiring high thermal stability and longevity under thermal stress.

When comparing the differences in thermal stability between thermal ageing and oxidative ageing of MO immersed pressboard, all fresh and aged samples exhibit the same mass reduction in Stage I, as shown in Figure 4.8a. However, for thermally aged MO, the immersed pressboard samples exhibit less mass reduction, only up to 80%, indicating that thermal ageing has a lesser impact on MO than oxidative ageing. In Stage II, oxidative ageing results in a mass reduction of 10-15%, whereas thermally aged samples show a comparatively lower mass reduction of around 20%. Similar trends are observed in Stage III. Overall, these findings demonstrate that oxidative ageing has a more significant effect on the thermal

stability of MO compared to thermal ageing. In case of FR3 in stages I, II and III in thermally aged samples there is a 5% more mass reduction than oxidatively aged samples as seen in Figures 4.8b and 4.9b. This shows that thermal ageing has high impact on FR3 than on MO.

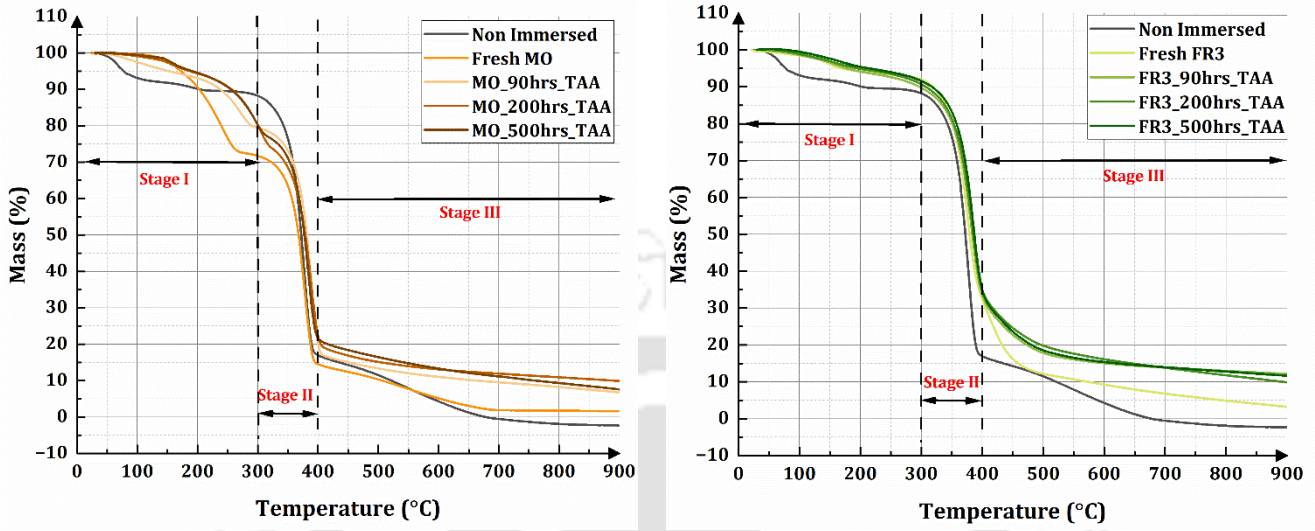

Fig. 4.9. Mass (%) vs Temperature (°C) of thermally aged (a) MO immersed pressboard samples; b) FR3 immersed pressboard samples

The FR3 immersed pressboard has superior thermal stability compared to MO immersed pressboard in maintaining structural integrity and performance over extended periods of thermal exposure, for both oxidative and thermal ageing making it a more robust and reliable option in thermal management applications.

4.3.2. Experimental Results of FTIR of Oil Immersed Pressboard

The FTIR analysis demonstrates significant changes in the chemical composition of cellulose Kraft pressboard due to oxidative aging in MO and NEO-FR3. This method provides insights into the degradation effects on the composition of cellulose Kraft pressboard. Figure 4.10 depicts the FTIR spectra for non-immersed, fresh oil-immersed, and oxidatively aged pressboard in both MO and FR3, highlighting the changes in the chemical structure of transformer pressboard insulation which is indicated by the variations in peak absorbance intensity of different functional groups. This figure presents the FTIR spectra for pressboard insulation after undergoing oxidative ageing in MO and FR3 at 115°C over periods of 90, 200, and 500 hours. In Figure 4.11, the peak absorbance intensities of various samples of transformer pressboard insulation are presented. According to available literature, these spectra are categorized based on specific functional groups. These include peaks around 3200 cm^{-1} corresponding to O-H groups, 2900 cm^{-1} for CH groups, 1750 cm^{-1} associated with

C=O groups of esters, and 1200 cm^{-1} for C-O groups [174-175]. These spectra allow for the examination of oxidative ageing mechanisms in pressboard, such as hydrolysis of natural ester, transesterification, and oxidation of transformer insulation paper.

Figure 4.12 displays the detailed FTIR spectra for transformer pressboard insulation undergoing oxidative aging in MO and FR3 at 115°C, with a focus on absorbance peaks around 2900 cm^{-1}. The absorbance peak observed in non-immersed pressboard insulation is comparatively lower than that in both aged and freshly oil-immersed samples, indicating the absence of structural deterioration. However, when the pressboard samples are immersed in fresh mineral oil (MO) and FR3 oil, there is an enhancement in absorbance, reaching levels of 0.13 a.u. and 0.15 a.u., respectively. But, the intensity of C-H group absorbance peaks has increased with ageing duration, possibly due to the absorption of MO and FR3 to the pressboard surface during aging. This increase is linked to the hydrolysis in FR3 and the transesterification process in transformer insulating paper, which leads to the degradation of triglycerides into glycerol and fatty acids [176]. Fatty acids, with their long alkyl chains comprising C-H groups, bond to cellulose, resulting in the trans-esterified cellulose polymer. Similarly, in the case of MO-immersed samples, the absorbance range due to the C-H group is significantly greater than that of FR3-immersed pressboard samples, indicating a higher level of deterioration.

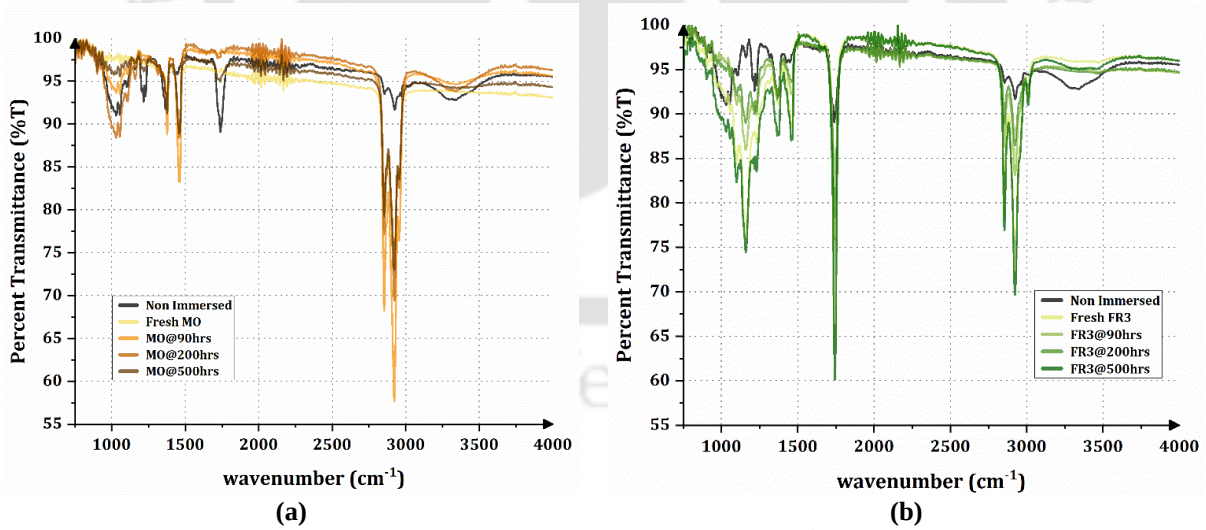

Fig. 4.10. Percentage transmittance (%T) vs wavenumber (cm^{-1}) of (a) MO immersed pressboard samples; b) FR3 immersed pressboard samples

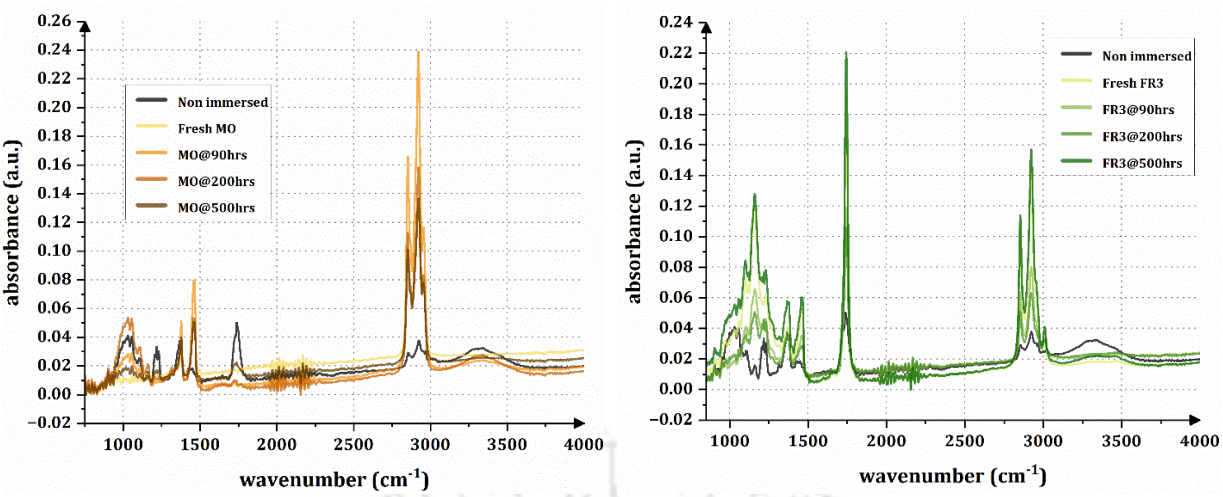

(a) (b)

Fig. 4.11. Absorbance (a.u.) vs wavenumber (cm^{-1}) of (a) MO immersed pressboard samples; b) FR3 immersed pressboard samples

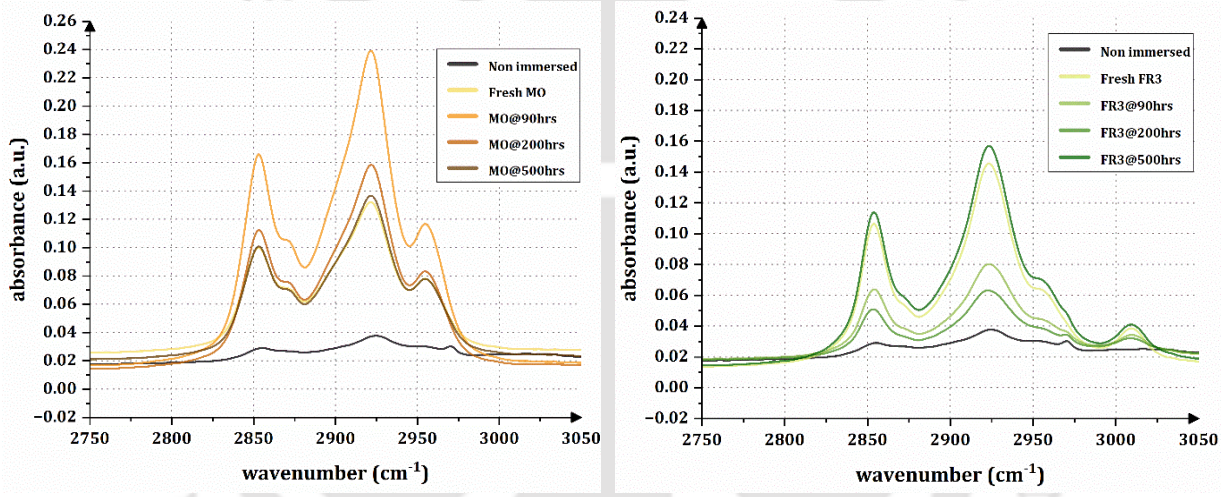

(a) (b)

Fig. 4.12. Absorbance (a.u.) vs wavenumber (cm^{-1}) of (a) MO immersed pressboard samples at a range of 2800-3000 cm^{-1}; b) FR3 immersed pressboard samples at a range of 2800-3000 cm^{-1}

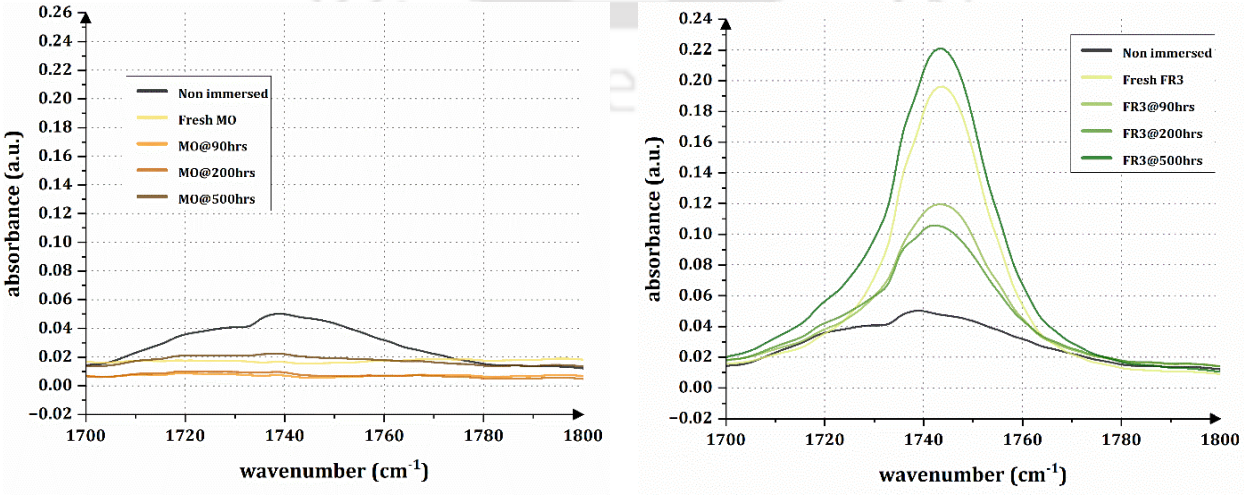

(a) (b)

Fig. 4.13. Absorbance (a.u.) vs wavenumber (cm^{-1}) of (a) MO immersed pressboard samples at 1700 cm^{-1}; b) FR3 immersed pressboard samples at 1700 cm^{-1}

Figure 4.13 presents the FTIR spectra for transformer pressboard insulation subjected to oxidative ageing at 115°C in MO and FR3, focusing on the peak around 1750 cm-1. The observed peak absorbance at 1743 cm-1, which corresponds to the C=O groups, increases with the age of insulation. This particular carbonyl band is indicative of an ester-cellulose linkage, thereby confirming the occurrence of transesterification [177]. This peak serves as indirect evidence of the transesterification process in transformer insulating paper using NEO, where the long alkyl chains of fatty acids bond with the cellulose polymer, forming a trans-esterified cellulose polymer. This transesterification process, which involves bonding fatty acids long alkyl chains with cellulose, is believed to preserve the cellulose insulation from degradation and create a barrier against water penetration [175]. In contrast, the pressboard immersed in MO shows completely flat peaks, indicating no significant impact of the carbonyl group. The intensity of this peak suggests that FR3 offers considerable protection to the cellulose components of the pressboard, especially in terms of reducing water absorption, when compared to its counterpart immersed in MO. In Figure 4.14, the FTIR spectra of pressboard subjected to oxidative ageing in FR3 and MO at 115°C are shown, with a notable absorption around 900-1500 cm^{-1}. These peaks are associated with the C-O groups, is more intense in aged transformer insulation paper compared to fresh insulation paper.

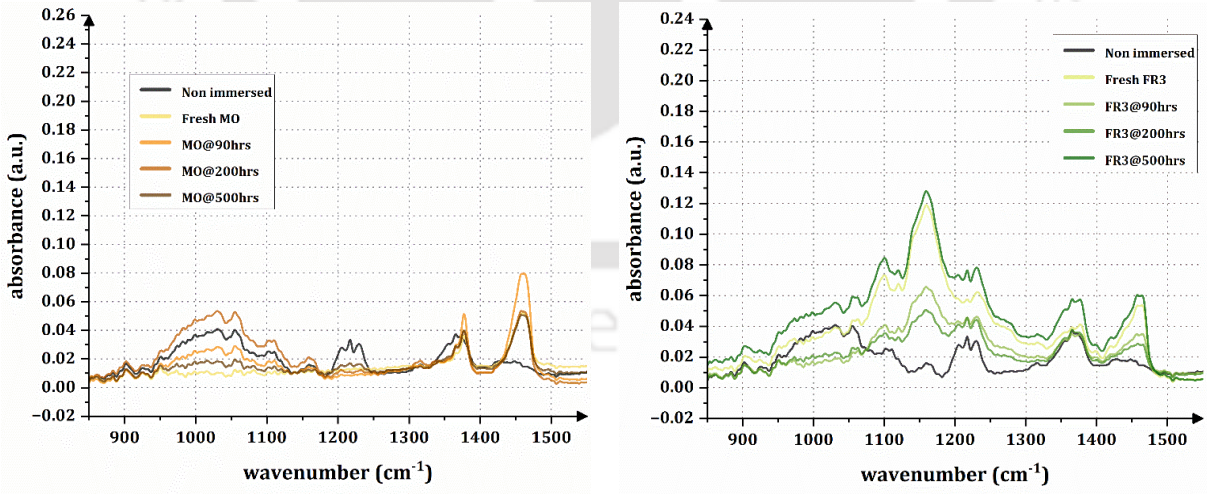

(a) (b)

Fig. 4.14. Absorbance (a.u.) vs wavenumber (cm^{-1}) of (a) MO immersed pressboard samples at a range of 900-1500cm^{-1}; b) FR3 immersed pressboard samples at a range of 900-1500cm^{-1}

This increased intensity suggests a reinforcement of C-O groups in the cellulose during the aging process, likely due to transesterification [175]. For FR3-immersed pressboard, the

presence of a peak at 1159 cm^{-1} indicates the strengthening of C-O bonds within the cellulose, contributing to the enhanced durability of the cellulose insulation and reducing degradation due to aging [175]. Conversely, in the case of MO-treated pressboard, the absence of distinct peaks in this spectrum range suggests that FR3 is more effective than MO in protecting pressboard against ageing.

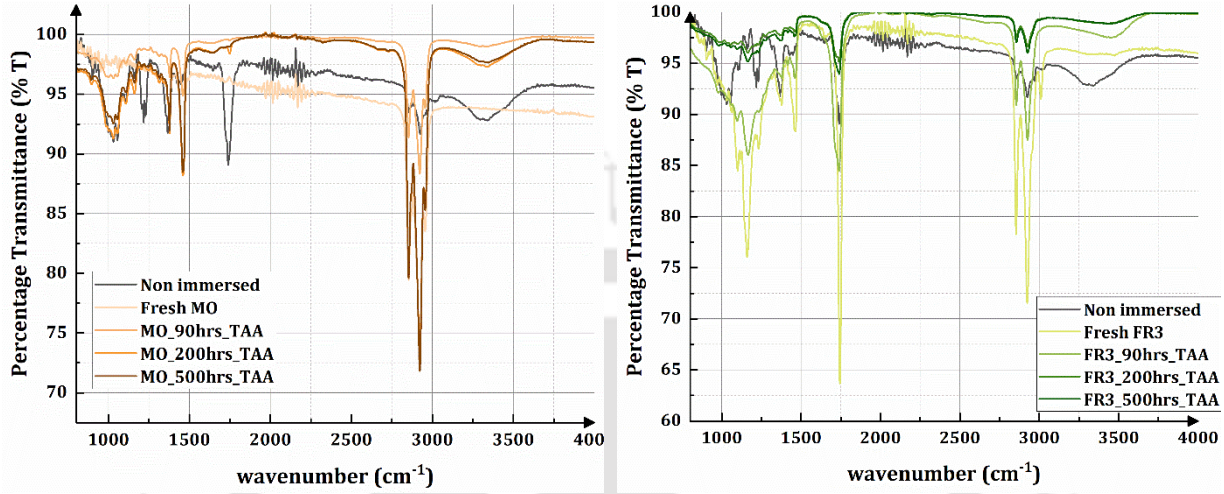

Fig. 4.15. Percentage transmittance (%T) vs wavenumber (cm^{-1}) for thermally aged (a) MO immersed pressboard samples; b) FR3 immersed pressboard samples

In case of thermal ageing the FTIR results for thermally aged samples of MO and FR3 immersed pressboard (PB) samples reveal significant insights into their degradation patterns. The fresh samples of both oils exhibit high transmittance, indicating minimal initial chemical changes. However, as the thermal ageing progresses (90 hours, 200 hours, and 500 hours), there is a noticeable decline in transmittance, particularly around 1500-1700 cm^{-1} and 2800-3000 cm^{-1}. This suggests the formation of oxidation products, such as carbonyl (C=O) and hydroxyl (O-H) groups, indicating the onset and progression of oil degradation.

In the case of MO immersed PB samples, figure 4.15a shows that the percentage transmittance of aged samples is significantly lower compared to non-aged samples, indicating that thermal ageing has a pronounced effect on MO. Conversely, in Figure 4.10a, the difference in transmittance between non-aged and oxidatively aged MO immersed pressboard samples is minimal, demonstrating that oxidative ageing has a lesser effect. For FR3 immersed samples as shown in figure 4.15b, the transmittance of oxidatively aged samples is similar to that of fresh samples, suggesting that oxidative ageing has a minimal impact on FR3 immersed samples. However, with thermal ageing, the transmittance of aged

FR3 immersed samples is noticeably lower than that of fresh oil-immersed pressboard samples. This distinct difference in transmittance indicates that thermal ageing significantly impacts FR3 immersed samples compared to oxidative ageing.

4.3.3. Tensile Strength of Oil Immersed Pressboard

The tensile strength is measured to assess the strength of the pressboard when the sample is secured to an axial loading frame, as seen in figure 4.6. The results of this test are analysed to measure the mechanical strength of the pressboard samples. Figure 4.16a displays the tensile strength (MPa) and load (kN) required to break pressboard samples; as the oxidative ageing of these pressboard samples progresses with time, the tensile strength and load required for mechanical failure decrease. Figure 4.16b demonstrates that as ageing advances, the tensile strength diminishes significantly. Interestingly, after 90 hours of ageing, the mechanical strength of pressboard samples immersed in FR3 is lower than that of pressboard samples immersed in MO. Where a non-immersed pressboard has greater mechanical strength than an oil-immersed pressboard.

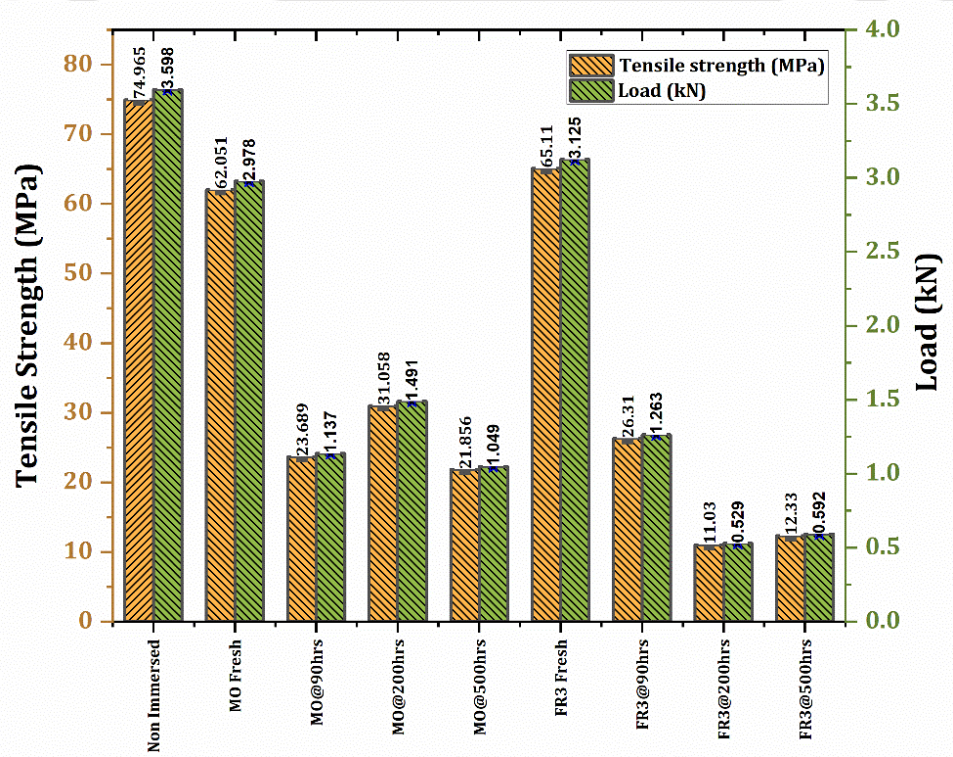

(a)

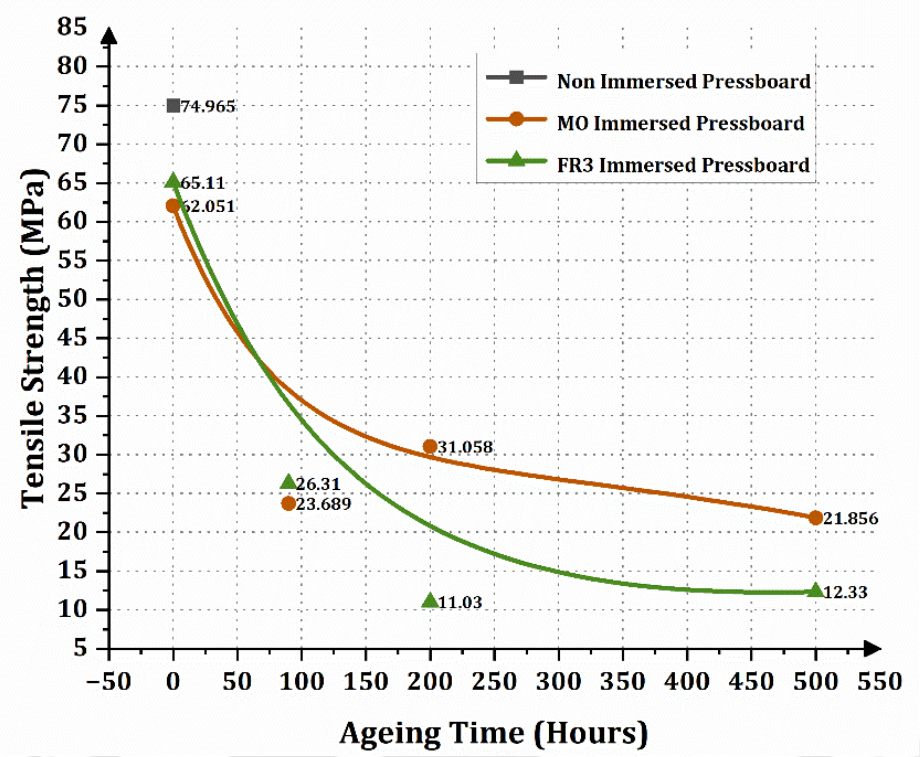

(b)

Fig. 4.16. a) Tensile strength (MPa) and the Load (kN) of pressboard samples for oxidatively aged b) Tensile Strength (MPa) vs Ageing Time (Hours) of oxidatively aged pressboard samples

After immersion in fresh MO and FR3, the tensile strength of the pressboard drops marginally, by 17.2% in the case of MO immersed pressboard and 13.1% in the case of FR3 immersed pressboard, demonstrating the superior advantages of FR3 as a fresh oil on pressboard compares to MO. Pressboards immersed in MO and FR3 undergo oxidative ageing at 115℃. The tensile strength of the pressboard decreases by 61.8%, 49.9%, and 64.7% after ageing in MO for 90, 200, and 500 hours. However, the tensile strength of immersed FR3 pressboards decreases to 59.59%, 83.15%, and 81.06% after 90, 200, and 500 hours.

Similarly, tensile strength of thermally aged immerse samples in MO and FR3 are illustrated in figure 4.17. The tensile strength of the pressboard decreases by 72.09%, 55.8%, and 68.8% after ageing in MO for 90, 200, and 500 hours. However, the tensile strength of immersed FR3 pressboards decreases to 50.1%, after 90hours.

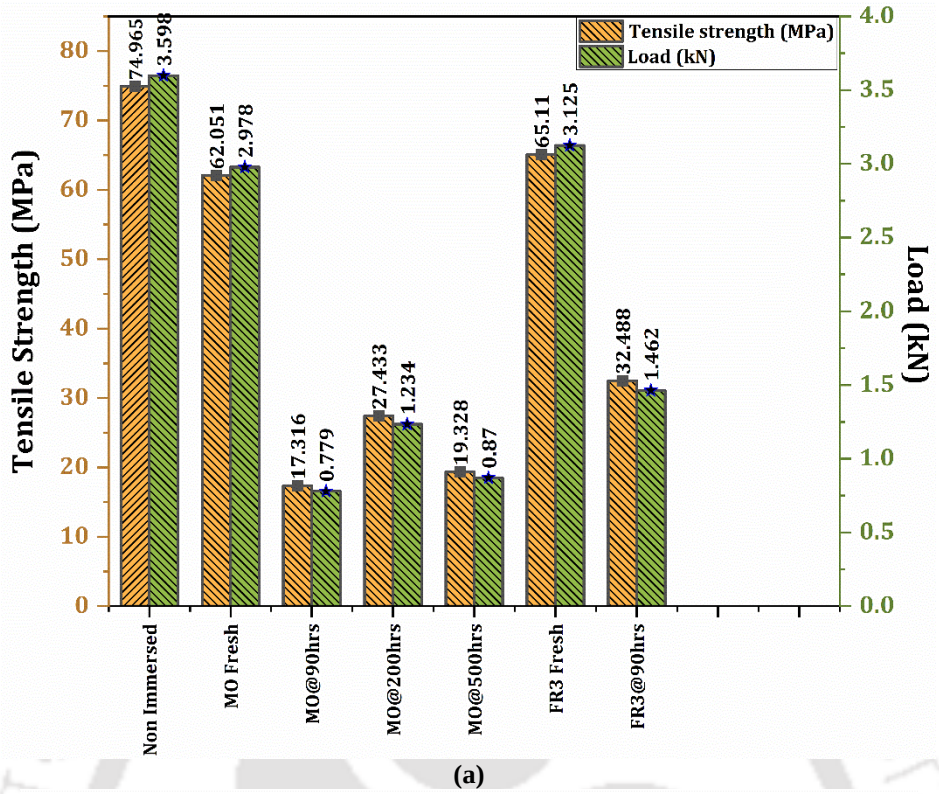

(a)

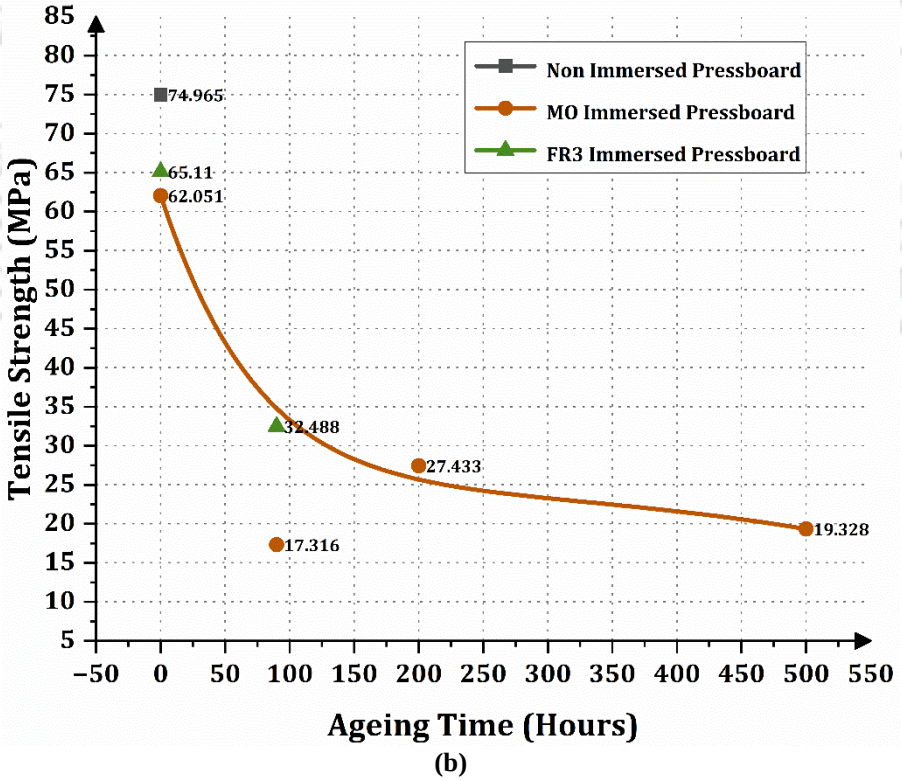

(b)

Figure. 4.17. a) Tensile strength (MPa) and the Load (kN) of pressboard samples for thermal ageing b) Tensile Strength (MPa) vs Ageing Time (Hours) of thermally aged pressboard samples for thermal ageing

4.3.4. AC and DC Breakdown Voltage

This test analyses the influence of oxidation on the pressboard's dielectric strength as it degrades due to oxidative ageing. Figures 4.18a, 4.18b, and 4.18**c** depict the AC, positive and negative DCBDV of oil-immersed and oxidatively aged MO and FR3 immersed pressboard samples. ACBDV illustrated in figure 4.18a shows FR3-immersed pressboard samples have a higher dielectric strength than MO-based pressboard samples. The graph shows that the pressboard immersed in fresh oil has nearly the same dielectric strength as the pressboard immersed in MO but that the ACBDV of the pressboard immersed in MO decreases over time. The dielectric breakdown strength of the MO-immersed pressboard is nearly identical to that of the FR3-immersed pressboard. However, MO-immersed pressboard has a slightly higher value for fresh oil or non-aged samples, at 0.46%. MO immersed pressboard deteriorates and lost its dielectric properties compared to FR3 immersed pressboard by 5.09 % at 90 hours, 1.10 % at 200 hours, and 5.03 % at 500 hours.

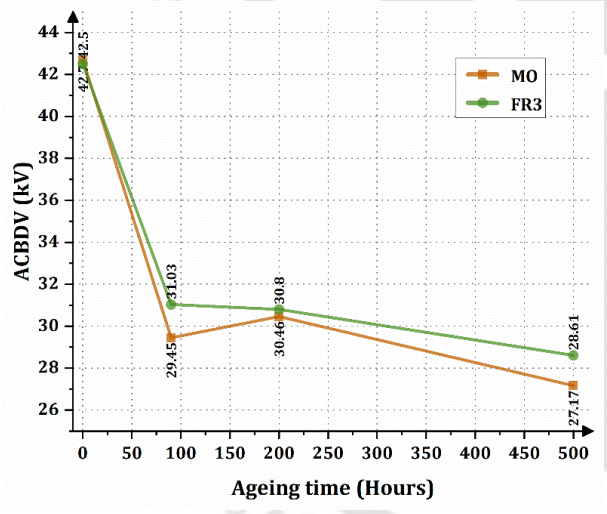

(a)

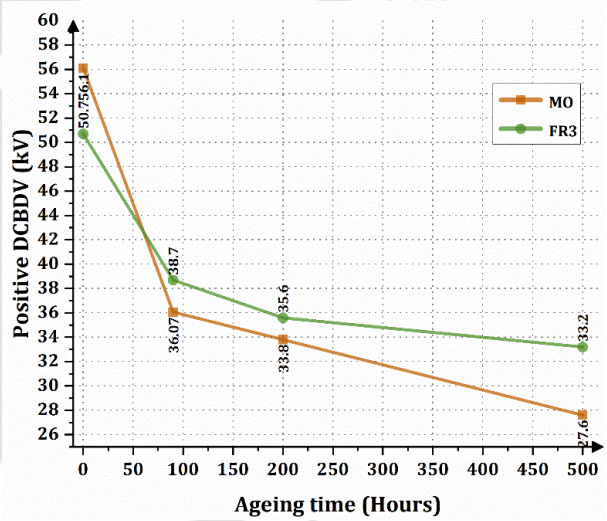

(b)

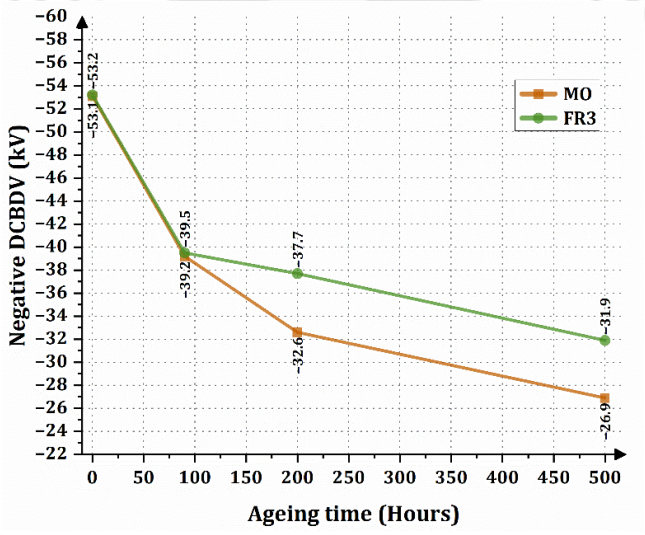

(c)

Fig. 4.18. a) ACBDV vs Ageing time (Hours) of oxidatively aged pressboard samples; b) Positive DCBDV vs Ageing time (Hours) of oxidatively aged pressboard samples; c) Negative DCBDV vs Ageing time (Hours) of oxidatively aged pressboard samples

Figures 4.18b and 4.18c depict the DCBDV plots for positive and negative polarity respectively. As with ACBDV, DCBDV must be explored because the world is transitioning to renewable energies, and power equipment transfers HVDC power directly. This section examines the effects of oxidative ageing on MO and FR3 pressboards immersed in DC voltage. For fresh oil-immersed or non-aged pressboard samples in MO and FR3, the MO-immersed pressboard has a 9.62% greater DCBDV with positive polarity than the FR3-immersed pressboard. As ageing progresses, the BDV values for MO immersed pressboard decline by 6.79% for 90 hours, 5.05 % for 200 hours, and 16.86% at 500 hours compared to FR3 immersed pressboard. Compared to FR3 immersed pressboard, the dielectric strength of MO immersed pressboard decreases by 0.187% for fresh or unaged samples, 0.75 % for 90 hours, 13.52 % for 200 hours, and 15.62 % for 500 hours when subjected to DCBDV under negative polarity. If the patterns in the BDV plots for ACBDV are scrutinized, the degradation of oil-immersed pressboards is approximately 5% less for MO than FR3 during the aging period. However, at 200 and 500 hours, the dielectric strength of DCBDV in both the positive and negative polarity decreases significantly for MO-immersed pressboard samples. It indicates that natural ester oil has reduced the oxidative ageing effect of pressboard insulation. Moisture and temperature are two of the primary causes of deterioration of the pressboard. In both cases, natural ester oil has superior properties; one of them is moisture retention properties; thus, pressboard insulation is less affected by ageing.

The figures 4.19a, 4.19b, and 4.19c show a clear decrease in AC and DC Breakdown Voltage (BDV) for samples aged thermally in MO and FR3. For AC BDV, the voltage decreases by 49.3% for MO samples from fresh to 500 hours of ageing, while for FR3, the reduction is 65.8%. This reduction occurs steadily after 90 hours of thermal ageing. In the case of DC BDV under positive polarity, the voltage decreases initially at 90 hours, then slightly increases up to 500 hours due to the formation of aging by-products.

The overall reduction in DC BDV is 52.2% for MO and 68.5% for FR3 immersed pressboard samples. Under negative polarity, a similar trend is observed, with BDV reductions of 49.9% for MO immersed samples and 66.29% for FR3. And in all cases, MO

immersed PB samples exhibits higher BDV compared to FR3 immersed, indicating a more significant effect of thermal ageing on FR3. This ageing process also includes sludge formation, affecting the BDV of pressboard samples in AC and DC conditions.

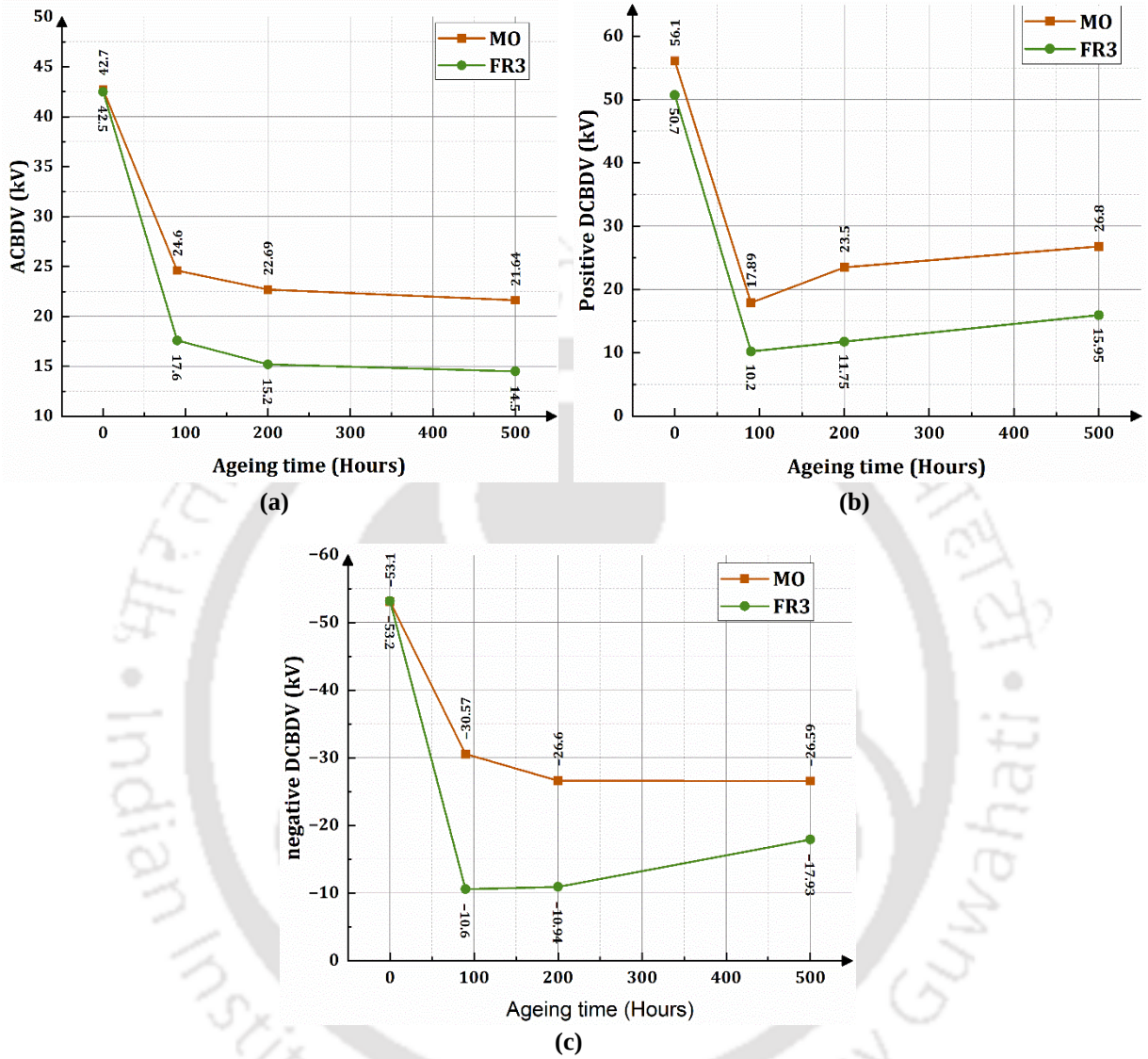

Fig. 4.19. a) ACBDV vs Ageing time (Hours) of thermally aged pressboard samples; b) Positive DCBDV vs Ageing time (Hours) of thermally aged pressboard samples; c) Negative DCBDV vs Ageing time (Hours) of thermally aged pressboard samples

4.4. Summary of the chapter

In this investigation, the pressboard insulation of transformers is immersed in FR3 (NEO) and conventional MO, and these pressboard samples are exposed to open-beaker oxidative ageing following ASTM D1934 standard and thermal ageing. In general, the effect of oxidative and thermal ageing degrading behaviour of pressboard on FR3 and MO immersed is explored. In the present work, MO and FR3 immersed pressboards have oxidatively and

thermally aged for 90, 200 and 500 hours in an open beaker and the changes in pressboard insulating properties are studied and analysed. FTIR allows one to comprehend the changes in the chemical behaviour of pressboard insulation. TGA is also used to examine the influence of oxidation on the thermal stability of pressboard samples immersed in MO and FR3. From tensile strength analysis, it is determined that the mechanical strength of insulation decreases as it aged. This deterioration also affects the electrical properties; hence, the AC and DCBDV are evaluated for the aged pressboard insulation immersed in MO and FR3. The summary of the present study are as follows.

a) Pressboard samples immersed in MO and FR3 are subjected to TGA analysis, which reveals that mass loss is significantly affected between 300 and 400℃. Here, the non-immersed pressboard sample serves as a reference sample. The FR3 sample exhibits excellent properties than the MO-immersed pressboard samples and even more remarkable properties than the non-immersed sample across the whole temperature range. In the range of transformer operating temperature, FR3 has a lower percentage of mass loss. Overall, these findings demonstrate that oxidative ageing has a more significant effect on the thermal stability of MO compared to FR3. And in case of FR3 thermal ageing FR3 immersed pressboard has high impact than MO immersed pressboard.

b) The changes in chemical composition are investigated to identify the impacts of oxidative and thermal ageing on pressboard insulation. The various functional groups of samples of immersed MO and FR3 pressboards are discussed. Additionally, the findings reveal that pressboard samples immersed in both MO and FR3 are prone to aging. However, it is observed that the impact of oxidative is less pronounced in pressboard samples immersed in FR3 compared to those immersed in MO. In case of thermal ageing the FR3 immersed samples has more effect compared to MO immersed samples in view of chemical changes.

c) Tensile strength measurements are used to investigate the effects of oxidative ageing on the mechanical strength of pressboard insulation. As the ageing period increases, the tensile strength of both MO and FR3-immersed pressboard samples decreases. Interestingly, after 90 hours of ageing, the tensile strength of FR3-immersed samples decreases below that of MO-immersed samples, despite FR3's superior strength for fresh oil-immersed samples compared to MO-immersed samples.

d) Non-immersed, fresh oil immersed, and oxidatively aged samples of pressboard are subjected to the BDV test with both AC and DC voltage sources to determine the adverse effects of ageing on pressboard insulation. FR3 is reported to have superior electrical properties even after aging compared to MO. In case of thermal ageing, the AC and DCBDV of MO immersed pressboards is greater than the FR3 immersed pressboard samples showcasing the thermal ageing effect of FR3 is greater than MO.

This thesis studies the DC BDV of liquid and solid insulation under various conditions, including ageing and geometric effects. Breakdown occurs when an arc forms, creating a short circuit through the liquid and allowing large currents to flow between terminals. Before an arc forms, highly conductive structures called electrical streamers appear in the liquid. Studying these structures is crucial to understanding the behaviour of DCBDV. To investigate this pre-breakdown phenomenon, a specialized apparatus must be designed to replicate the conditions within a transformer which is explained in detail in the next chapter.

***Note**: This work is partially submitted to,*

D. Kanumuri, A. Kumar, S. S. Sahu, S. Anand, N. Baruah and S. K. Nayak, "Degradation Study of Oxidatively Aged Natural Ester Oil Immersed Pressboard Insulation," ***2024 IEEE 7th International Conference on Condition Assessment Techniques in Electrical Systems (CATCON),*** Kolkata, India, 2024, pp. 1-6.

5

Design of experimental setup for pre-breakdown phenomena in liquid and solid dielectrics

Contents

5.1 Introduction …….. 122

5.2 Design of experimental setup for studying pre-breakdown phenomena in liquid dielectrics……..…..……. 123

5.3 Design of experimental setup to study the streamers along the surface of solid dielectrics immersed in liquid insulation …… 132

5.4 Summary of the chapter …..…… 138

5.1. Introduction

Electricity generation around the world is expected to be increased by 69% in the next two decades to satisfy the consumer demand across the globe [178]. This poses a challenge to existing power system which requires new strategies for both transmission and generation of electricity that is more reliable, efficient and flexible. So, high voltage power apparatus in a power system such as cables, capacitors, transformers etc. also need to improve their reliability, efficiency and performance to satisfy the requirements of future grids. Nowadays power systems require higher voltage components (level greater than 1MV) and the insulation systems in these apparatus needs to be improved to offer a good performance.

Insulation in high voltage apparatus provides dielectric performance for power apparatus which is in working environment. Dielectric failure in high voltage power apparatus can be prevented by their insulation system that can work under higher thermal, electrical and mechanical stresses. Due to rapid advancements in material science and nanotechnology dielectric performances of insulation like new materials such as polymers, cellulose-based materials, non-polar liquids etc. can be engineered to work under extreme conditions. It is important to understand the mechanisms like conduction, pre-breakdown and breakdown phenomena that are involved in material degradation and dielectric failure in order to implement these materials in real time equipment. Rapid technological advancements in multi frame and high-speed cameras can be combined with optical techniques for imaging streamers during their initiation and propagation.

In recent studies, conceptualization and description of streamers for positive and negative polarity are classified for different modes [179-180]. Nevertheless, the physical processes involved for independent modes are still not established for different insulating samples under aging, nanofluids, natural esters and blending oils, effect of moisture, temperature, flow on pre-breakdown mechanisms etc. This experimental setup has been designed to carry out the breakdown and pre-breakdown tests to study the limitations and relative durability of an insulating oil kept in real time environment for a HVDC transformer.

There are some experimental setups available which are developed by some researchers. In [181], an experimental setup consists of test chamber made of glass with a point plane electrode system in which point electrode was connected to high voltage source and plane electrode was grounded is disclosed. A Marx generator with a step supply voltage of

0.5/1700μs was used as source with an electrode gap of 8 cm throughout their study. To limit the breakdown current and dampen the oscillations a 76 Ω resistor was used. With the help of gas overvoltage protector and some attenuators that are connected to an oscilloscope at the grounded side of chamber streamer current was measured. Light emitted pulses from a streamer were recorded by a photomultiplier and streak images were captured with the help of Imacon 468 an image converter camera. Xenon flash was utilized to produce shadow-graphic images. Marx generator, Xenon flash, and the camera were synchronized by a trigger system. This system is utilized to study characteristics of non-breakdown and breakdown streamers through the effects of dissolved gases/air, carbon particles, additives, reduced pressure, liquid chemistry and voltage polarities on streamers. In [182], an experimental setup to study the streamers in liquid and liquid-solid insulation system with the help of point plane electrode configuration is disclosed. The experimental setup is capable to detect streamer parameters such as velocity, length, propagation time, emitted light and charge. And, in [183] an experimental setup to study the streamer and breakdown characteristics of mineral and synthetic ester oils under both positive and negative DC voltages using point plane electrode configuration is disclosed. Analysis of streamer characteristics such as streamer length, propagation, velocity, shape based on images captured through shadow graphic method by using an ultra-high-speed camera in between the electrode gap distance is performed.

However, while some researchers have experimentally studied and developed theories on pre-breakdown phenomena, many aspects remain unexplored. For instance, the distinct propagation modes of positive and negative streamers in MO have yet to be thoroughly analysed. Additionally, the pre-breakdown phenomena for new natural ester oils (NEOs) must be established under all in-service conditions, such as flow, temperature, and pressure. To meet these requirements, it is necessary to develop an apparatus and experimental method to study the inception and propagation of both positive and negative streamers in liquid insulation. This apparatus should also be suitable for studying NEOs used in HVDC equipment and be capable of handling all types of stresses, including AC, DC, and impulse.

5.2. Design of experimental setup for studying pre-breakdown phenomena in liquid dielectrics

Referring to Figure 5.1, a block diagram of an apparatus for analyzing breakdown and pre-breakdown phenomena in liquid-dielectrics is illustrated. From the figure**,** a complete

schematic of the test setup is depicted wherein “a” is a stainless-steel test chamber where the liquid insulation and streamers along the surface of solid insulation is tested. From the figure 5.1 the “b” and “c” represents the filtering and degassing system & shadow graphic and photon detection systems connected to test chamber in order to replicate the real time conditions of transformer.

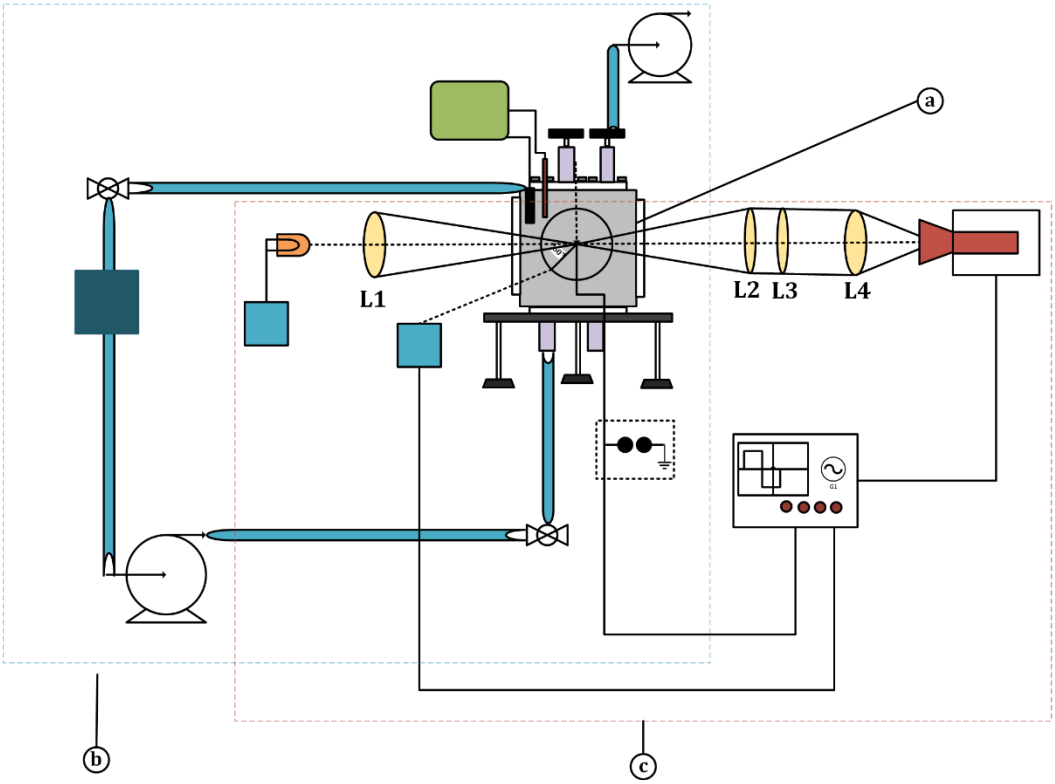

Fig. 5.1. Exemplary profile of an apparatus for analyzing breakdown and pre-breakdown phenomena in liquid-dielectrics

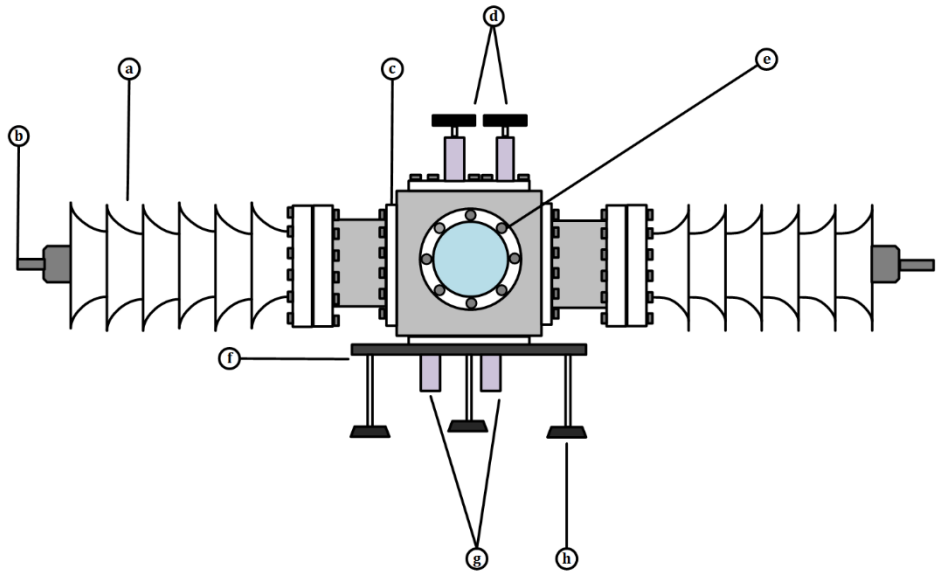

Fig. 5.2. Schematic of test chamber

Figure 5.2 illustrates a schematic of test chamber that is made up of stainless-steel. From this figure ‘a’ shows the high voltage bushing connected to the electrodes present inside the test chamber. The high voltage lead configured to which a high voltage source is connected is indicated in ‘b’. The square stainless-steel test chamber with the dimensions of 120 mm on all sides with a width of 10 mm of all the plates is shown in ‘c’. The capacity of oil required for this test chamber is around 1500-1800 ml. The components ‘d’ and ‘g’ as shown in figure 5.2 are inlets and outlets of chamber respectively through which the flow of oil is maintained and also used for cleaning and maintenance. Whereas ‘e’ indicates the view port made of glass through which complete pre-breakdown phenomena between the electrodes is viewed. The diameter of this view port is 60 mm from the center of wall. This complete test chamber is placed on the circular stainless-steel disk with a diameter of 150 mm as shown in ‘f”. The component ‘h’ represents the stand on which the test chamber along with steel disk is placed. It has three legs with a rubber knob at the bottom and welded to the stainless-steel disk. The height of the chamber from ground is 100 mm that provides clearance to high voltage leads from ground.

The test chamber is fabricated with stainless steel in which two view ports as shown in ‘e’ are attached to the walls of the chamber in order to observe the streamer phenomena. These are attached to the chamber with the help of stainless-steel bolts. Now two bushings are fitted on the opposite sides of these view ports and these are also fitted to the walls by carving the plates and attaching them with the tube between them as shown in figure 5.2. There are two openings at the top and at the bottom of the chamber in which one inlet will be used to pour the liquid into chamber and other is used by vacuum pump to maintain the pressure in the chamber. The outlets present at the bottom of the chamber will help in circulating oil that is described in figure 5.5 and other outlet is utilized to drain the oil from the chamber. The complete setup is placed on the three-legged stand with rubber knobs at the bottom the height will provide enough clearance for high voltage leads from base. The high voltage terminals are connected to the high voltage leads that will energize the electrodes immersed in the oil leading to streamer formation.

Figure 5.3 illustrates an inner view of test chamber. ‘a’ in figure 5.3 represents the test chamber which consists a point plane electrode system to test the oil samples. The electrodes on the other end is connected to high voltage leads through which a source is provided for testing. When the high voltage side is connected to point electrode and ground is connected to

plane electrode, a positive streamer is generated. Similarly, with same electrode configuration and polarity change in source end by changing the diode direction, negative streamers are formed in the electrode gap distance. From the figure 5.3, component ‘b’ is the gap between electrodes generally varies from 1-50 mm in distance between the electrodes. Whereas ‘c’ and ‘e’ are two openings in the test chamber for the filtered oil and for the optical fiber cable respectively in order to detect streamers in the chamber and ‘d’ indicates the screw gauge connected strongly to the electrode so that the distance between the electrodes can be adjusted depending on the application.

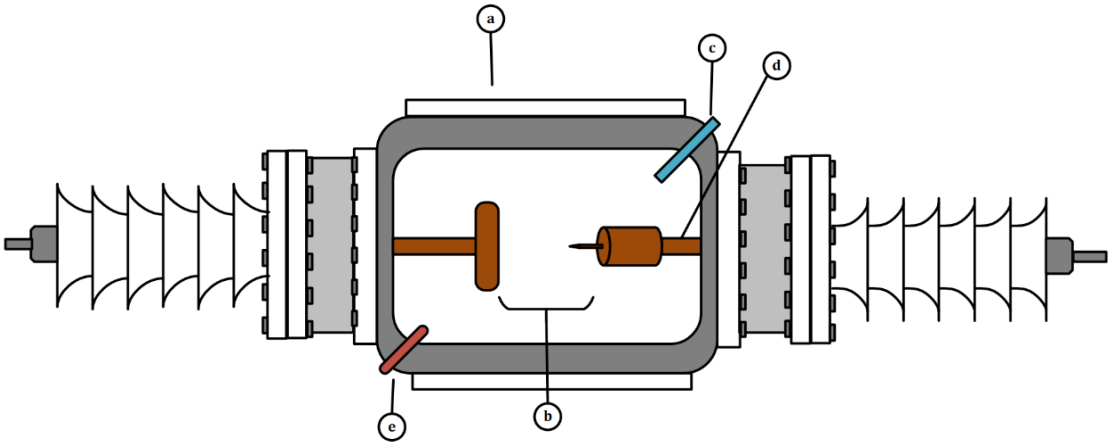

Fig 5.3. Inner view of test chamber

From the above figure it is shown that the electrodes are placed inside the chamber attached to the high voltage bushings. These can be interchanged with other electrode configurations. This is possible as the electrodes are attached at the end of the rods connected to the bushings that are detachable. The needle electrode has a screw gauge that can be adjusted so that the distance between electrodes is varied depending on the application. Apart from this there are two openings in the walls of the chamber in which blue opening represents the pipe which carries the circulating oil into the chamber after filtering and the red opening is for placing the optical fiber 5.6e inside the chamber that detects the streamers formed in between the electrodes.

Figure 5.4 illustrates different electrodes shapes that are placed inside a test chamber. Where “a, b, c and d” indicate the different type of electrode systems that can be changed in the test chamber for studying the breakdown and prebreak down phenomena in liquid dielectrics. These electrodes shape and size are considered as per the standards like ASTM D3300-20, ASTM D877, ASTM D1816-12, IEC60156, IEC 60897 etc. The materials that are

likely to be used in these electrodes are either copper/ brass/tungsten etc. Depending on the application these electrode configurations are interchanged inside the test chamber. (a) illustrates needle-Plane electrode configuration system. (b) illustrates uniform Disk electrode configuration system. (c) illustrates uniform Sphere-Sphere electrode configuration system, and (d) illustrates needle-Sphere electrode configuration system.

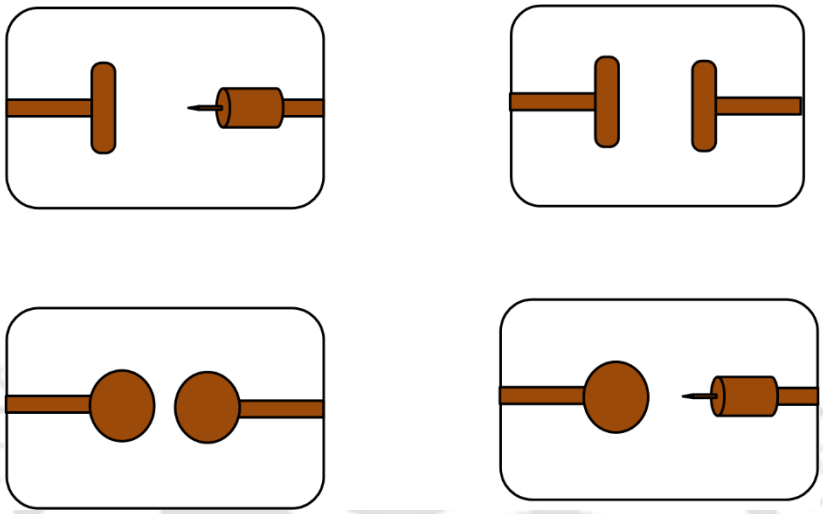

Fig 5.4. Different electrodes shapes that are placed inside a test chamber

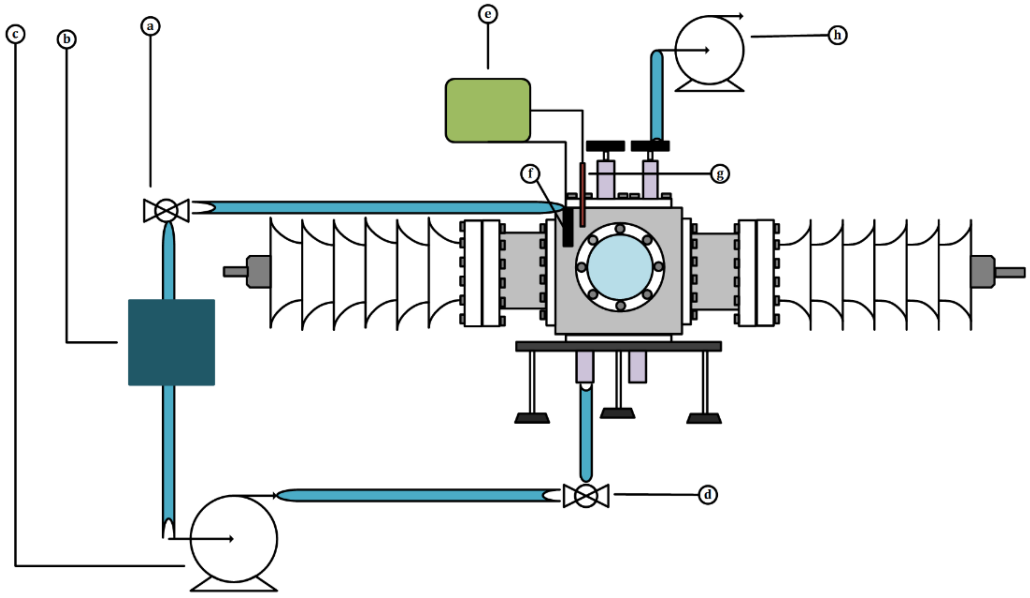

Fig 5.5. Filtering and degassing system with temperature controller

Figure 5.5 illustrates a filtering and degassing system with temperature controller. This setup indicates the degassing and filtration system that is also equipped with a heating rod and an RTD sensor. ‘a’ and ‘d’ of the figure indicate the valves for the test chamber through which the oil flow can be controlled. Whereas ‘b’ shows the hydraulic filter with a pore size

of 2 µm that filters all the impurities in the oil. Component 'c' shows the magnetic pump that allows the oil to circulate through the filter and again reach to test chamber through the filtering system. The speed of pump should be varied from 2 rpm to 50 rpm in order to replicate the laminar flow of transformer oil in service conditions. 'e' is a temperature controller circuit that is used to maintain the temperature of oil in the test chamber ranging from 30 to 90˚C replicating the real time environment conditions. 'f' and 'g' indicate the stainless-steel heating rod (cartridge heater) and RTD sensor placed inside the test chamber in which the heating rod is used to maintain the temperature of oil and sensor is used to monitor and maintain the temperature of test chamber. 'h' indicates the vacuum pump connected to the test chamber in order to maintain the pressure below 5 mbar. Once the oil is filled in the chamber with the support of degassing and filtering system, the impurities in the oil are removed. The complete process is briefly explained in the experimental procedure and operation section. The temperature controller is used to control the temperature of the chamber by RTD sensor and heater rod. Oil circulation is controlled by controlling the speed of pump and vacuum pressure inside chamber. Tests can be performed in stationary condition, with and without temperature, with and without pressure and by combining all these as per the desired application.

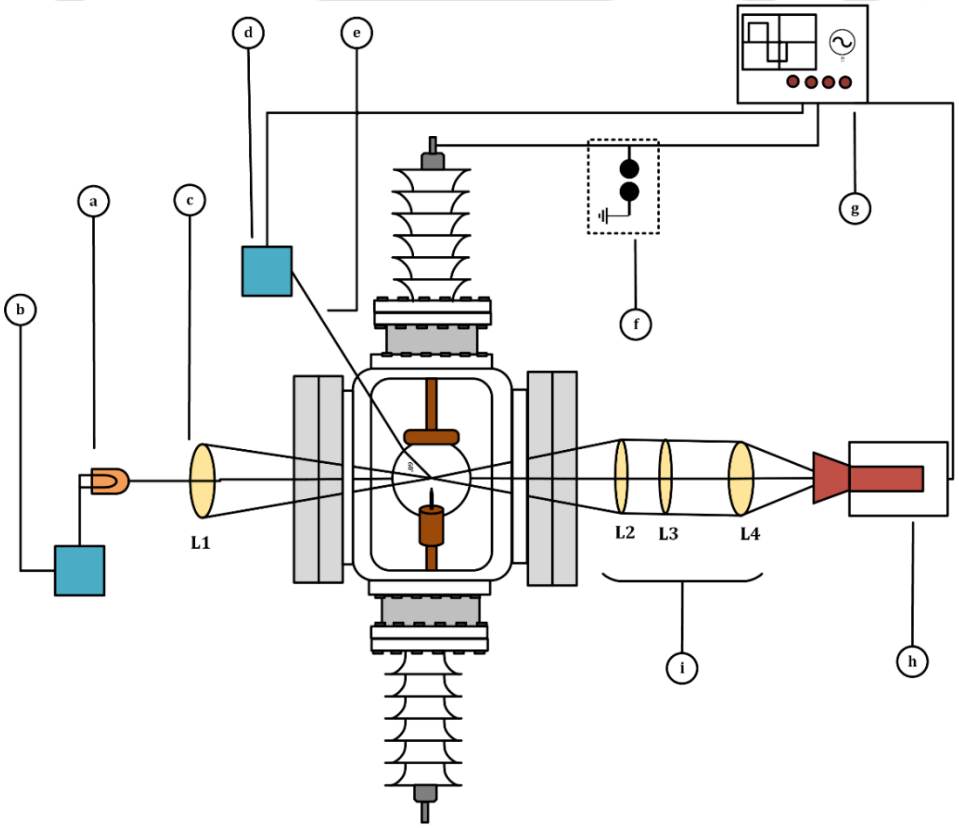

Fig 5.6. Shadow graphic and photon detection system

Figure 5.6 illustrates a shadow graphic and photon detection system. Figure 5.6 shows the shadow graphic and photon detection systems connected to the test chamber in order to track, measure and study the streamers generated in the electrode gap area. ‘a’ and ‘b’ indicates xenon lamp and lamp source. ‘c’ in figure 5.6 is a lens that is collimated with xenon lamp through the test chamber view port illuminating the electrode gap from tip of point electrode to plane electrode. The components ‘d’ and ‘e’ indicate the photo multiplier and optical fiber. ‘g’ shows an oscilloscope connected from grounded terminal through an over voltage protector ‘f’ to protect the oscilloscope from high voltages. A high-speed camera with computer as shown in ‘h’ and ‘i’ indicates the far field microscope is placed on the opposite side of view port aligned with light beam. The diameter of the optical fiber ‘e’ is 2 mm and is placed at 10 mm away from tip of point electrode. In order to reduce the effect of shadow graphic system on photon detection system, the core of the fiber is placed at an angel of 60˚ to the line of light beam on the path of xenon lamp. In addition to this, a long pass filter with 650 nm wavelength is placed in front of the lamp. The photomultiplier spectral sensitivity ranges from 200-700 nm (10% of sensitivity is 650 nm). And in order to shield the photomultiplier ‘d’ from electromagnetic interference from high voltage source it is installed inside a dark box. The light beam produced will be projected on to the high-speed camera through the far field microscope ‘i’. The far field microscope should magnify the image at the tip of the point to 20 times so that the image obtained will be a minimum of 1000×1000 μm^2 with a maximum resolution of 1µm /pixel. The photomultiplier and camera sensor should be synchronized so that whenever the streamer is formed, the camera is triggered through the oscilloscope. Now the camera will capture the streamer phenomena once the trigger is received.

From the captured streamer images, the time and distance between the electrodes is determined. From this experimental result, the streamer length/ stopping length (mm) and time (µs) taken to reach that point for an applied voltage (kV) can be determined from the images. Now as the distance and time of streamers is known, streamer velocity can be determined for the applied voltage. As the phenomenon occurs, the current is captured by the current probe from high voltage bushings and this streamer current vs applied voltage and time can be observed in oscilloscope. From this current, charge is measured and streamers charge vs applied voltage and time are plotted. This process is repeated for various types of liquid dielectric (conventional, alternative and engineered samples) under various in-service

conditions.

Experimental Procedure and Operation:

a. The first step to start this experiment is by conditioning the liquid dielectric that needs to be tested. As these streamers directly correspond to dielectric strength, the major factor that influences this is moisture. In order to remove the moisture from the oil, the sample is placed in a vacuum over at 60˚C under vacuum conditions for 48 hours.

b. Moisture content should be noted before and after the conditioning as to determine the effect of moisture on the dielectric strength. Same procedure must be maintained for all the materials (i.e. liquid insulation) including the engineered materials. The test chamber should be cleaned thoroughly before experiment with the help of cleaning agents like acetone, methanol etc.

c. The electrode configuration and gap between the electrodes should be chosen and replaced with respect to the application. The electrode configurations and setup are shown in Figure 5.3 and 5.4. Once the procedure is done, the oil should be filtered and degassed for 24 hours as described below.

d. Filtering and degassing of oil are very important in order to reduce impurities in oil and air present in the test chamber during handling before the experiments. So before test the test chamber can be partially filled with the liquid dielectric to a level that immerses the electrodes in the oil. The oil that is poured in test chamber should be circulated through the filter for 24 hours in a loop.

e. During this process oil is poured on to the heating rod which should be in operation throughout the process until the oil temperature is maintained to 60˚C. This temperature can be controlled with the help of temperature controller and RTD sensors present in the test chamber. This complete setup is shown in Figure 5.5.

f. As the oil is circulated and heated, the pressure of the chamber should be lowered from atmospheric pressure to 5mbar during these 24 hours. Once the filtering and degassing of oil is done the circulation of oil stops and cooled down to room temperature. Now the oil

is filtered and degassed and ready for testing. These are the recommendations and techniques considered for filtration and degassing from.

g. Now the electrical test is performed at atmospheric pressure and room temperature by subjecting the sample with the voltage stresses like DC, Lightning Impulse and Switching Impulse. At first, breakdown voltage for selected electrode configuration and gap will be measured. Thereafter, random voltages lesser than the breakdown voltage are applied to form streamers between the electrodes. The data is then collected with the help of photomultiplier, camera, photon detection system and shadow graphic system and oscilloscope that are synchronized with each other help to visually capture the time, length of propagation, size and shape of streamers formed. Streamer current and charge can be obtained from oscilloscope.

h. The polarity of the applied voltage can be changed when the high voltage terminals are interchanged (i.e. the negative polarity is applied when the positive terminal is given to plane electrode and negative terminal is given to point electrode).

i. Similarly, when the streamer phenomena are observed the flow of oil can be applied by the means of circulating system and temperature of the oil can also be varied to obtain more in-service conditions while testing.

j. From the experimental results the streamer characteristics like propagation length, stopping length, current, charge, velocity with respect to applied voltage and time for different liquid dielectrics are measured, plotted and analyzed.

The developed apparatus as shown in figure 5.1 facilitates in studying the streamers is meant for all kind of insulating oil used in power and distribution transformers. The apparatus can be utilized to analyze various thermochemical, physical and electrical stressed samples along with nanoparticles dispersed insulating oil. The apparatus effectively performs for both new and service insulating oil for transformer. All parts including test chamber, filtering and degassing system, shadow graphic and photon detection systems are depicted individually and each system is briefly described as follows. Different systems of streamer experimental test setup are mentioned in order to have a detailed understanding about every part in the apparatus. The complete setup is placed on the table with the help of optical bread board and

the dimensions required for the table is 7ft×4ft (length ×breadth). The complete setup is properly grounded. The test chamber is connected to a high voltage source that is having a variety of options such as DC voltage source, Lightning Impulse and Switching Impulse in order to study streamers formed in insulating oil in the presence of these high levels of electric fields.

The apparatus can study and analyze the pre-breakdown and breakdown phenomena of NEOs used in HVDC equipment. In addition to liquid insulation, solid insulation is also crucial. Therefore, studying streamer formation on solid insulation is equally important. The current apparatus has also been modified to capture images of the surface of solid insulation, enabling comprehensive analysis.

5.3. Design of experimental setup to study the streamers along the surface of solid dielectrics immersed in liquid insulation

Particularly for solid insulation, it's crucial to understand streamers, as pre-breakdown events create conductive paths on the insulation. These paths lead to persistent leakage currents during equipment operation, resulting in gradual insulation degradation and ultimately shortening the lifespan of the equipment. Therefore, assessing and comprehensively understanding the nature of streamers in solid insulation is of paramount importance. Apparatus discussed above remains same, however some of its parts are modified to study streamer formation on the surface of solid insulation.

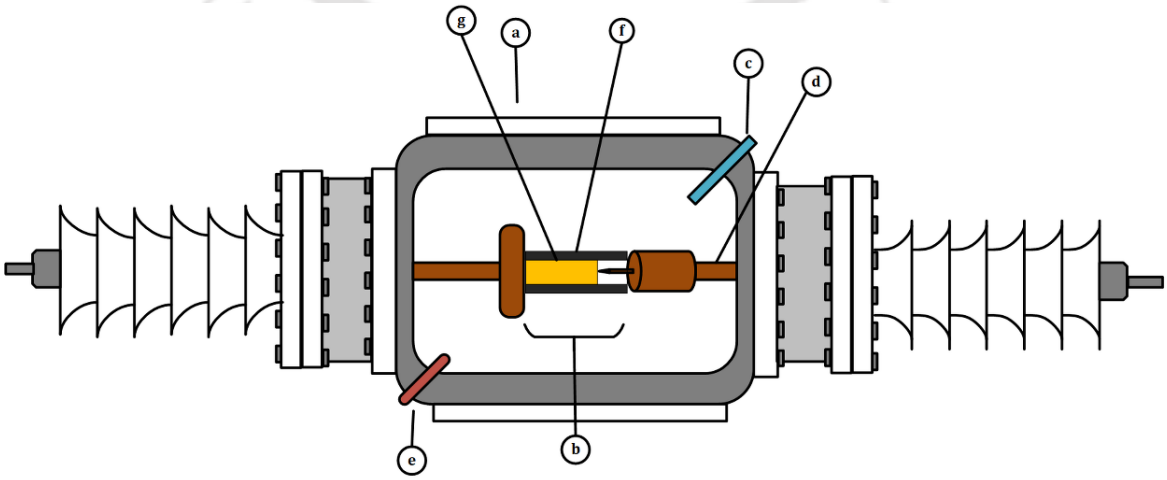

Fig 5.7: Inner view of test chamber (Top view)

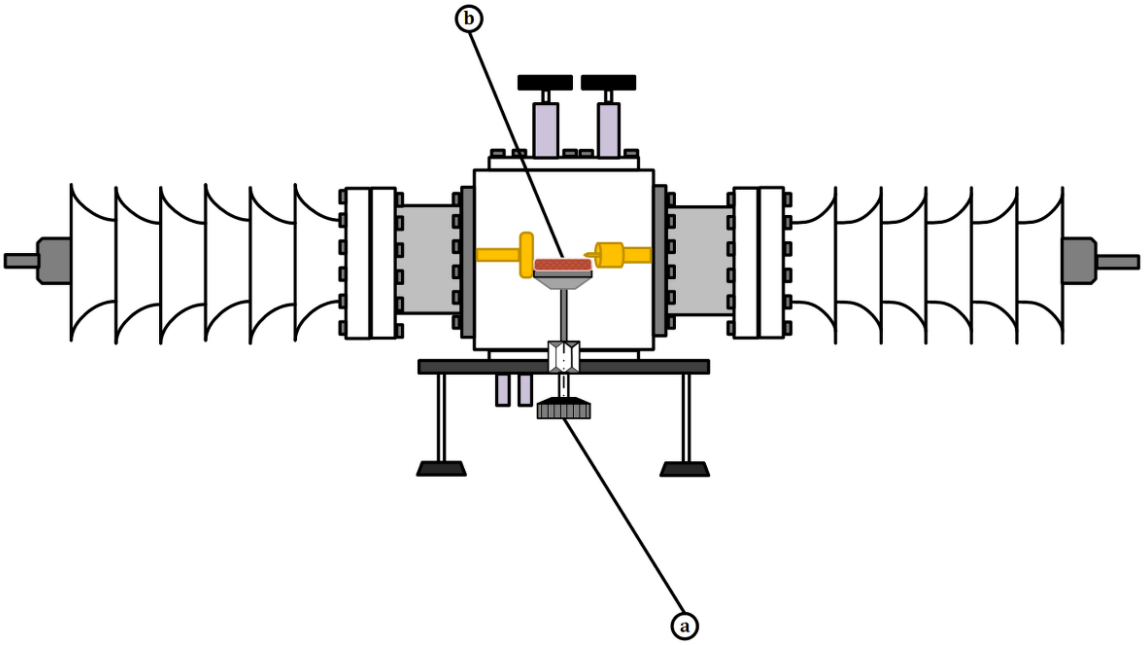

Fig 5.8: Side view/cross-sectional view of high voltage electrodes with solid insulation sample holder that are placed inside a test chamber

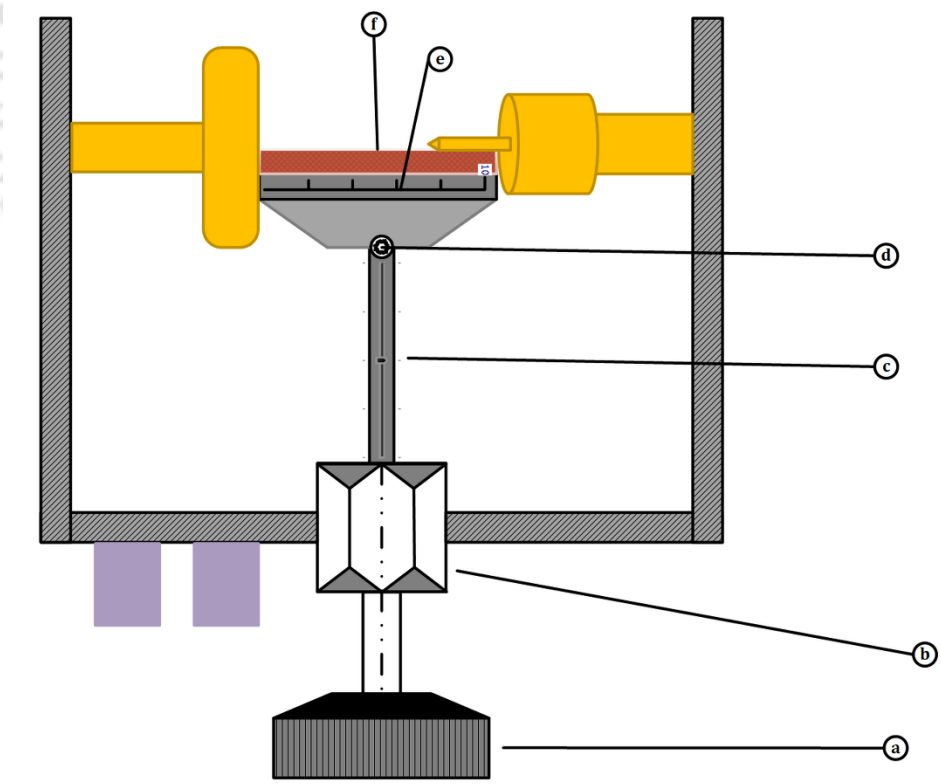

Fig 5.9: Schematic of solid insulation sample holder

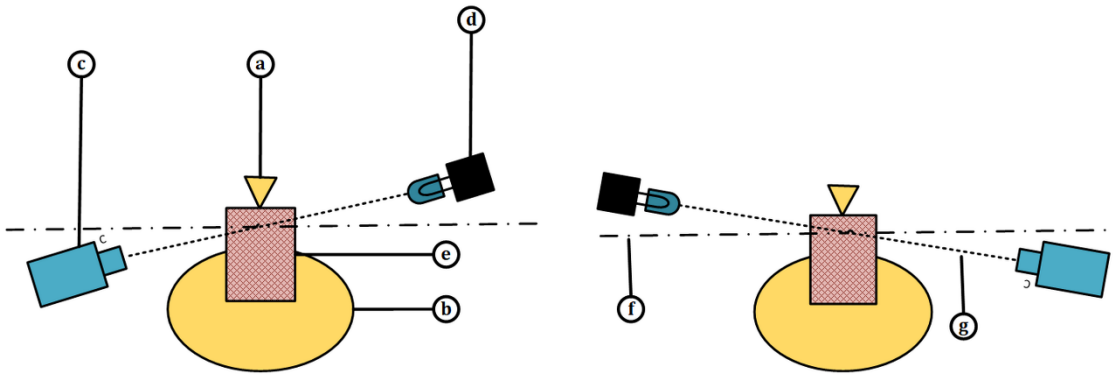

Fig 5.10: Schematic of needle plane electrode configuration and alignment of xenon lamp and high-speed camera

Figure 5.7 illustrates an inner view of test chamber (top view). From this figure ‘a’ shows the test chamber which consists of a point plane electrode system to test the oil immersed solid samples. The electrodes on the other end are connected to high voltage leads through which a source is provided for testing. When the high voltage side is connected to point electrode and ground is connected to plane electrode, a positive streamer is generated. Similarly, with same electrode configuration and polarity change in source end by changing the diode direction, negative streamers are formed in the electrode gap distance. From the figure 5.7, ‘b’ is the gap between electrodes generally varies from 1-50 mm in distance between the electrodes. And, ‘c’ and ‘e’ are two openings in the test chamber for the filtered oil and for the optical fiber cable respectively in order to detect streamers in the chamber. The screw gauge connected strongly to the electrode so that the distance between the electrodes as indicated in ‘d’ can be adjusted depending on the application. Component ‘f’ illustrates the solid insulation sample holder situated within the needle-plane electrode system, while ‘g’ shows the solid insulation sample positioned on this holder, contacting both the needle and ground electrodes. The needle electrode has a screw gauge that can be adjusted so that the distance between electrodes is varied depending on the application. Apart from this there are two openings in the walls of the chamber in which ‘c’ represents the pipe which carries the circulating oil into the chamber after filtering and the red opening is for placing the optical fiber ‘e’ inside the chamber that detects the streamers formed in between the electrodes.

Figure 5.8 illustrates side view/cross-sectional view of high voltage electrodes with solid insulation sample holder that are placed inside a test chamber. From this figure ‘a’ depicts the

sample holder, and ‘b’ shows the solid sample that is set up for testing. This figure provides a clear cross-sectional view of how the samples are positioned within the test chamber. A more detailed and schematic representation of this sample holder is provided in Figure 5.9.

Figure 5.9 illustrates an arrangement and schematic of solid insulation sample holder it provides a comprehensive schematic detailing the structure and positioning of the solid insulation sample holder within the test chamber. From figure 5.9 ‘a’ shows the screw gauge located outside the test chamber and ‘b’ illustrates the gauge's opening, which is used for adjusting the height of the holder inside the test chamber. Component ‘c’ depicts the scale used to measure the height of the platform inside the chamber and ‘d’ presents a flexible screw hinge, enabling the adjustment of the sample platform to angles between 10 and 20 degrees for perfect alignment with the needle electrode. Component ‘e’ displays the scale on the sample holder platform, which is useful for checking the gap distance between the electrode systems. Finally, ‘f’ shows the solid insulation sample in contact with the electrode configuration. When positioning the sample on the holder, both its height and angle are carefully adjusted to ensure precise alignment with the needle electrode.

Figure 5.10 illustrates a schematic of solid insulation sample with needle plane electrode configuration and alignment of xenon lamp and high-speed. A shadow graphic system, utilizing a xenon lamp light beam, is employed to track streamers as they move along various oil/solid interfaces. The shadow of a streamer is cast onto the sensor of a high-speed, non-intensified camera through a set of lenses aligned with both the light beam and the camera, as depicted in Figure 5.6. The positioning of the solid sample in relation to the light beam is arranged in two different setups. The first setup, shown in Figure 5.10 (i), aligns the solid surface parallel to the light beam, enabling observation of the oil/solid interface. The second setup, illustrated in Figure 5.11 (ii), involves rotating the solid sample by 90°, which allows for the observation of streamer branching on the solid surface. 6.10a and 6.10b are the needle and plane/ground electrodes. 5.10c and 5.10d depict the high-speed camera and xenon lamp, respectively. 5.10e represents the solid insulation sample, while 6f indicates the line of sight through viewports. 5.10g highlights the angle optimal for clear streamer observation, which is typically between 10 to 20 degrees from the line of sight.

Once the oil is filled in the chamber with the support of degassing and filtering system, the impurities in the oil are removed and then the solid insulation sample is placed in the test

chamber for testing. The complete process is briefly explained in the experimental procedure and operation section. The temperature controller is used to control the temperature of the chamber by RTD sensor and heater rod. Oil circulation is controlled by controlling the speed of pump and vacuum pressure inside chamber. Tests can be performed in stationary condition, with and without temperature, with and without pressure and by combining all these as per the desired application.

Experimental Procedure and Operation:

a) The first step to start this experiment is by conditioning the liquid dielectric in which the solid insulation is immersed that needs to be tested. As these streamers directly correspond to dielectric strength, the major factor that influences this is moisture. In order to remove the moisture from the oil, the sample is placed in a vacuum over at 60˚C under vacuum conditions for 48 hours.

b) Moisture content should be noted before and after the conditioning as to determine the effect of moisture on the dielectric strength. Same procedure must be maintained for all the materials (i.e. liquid insulation) including the engineered materials. The test chamber should be cleaned thoroughly before experiment with the help of cleaning agents like acetone, methanol etc.

c) The electrode configuration and gap between the electrodes should be chosen and replaced with respect to the application. The electrode configurations and setup are shown in Figure 5.7 and 5.8. Once the procedure is done the oil should be filtered and degassed for 24 hours as described below.

d) Filtering and degassing of oil are very important in order to reduce impurities in oil and air present in the test chamber during handling before the experiments. So before test the test chamber can be partially filled with the liquid dielectric to a level that immerses the electrodes in the oil. The oil that is poured in test chamber should be circulated through the filter for 24 hours in a loop.

e) During this process oil is poured on to the heating rod which should be in operation throughout the process until the oil temperature is maintained to 60˚C. This temperature can be controlled with the help of temperature controller and RTD sensors present in the test chamber. This complete setup is shown in Figure 5.9.

f) As the oil is circulated and heated, the pressure of the chamber should be lowered from atmospheric pressure to 5mbar during these 24 hours. Once the filtering and degassing of oil is done the circulation of oil stops and cooled down to room temperature. Now the oil is filtered and degassed and ready for testing. These are the recommendations and techniques considered for filtration and degassing from.

g) The solid samples designated for testing are first impregnated in liquid insulation. These samples, which can range from Kraft paper to pressboard insulation commonly used in power equipment construction, are cut into dimensions of 10mm in width by 60mm in height, with a thickness varying from 0.5mm to 50mm. They are then placed in a petri dish and kept in a vacuum oven at 80°C for 24 hours under a low pressure of 5mbar, a process intended to remove any moisture in the solid insulation samples. After this period, the oven's temperature is reduced, and degassed oil is added to the petri dish, where it remains under vacuum for another 24 hours to ensure thorough impregnation. Once this impregnation process is complete, the solid insulation sample is positioned on the sample holder within the test chamber, which is already filled with filtered and degassed oil. The chamber is then sealed, and the sample is finely adjusted using the sample holder's screw gauge. These prepared samples are now ready for breakdown and pre-breakdown testing.

h) Now the electrical test is performed at atmospheric pressure and room temperature by subjecting the sample with the voltage stresses like AC, DC, Lightning Impulse and Switching Impulse. At first, breakdown voltage on the surface of the solid samples for various gaps will be measured. Thereafter, random voltages lesser than the breakdown voltage are applied to form streamers on the surface of solid samples are tested between the electrodes. The data is then collected with the help of photomultiplier 5.6d, camera, photon detection system and shadow graphic system and oscilloscope that are synchronized with each other help to visually capture the time, length of propagation, size

and shape of streamers formed. Streamer current and charge can be obtained from oscilloscope.

i) The polarity of the applied voltage can be changed when the diodes direction is high voltage source is interchanged both the positive and negative streamers are observed at needle tip.

j) Similarly, when the streamer phenomena are observed on the surface of solid samples the flow of oil can be applied by the means of circulating system and temperature of the oil can also be varied to obtain more in-service conditions while testing.

From the experimental results the streamer characteristics like propagation length, stopping length, current, charge, velocity with respect to applied voltage and time for different liquid-solid dielectrics are measured, plotted and analyzed.

5.4. Summary of the chapter

This chapter discusses the streamer formation characteristics, and breakdown strength along the surface of solid insulation immersed in liquid dielectrics under high voltage stresses. Obtained results can be studied by product design engineers, scientists and researchers in industries to develop a reliable and efficient material for high voltage liquid filled power apparatus. The present design generally relates to an apparatus for analyzing breakdown and pre-breakdown phenomena in liquid-solid dielectrics comprises a test chamber with electrodes, solid insulation sample holder, a filtration and degassing system, and a shadow graphic and photon detection systems. The apparatus can be used separately or simultaneously for all the experimental variations (i) streamer study (ii) degassing and (iii) photo detection depending on the applications.

***Note**: This work is granted and applied for Indian patent,*

1. **Deepak Kanumuri**, Niharika Baruah, Ambuj Kumar and Sisir Kumar Nayak, "An Apparatus for Analysing Breakdown and Pre-Breakdown Phenomena in Liquid Dielectrics" ***Indian patent number**: **432202*** (**Granted on 18/05/2023**; **Filed on: 04/07/2022**).

2. **Deepak Kanumuri**, Niharika Baruah, Ambuj Kumar and Sisir Kumar Nayak," Apparatus and Method for Measuring and Analysing Breakdown and Pre-Breakdown Phenomena along the Surface of Oil-Immersed Solid Insulation for Oil-Filled Power Equipment" ***Indian patent application number: 202433034553***. (**filed on 01/05/2024, FER reply filed**).

6

Conclusion and future work

Contents

6.1	Summary of the present work…….....	142
6.2	Contribution of the thesis……...……..	143
6.3	Suggestions for future research work…….....	144

6.1. Summary of the present work

This thesis investigates the dielectric insulating properties of natural ester oil (FR3) under oxidative and thermal ageing conditions, with a focus on their applicability in HVDC applications. The research addresses the significant gap in understanding the long-term performance of NEOs under DC voltage stresses and provides valuable insights into the ageing mechanisms affecting these insulating fluids.

Chapter 2 presents the experimental methodology and sample preparation for investigating the dielectric properties of MO and FR3 under oxidative and thermal ageing. The chapter details the ageing processes, post-ageing tests, storage conditions, and the experimental setup for DCBDV testing. This ensures a robust and comprehensive approach to understanding the insulation properties under DC stresses. Statistical analyses of the DCBDV using normal distribution, two-parameter Weibull, and three-parameter Weibull distributions are carried out. For further strengthen the reliability of the DCBDV data, the statistical analysis of the results are validated by Anderson-Darling and goodness-of-fit test . Additionally, this chapter provides a detailed explanation of the theory on how and why DC conductivity is obtained from FDS results and Cole-Cole plots. A detailed examination of the DCBDV and DC conductivity results for MO and FR3 under oxidative and thermal ageing is done. The findings highlight the superior performance of FR3, which exhibits higher DCBDV than MO, especially under positive polarity. The study also reveals that FR3 experiences less severe deterioration in DCBDV and conductivity compared to MO, underscoring the advantageous properties of NEOs in maintaining electrical insulation performance over time.

Chapter 3 investigates the effects of electrode-stressed areas (EESA) on the dielectric strength of NEOs under DC stresses. The experimental results demonstrate that the average DCBDV is higher for sphere electrode configurations, followed by plane and VDE configurations. The study emphasizes the importance of considering geometric effects in the measurement of BDV values and proposes normalization techniques to improve the reliability and consistency of these measurements.

Chapter 4 delves into the effects of ageing on solid insulation, particularly on pressboards immersed in FR3 and MO. The study examines the pressboard insulations chemical, thermal, and mechanical changes due to oxidative and thermal ageing. The findings reveal that FR3-immersed pressboard exhibits superior thermal stability and electrical properties compared to

MO-immersed pressboard under both ageing conditions, although FR3 shows a higher impact of thermal ageing on mechanical strength.

Chapter 5 discusses streamer characteristics and breakdown strength along the surface of solid insulation immersed in liquid dielectrics. The chapter outlines the design of a specialized apparatus for analyzing breakdown and pre-breakdown phenomena, providing a valuable tool for researchers and engineers to develop reliable and efficient materials for high-voltage liquid-filled power apparatus.

6.2. Contribution of the thesis

The major contributions of the thesis for application of NEOs to HVDC transformer are given as follows:

- This thesis presents a detailed and systematic approach to investigate the dielectric properties of insulating oils under oxidative and thermal ageing. The preparation of aged samples, post-ageing tests, and the experimental setup for DCBDV testing contribute to the robustness and reliability of the findings.

- Using the normal distribution, two-parameter Weibull, and three-parameter Weibull distributions, validated by Anderson-Darling and goodness-of-fit tests, provides a thorough statistical framework for analyzing the dielectric breakdown voltage of aged insulating oils. Also, DC conductivity is obtained from Cole-Cole plots through frequency domain analysis.

- This research highlights the superior performance of FR3 compared to MO under oxidative and thermal ageing conditions. The findings on DCBDV and conductivity offer valuable insights into the ageing mechanisms and long-term applicability of natural ester oils in HVDC applications.

- The thesis emphasizes the significance of electrode-stressed areas on the dielectric strength of insulating oils and proposes normalization techniques to improve the accuracy and consistency of BDV measurements.

- By investigating the ageing effects on pressboard insulation immersed in FR3 and MO, this thesis provides a comprehensive understanding of the chemical, thermal, and

mechanical changes in solid insulation, which is crucial for the overall reliability of HVDC transformers.

- The design of a specialized apparatus for analyzing breakdown and pre-breakdown phenomena in liquid-solid dielectrics offers a valuable tool for further research and development in high-voltage insulation systems.

6.3. Suggestions for future research work

The suggestions for further research are given as follows:

- For HVDC applications, this thesis primarily studies DC stresses. However, AC and DC stresses are simultaneously present in converter transformers. Future research should focus on the breakdown voltage (BDV) under DC stresses superimposed with AC stresses, as this approach would provide more accurate and real-time relevant data.

- While this thesis focuses on FR3, future research could explore other NEOs dielectric properties and ageing mechanisms. Investigating a broader range of NEOs could help identify the most suitable materials for HVDC applications and expand the understanding of their performance under different environmental and electrical stress conditions.

- Future studies should consider the effects of particle and water contamination on the dielectric properties of insulating oils. By incorporating contaminant analysis, researchers can develop more accurate models for predicting insulating oils long-term performance and reliability in real-world conditions.

- The current research highlights the importance of electrode-stressed areas. Extending this investigation to include the effects of electrode surface roughness and size variations will provide a more detailed understanding of their impact on BDV measurements. This could lead to the development of standardized electrode configurations for more reliable testing.

- Incorporating advanced computational modelling and simulation techniques can enhance the understanding of complex ageing mechanisms in insulating materials. Future research could develop a predictive model to simulate the long-term behaviour of insulating oils

and solid insulation, allowing for more accurate lifespan predictions and optimized maintenance strategies for HVDC equipment.

List of Publications

Patents

1. **Deepak Kanumuri**, Niharika Baruah, Ambuj Kumar and Sisir Kumar Nayak, "An Apparatus for Analysing Breakdown and Pre-Breakdown Phenomena in Liquid Dielectrics" ***Indian patent number***: **432202** (**Granted on 18/05/2023**; **Filed on: 04/07/2022**).

2. **Deepak Kanumuri**, Niharika Baruah, Ambuj Kumar and Sisir Kumar Nayak," Apparatus and Method for Measuring and Analysing Breakdown and Pre-Breakdown Phenomena along the Surface of Oil-Immersed Solid Insulation for Oil-Filled Power Equipment" ***Indian patent application number*: 202433034553**. (**filed on 01/05/2024; FER reply filed**).

3. Niharika Baruah, Rohith Sangineni, **Deepak Kanumuri**, and Sisir Kumar Nayak, " Long Term Accelerated Multi-Stress Ageing Chamber for Transformer Insulation" ***Indian patent application number*: 202331008919**. (**Granted on 18/05/2023**, **filed on 29/10/2024**).

4. Subhendu Sekhar Sahu, **Deepak Kanumuri**, Sisir Kumar Nayak, “Method and apparatus for Analyzing Partial Discharges in Liquid Insulation and Solid Insulation” ***Indian patent application number*: 202431074410.** (**filed on 01/10/2024; FER reply filed**).

Journal publications

1. **D. Kanumuri,** N. Baruah, A. Kumar and S. K. Nayak, "Effects of Oxidative Aging on Dielectric Strength of Natural Ester Oil Under DC Voltage Stresses," in ***IEEE Transactions on Dielectrics and Electrical Insulation***, vol. 30, no. 4, pp. 1517-1524, Aug. 2023.

2. **D. Kanumuri,** A. Kumar, D. Kanumuri, A. Kumar, N. Baruah and S. K. Nayak, "Influence of Thermal Aging on DC Conductivity and Breakdown Strength of Natural Ester Oils for HVDC Applications," in ***IEEE Transactions on Dielectrics and Electrical Insulation***, vol. 31, no. 6, pp. 3444-3452, Dec. 2024.

3. **D. Kanumuri,** A. Kumar, N. Baruah and S. K. Nayak, " Effects of Electrode Geometry on Dielectric Breakdown Strength of Natural Ester Oils for HVDC Applications," is

submitted in ***IEEE Transactions on Dielectrics and Electrical Insulation,*** Jan. 2025. [**Under Review**]

Conference publications

1. **D. Kanumuri**, A. Kumar, S. S. Sahu, S. Anand, N. Baruah and S. K. Nayak, "Degradation Study of Oxidatively Aged Natural Ester Oil Immersed Pressboard Insulation," ***2024 IEEE 7th International Conference on Condition Assessment Techniques in Electrical Systems (CATCON),*** Kolkata, India, 2024, pp. 1-6.

2. **D. Kanumuri,** R. Sangineni, N. Baruah and S. K. Nayak, "Study of magnetic properties of mineral oil based nanofluids," ***2021 IEEE International Conference on the Properties and Applications of Dielectric Materials (ICPADM),*** Johor Bahru, Malaysia, 2021, pp. 226-229.

3. A. Kumar, **D. Kanumuri**, S. S. Sahu, N. Baruah and S. K. Nayak, "Effect of Furfural on Dielectric Characteristics of Mineral Oil," ***2024 IEEE 7th International Conference on Condition Assessment Techniques in Electrical Systems (CATCON),*** Kolkata, India, 2024, pp. 177-180.

4. S. S. Sahu, **D. Kanumuri**, A. Kumar and S. K. Nayak, "Effect of TiO_2 and ZnO on the Dielectric Properties of Natural Ester Oil Nanofluid Impregnated Pressboard Insulation," ***2024 IEEE 7th International Conference on Condition Assessment Techniques in Electrical Systems (CATCON),*** Kolkata, India, 2024, pp. 171-176.

5. R. Sangineni, **D. Kanumuri**, N. Baruah, S. K. Nayak, “Non-Isothermal Thermo Gravimetric Analysis (TGA) Measurements of Oxidative Aged Solid Insulation,” in ***IEEE 5th International Conference on Condition Assessment Techniques in Electrical Systems (CATCON)***, December, (2021), India.

6. R. Sangineni, N. Baruah, **D. Kanumuri**, S. K. Nayak, “Comparison of magnetic nature of vegetable oil based nanofluids,” in ***39th Electrical Insulation Conference (EIC),*** online from 7-20 June, (2021), USA.

7. N. Baruah, R. Sangineni, C. Saha, **D. Kanumuri**, M. Chakraborty, S. K. Nayak, "Supervised machine learning model for predictive analysis of dielectric response of insulating liquids," in ***IEEE Conference on Electrical Insulation and Dielectric Phenomena (CEIDP)***, 12-15 December, (2021), Vancouver, Canada.

Bibliography

[1]. T. Le, "HVDC Technologies & ABB Experience," *ABB22* April 2013.

[2]. O. E. Oni, I. E. Davidson, and K. N. Mbangula, "A review of LCC-HVDC and VSC-HVDC technologies and applications," in *IEEE 16th International Conference on Environment and Electrical Engineering (EEEIC)*, 2016, pp. 1-7.

[3]. M. P. Bahrman and B. K. Johnson, "The ABCs of HVDC transmission technologies," *IEEE Power Energy M*, vol. 5, no. 2, pp. 32-44, 2007.

[4]. Z.D. Yang, W.Y. Yin, and Y.N. Li, "Reactive Power Compensation and Control Scheme for the Three Gorges to Shanghai DC Project," *Electric Power Construction*, vol. 12, p. 004, 2007.

[5]. Siemens, "The world's first HVDC transformer passes the test for ±1,100 kV level", January, 2018.

[6]. Zhou Mu, "Space Charge Behaviors of Mineral Oil and Ester Liquids Impregnated Cellulose Paper Insulations under DC Stress" *PhD Thesis*, *Univ of Manchester*, 2018.

[7]. IEC 61378-3:2015, "Converter transformers Part 3: Application guide".

[8]. A. Carlson, "Specific requirements on HVDC converter transformers," *ABB Transformers* AB, Ludvika, Sweden, 1996.

[9]. H. Jin, P. Morshuis, A. R. Mor, and J. J. Smit, "Partial discharge behaviour of mineral oil based nanofluids," *IEEE Trans. Dielectr. Electr. Insul.*, vol. 22, pp 2747-2753, 2015.

[10]. T. V. Oommen, "Vegetable oils for liquid-filled transformers," *IEEE Electr. Insul. Mag.*, vol. 18, no. 1, pp. 6-11, 2002.

[11]. C. P. McShane, "Vegetable-oil-based dielectric coolants," *IEEE Ind. Appl. Mag.*, vol. 8, no. 3, pp. 34-41, 2002.

[12]. T. V. Oommen, C. C. Claiborne, and J. T. Mullen, "Biodegradable electrical insulation fluids," in *IEEE Electr. Insul., Electr. Manufacturing and Coil Winding Conf.*, 1997, pp. 465-468.

[13]. D. M. Nail and P. H. Shoun, "Retrofilling-a technique to reduce polychlorinated biphenyls (pcb's)," *IEEE Power Engg. Rev.*, vol. 4, no. 3, pp. 26-26, 1984.

[14]. I. Webber, D. B. Pilgrim, and M. A. Thompson, "The safe disposal of polychlorinated biphenyls," *IEEE Trans. Ind. Appl.*, vol. IA-20, no. 1, pp. 159-166. 1984.

[15]. U. M. Rao, I. Fofana, T. Jaya, E. M. Rodriguez-Celis, J. Jalbert, and P. Picher, "Alternative dielectric fluids for transformer insulation system: progress, challenges, and future prospects," *IEEE Access*, vol. 7, pp. 184552 – 184571, 2019.

[16]. EPRI EL-4004, “HVDC Converter Transformer Insulation”, *final Report*, May 1985.

[17]. A. Emsley and G. Stevens, "Review of chemical indicators of degradation of cellulosic electrical paper insulation in oil-filled transformers," *IEE Proceedings-Science, Measurement and Technology*, vol. 141, no. 5, pp. 324- 334, 1994.

[18]. *IEC 60422: 2013*, “Mineral insulating oils in electrical equipment - Supervision and maintenance guidance.”.

[19]. R. Heywood, A. Emsley, and M. Ali, "Degradation of cellulosic insulation in power transformers. Part 1: Factors affecting the measurement of the average viscometric degree of polymerisation of new and aged electrical papers," *IEE Proceedings-Science, Measurement and Technology*, vol. 147, no. 2, pp. 86- 90, 2000.

[20]. IEC 60156, “Insulating liquids - Determination of the breakdown voltage at power frequency - Test method”, 2018.

[21]. ASTM D1816-12 “Standard Test Method for Dielectric Breakdown Voltage of Insulating Liquids Using VDE Electrodes”, 2019.

[22]. ASTM D877, “Standard Test Method for Dielectric Breakdown Voltage of Insulating Liquids Using Disk Electrodes”, 2018.

[23]. J. Jadidian, “Charge transport and breakdown physics in liquid/solid insulation systems.” *PhD. Diss*, *Massachusetts Institute of Technology*, 2013.

[24]. T. V. Oommen, C. C. Claiborne, E. J. Walsh, and J. P. Baker, “A new vegetable oil-based transformer fluid: development and verification,” in *IEEE Conf. Electr. Insul. Dielectr. Phenomena*, Victoria, BC, Canada, 2000, pp. 308-312.

[25]. C. P. McShane, “Relative properties of the new combustion-resist vegetable-oil-based dielectric coolants for distribution and power transformers,” *IEEE Trans. Dielectr. Electr. Insul.*, vol. 37, no. 4, pp. 1132-1139, 2001.

[26]. M. Hrkac, P. Papageorgiou, I. Kosmoglou, and G. Miatto, “BIOTEMP® transformer technology for innovative compact substation,”in *7th Mediterranean Conference and Exhibition on Power Generation, Transmission, Distribution and Energy Conversion (MedPower 2010)*, Agia Napa, Cyprus, 2010, pp. 1-6.

[27]. C. P. McShane, “New dielectric coolant concepts for distribution and power transformers,” in *IEEE Pulp and Paper, Ind. Technical Conf.*, 1999, pp. 55 –62.

[28]. M. Mazzaro, et.al., “Power transformer fire and environmental risk reduction by using natural esters,” in *Int’l. Conf. Dielectr. Liquids (ICDL)*, Manchester, UK, 2017, pp. 1-4.

[29]. L. Pompili, A. Calcara, and C. F. Sturchio, “Natural esters distribution transformers: a solution for environmental and fire risk prevention,” in *Int.l’ Annu. Conf. Sustainable Development in the Mediterranean Area, Energy and ICT Networks of the Future*, Capri, Italy, 2017.

[30]. T. A. Prevost and T. V. Oommen, "Cellulose insulation in oil-filled power transformers: part I - history and development," *IEEE Electr. Insul. Mag*., vol. 22, no. 1, pp. 28-35, 2006.

[31]. D. Martin and Z. D. Wang, "Statistical analysis of the AC breakdown voltages of ester-based transformer oils," *IEEE Trans. Dielectr. Electr. Insul.*, vol.15, pp. 1044-1050, 2008.

[32]. P. Totzauer and P. Trnka, "Different ways to improve natural ester oils," *Transportation Research Procedia*, vol.40, pp. 102–106, 2019.

[33]. H. B. H. Sitorus, R. Setiabudy, S. Bismo, and A. Beroual, "Jatropha curcas methyl ester oil obtaining as vegetable insulating oil," *IEEE Trans. Dielectr. Electr. Insul.*, vol. 23, no. 4, pp. 2021-2028, 2016.

[34]. D. M. Mehta, P. Kundu, A. Chowdhury, V.K. Lakhiani, and A.S. Jhala, "A review on critical evaluation of natural ester vis-a-vis mineral oil insulating liquid for use in transformers: part 1," *IEEE Trans. Dielectr. Electr. Insul.*, vol. 23, pp.873-880, 2016.

[35]. V-H. Dang, A. Beroual, and C. Perrier, "Comparative study of statistical breakdown in mineral, synthetic and natural ester oils under AC voltage," *IEEE Trans. Dielectr. Electr. Insul.*, vol. 19, pp. 1508-1513, 2012.

[36]. B. X. Diu and X. L. Li, "Dielectric and thermal characteristics of vegetable oil filled with BN nanoparticles," *IEEE Trans. Dielectr. Electr. Insul.*, vol. 24, no. 2, pp.956-963, 2017.

[37]. H. B. H. Sitorus, A. Beroual, and R. Setiabudy, "Pre-breakdown phenomena in new vegetable oil - based jatropha curcas seeds as substitute of mineral oil in high voltage equipment," *IEEE Trans. Dielectr. Electr. Insul.*, vol. 22, no. 5, pp. 2442-2448, 2015.

[38]. V-H. Dang, A. Beroual, and C. Perrier, "Investigations on streamers phenomena in mineral, synthetic and natural ester oils under lightning impulse voltage," *IEEE Trans. Dielectr. Electr. Insul.*, vol. 19, no. 5, pp. 1521-1527, 2012.

[39]. Nynas Naphthenics AB, "Base oil handbook", *Nynas Naphthenics AB*, Sweden, 2001.

[40]. H. G. Erdman, "Electrical Insulating Oils", *American Society for Testing and Materials*, USA, 1988.

[41]. L. Lewand, "Laboratory Evaluation of Several Synthetic and Agricultural-Based Dielectric Liquids", *Doble International Client Conference*, USA, 2001.

[42]. Ab Ghani, Sharin, et.al., "Methods for improving the workability of natural ester insulating oils in power transformer applications: A review," *Electr. Power Syst. Res* 163, 2018, pp: 655-667.

[43]. I. Fofana, "50 years in the development of insulating liquids," in *IEEE Electr. Insul. Mag*, vol. 29, no. 5, pp. 13-25, September-October 2013.

[44]. U. Piovan, "Insulation systems for HVDC transformers: Present configurations, trends, challenges, solutions and open points," *2013 IEEE International Conference on Solid Dielectrics (ICSD)*, Bologna, Italy, 2013, pp. 254-257.

[45]. *Cigre*, "Analysis of HVDC Thyristor Converter Transformer Performance", 2004.

[46]. CIGRE, "HVDC Converter Transformers, Design Review, Test Procedures, Ageing Evaluation and Reliability in Service." *Joint working group A2-B4 (28), CIGRÉ*, 2010.

[47]. U. Khaled, and A. Beroual, "DC breakdown voltage of natural ester oil-based Fe_3O_4, Al_2O_3, and SiO_2 nanofluids." *Alex. Eng. J*, 59, no. 6 ,2020, pp. 4611-4620.

[48]. S. O. Oparanti, F. R. Tambuwal, A. A. Khaleed and A. A. Abdelmalik, "DC and AC Breakdown Analysis of Neem Ester/ SiO2 Nanofluid for High Voltage Insulation," 2021 *IEEE Conference on Electrical Insulation and Dielectric Phenomena (CEIDP)*, Vancouver, BC, Canada, 2021, pp. 383-386.

[49]. G. D. P. Mahidhar, R. Sarathi, N. Taylor and H. Edin, "Study on performance of silica nanoparticle dispersed synthetic ester oil under AC and DC voltages," in *IEEE Trans. Dielectr: Electr. Insul.*, vol. 25, no. 5, pp. 1958-1966, Oct. 2018.

[50]. K. Swati, K. S. Yadav, R. Sarathi, R. Vinu and M. G. Danikas, "Understanding Corona discharge activity in titania nanoparticles dispersed in transformer oil under AC and DC voltages," in *IEEE Trans. Dielectr: Electr. Insul.*, vol. 24, no. 4, pp. 2325-2336, 2017.

[51]. J. Hao, et al. "Comparative study on the dynamic migration of cellulose particles and its effect on the conductivity in natural ester and mineral oil under DC electrical field", *IET Gener. Transm. Distrib*,11(9), 2017, pp. 2375-2383.

[52]. J. Hao, L. Ruijin, Y. Li, M. Dan, and Y. Lijun, "A comparative study of the particle accumulation in natural ester and mineral oil under DC electric field." In 2017 *IEEE 19th Int. Conf. Dielectric Liquids (ICDL)*, pp. 1-4. IEEE, 2017.

[53]. Y. Li, J. Hao, M. Dan, R. Liao and L. Yang, "A comparative study of the migration behaviors of cellulose particles in natural ester and mineral oil under DC electrical field," *2017 1st International Conference on Electrical Materials and Power Equipment (ICEMPE)*, Xi'an, China, 2017, pp. 301-304.

[54]. F. Vahidi, K. Rapp, J. Luksich and S. Tenbohlen, "Comparative Study on Impact of Cellulose Particles on Electrical Conductivity of Mineral Oil and Natural Ester," *VDE High Voltage Technology 2016; ETG-Symposium*, Berlin, Germany, 2016, pp. 1-6.

[55]. T. Zhao, N. Chao, Y. Liu and Y. Tong, "Experiment and Mechanism of Bridging Effect of Cellulose Particles in Natural Ester Oil Gap under DC Voltage," *2020 5th Asia Conference on Power and Electrical Engineering (ACPEE)*, Chengdu, China, 2020, pp. 1918-1922.

[56]. L. Cheng, Yi Jiang, M. Dan, W. Hao, Y. Li, W. Qin, and J. Hao, "Effects of fiber and copper particles on conductivity and breakdown characteristics of natural ester and mineral oil under DC voltage." *Energies* 13, no. 7 ,2020, pp. 1818.

[57]. R. Zou, et al. "DC breakdown characteristics and charges accumulation behaviour of thermally upgraded paper aged in natural ester." *IET sci. meas. technol.* 15.9 (2021): 701-709.

[58]. H. Yoon, G. Chen and I. L. Hosier, "Influence of Thermal Aging on Dielectric Properties of Natural Ester Oil-Impregnated Paper," in *IEEE Trans. Dielectr: Electr. Insul*, vol. 30, no. 3, pp. 1337-1344, June 2023.

[59]. H. Nadarajah, et.al. "Breakdown Characteristics of Unused Transformer Oil and Olive Oil under AC and DC Voltages at Different Temperature Rate." *nt. J. Integr. Eng*, 14, no. 3, 2022, pp. 33-40.

[60]. P. Rumpelt and F. Jenau, "A study of oil impregnated pressboard insulation based on ester fluids for an application in HVDC insulation systems," *2017 IEEE International Conference on Environment and Electrical Engineering and 2017 IEEE Industrial and Commercial Power Systems Europe (EEEIC / I&CPS Europe)*, Milan, Italy, 2017, pp. 1-4.

[61]. F. Schober, "Electrical conductivity of pressboard as a diagnostic quantity for HVDC equipment." *Diegnostik Elektrischer Betriebsmittel*, Berlin, 2014.

[62]. M. H. S. Zainoddin, H. Zainuddin and A. Aman, "Effects of viscosity of ester oils and different sizes of suspended cellulose particles on bridging phenomenon under non-uniform DC electric field," *2016 IEEE International Conference on Power and Energy (PECon)*, Melaka, Malaysia, 2016, pp. 285-289.

[63]. A. Beroual, U. Khaled, P. Seraphine Mbolo Noah, and H. Sitorus. "Comparative study of breakdown voltage of mineral, synthetic and natural oils and based mineral oil mixtures under AC and DC voltages." *Energies* 10, no. 4, 2017, pp. 511.

[64]. J. Hao, M. Dan, R. Liao and J. Li, "Effect of Moisture on Particles Accumulation and Oil Breakdown Characteristics in Mineral Oil and Natural Ester Under Non-Uniform DC Electrical Field," in *IEEE Access*, vol. 7, pp. 101785-101794, 2019.

[65]. R.Liao, et al, "Influence of oil aging on the motion characteristics of cellulose particles and conductivity in contaminated mineral oil and natural ester under DC

electric field." *IEEJ Transactions on Electrical and Electronic Engineering*, 13(10), 2018, pp: 1384-1393.

[66]. J. Fabian, B. Jocham, B. Nader, R. Woschitz and M. Muhr, "Current challenges and issues of designing HVDC converter transformers," *2011 Annual Report Conference on Electrical Insulation and Dielectric Phenomena*, Cancun, Mexico, 2011, pp. 432-435.

[67]. Y. Jing et al., "DC Breakdown Properties and Mobility Characteristics of Different Insulation Liquids Applying in Transformer," *2021 International Conference on Advanced Electrical Equipment and Reliable Operation (AEERO)*, Beijing, China, 2021, pp. 1-4.

[68]. Y. Jing et al., "Dielectric properties of natural ester, synthetic ester midel 7131 and mineral oil diala D," in *IEEE Trans. Dielectr: Electr. Insul.*, vol. 21, no. 2, pp. 644-652, April 2014.

[69]. G. G. Muscio, L. Calcara, M. Pompili and G. De Bellis, "Effect of strong DC Electric Fields on the flow properties of insulating liquids at different temperatures," 2023 *IEEE 22nd Int. Conf. Dielectric Liquids (ICDL)*, Worcester, MA, USA, 2023, pp. 1-4.

[70]. R. Patrick, and F. Jenau, "Oil impregnated pressboard barrier systems based on ester fluids for an application in HVDC insulation systems." 2017: 2147.

[71]. J. Xiang, Q. Liu and Z. D. Wang, "Streamer characteristic and breakdown in a mineral oil and a synthetic ester liquid under DC voltage," in *IEEE Trans. Dielectr: Electr. Insul.*, vol. 25, no. 5, pp. 1636-1643, Oct. 2018.

[72]. A. M. Alshehawy, Z. Mu, S. Matharage, Q. Liu and Z. Wang, "Space Charge Behaviors of Ester Liquid and Kraft Paper Double-Layer Insulation Systems at Polarity Reversal," 2022 *IEEE 21st Int. Conf. Dielectric Liquids (ICDL)*, Sevilla, Spain, 2022, pp. 1-4.

[73]. A. Fatih, A. Ersoy, and P. Rozga. "Investigation of effects of different high voltage types on dielectric strength of insulating liquids." *Energies*, 15(21), 2022, pp: 8116.

[74]. Bo Huang," Space Charge Behaviour of Thick Oil and Pressboard in a HVDC Converter Transformer", *PhD Thesis, University of Southampton*, 2018.

[75]. Zhou Mu," Space Charge Behaviours of Mineral Oil and Ester Liquids Impregnated Cellulose Paper Insulations under DC Stress", *PHD thesis, The University of Manchester*.

[76]. H. Yoon and G. Chen, "Space Charge Characteristics of Natural Ester Oil-Impregnated Paper with Different Moisture Contents," in *IEEE Trans. Dielectr: Electr. Insul.*, vol. 29, no. 6, pp. 2139-2146, Dec. 2022.

[77]. C. G. Azcarraga, “Partial Discharge Phenomena in Converter and Traction Transformers: Identification and Reliability.” *PhD dissertation*, *University of Bologna*, 2014.

[78]. P. Trnka, J. Hornak, M. Svoboda and J. Pihera, "Partial discharges under DC voltage in paper-oil insulating system," 2015 *IEEE 11th International Conference on the Properties and Applications of Dielectric Materials (ICPADM*), Sydney, NSW, Australia, 2015, pp. 436-439.

[79]. Q. Wang, B. Bai, D. Chen, T. Fu and Q. Ma, ""Study of Insulation Material Properties Subjected to Nonlinear AC–DC Composite Electric Field for Converter Transformer,"" in *IEEE Trans. Magn*, vol. 55, no. 2, pp. 1-4, Feb. 2019, Art no. 8400604.

[80]. Y. Shuai, X. Han, L. Zhang, C. Yang, X. Hu and H. Wu, "Major insulation design consideration of converter transformer," *2016 International Conference on Condition Monitoring and Diagnosis (CMD),* Xi'an, China, 2016, pp. 1004-1007.

[81]. S. Liang, J. Li, L. Chen, F. Wang, X. Lin and Y. Wang, "Measurement and influence factor analysis of ion mobility of vegetable insulation oil," *2017 IEEE 19th Int. Conf. Dielectric Liquids (ICDL),* Manchester, UK, 2017, pp. 1-4.

[82]. H. B. H. Sitorus, A. Beroual, R. Setiabudy and S. Bismo, "Statistical analysis of AC and DC breakdown voltage of JMEO (Jatropha methyl ester oil), mineral oil and their mixtures," 2017 *IEEE 19th International Conference on Dielectric Liquids (ICDL*), Manchester, UK, 2017, pp. 1-4.

[83]. M. Yea, K. J. Han, J. Park, S. Lee and J. Choi, "Design optimization for the insulation of HVDC converter transformers under composite electric stresses," in *IEEE Trans. Dielectr: Electr. Insul*, vol. 25, no. 1, pp. 253-262, Feb. 2018.

[84]. “MIDEL Selection Guide”, *M&I Mater. Ltd*., Manchester, U.K., Mar. 2017.

[85]. Envirotemp, "Dielectric Fluids.", *Envirotemp FR3 Dielectric Fluid-Technical Data Sheets* (2013).

[86]. Brochure, “A. B. B. "BIOTEMP® dielectric insulating fluid." *Zürich*: *ABB (2011).*

[87]. D. Martin, N. Lelekakis, W. Guo and Y. Odarenko, "Further studies of a vegetable-oil-filled power transformer," in *IEEE Electr. Insul. Mag*., vol. 27, no. 5, pp. 6-13, September-October 2011.

[88]. J. Carcedo, I. Fernández, A. Ortiz, F. Delgado, C. J. Renedo and C. Pesquera, "Aging assessment of dielectric vegetable oils," in *IEEE Electr. Insul.* Mag, vol. 31, no. 6, pp. 13-21, November-December 2015.

[89]. D. Martin, “Evaluation of the dielectric capabilities of ester-based oils for power transformers”, *Ph.D. thesis, The Univ. of Manchester*, UK, 2007.

[90]. D. Martin, Z. D. Wang, A. W. Darwin and I. James, "A Comparative Study of the Chemical Stability of Esters for Use in Large Power Transformers," *IEEE Conf. Electr. Insul. Dielectr. Phen. (CEIDP)*, 2006, pp. 493-496,

[91]. H. M. Wilhelm, L. Tulio, R. Jasinski and G. Almeida, "Aging markers for in-service natural ester-based insulating fluids," in *IEEE Trans. Dielectr. Electr. Insul*., vol. 18, no. 3, pp. 714-719, June 2011.

[92]. S. Tenbohlen and M. Koch, "Aging Performance and Moisture Solubility of Vegetable Oils for Power Transformers," in *IEEE Trans. Power Deliv*., vol. 25, no. 2, pp. 825-830, April 2010.

[93]. N. Baruah, R. Sangineni, M. Chakraborty and S. K. Nayak, "Estimation of Dielectric Parameters of Aged Natural Ester based Insulating Liquid using Open Beaker Oxidative Ageing technique," 2021 *IEEE 12th Energy Convers. Congr. Expo, - Asia (ECCE-Asia)*, 2021, pp. 1833-1838.

[94]. N. Baruah, R. Sangineni, M. Chakraborty and S.K. Nayak “Investigation of Natural Ester based Insulating Liquid using Statistical Hypothesis Testing”. *IEEJ Trans. Fundam. Mater*., 141(10), 560-566. (2021).

[95]. T. Zhao, M. Fan, H. Yue, Y. Liu and Z. Zhang, "Effect of Cellulose Particles on Breakdown Voltage in Wet FR3 Natural Ester," in *IEEE Access*, vol. 7, pp. 119357-119366, 2019.

[96]. T. Zhao, M. Fan, N. Chao, Y. Liu and Z. Zhang, "The Analysis of Cellulose Particles Bridging in Natural Ester Oil under DC Voltage," 2019 *IEEE 20th Int. Conf. on Dielectric Liquids (ICDL))*, 2019, pp. 1-4.

[97]. P. Rumpelt, E. Burkhardt and F. Jenau, "DC-conductivity of insulating oil at lower temperatures," 2017 IEEE 19th *Int. Conf. Dielectric Liquids (ICDL)*, Manchester, UK, 2017, pp. 1-3.

[98]. B. S. H. M. S. Y. Matharage, M. A. R. M. Fernando, M. A. A. P. Bandara, G. A. Jayantha and C. S. Kalpage, "Performance of coconut oil as an alternative transformer liquid insulation," in *IEEE Trans. Dielectr. Electr. Insul*, vol. 20, no. 3, pp. 887-898, June 2013.

[99]. J. Liu, L. Zhou, G. Wu, Y. Zhao, P. Liu and Q. Peng, "Dielectric frequency response of oil-paper composite insulation modified by nanoparticles," in *IEEE Trans. Dielectr. Electr. Insul*, vol. 19, no. 2, pp. 510-520, April 2012.

[100]. ASTM D1934-20, "Standard Test Method for Oxidative Aging of Electrical Insulating Liquids by Open-Beaker Method,".

[101]. "IEEE Standard Test Procedure for Thermal Evaluation of Liquid-Immersed Distribution and Power Transformers," in *IEEE Std C57.100-1999*, vol., no., pp.1-17, 7 Oct. 1999.

[102]. "SMaRT, user guide", *solartron analytical*, Feb. 2003.

[103]. K. S. Cole and R. H. Cole, "Dispersion and absorption in dielectrics – I: alternating current characteristics," *J. Chem. Phys*., vol. 9, no. 4, p. 341-351, 1941.

[104]. K. S. Cole and R. H. Cole, "Dispersion and absorption in dielectrics – II: direct current characteristics," *J. Chem. Phys*., vol. 10, no. 2, p. 98-105, 1942.

[105]. E. Tuncer, Y. V. Serdyuk, and S. M. Gubanski, "Dielectric mixtures: electrical properties and modeling," *IEEE Trans. Electr. Insul.*, vol. 9, no. 5, pp. 809– 828, 2002.

[106]. K. Kondo, T. Chiba, S. Ando, S. Yoshida, Y. Shimada, T. Nakamura, N. Matsushita, and M. Abe, "Cole-Cole impedance analysis on spin sprayed Ni-Zn-Co ferrite films exhibiting strong magnetic loss in gigahertz range," *IEEE Trans. Magnetics*, vol. 39, no. 5, pp. 3130–3132, 2003.

[107]. A. N. Asokan, A. P. Anagha, P. Preetha, and K. Sunitha, "Effect of interphase on dielectric relaxation mechanisms in epoxy-alumina nanocomposite," *IEEE Trans. Dielectr. Electr. Insul*., vol. 26, no. 4, pp. 1211–1219, 2019.

[108]. D. Kanumuri, N. Baruah, A. Kumar and S. K. Nayak, "Effects of Oxidative Aging on Dielectric Strength of Natural Ester Oil Under DC Voltage Stresses," in *IEEE Trans. Dielectr. Electr. Insul*, vol. 30, no. 4, pp. 1517-1524, Aug. 2023.

[109]. A. Reffas, A. Beroual and H. Moulai, "Comparison of breakdown voltage of vegetable olive with mineral oil, natural and synthetic ester liquids under DC voltage," in *IEEE Trans. Dielectr. Electr. Insul*, vol. 27, no. 5, pp. 1691-1697, Oct. 2020.

[110]. U. Khaled and A. Beroual, "Statistical Investigation of AC Dielectric Strength of Natural Ester Oil-Based Fe_3O_4, Al_2O_3, and SiO_2 Nano-Fluids," in *IEEE Access*, vol. 7, pp. 60594-60601, 2019.

[111]. T. Nakagawa and S. Osaki, "The Discrete Weibull Distribution," in *IEEE Trans* Reliab, vol. R-24, no. 5, pp. 300-301, Dec. 1975.

[112]. L. Jäntschi and S. D. Bolboacă, "Computation of probability associated with Anderson–Darling statistic". *Mathematics*, 6(6), 88. (2018).

[113]. M. Maharana, N. Baruah, S.K. Nayak, and N. Sahoo, “Effect of oxidative ageing on the thermophysical and electrical properties of the nanofluid with statistical analysis of AC breakdown voltage”. *IET Sci. Meas. Technol*, 12(8), pp.1074-1081. 2018.

[114]. P Rozga, S. Marcin. “Characteristics of streamers developing at inception voltage in small gaps of natural ester, synthetic ester and mineral oil under lightning impulse”. *IET Sci. Meas. Technol*, 2016, 10, 50-57.

[115]. B. Chakraborty, S. Maur, A. K. Pradhan, B. Chatterjee and S. Dalai, "Insight the Impact of TiO_2 and Al_2O_3 Nanoparticles in Mineral, Vegetable Oil Based on AC Dielectric Properties—Conformity with Weibull Distribution," in *IEEE Trans Plasma Sci*, vol. 51, no. 10, pp. 3095-3102, Oct. 2023.

[116]. M. Koch, S. Tenbohlen, M. Krüger, and A. Kraetge, "A comparative test and consequent improvements on dielectric response methods", *In Proceedings of the XVth International Symposium on High Voltage Engineering*, ISH, Ljubljana, Slovenia. 2007.

[117]. A. A. Abdelmalik, J. C. Fothergill and S. J. Dodd, "Electrical conduction and dielectric breakdown characteristics of alkyl ester dielectric fluids obtained from palm kernel oil," in *IEEE Trans. Dielectr. Electr. Insula*. vol. 19, no. 5, pp. 1623-1632, October 2012.

[118]. F. Schober, A. Küchler, and C. Krause, “Oil conductivity–an important quantity for the design and the condition assessment of HVDC insulation systems” *FHWS Science Journal*, 1(2), 59-78, 2014.

[119]. N. Baruah, S. K. Nayak and S. K. Pratihar, "Quantitative Effect of Aging Duration on Dielectric Parameters Based on Frequency Response," in *IEEE Trans Instrum Meas*, vol. 71, pp. 1-9, 2022.

[120]. J. Liu, T. Sun, X. Fan, Y. Zhang and B. Lai, "A Modified Simulation Model for Predicting the FDS of Transformer Oil-Paper Insulation Under Nonuniform Aging," in *IEEE Trans Instrum Meas*, vol. 70, pp. 1-9, 2021.

[121]. D. Mishra, A. Baral, N. Haque and S. Chakravorti, "Condition Assessment of Power Transformer Insulation Using Short-Duration Time-Domain Dielectric Spectroscopy Measurement Data," in *IEEE Trans Instrum Meas*, vol. 69, no. 7, pp. 4404-4411, July 2020

[122]. M. Maharana, N. Baruah, S. K. Nayak, N. Meher and P. K. Iyer, "Condition Assessment of Aged Ester-Based Nanofluid Through Physicochemical and Spectroscopic Measurement," in *IEEE Trans Instrum Meas*, vol. 68, no. 12, pp. 4853-4863, Dec. 2019.

[123]. W. M. F. Al-Masri, M. F. Abdel-Hafez and A. H. El-Hag, "A Novel Bias Detection Technique for Partial Discharge Localization in Oil Insulation System," in *IEEE Trans Instrum Meas,* vol. 65, no. 2, pp. 448-457, Feb. 2016.

[124]. M. Chakraborty, R. Sangineni, N. Baruah and S. K. Nayak, "A Sandwich Layer Method for Moisture Extraction in Transformer Insulating Oils Using Metal Organic Frameworks," in *IEEE Trans Instrum Meas,* vol. 72, pp. 1-8, 2023.

[125]. X. Fan, J. Liu, B. Lai, Y. Zhang and C. Zhang, "FDS Measurement-Based Moisture Estimation Model for Transformer Oil-Paper Insulation Including the Aging Effect," in *IEEE Trans Instrum Meas*, vol. 70, pp. 1-10, 2021.

[126]. M. G. Danikas, "Breakdown of transformer oil," in *IEEE Electr. Insul. Mag*., vol. 6, no. 5, pp. 27-34, Sept.-Oct. 1990.

[127]. K. H. Weber and H. S. Endicott, "Area Effect and Its Extremal Basis for the Electric Breakdown of Transformer Oil," in *Transactions of the American Institute of Electrical Engineers. Part III: Power Apparatus and Systems,* vol. 75, no. 3, pp. 371-381, Jan. 1956.

[128]. K. H. Weber and H. S. Enditott, "Extremal area effect for large-area electrodes for the electric breakdown of transformer oil," *1956 Conference on Electrical Insulation,* Schenectady, NY, USA, 1956, pp. 53-56.

[129]. W. R. Wilson, "A fundamental factor controlling the unit dielectric strength of oil," in *Transactions of the American Institute of Electrical Engineers. Part III: Power Apparatus and Systems*, vol. 72, no. 1, pp. 68-74, Feb. 1953.

[130]. Y. Kawaguchi, H. Murata and M. Ikeda, "Breakdown of Transformer Oil," in *IEEE Trans. Power App. Syst.*, vol. PAS-91, no. 1, pp. 9-23, Jan. 1972.

[131]. K. Kato, X. Han and H. Okubo, "Insulation optimization by electrode contour modification based on breakdown area/volume effects," in *IEEE Trans Dielectr Electr Insul*., vol. 8, no. 2, pp. 162-167, April 2001.

[132]. R. M. Del Vecchio, "Geometric effects in the electrical breakdown of transformer oil," in *IEEE Trans. Power Deliv*, vol. 19, no. 2, pp. 652-656, April 2004.

[133]. X. Wang, Z. D. Wang, C. Perrier, and S. Northcote. "Electrode area effect on dielectric breakdown strengths of mineral oil and esters." in *XVII International Symposium on High Voltage Engineering,* Hannover. 2011.

[134]. X. Wang and Z. D. Wang, "Study of dielectric behavior of ester transformer liquids under ac voltage," in *IEEE Trans. Dielectr. Electr. Insul*., vol. 19, no. 6, pp. 1916-1925, December 2012.

[135]. H. Goshima, N. Hayakawa, M. Hikita, H. Okubo and K. Uchida, "Weibull statistical analysis of area and volume effects on the breakdown strength in liquid nitrogen," in *IEEE Trans. Dielectr. Electr. Insul*., vol. 2, no. 3, pp. 385-393, June 1995.

[136]. W. Hauschild, W. Mosch "Statistical techniques for high-voltage engineering", *IET*, 1992.

[137]. W. Weibull "A statistical distribution function of wide applicability". *J. Appl. Mech*., pp. 293-297, Sept.1951.

[138]. S. Ul-Haq and G. R. G. Raju, "Weibull statistical analysis of area effect on the breakdown strength in polymer films," *Annual Report Conference on Electrical Insulation and Dielectric Phenomena*, Cancun, Mexico, 2002, pp. 518-521.

[139]. N. Hayakawa, H. Sakakibara, H. Goshima, M. Hikita and H. Okubo, "Mutual contribution of area and volume effects on breakdown strength in liquid nitrogen," *ICDL'96. 12th International Conference on Conduction and Breakdown in Dielectric Liquids*, Roma, Italy, 1996, pp. 333-336.

[140]. KJ Rapp, CP McShane, J. Luksich, "Interaction mechanisms of natural ester dielectric fluid and Kraft paper", In *IEEE Int. Conf. Dielectr. Liq.*, 2005. ICDL 2005. 2005 Jun 26, pp. 393-396.

[141]. McShane CP, Rapp KJ, Corkran JL, Gauger GA, Luksich J. "Aging of paper insulation in natural ester dielectric fluid". *In IEEE/PES Transmission and Distribution Conf. and Expos. Developing New Perspectives.* 2001 Nov 2 (Vol. 2, pp. 675-679). IEEE.

[142]. Sun C, Li J, Li X, Grzybowski S. "Electric properties of vegetable oil-based dielectric liquid and lifetime estimation of the oil-paper insulation". *In 2006 IEEE Conf. Electr. Insul. Dielectr. Phenomena* 2006 Oct 15 (pp. 680-683). IEEE.

[143]. SA Wani, AS Rana, S Sohail, O Rahman, S Parveen, SA Khan, "Advances in DGA based condition monitoring of transformers: A review" *Renew. Sust. Energ.* Rev. 2021 Oct 1, pp. 149:111347.

[144]. M. Rafiq, YZ Lv, Y Zhou, Ma KB, W Wang, CR Li, Q Wang, "Use of vegetable oils as transformer oils–a review.", *Renew. Sust. Energ*. Rev. 2015 Dec 1; 52:308-24.

[145]. HP. Shanmugasundram, E. Jayamani, KH. Soon, "A comprehensive review on dielectric composites: Classification of dielectric composites." *Renew. Sust. Energ. Rev*, 2022 Apr 1; 157:112075.

[146]. M. Karatas, Y. Bicen, "Nanoparticles for next-generation transformer insulating fluids: A review.", *Renew. Sust. Energ. Rev*, 2022 Oct 1; 167:112645.

[147]. H .de Faria Jr, JG. Costa, JL. Olivas, "A review of monitoring methods for predictive maintenance of electric power transformers based on dissolved gas analysis", *Renew. Sust. Energ. Rev*, 2015 Jun 1; 46:201-9.

[148]. A Christina, MA Salam, QM Rahman, F Wen, SP Ang, W Voon., "Causes of transformer failures and diagnostic methods–A review", *Renew. Sust. Energ. Rev,* 2018 Feb 1; 82:1442-56.

[149]. T Mariprasath, V Kirubakaran. "A critical review on the characteristics of alternating liquid dielectrics and feasibility study on pongamia pinnata oil as liquid dielectrics."" *Renew. Sust. Energ. Rev*., 2016 Nov 1; 65:784-99.

[150]. A Azmi, J Jasni, N Azis, MA Kadir, "Evolution of transformer health index in the form of mathematical equation", *Renew. Sust. Energ. Rev*, 2017 Sep 1; 76:687-700.

[151]. Z Shen, F Wang, Z Wang, J Li, "A critical review of plant-based insulating fluids for transformer: 30-year development." *Renew. Sust. Energ. Rev*, 2021 May 1; 141:110783.

[152]. AK Das, DC Shill, S Chatterjee, "Coconut oil for utility transformers–Environmental safety and sustainability perspectives." *Renew. Sust. Energ. Rev*, 2022 Aug 1; 164:112572.

[153]. JP Van Bolhuis, E Gulski, JJ Smit, "Monitoring and diagnostic of transformer solid insulation", *IEEE Trans. Power Deliv*. 2002 Apr,17(2):528-36.

[154]. I Fofana, H Borsi, E Gockenbach, M Farzaneh, "Aging of transformer insulating materials under selective conditions", *Eur. Trans. Electr. Power*. 2007 Sep;17(5):450-70.

[155]. R Sanghi, "Chemistry behind the life of a transformer", *Resonance*, 2003 Jun; 8:17-23.

[156]. LE Lundgaard, W Hansen, D Linhjell, TJ Painter, "Aging of oil-impregnated paper in power transformers", *IEEE Trans. Power Deliv*, 2004, Jan 7,19(1), pp.:230-9.

[157]. C Homagk, K Mossner, T Leibfried, "Investigation on degradation of power transformer solid insulation material", *In 2008 IEEE Annual Report Conf. Electr. Insul. Dielectr. Phenomena*, 2008, Oct 26, pp. 75-78.

[158]. AM Emsley, RJ Heywood, M Ali, X Xiao, "Degradation of cellulosic insulation in power transformers. Part 4: Effects of ageing on the tensile strength of paper", *IEE Proc. Sci. Meas. Technol*, 2000, Nov 1,147(6), pp.285-90.

[159]. A Munajad, C Subroto, Suwarno, "Study on the effects of thermal aging on insulating paper for high voltage transformer composite with natural ester from palm oil using

Fourier transform infrared spectroscopy (FTIR) and energy dispersive X-ray spectroscopy (EDS)", *Energies*, 2017, Nov 13,10(11), pp.1857.

[160]. LS Nasrat, N Kassem, N Shukry, "Aging effect on characteristics of oil impregnated insulation paper for power transformers", *Engineering*, Vol. 5 No. 1, 2013, pp. 1-7.

[161]. AR Suwarno, "Study of Thermally accelerated aging of Transformer Insulation Paper in Mineral Oil and Gas-to-Liquid Dielectrics using Scanning Electron Microscopy (SEM), Thermogravimetric Analysis (TGA) and X-ray Diffraction (XRD)." *Int. J. Electr. Eng. Inform.*, 2021 Sep 1, 13(3).

[162]. U. M. Rao, I. Fofana, P. Rozga, P. Picher, D. K. Sarkar and R. Karthikeyan, "Influence of Gelling in Natural Esters Under Open Beaker Accelerated Thermal Aging," in *IEEE Trans Dielectr Electr Insul*, vol. 30, no. 1, pp. 413-420, Feb. 2023.

[163]. R. Liao, J. Hao, G. Chen, Z. Ma and L. Yang, "A comparative study of physicochemical, dielectric and thermal properties of pressboard insulation impregnated with natural ester and mineral oil," in *IEEE Trans Dielectr Electr Insul*., vol. 18, no. 5, pp. 1626-1637, October 2011.

[164]. I Fofana, A Bouaicha, M Farzaneh, "Characterization of aging transformer oil–pressboard insulation using some modern diagnostic techniques",. *Eur. Trans. Electr. Power*, 2011, Jan, 21(1):1110-27.

[165]. N Irahhauten, "Optimization of the Impregnation Process of Cellulose Materials in High Voltage Power transformers-susceptibility of high-density materials to partial discharge activity." *TU Delft*, 2015.

[166]. E. L., Charsley, "Warrington S. B. Thermal analysis-techniques and applications". 1992.

[167]. PJ.Haines, "Thermogravimetry. In Thermal Methods of Analysis: Principles, Applications and Problems", *Dordrecht: Springer Netherlands*, 1995, pp. 22-62.

[168]. PK Gallagher, ME Brown, "Handbook of thermal analysis and calorimetry". *Amsterdam: Elsevier Science*, 1998.

[169]. N. A. Bakar, Huize Cui, A. Abu-Siada and Shengtao Li, "A review of spectroscopy technology applications in transformer condition monitoring," *2016 International Conference on Condition Monitoring and Diagnosis (CMD)*, Xi'an, China, 2016, pp. 372-375.

[170]. D Kanumuri, V Sharma, OP Rahi, "Analysis using various approaches for residual life estimation of power transformers" *Int. J. Electr. Eng. Inform*, Jun 2019, 11(2), pp: 389-407.

[171]. Y. E. Sari, A. D. S. Ritonga and Suwarno, "Comparative Study of Kraft Paper Aged in Natural Ester with XRD and TG/DTG Analysis," *2019 International Conference on Electrical Engineering and Informatics (ICEEI),* Bandung, Indonesia, 2019, pp. 564-569.

[172]. Qiang Fu et al., "Correlation analysis between crystalline behavior and aging degradation of insulating paper," *2016 IEEE International Conference on Dielectrics (ICD),* Montpellier, 2016, pp. 617-620.

[173]. S. Rohith, D. Kanumuri, N. Baruah and S. K. Nayak, "Non-Isothermal Thermo Gravimetric Analysis (TGA) Measurements of Oxidative Aged Solid Insulation," *2021 IEEE 5th International Conference on Condition Assessment Techniques in Electrical Systems (CATCON),* Kozhikode, India, 2021, pp. 252-255.

[174]. CS Abi Munajad, "Fourier transform infrared (FTIR) spectroscopy analysis of transformer paper in mineral oil-paper composite insulation under accelerated thermal aging", *Energies*, 2018, Feb 4;11(2):364.

[175]. A Munajad, C Subroto, "Fourier transform infrared spectroscopy (FTIR) analysis of transformer insulation paper in natural ester", *In 2017 International Conference on High Voltage Engineering and Power Systems (ICHVEPS)* 2017 Oct 2 (pp. 446-450). IEEE.

[176]. MB García de Burgos, T García Ordóñez, VA Primo Cano, JC Burgos Díaz, DJ Urquiza Cuadros, "Studying the Loss of Life of Natural-Ester-Filled Transformer Insulation: Impact of Moisture on the Aging Rate of Paper", *IEEE Electr. Insul. Mag,* vol. 33, no. 1, pp. 15-23, January-February 2017.

[177]. U Mohan Rao, I Fofana, R Kartheek, KM Yapi, T Jaya, "Mineral oil and ester-based oil/paper insulation decaying assessment by FTIR measurements", *In Proceedings of the 21st International Symposium on High Voltage Engineering:* Volume 1 2020 (pp. 615-624), Springer International Publishing.

[178]. U.S. Energy Information Administration, "International Energy Outlook 2016", vol. 0484(2016), no. May 2016. 2016

[179]. O. Lesaint, "Prebreakdown phenomena in liquids: propagation 'modes' and basic physical properties," *J. Phys. D. Appl. Phys*., vol. 49, no. 14, p. 144001, 2016.

[180]. A. Beroual, M. Zahn, A. Badent, K. Kist, A. J. Schwabe, H. Yamashita, K. Yamazawa, M. Danikas, W. D. Chadband, and Y. Torshin, "Propagation and structure of streamers in liquid dielectrics," *IEEE Electr. Insul. Mag*., vol. 14, no. 2, pp. 6–17, Mar. 1998.

[181]. Nguyen, Dung Van. "Experimental studies of streamer phenomena in long oil gaps." (2013).

[182]. Ariza, David. On the inception and propagation of streamers along mineral-oil/solid interfaces", *Diss. KTH Royal Institute of Technology*, 2017.

[183]. Xiang, Jing, "Pre-Breakdown and Breakdown Study of Transformer Oil under DC and Impulse Voltages", *PhD thesis*, *The University of Manchester* (United Kingdom), 2017.

[184]. K. Wen, Y. Zhou, J. Fu and T. Jin, "A calculation method and some features of transient field under polarity reversal voltage in HVDC insulation," in *IEEE Transactions on Power Delivery*, vol. 8, no. 1, pp. 223-230, Jan. 1993.

[185]. G. C. Stone and R. G. Van Heeswijk, "Parameter Estimation for the Weibull Distribution," in *IEEE Transactions on Electrical Insulation*, vol. EI-12, no. 4, pp. 253-261, Aug. 1977.

[186]. A. V. Roggen, "Distributions of Relaxation Times and Their Diagrams," in *IEEE Transactions on Electrical Insulation*, vol. EI-5, no. 2, pp. 47-52, June 1970.

[187]. F. Pizzitutti, and F. Bruni, "Electrode and interfacial polarization in broadband dielectric spectroscopy measurements", *Review of Scientific Instruments*, 72(5), pp.2502-2504, 2001.

[188]. L. Yao-nan and L. Chyi-chang, "The study of apparent negative value in measuring dielectric loss," in *IEEE Transactions on Electrical Insulation*, vol. EI-17, no. 1, pp. 20-26, Feb. 1982.

Appendix A

Experimental results of Fresh and Aged samples

- The raw data and plots in this appendix are for results discussed in chapter 2.

Table A.1: Experimental results of DCBDV (kV) of fresh samples

Sets	Breakdown Series	MO (kV)		FR3 (kV)	
		Positive (+)	Negative (-)	Positive (+)	Negative (-)
Set 1	1	22	-34.1	61.2	-47.3
	2	26.5	-31.3	36.2	-43.2
	3	19.3	-33.1	27.6	-41.9
	4	38	-31.7	39.2	-36.7
	5	26.2	-41	36.6	-24.2
	6	36.1	-34.5	38.7	-32.6
Set 2	7	30	-37.3	45.2	-34.8
	8	29.5	-30.9	39.2	-29.3
	9	29.7	-36.2	33.2	-35.6
	10	24.5	-32.3	40.3	-32.4
	11	26.8	-35.9	30.9	-31.6
	12	29.3	-32.4	39.1	-34.3
Set 3	13	22.4	-36.3	46.7	-38.4
	14	26.3	-27.3	36.8	-27.8
	15	27.2	-29.2	39.2	-35.2
	16	30.7	-29.7	38.7	-30.1
	17	24.9	-32.1	40.6	-32.6
	18	27.3	-30.5	32.4	-33.2
Set 4	19	26.7	-34.3	32.1	-38.3
	20	24.3	-26.1	42.4	-22.8
	21	23.1	-29.4	36.1	-30.9
	22	24.3	-24.6	33.7	-35.7
	23	26.1	-24.3	36.9	-27.2
	24	27.2	-29.3	30.6	-23.5
Average Breakdown		**27.017**	**-31.825**	**38.067**	**-33.317**
Standard Deviation		**4.137**	**4.061**	**6.712**	**6.049**
Standard Error		**0.845**	**0.829**	**1.370**	**1.235**

I. Experimental results of DCBDV of Open Beaker Oxidative Ageing (OBOA) Samples:

Table A.2: Experimental results of DCBDV (kV) of oxidatively aged MO samples

Sets	Breakdown Series	MO _ 90hrs_OBOA		MO_ 200 hrs_OBOA		MO_500 hrs_OBOA	
		(+)	(-)	(+)	(-)	(+)	(-)
Set 1	1	16.8	-39.5	21.1	-33.8	18.6	-16.2
	2	30.5	-36.8	17.1	-31.2	6.44	-9.8
	3	13.2	-32.6	10.1	-34.1	5.8	-15.2
	4	11.5	-22.9	12.65	-33.6	13.4	-17.6
	5	18.2	-32.4	17.55	-36.7	12.3	-18.2
	6	21.7	-27.1	16.05	-19.6	14.8	-21.2
Set 2	7	13.7	-35.9	17.1	-37.6	18.3	-15.9

	8	22.3	-30.8	15.8	-32.5	12.4	-16.6
	9	16.8	-24.6	13.8	-33.2	13.08	-16.9
	10	15.7	-25.8	15.6	-29.6	10.7	-21.59
	11	21.2	-32.5	16.9	-30.5	16.5	-15.8
	12	16.2	-26.7	21.35	-28.7	13.4	-16.6
Set 3	13	18.7	-28.3	10.6	-30.3	21.2	-17.48
	14	22.3	-30.2	19.8	-25.5	16.4	-17.8
	15	21.5	-25.1	26.3	-38.1	11.3	-17.2
	16	19.7	-23.8	17.2	-30.8	12.8	-16.3
	17	14.5	-27.6	21.3	-33.7	14.6	-18.3
	18	11.2	-21.3	17.6	-34.5	13.4	-17.2
Set 4	19	20.8	-23.5	14.4	-30.4	15.4	
	20	17.2	-26.8	17.7	-32.8	13.2	
	21	16.7	-14.9	22.1	-34.2	14.8	
	22	10.3	-19.6	20.8	-30.7	15.6	
	23	19.3	-16.8	12.8	-28.1	11.9	
	24	16.2	-19.3	21.7	-30.3	15.4	
Average Breakdown		**17.758**	**-26.867**	**17.392**	**-31.688**	**13.822**	**-16.993**
Standard Deviation		**4.470**	**6.241**	**3.929**	**3.940**	**3.409**	**2.454**
Standard Error		**0.912**	**1.274**	**0.802**	**0.804**	**0.696**	**0.578**

Table A.3: Experimental results for DCBDV (kV) of oxidatively aged FR3 samples

Sets	**Breakdown Series**	**FR3 _ 90hrs_OBOA**		**FR3_ 200 hrs_OBOA**		**FR3_500 hrs_OBOA**	
		(+)	**(-)**	**(+)**	**(-)**	**(+)**	**(-)**
Set 1	1	57.2	-61.2	52.5	-57.3	59.8	-63.2
	2	38.6	-51.3	35.7	-41.2	34.3	-42.7
	3	44.5	-37.3	36.3	-36.1	24.1	-46.2
	4	43.8	-39.1	35.4	-35.7	42.8	-34.5
	5	45.7	-38.2	36.9	-37.3	24.8	-37.6
	6	41.8	-22.8	35.8	-39.3	23.5	-41.1
Set 2	7	52.8	-48.5	50.3	-54.6	54.2	-56.1
	8	35.1	-31.7	34.1	-33.9	39.6	-40.6
	9	35.6	-36.3	36.2	-27.3	34.4	-34.2
	10	32.7	-38.9	35.8	-24.6	33.8	-36.3
	11	33.2	-40.7	33.9	-34.6	36.6	-32.8
	12	36.5	-39.2	37.2	-19.1	24.3	-31.7
Set 3	13	53.6	-47.3	54.2	-48.7	45.7	-48.2
	14	32.7	-39.2	32.2	-24.2	31.2	-37.2
	15	35.5	-34.6	23.5	-36.3	25.3	-21.5
	16	38.2	-36	27.8	-17.7	32.5	-22.8
	17	26.4	-35.9	31.3	-29.8	30.9	-33.2
	18	33.8	-36.5	24.7	-33.3	19.5	-34.6
Set 4	19	56.2	-42.6	43.3	-43.5	35.5	-43.7
	20	34.4	-36.2	29.1	-34.9	25.2	-31.9
	21	35.7	-35.9	32.6	-30.2	34.6	-24.6
	22	38.2	-38.3	18.6	-31.7	30.8	-29.5
	23	35.2	-35.1	29.8	-22.9	31.5	-34.5
	24	37.2	-32.3	31.2	-36.1	18.7	-37.2
Average Breakdown		**39.775**	**-38.963**	**34.933**	**-34.596**	**33.067**	**-37.329**

Standard Deviation		**8.123**	**7.425**	**8.485**	**9.895**	**10.062**	**9.626**
Standard Error		**1.658**	**1.516**	**1.732**	**2.020**	**2.054**	**1.965**

Histograms of fresh and oxidatively aged samples for positive DCBDV

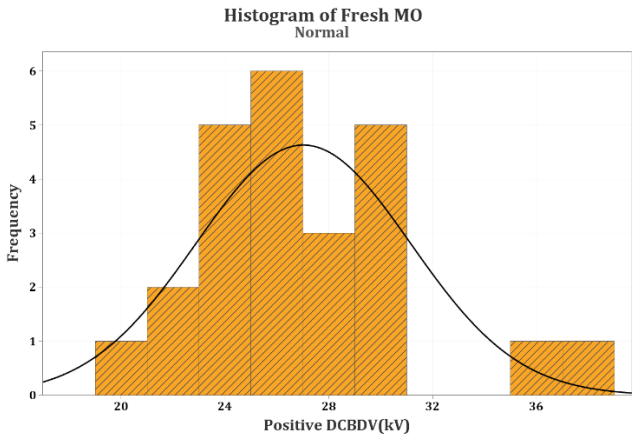

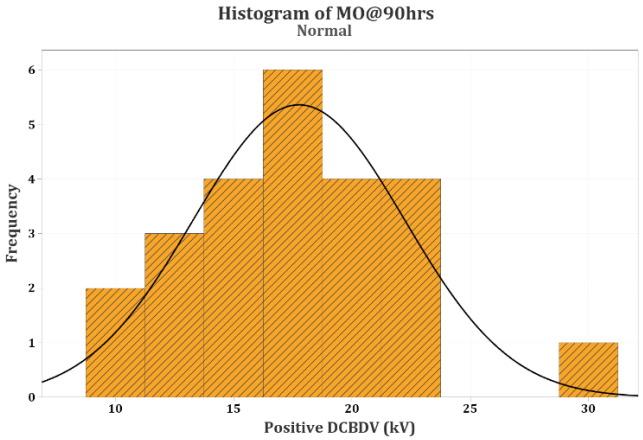

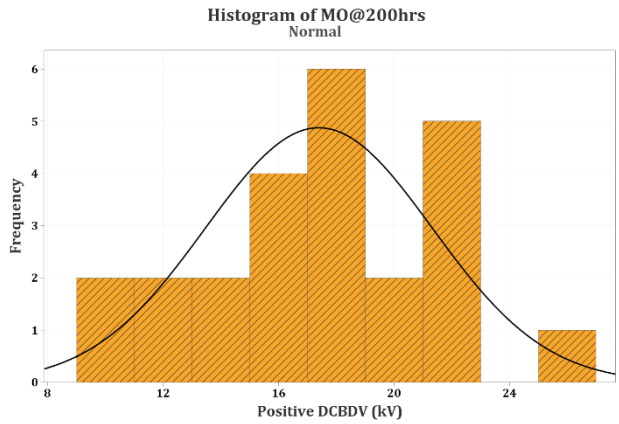

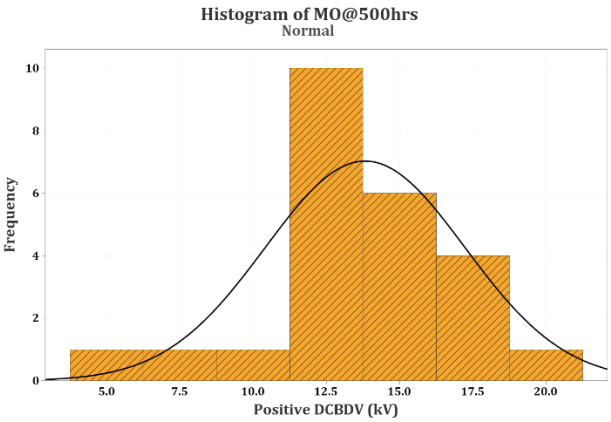

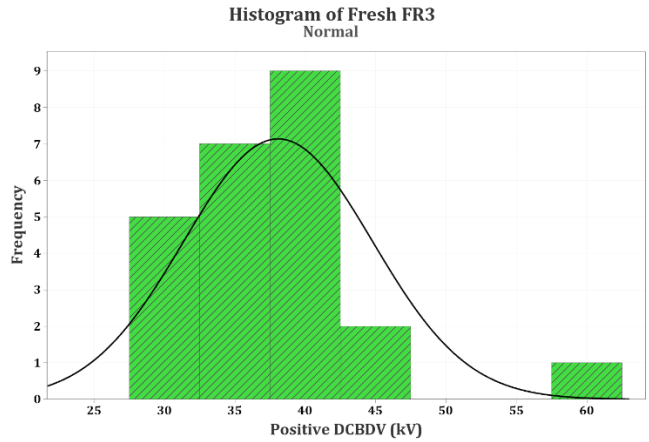

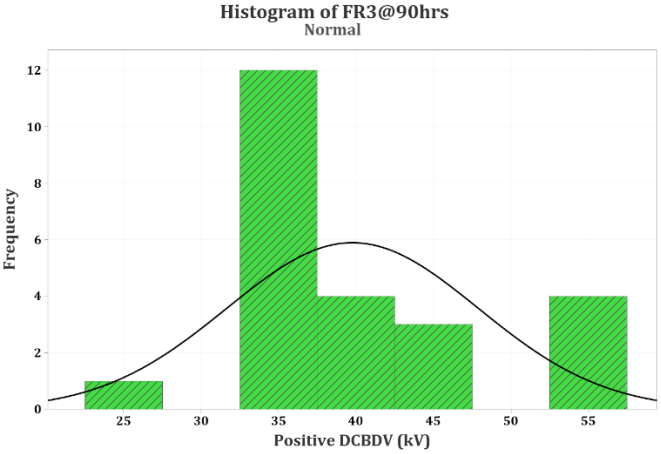

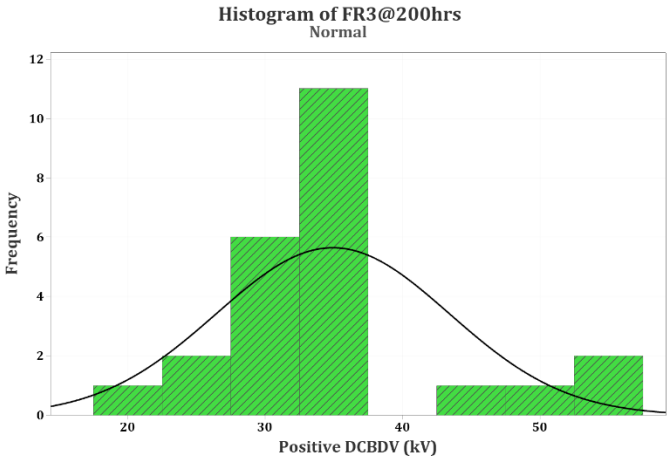

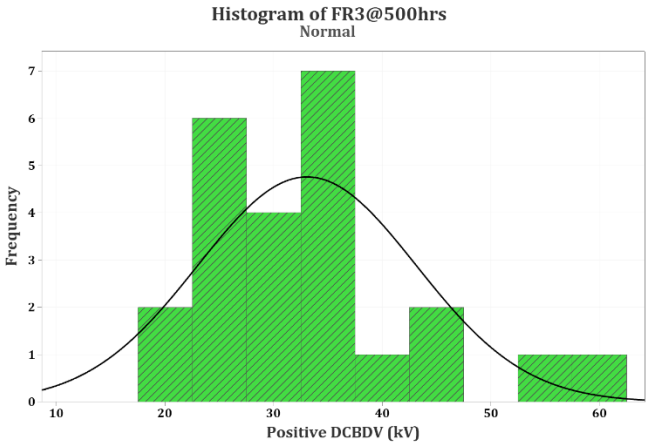

Histograms of fresh and oxidatively aged samples for negative DCBDV

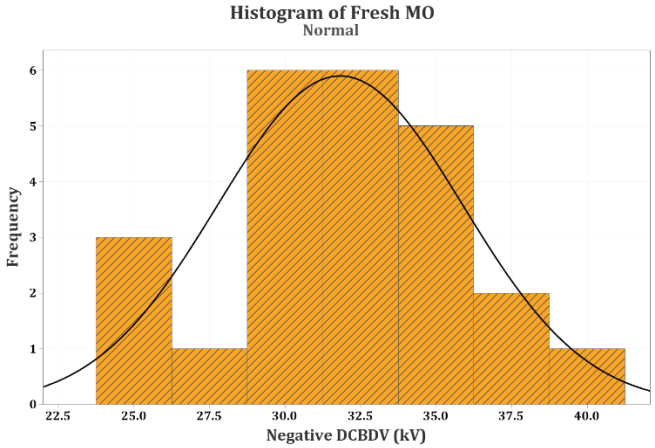

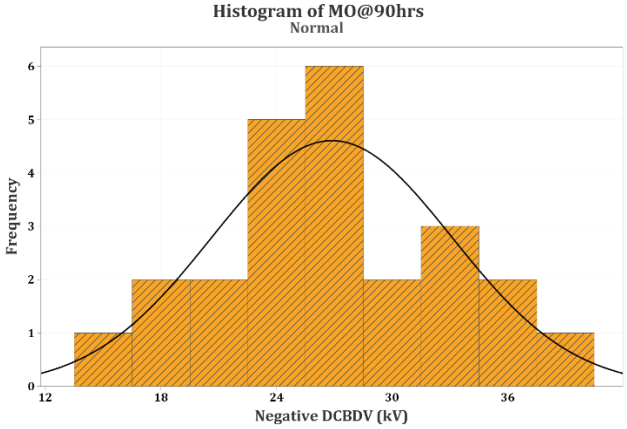

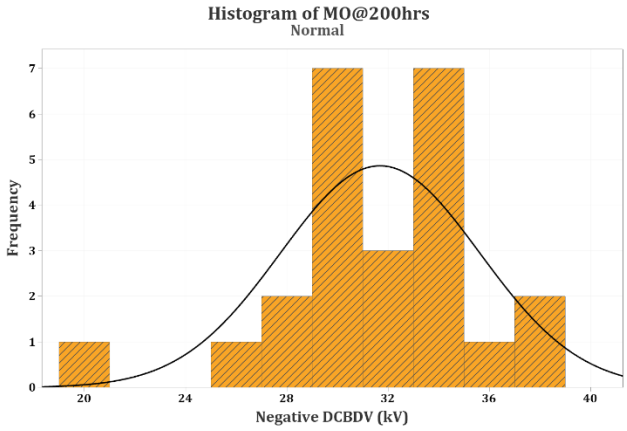

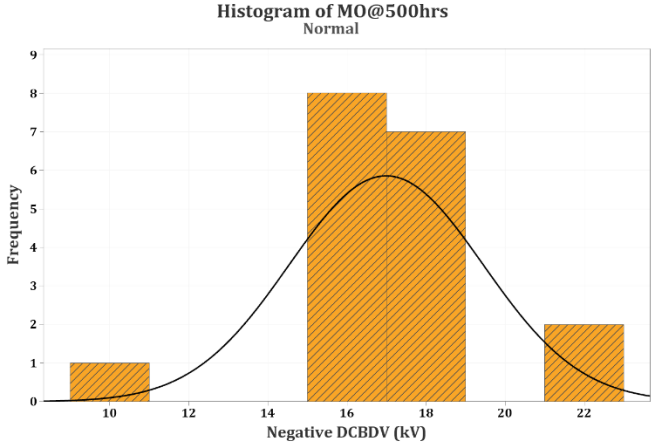

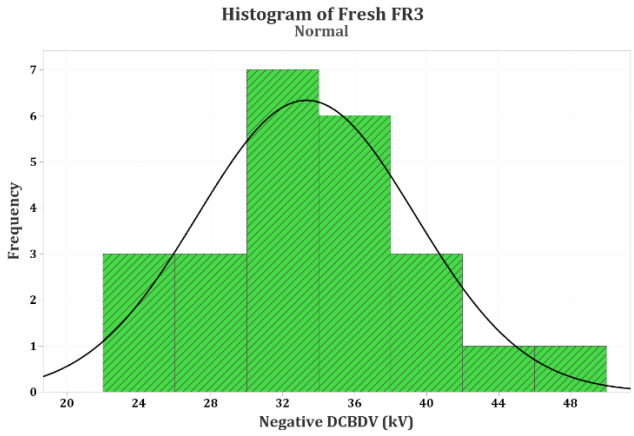

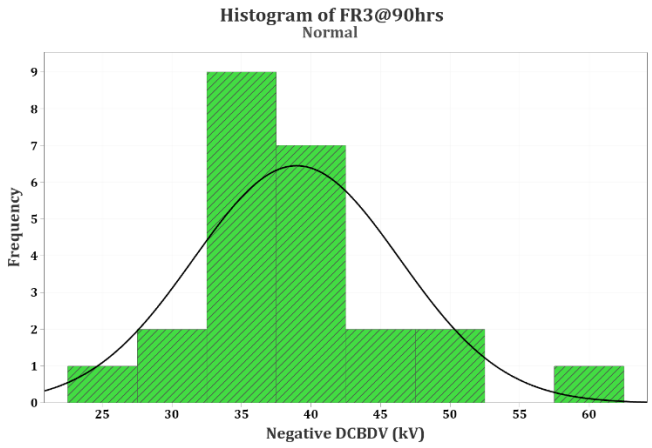

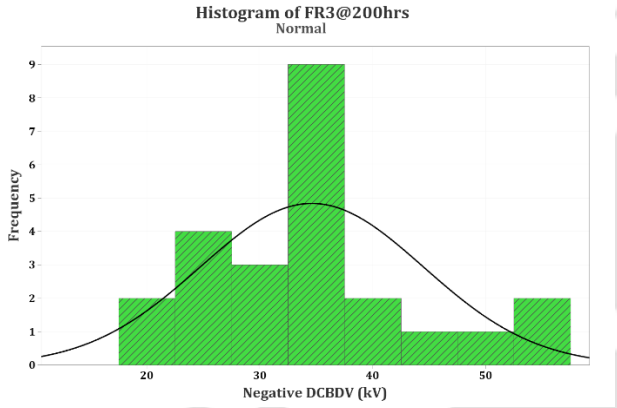

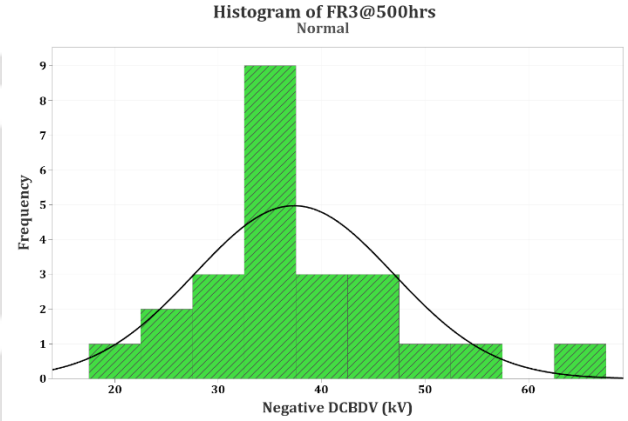

Parameters of normal distribution:

For Positive DCBDV:

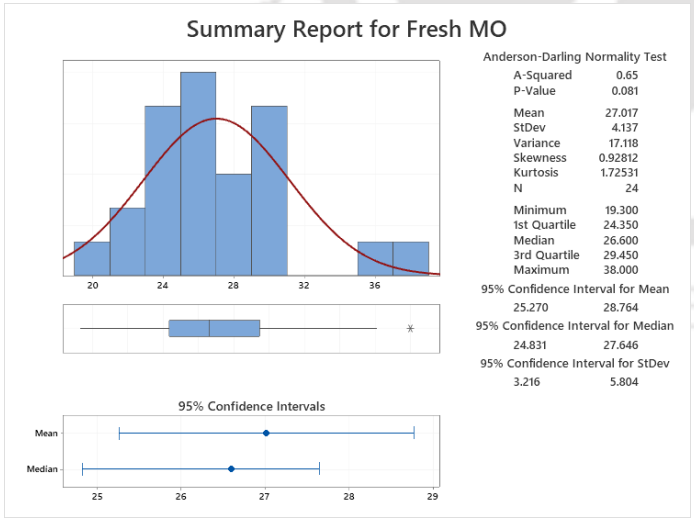

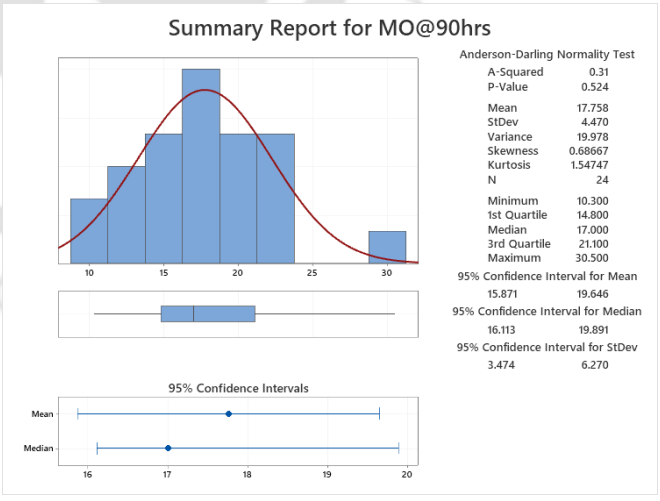

Summary Report for MO@200hrs

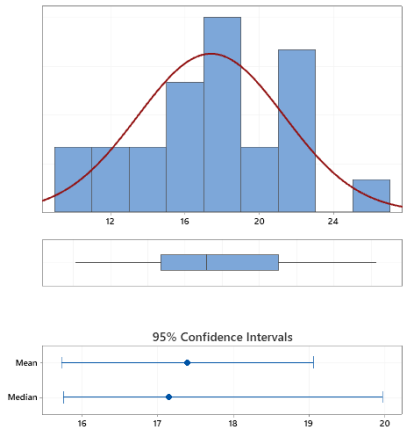

Anderson-Darling Normality Test	
A-Squared	0.31
P-Value	0.532
Mean	17.392
StDev	3.929
Variance	15.438
Skewness	0.0998999
Kurtosis	-0.0845979
N	24
Minimum	10.100
1st Quartile	14.700
Median	17.150
3rd Quartile	21.025
Maximum	26.300
95% Confidence Interval for Mean	
15.733	19.051
95% Confidence Interval for Median	
15.765	19.973
95% Confidence Interval for StDev	
3.054	5.512

Summary Report for MO@500hrs

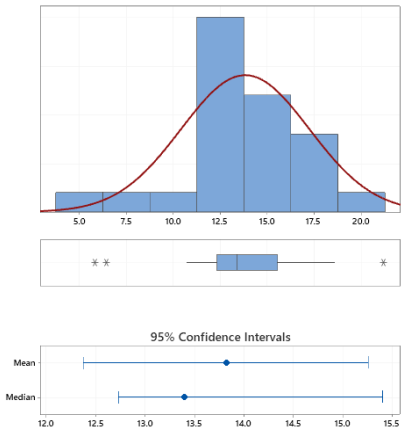

Anderson-Darling Normality Test	
A-Squared	0.50
P-Value	0.189
Mean	13.822
StDev	3.409
Variance	11.622
Skewness	-0.39208
Kurtosis	1.27961
N	24
Minimum	5.800
1st Quartile	12.325
Median	13.400
3rd Quartile	15.550
Maximum	21.200
95% Confidence Interval for Mean	
12.382	15.261
95% Confidence Interval for Median	
12.731	15.400
95% Confidence Interval for StDev	
2.650	4.782

Summary Report for Fresh FR3

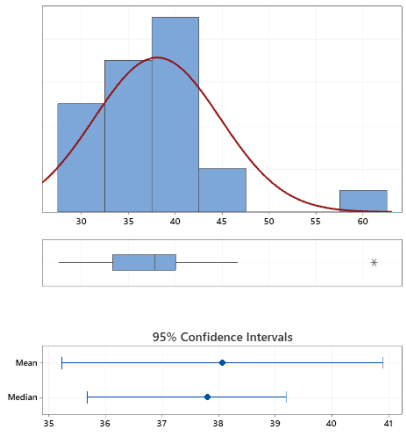

Anderson-Darling Normality Test	
A-Squared	0.87
P-Value	0.021
Mean	38.067
StDev	6.712
Variance	45.047
Skewness	1.71881
Kurtosis	5.35704
N	24
Minimum	27.600
1st Quartile	33.325
Median	37.800
3rd Quartile	40.025
Maximum	61.200
95% Confidence Interval for Mean	
35.233	40.901
95% Confidence Interval for Median	
35.684	39.200
95% Confidence Interval for StDev	
5.216	9.415

Summary Report for FR3@90hrs

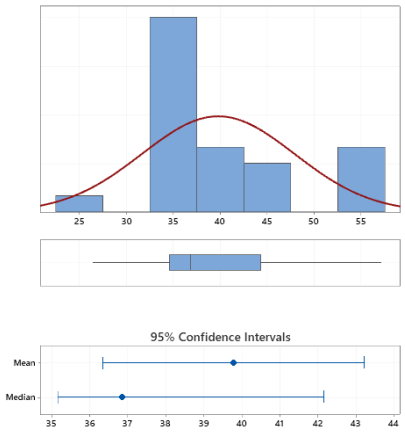

Anderson-Darling Normality Test	
A-Squared	1.27
P-Value	<0.005
Mean	39.775
StDev	8.123
Variance	65.980
Skewness	0.949515
Kurtosis	0.135550
N	24
Minimum	26.400
1st Quartile	34.575
Median	36.850
3rd Quartile	44.325
Maximum	57.200
95% Confidence Interval for Mean	
36.345	43.205
95% Confidence Interval for Median	
35.183	42.146
95% Confidence Interval for StDev	
6.313	11.394

Summary Report for FR3@200hrs

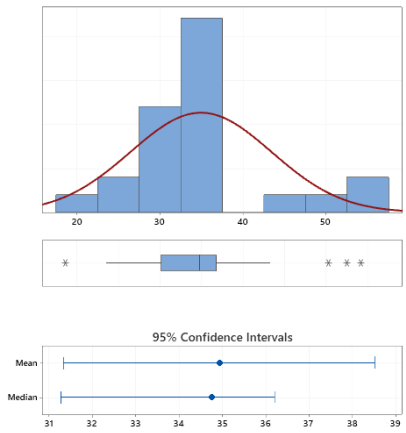

Anderson-Darling Normality Test	
A-Squared	0.88
P-Value	0.021
Mean	34.933
StDev	8.485
Variance	72.001
Skewness	0.703182
Kurtosis	0.898333
N	24
Minimum	18.600
1st Quartile	30.150
Median	34.750
3rd Quartile	36.750
Maximum	54.200
95% Confidence Interval for Mean	
31.350	38.516
95% Confidence Interval for Median	
31.283	36.217
95% Confidence Interval for StDev	
6.595	11.903

Summary Report for FR3@500hrs

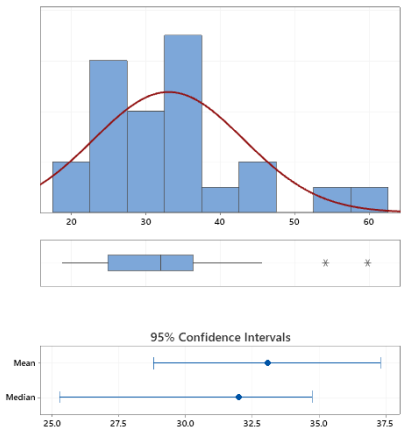

Anderson-Darling Normality Test	
A-Squared	0.67
P-Value	0.071
Mean	33.067
StDev	10.062
Variance	101.251
Skewness	1.04948
Kurtosis	1.28034
N	24
Minimum	18.700
1st Quartile	24.900
Median	32.000
3rd Quartile	36.325
Maximum	59.800
95% Confidence Interval for Mean	
28.818	37.316
95% Confidence Interval for Median	
25.283	34.756
95% Confidence Interval for StDev	
7.821	14.115

For Negative DCBDV:

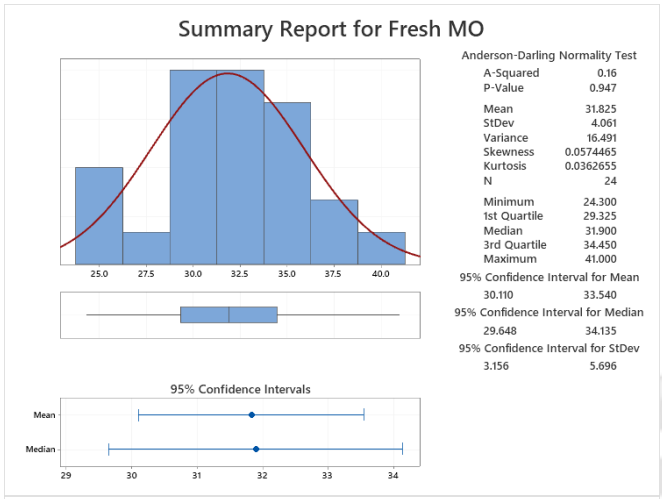

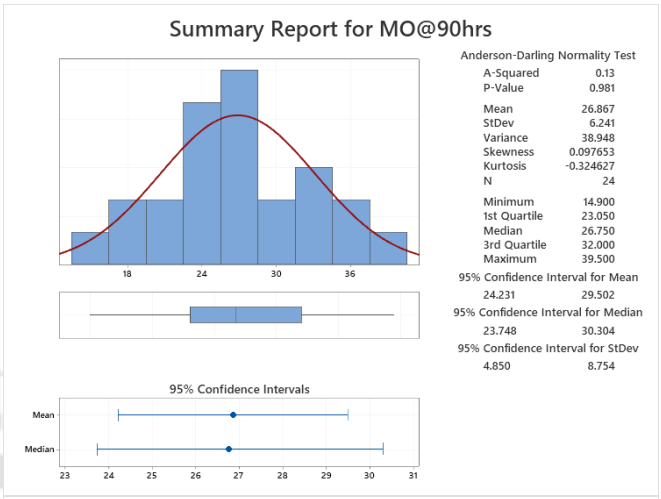

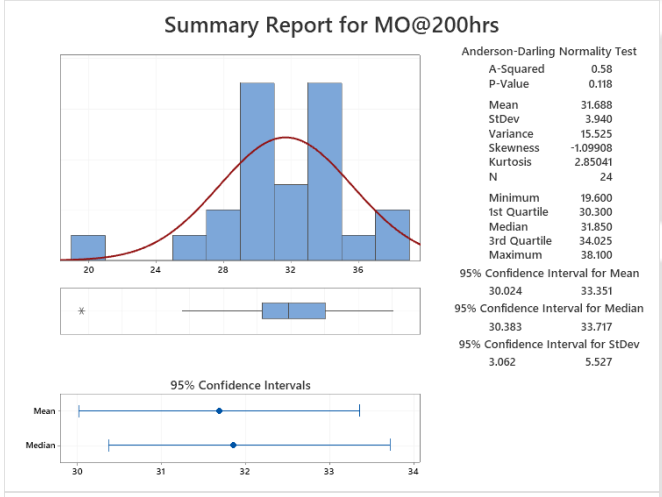

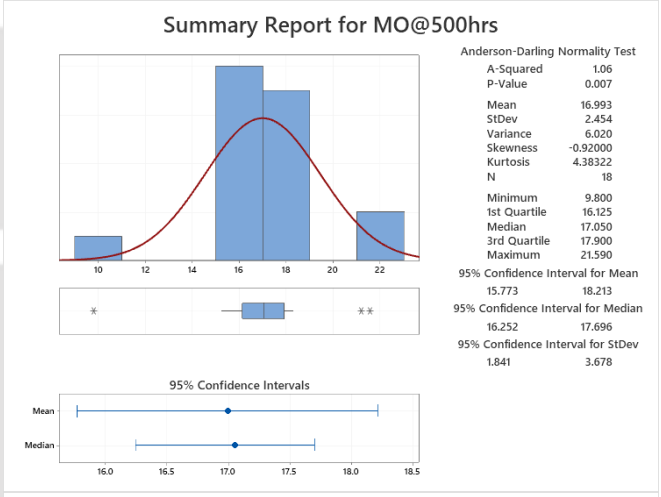

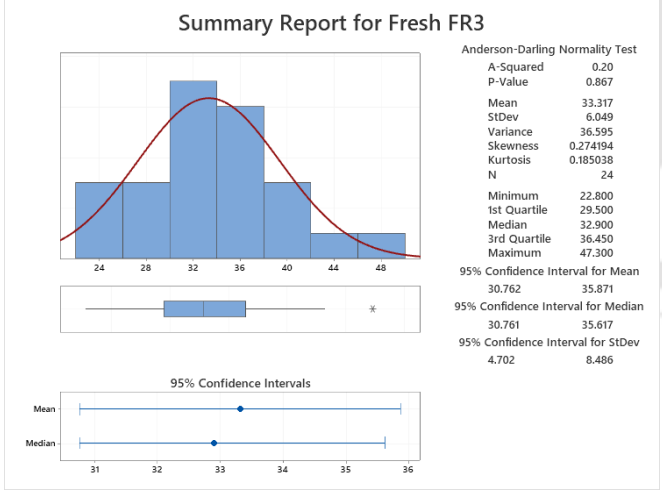

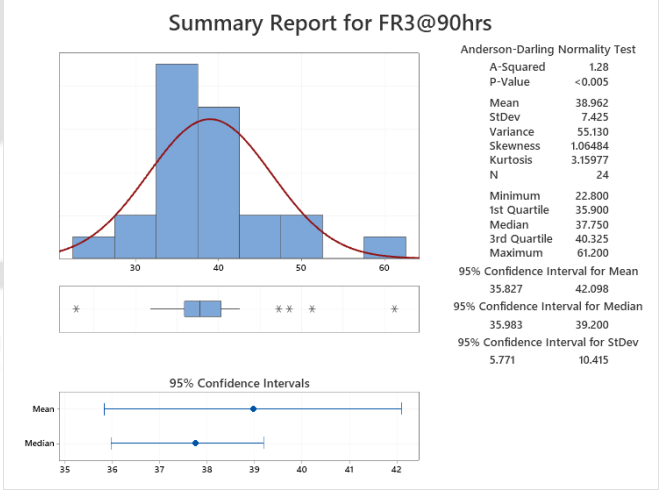

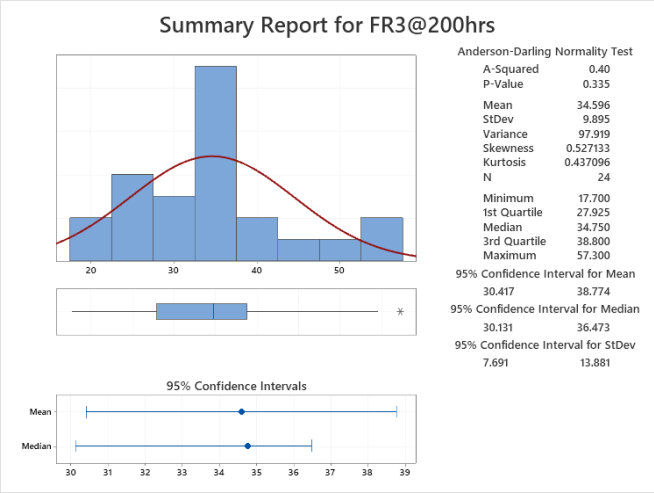

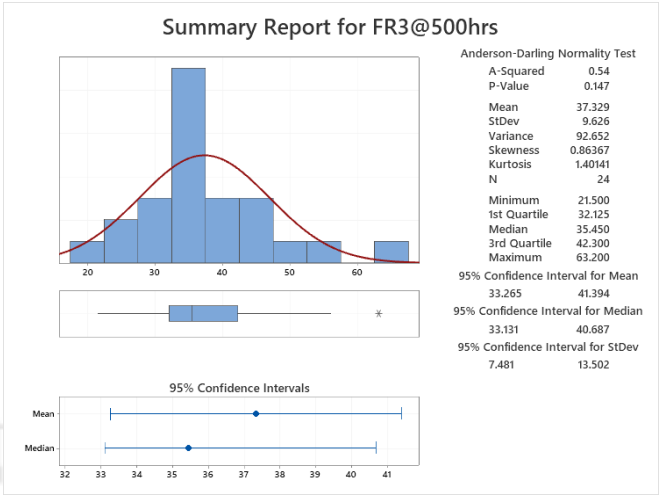

Weibull parameters for fresh and oxidatively aged samples:

Oil Samples	2-parameter Weibull						3-parameter Weibull					
	For Positive DCBDV			For Negative DCBDV			For Positive DCBDV			For Negative DCBDV		
	α	β	γ	α	β	γ	α	β	γ	α	β	γ
Fresh MO	28.82	6.374	-	33.58	8.569	-	9.922	2.263	18.21	12.22	3.016	20.91
MO@90	19.46	4.154	-	29.3	4.862	-	9.715	2.043	9.131	18.16	2.903	10.68
MO@200	18.93	4.963	-	33.27	10.16	-	11.34	2.872	7.286	51.24	15.83	-17.9
MO@500	15.08	4.686	-	17.97	8.084	-	16.14	5.037	-1.03	16.09	7.223	1.865
Fresh FR3	40.92	5.135	-	35.81	5.952	-	12.57	1.768	26.86	15.35	2.458	19.69
FR3@90	43.13	5.028	-	42.03	5.096	-	16.39	1.909	25.24	21.29	2.672	19.93
FR3@200	38.23	4.323	-	38.23	3.786	-	21.59	2.421	15.75	22.54	2.16	14.61
FR3@500	36.69	3.438	-	41	4.025	-	16.89	1.554	17.83	20.24	1.97	19.34

II. Experimental results of DCBDV of thermally accelerated aged (TAA) samples

Table A.4: Experimental results of DCBDV (kV) of thermally aged MO samples

Sets	Breakdown Series	MO _ 90hrs_TAA		MO_ 200 hrs_TAA		MO_500 hrs_TAA	
		Positve (+)	Negative (-)	Positve (+)	Negative (-)	Positve (+)	Negative (-)
Set 1	1	15.16	-23.7	21.2	-19.6	10.6	-13.5
	2	16.7	-20.3	24.4	-18.5	15.4	-7.6
	3	13.5	-16.1	21.7	-23.3	7.6	-12.2
	4	13.9	-18.3	21.3	-21.5	20.5	-15.7
	5	15.2	-17.8	19.5	-29.2	18.3	-16.8
	6	16.8	-20.1	21.1	-32.1	13.2	-7.6
Set 2	7	12.9	-16.8	15.7	-18.4	13.6	-5.6
	8	17.3	-21.6	22.6	-31.1	9.7	-6.8
	9	17.6	-24.2	16.8	-33.7	18.5	-13.1
	10	16.5	-18.7	17.6	-33.5	13.2	-13.8
	11	15.8	-21.4	20.2	-20.9	11.8	-18.7

	12	18.5	-19.3	25.3	-24.6	12.7	-10.3
Set 3	13	16.7	-21.2	18.6	-29.4	17.2	-9.1
	14	17.6	-17.5	22.3	-23.4	11.1	-10.4
	15	19.4	-13.3	15.8	-28.9	18.3	-17.9
	16	18.8	-18.9	17.4	-28.5	11.4	-13.1
	17	15.3	-17.1	24.5	-27.6	17.2	-11.8
	18	19.2	-20.2	20.4	-31.3	17.4	-17.2
Set 4	19	18.7	-21.6	26.1	-27.4	12.8	-13.1
	20	18.1	-21.7	22.5	-16.7	11.2	-13.6
	21	15.2	-15.9	20.7	-30.8	15.6	-5.3
	22	15.6	-20.8	16.4	-17.4	15.9	-13.9
	23	19.2	-16.2	18.3	-26.2	15.7	-11.2
	24	14.5	-18.7	22.6	-32.7	8.7	-12.7

Average Breakdown		**16.590**	**-19.225**	**20.542**	**-26.113**	**14.067**	**-12.125**
Standard Deviation		**1.904**	**2.622**	**3.006**	**5.490**	**3.451**	**3.759**
Standard Error		**0.389**	**0.535**	**0.614**	**1.121**	**0.704**	**0.767**

Table A.5: Experimental results of DCBDV (kV) of thermally aged FR3 samples

Sets	**Breakdown Series**	**FR3 _ 90hrs_TAA**		**FR3_ 200 hrs_TAA**		**FR3_500 hrs_TAA**	
		Positve (+)	**Negative (-)**	**Positve (+)**	**Negative (-)**	**Positve (+)**	**Negative (-)**
Set 1	1	47.5	-55.3	45.7	-36.5	40.2	-38.9
	2	26.7	-28.9	35.9	-34.4	31.1	-30.3
	3	30.2	-25.7	29.6	-30.8	35.7	-28.4
	4	28.6	-33.8	31.3	-25.6	28.5	-30.7
	5	30.1	-18.5	25.1	-35.2	26.4	-26.3
	6	33.6	-27.4	28.5	-29.7	31.9	-30.9
Set 2	7	30.4	-38.1	45.2	-39.6	41.5	-32.1
	8	29.1	-24.4	24.2	-33.1	30.1	-24.5
	9	24.6	-32.2	29.6	-33.9	27.6	-24.7
	10	32.8	-25.7	30.4	-25.3	23.3	-29.9
	11	28.6	-27.6	29.5	-31.3	26.8	-27.1
	12	29.5	-33.5	27.7	-32.8	26.2	-26.8
Set 3	13	27.6	-39.8	37.3	-43.5	36.1	-28.3
	14	28.2	-26.7	32.1	-27.9	28.2	-29.6
	15	34.6	-32.1	27.6	-26.3	26.6	-19.2
	16	31.5	-33.5	24.3	-31.9	34.6	-27.9
	17	25.7	-27.6	28.2	-23.6	26.5	-24.2
	18	32.7	-26.3	27.5	-31.4	27.6	-25.1
Set 4	19	30.8	-36.2	36.6	-35.8	30.5	-23.7
	20	22.6	-24.7	23.1	-26.6	30.1	-27.2
	21	28.7	-32.3	19.7	-28.7	24.6	-28.9
	22	30.5	-22.8	27.2	-26.7	26.7	-25.6
	23	28.3	-29.8	16.3	-25.2	25.9	-23.4
	24	31.8	-27.1	25.6	-27.1	22.4	-28.3

Average Breakdown		**30.196**	**-30.417**	**29.508**	**-30.954**	**29.546**	**-27.583**
Standard Deviation		**4.630**	**7.291**	**6.890**	**4.985**	**4.957**	**3.813**
Standard Error		**0.945**	**1.488**	**1.406**	**1.018**	**1.012**	**0.778**

Histograms of fresh and thermally aged samples for positive DCBDV:

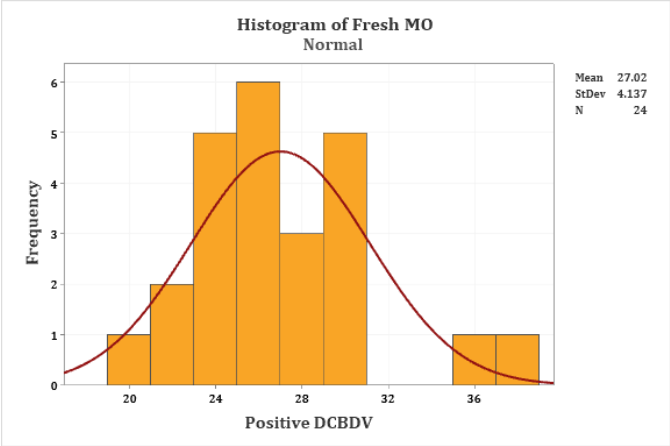

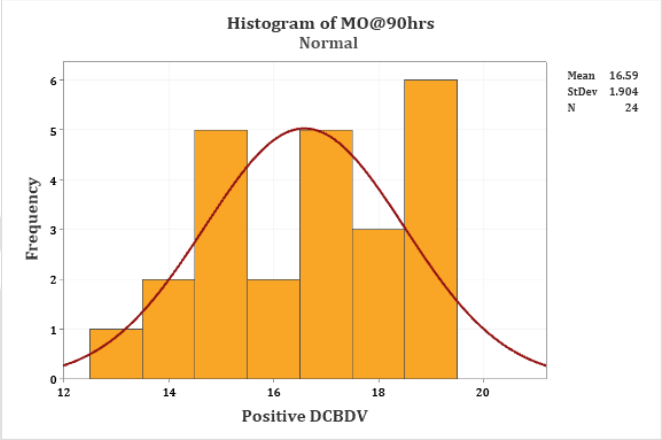

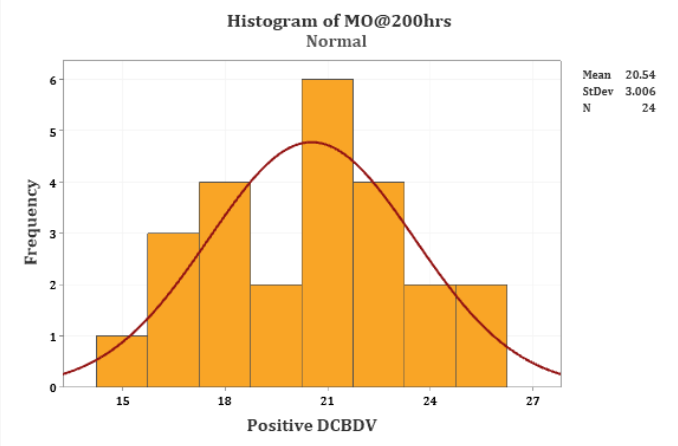

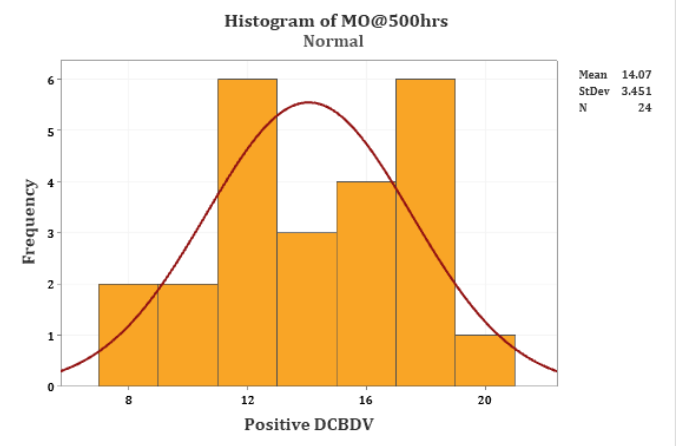

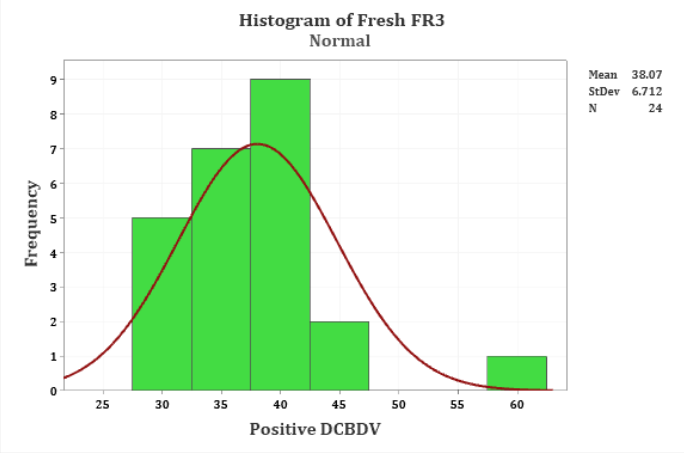

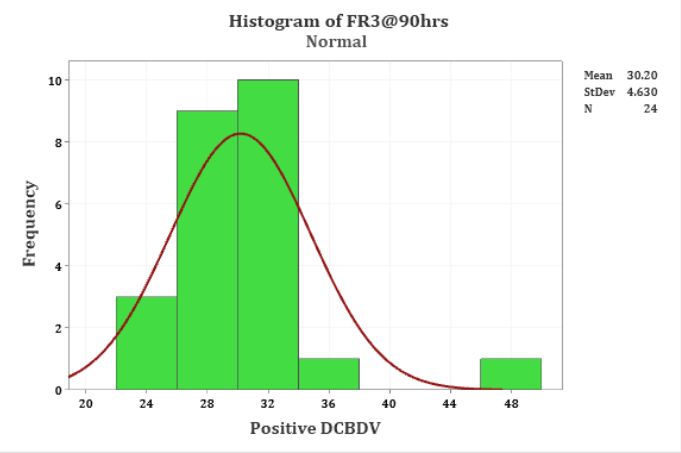

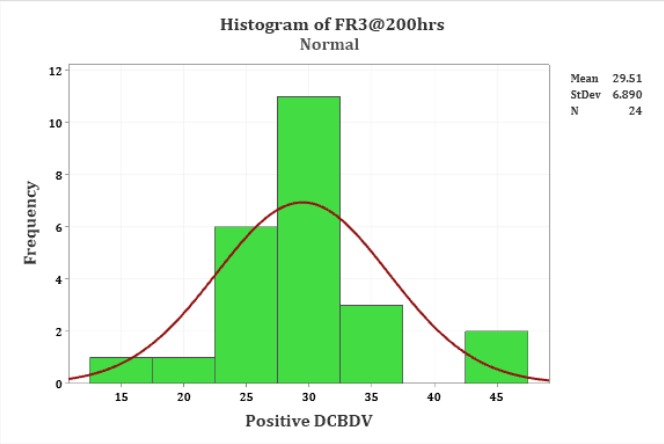

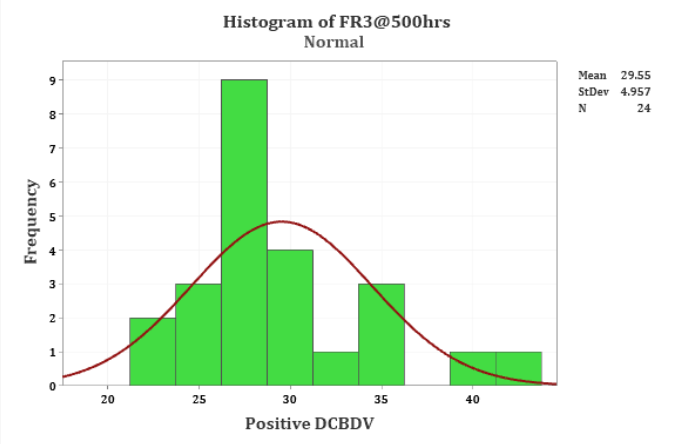

Histograms of fresh and thermally aged samples for negative DCBDV:

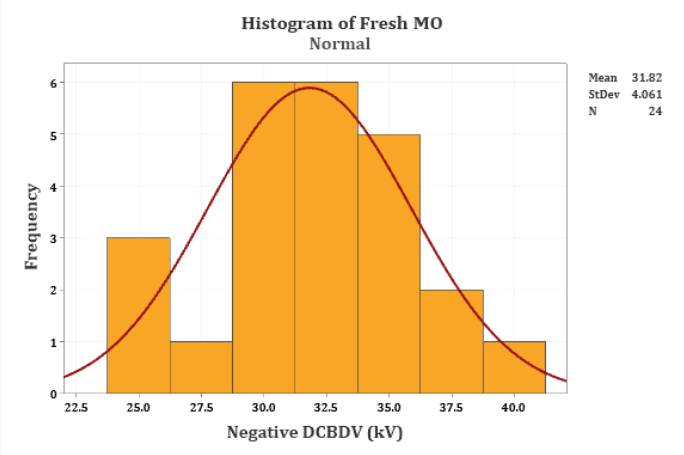

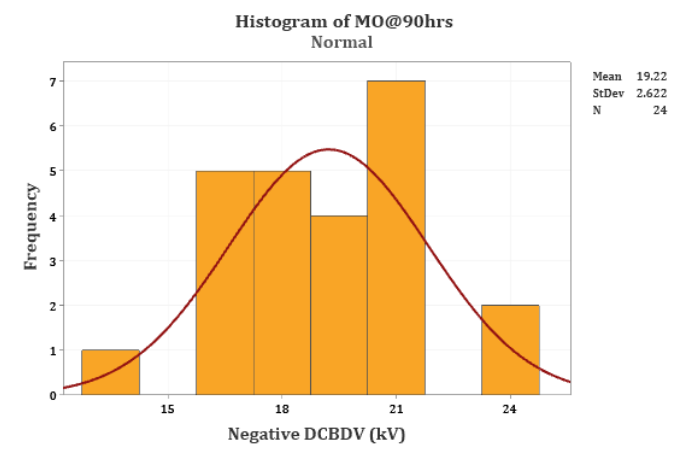

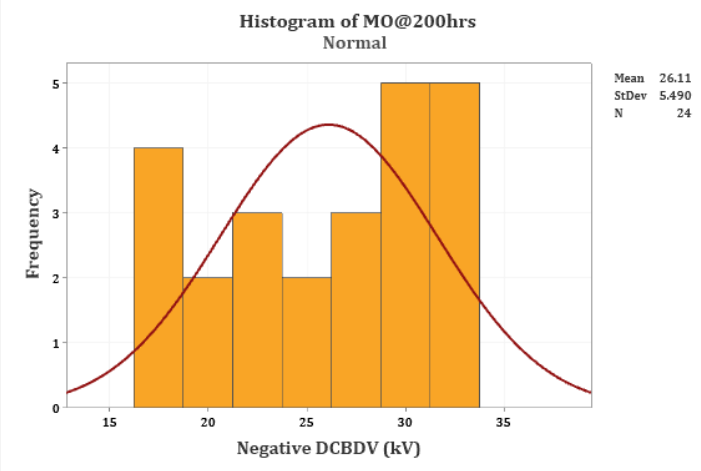

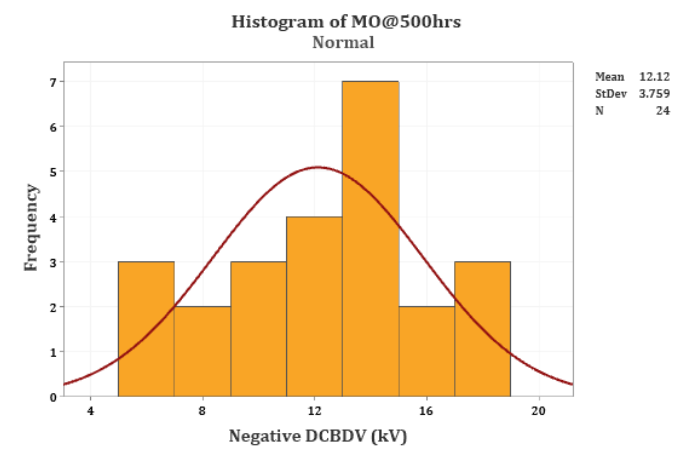

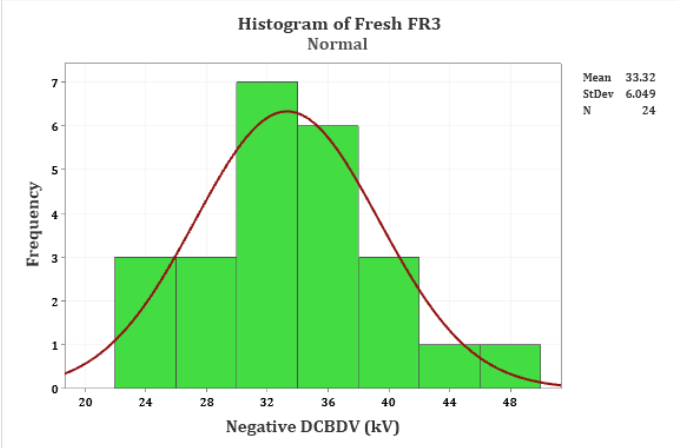

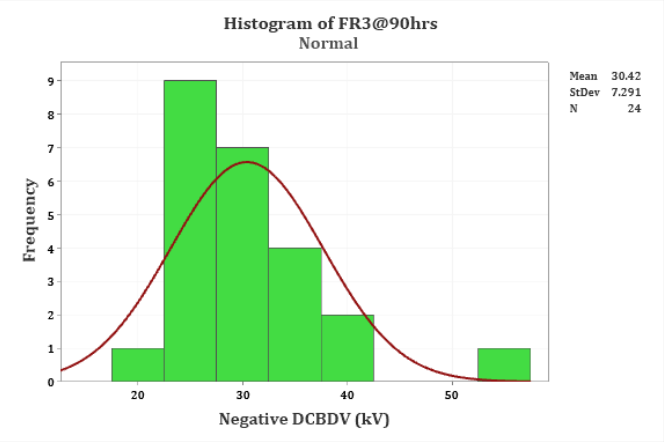

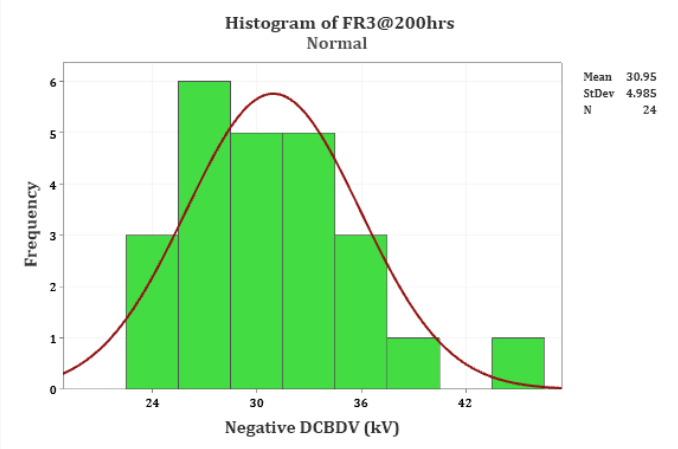

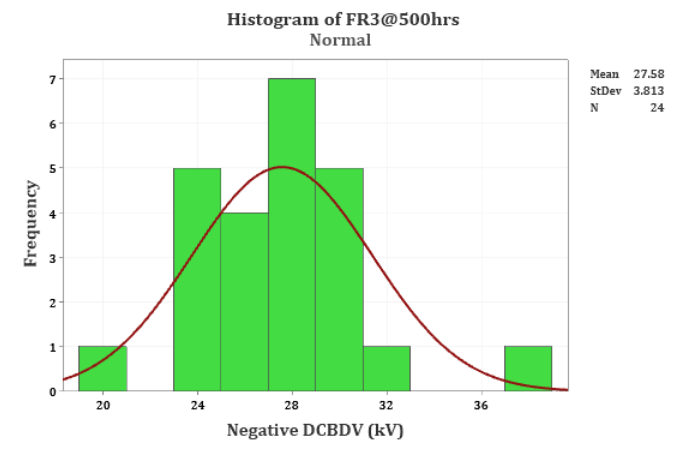

Parameters of normal distribution:

For Positive DCBDV:

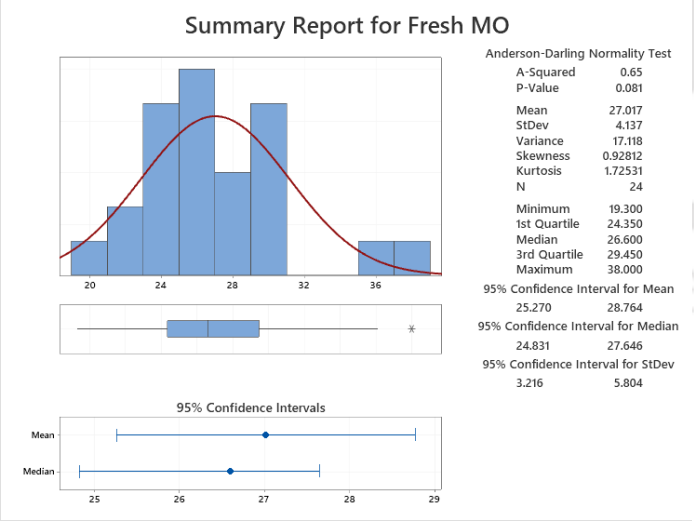

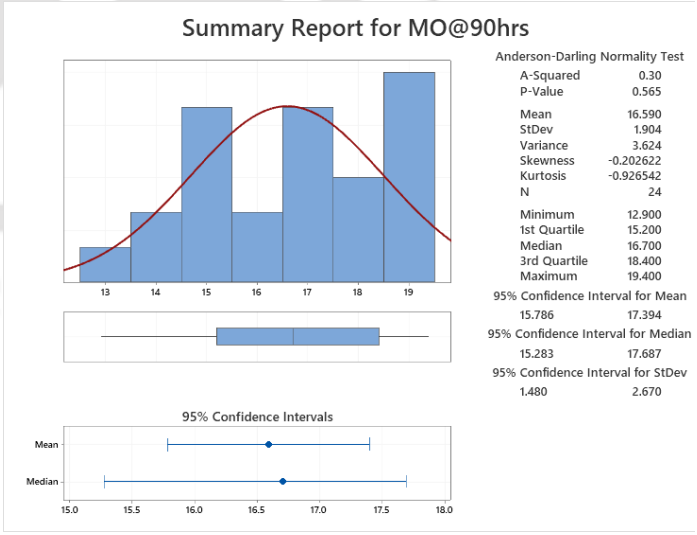

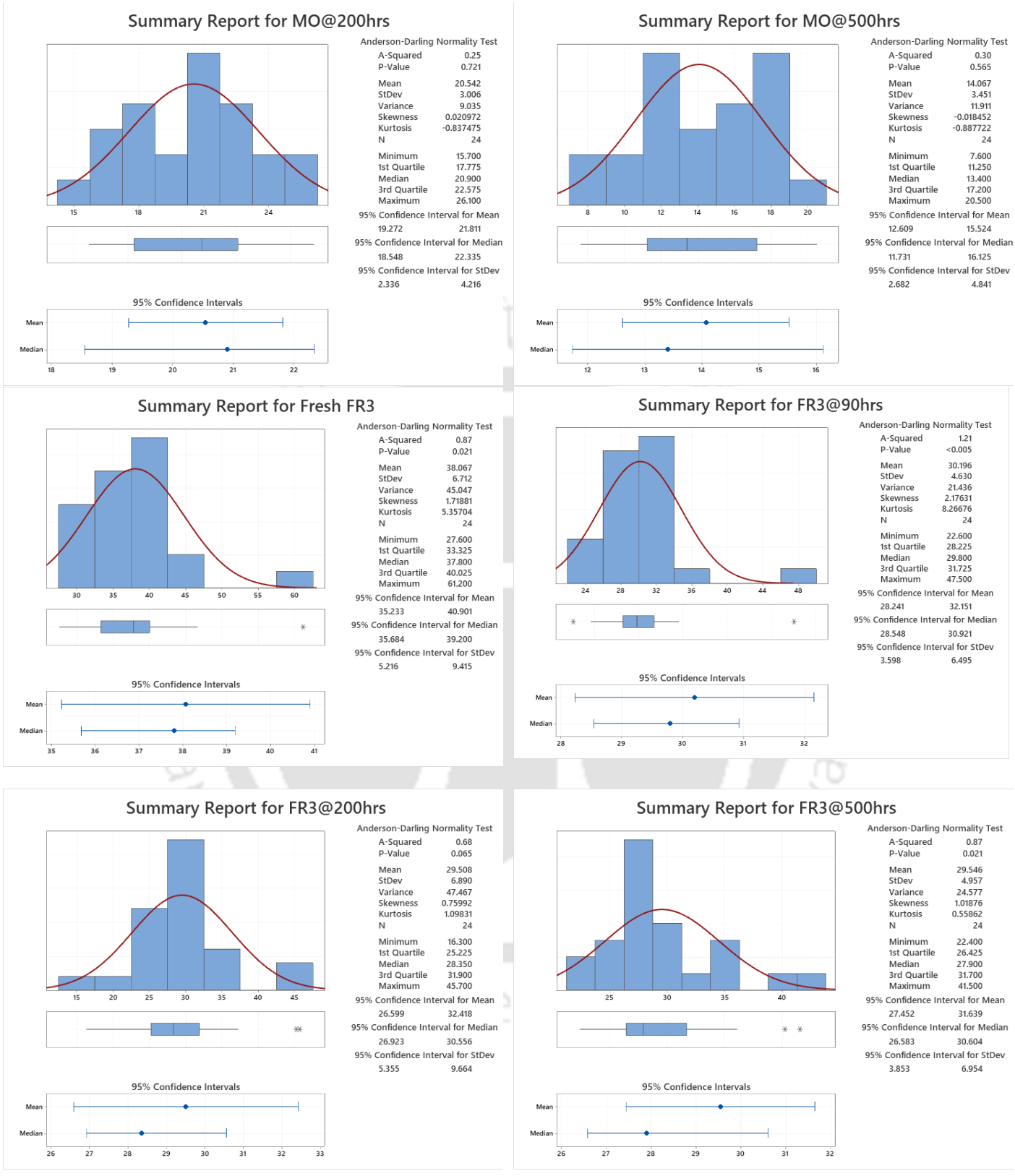

For negative DCBDV:

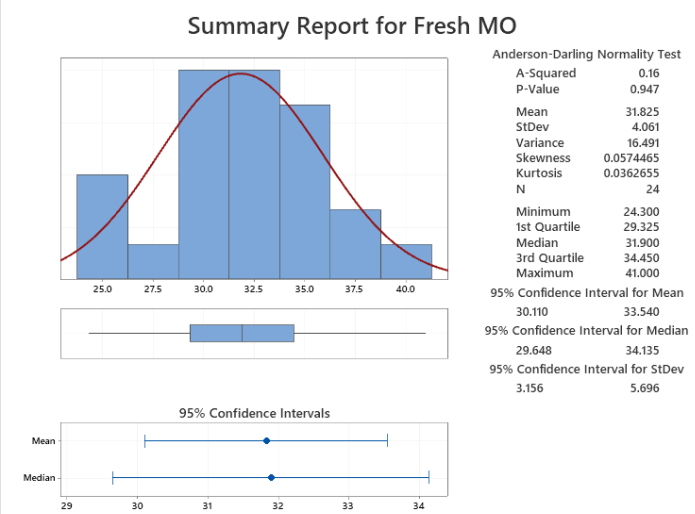

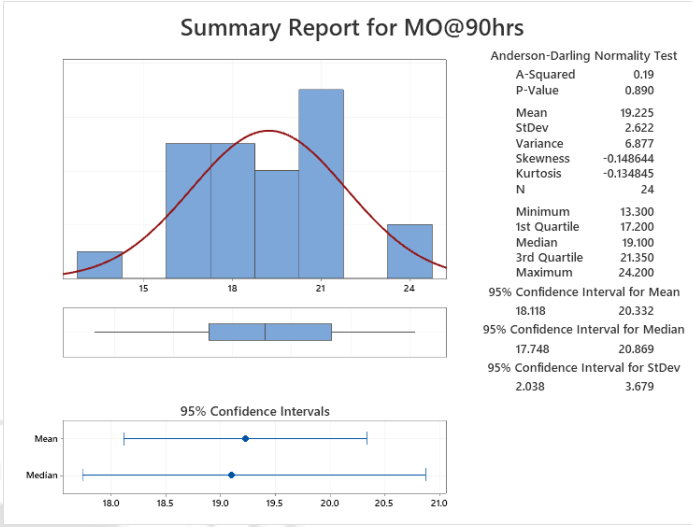

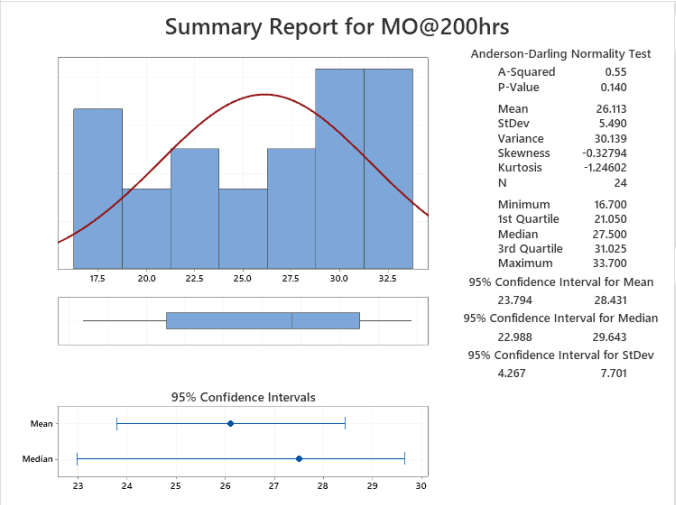

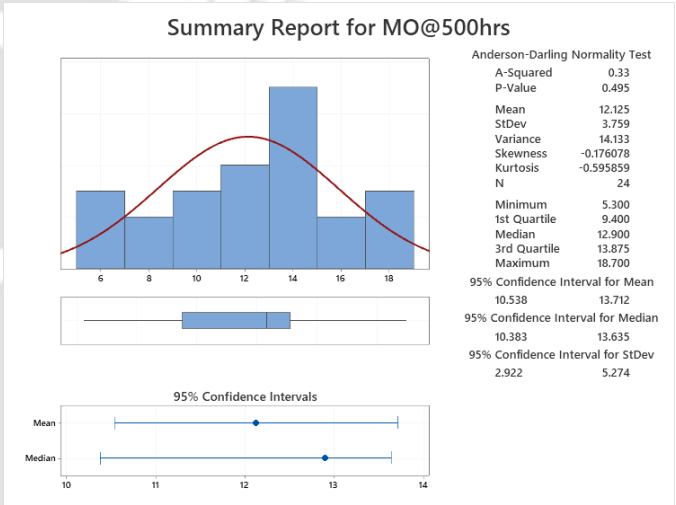

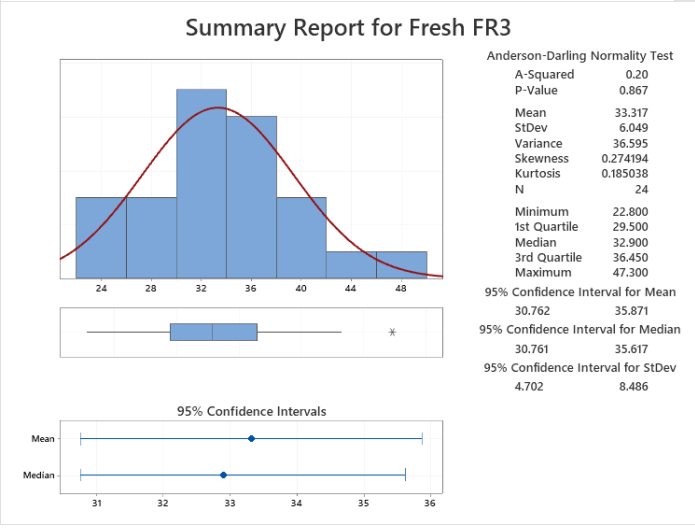

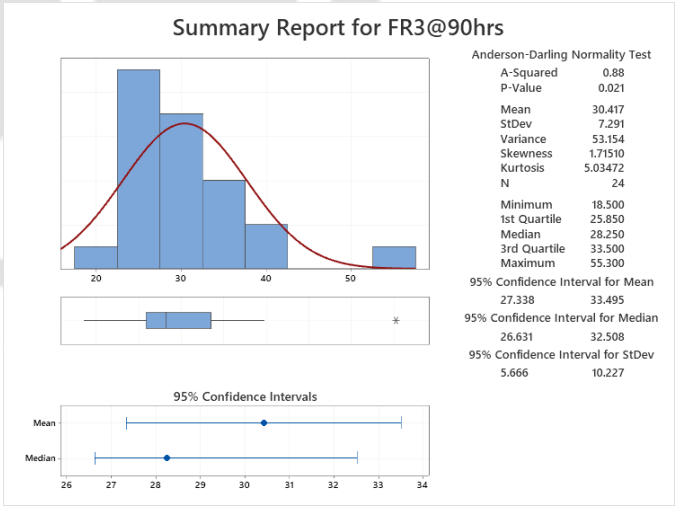

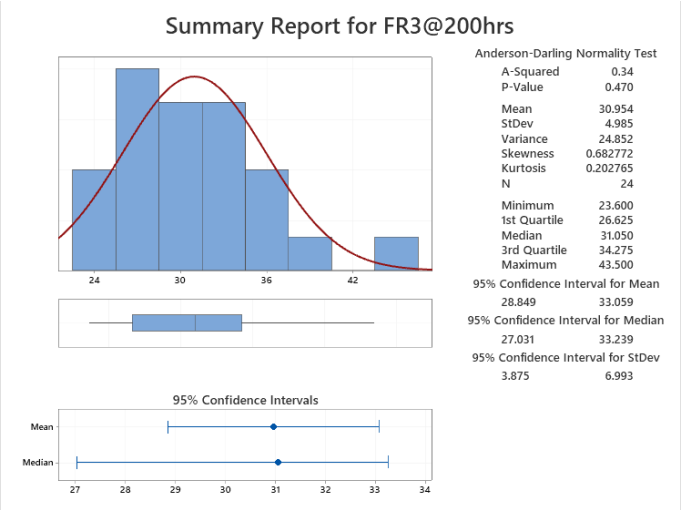

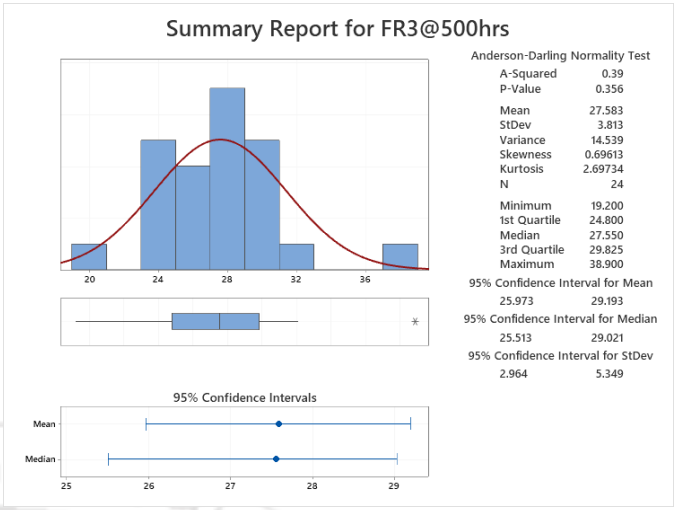

Weibull parameters for fresh and thermally aged samples:

Oil Samples	2-parameter Weibull						3-parameter Weibull					
	For Positive DCBDV			For Negative DCBDV			For Positive DCBDV			For Negative DCBDV		
	α	β	γ	α	β	γ	α	β	γ	α	β	γ
Fresh MO	28.82	6.374	-	33.58	8.569	-	9.922	2.263	18.21	12.22	3.016	20.91
MO@90	17.42	10.41	-	20.34	8.402	-	7.448	4.207	9.839	10.36	4.15	9.82
MO@200	21.82	7.797	-	28.28	5.877	-	7.39	2.407	14	47.51	10.24	-19.05
MO@500	15.39	4.734	-	13.45	3.768	-	10.17	2.987	5.005	13.34	3.734	0.1044
Fresh FR3	40.92	5.135	-	35.81	5.952	-	12.57	1.768	26.86	15.35	2.458	19.69
FR3@90	32.24	5.537	-	33.26	3.979	-	9.189	1.868	22.01	14.44	1.87	17.58
FR3@200	32.21	4.451	-	33.1	6.373	-	17.36	2.392	14.08	8.674	1.601	23.16
FR3@500	31.68	5.941	-	29.25	6.982	-	8.382	1.582	22.02	11.42	2.84	17.36

MATLAB code for extraction of DC conductivity through Cole- Cole plots:

Imaginary Permittivity Fit:

```
clc;
clear all;
double num;
x = importdata('Frequency.xlsx');
y=importdata('Fresh FR3.xlsx');


x0 = [300*(10^-12) 0.009 1.8 20 5 0.13 0.1 0.0195 0.152];
%'sig_DC','A','n','B','t1','a1','C','t2','a2'

fitfun= fittype('(sig_DC/((8.85*(10^-12))*2*pi*x))+((A*((2*pi*x)^(-n)))*cot((1-n)*pi*0.5))+imag((B/(1+((2*j*pi*x*t1)^(1-a1)))+(C/(1+((2*j*pi*x*t2)^(1-a2))))))', 'dependent',{'y'},'independent',{'x'},'coefficients',{'sig_DC','A','n','B','t1','a1','C','t2','a2'})
this_fit = fit (x, y, fitfun,'StartPoint', x0)


% Save the coeffiecient values for a,b,c and d in a vector
coeffvals = coeffvalues(this_fit);
```

```
% Plot results
p=log10(x);
scatter (p, y, 'r+')
hold on
plot(p,this_fit(x))
hold off
```

Data retrieval of curve fitting from MATLAB figures:

```
clear all;
close all;
clc;

h=openfig('MO_200.fig');
h=findobj (gca, 'Type','line');
x=get(h,'Xdata');
y=get(h,'Ydata');

A=[];
A(:,1)=x;
A(:,2)=y;
dlmwrite('data.txt',A,',');
```

Appendix B

Experimental results for geometric effects on DCBDV of MO and FR3 samples

- The raw data and plots in this appendix are for results discussed in chapter 3.

Experimental results of DCBDV of MO and FR3:

Table B.1: Experimental results for DCBDV of MO and FR3 with VDE electrode configuration

Sets	Breakdown Series	MO (kV)		FR3 (kV)	
		Positve (+)	Negative (-)	Positve (+)	Negative (-)
Set 1	1	22	-34.1	61.2	-47.3
	2	26.5	-31.3	36.2	-43.2
	3	19.3	-33.1	27.6	-41.9
	4	38	-31.7	39.2	-36.7
	5	26.2	-41	36.6	-24.2
	6	36.1	-34.5	38.7	-32.6
Set 2	7	30	-37.3	45.2	-34.8
	8	29.5	-30.9	39.2	-29.3
	9	29.7	-36.2	33.2	-35.6
	10	24.5	-32.3	40.3	-32.4
	11	26.8	-35.9	30.9	-31.6
	12	29.3	-32.4	39.1	-34.3
Set 3	13	22.4	-36.3	46.7	-38.4
	14	26.3	-27.3	36.8	-27.8
	15	27.2	-29.2	39.2	-35.2
	16	30.7	-29.7	38.7	-30.1
	17	24.9	-32.1	40.6	-32.6
	18	27.3	-30.5	32.4	-33.2
Set 4	19	26.7	-34.3	32.1	-38.3
	20	24.3	-26.1	42.4	-22.8
	21	23.1	-29.4	36.1	-30.9
	22	24.3	-24.6	33.7	-35.7
	23	26.1	-24.3	36.9	-27.2
	24	27.2	-29.3	30.6	-23.5
Average Breakdown		**27.017**	**-31.825**	**38.067**	**-33.317**
Standard Deviation		**4.137**	**4.061**	**6.712**	**6.049**
Standard Error		**0.845**	**0.829**	**1.370**	**1.235**

Table B.2: Experimental results for DCBDV of MO and FR3 with plane electrode configuration

Sets	Breakdown Series	MO (kV)		FR3 (kV)	
		Positve (+)	Negative (-)	Positve (+)	Negative (-)
Set 1	1	34.1	-38.6	59.5	-63.5
	2	30.1	-27.8	35.3	-59.7

	3	27.2	-30.5	44.7	-55.15
	4	29.1	-31.7	38.8	-49.5
	5	31.3	-27.6	37.2	-54.7
	6	25.7	-30.1	52.6	-54.5
Set 2	7	25.4	-30.7	58.2	-63.2
	8	27.3	-24.6	46.1	-42.5
	9	27.5	-29.5	47.5	-48.7
	10	23.1	-32.2	41.6	-43.2
	11	26.7	-27.3	45.7	-53.8
	12	27.8	-28.1	45.8	-49.7
Set 3	13	27.5	-27.7	55.6	-63.7
	14	26.6	-29.2	52.1	-38.9
	15	22.2	-24.4	38.3	-55.6
	16	24.1	-22.7	48.7	-42.7
	17	24.3	-29.4	31.5	-42.1
	18	30.1	-26.9	41.6	-47.9
Set 4	19	23.7	-26.3	60.6	-62.6
	20	24.5	-22.9	31.9	-45.3
	21	26.1	-25.2	48.4	-40.5
	22	21.6	-26.5	47.2	-37.8
	23	23.7	-25.4	39.2	-46.7
	24	21.6	-21.6	41.8	-41.5

Average Breakdown		**26.304**	**-27.788**	**45.413**	**-50.144**
Standard Deviation		**3.147**	**3.657**	**8.189**	**8.349**
Standard Error		**0.642**	**0.746**	**1.671**	**1.704**

Table B.3: Experimental results for DCBDV of MO and FR3 with sphere-sphere electrode configuration

Sets	**Breakdown Series**	**MO (kV)**		**FR3 (kV)**	
		Positve (+)	**Negative (-)**	**Positve (+)**	**Negative (-)**
Set 1	1	24.1	-32.7	63.2	-53.5
	2	29.8	-30.5	52.5	-34.5
	3	26.7	-24.5	61.3	-44.4
	4	32.1	-34.3	53.6	-44.7
	5	22.9	-32.7	50.7	-47.2
	6	28.5	-31.1	43.6	-47.5
Set 2	7	30.7	-34.4	55.3	-57.1
	8	30.9	-29.2	56.5	-63.3
	9	31.5	-29.6	40.6	-52.5
	10	33.6	-29.9	50.7	-53.8
	11	31.2	-32.2	61.9	-56.3
	12	31.3	-31.7	39.7	-45.5
Set 3	13	30.9	-33.6	59.3	-52.7
	14	28.7	-36.7	56.1	-52.2
	15	27.6	-38.2	51.2	-47.3
	16	25.1	-32.6	49.7	-52.1

	17	25.9	-26.3	42.5	-42.9
	18	27.7	-37.3	52.1	-49.3
Set 4	19	33.8	-33.4	57.2	-40.5
	20	28.6	-38.6	41.5	-45.7
	21	29.2	-40.8	45.5	-48.6
	22	27.1	-32.5	52.7	-44.6
	23	32.6	-40.3	44.3	-54.4
	24	26.5	-35.7	47.7	-46.7
Average Breakdown		**29.042**	**-33.283**	**51.225**	**-49.054**
Standard Deviation		**2.943**	**4.063**	**6.943**	**6.105**
Standard Error		**0.601**	**0.829**	**1.417**	**1.246**

For average and 90% confidence interval of β values: [mentioned in Table 4.5]

```
% Values of B for four sets
B1 = [11.79, 6.374, 8.513];
B2 = [8.523, 5.135, 6.167];
B3 = [9.17, 8.569, 7.268];
B4 = [8.696,5.952, 6.685];

% Calculate average, standard deviation, and confidence interval for each set

% Set 1
avg_B1 = mean(B1);
std_B1 = std(B1);
n1 = numel(B1);
alpha = 0.05; % Significance level (1 - confidence level)
t_critical = tinv(1-alpha/2, n1-1); % t-distribution critical value
margin_of_error1 = t_critical * std_B1 / sqrt(n1);
lower_bound1 = avg_B1 - margin_of_error1;
upper_bound1 = avg_B1 + margin_of_error1;

% Set 2
avg_B2 = mean(B2);
std_B2 = std(B2);
n2 = numel(B2);
t_critical = tinv(1-alpha/2, n2-1); % t-distribution critical value
margin_of_error2 = t_critical * std_B2 / sqrt(n2);
lower_bound2 = avg_B2 - margin_of_error2;
upper_bound2 = avg_B2 + margin_of_error2;

% Set 3
avg_B3 = mean(B3);
std_B3 = std(B3);
n3 = numel(B3);
t_critical = tinv(1-alpha/2, n3-1); % t-distribution critical value
margin_of_error3 = t_critical * std_B3 / sqrt(n3);
lower_bound3 = avg_B3 - margin_of_error3;
upper_bound3 = avg_B3 + margin_of_error3;

% Set 4
```

```
avg_B4 = mean(B4);
std_B4 = std(B4);
n4 = numel(B4);
t_critical = tinv(1-alpha/2, n4-1); % t-distribution critical value
margin_of_error4 = t_critical * std_B4 / sqrt(n4);
lower_bound4 = avg_B4 - margin_of_error4;
upper_bound4 = avg_B4 + margin_of_error4;

% Display results for each set
disp('Set 1:');
disp(['Average: ', num2str(avg_B1)]);
disp(['Standard Deviation: ', num2str(std_B1)]);
disp(['90% Confidence Interval: [', num2str(lower_bound1), ', ', num2str(upper_bound1), ']']);
disp(' ');

disp('Set 2:');
disp(['Average: ', num2str(avg_B2)]);
disp(['Standard Deviation: ', num2str(std_B2)]);
disp(['90% Confidence Interval: [', num2str(lower_bound2), ', ', num2str(upper_bound2), ']']);
disp(' ');

disp('Set 3:');
disp(['Average: ', num2str(avg_B3)]);
disp(['Standard Deviation: ', num2str(std_B3)]);
disp(['90% Confidence Interval: [', num2str(lower_bound3), ', ', num2str(upper_bound3), ']']);
disp(' ');

disp('Set 4:');
disp(['Average: ', num2str(avg_B4)]);
disp(['Standard Deviation: ', num2str(std_B4)]);
disp(['90% Confidence Interval: [', num2str(lower_bound4), ', ', num2str(upper_bound3), ']']);
disp(' ');
```

Results:

>> Final average B

Set 1:
Average: 8.8923
Standard Deviation: 2.7279
90% Confidence Interval: [2.116, 15.6687]

Set 2:
Average: 6.6083
Standard Deviation: 1.7366
90% Confidence Interval: [2.2944, 10.9222]

Set 3:
Average: 8.3357
Standard Deviation: 0.97223
90% Confidence Interval: [5.9205, 10.7508]

Set 4:
Average: 7.111
Standard Deviation: 1.4207
90% Confidence Interval: [3.5817, 10.7508]

Curve Fit Parameters Obtained from Figure 4.7 (from chapter 4)

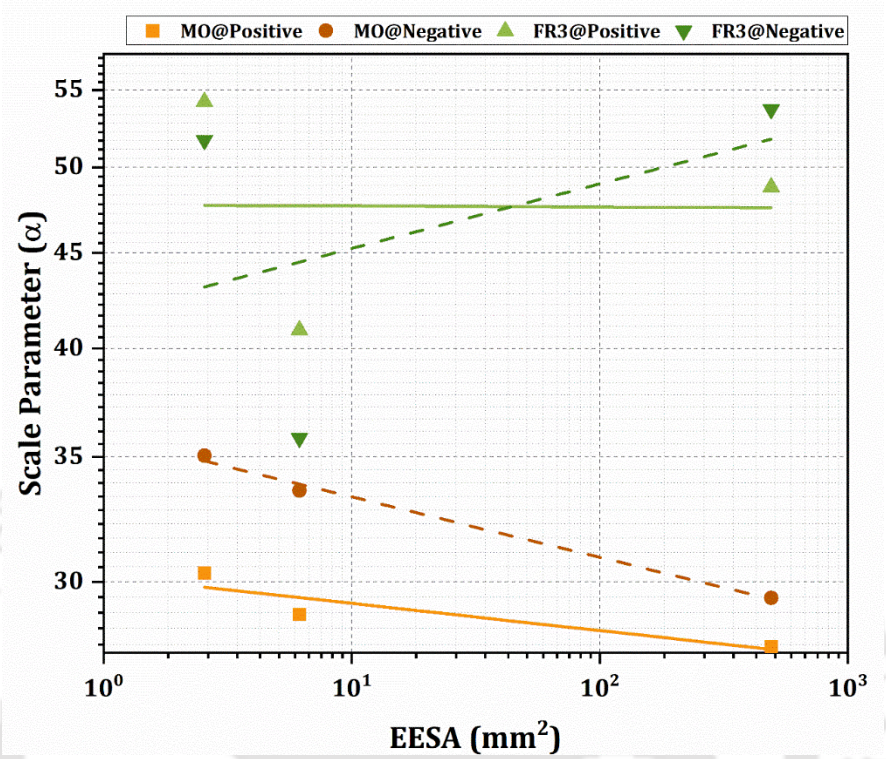

Fig. B.1. Correlation plot of Scale parameter (α) and EESA (mm^2) in logarithmic scale for various samples

Curve fit parameters obtained from this graph are

Equation	y = a + b*x
Plot	MO@Positive
Weight	No Weighting
Intercept	1.48024 ± 0.01124
Slope	-0.01454 ± 0.00687
Residual Sum of Squares	1.41408E-4
Pearson's r	-0.90406

Equation	y = a + b*x
Plot	MO@Negative
Weight	No Weighting
Intercept	1.55503 ± 0.0042
Slope	-0.03237 ± 0.00257
Residual Sum of Squares	1.97623E-5
Pearson's r	-0.99686
R-Square (COD)	0.99374
Adj. R-Square	0.98748

Equation	y = a + b*x
Plot	FR3@Positive
Weight	No Weighting

Intercept	1.67894 ± 0.08254
Slope	-5.89442E-4 ± 0.05045
Residual Sum of Squares	0.00762
Pearson's r	-0.01168
R-Square (COD)	1.36498E-4
Adj. R-Square	-0.99973

Equation	y = a + b*x
Plot	FR3@Negative
Weight	No Weighting
Intercept	1.62089 ± 0.11689
Slope	0.03463 ± 0.07145
Residual Sum of Squares	0.01528
Pearson's r	0.4362
R-Square (COD)	0.19027
Adj. R-Square	-0.61946

Experimental focus on furfurals a significant by products of insulation on DCBDV in various samples:

The research highlighted a concern regarding the purity of the samples used in the experiments, emphasizing the importance of utilizing pure, moisture-free, and sludge-free oil samples. Additionally, concern on the potential impact of furfurals, particularly 2-Furfuraldehyde a significant by-product of insulation on DCBDV measurements was pointed out. In response to this suggestion, the authors investigated the effects of presence of furfural additives in the test samples to assess their influence on DCBDV. The results of these tests, which yielded some intriguing findings, are briefly discussed below.

In this study, the insulating oils used, MO and FR3, underwent pre-treatment to ensure uniformity during testing. Although not completely moisture-free, both oils were conditioned at 65℃ for 48 hours to standardize their properties for comparability. Post-treatment moisture content was measured using a Metrohm 899 KF Coulometer, revealing water content levels of 189.7 ppm for MO and 839.7 ppm for FR3. Despite moisture, both oils were confirmed to be sludge-free, as they are fresh samples.

Now, addressing the furfural content, the literature on the formation of furfural in insulating oil within a transformer is studied to ensure that adding a furfural additive is practical and meaningful. According to Table 2 from [1], international standards for furfural content in oil vary across countries. China allows furfural levels ranging from 0.1 mg/L in transformers aged 1-5 years to 0.75 mg/L in

those aged 15-20. The USA has a maximum limit of less than 0.5 mg/L for transformer, switch, and electrical equipment oils, while Canada permits less than 0.4 mg/L in transformer, cable, and switch oils [1]. 0.5mg is very small so for experimental purposes so 10 mg/L of furfural to is added to MO which requires mixing 8.62µl/L based on MO's density; a similar approach applies to FR3 [2]. Prior to adding furfural, the oils undergo pre-treatment as detailed previously. To ensure uniform furfural dispersion, a litre of oil is mixed with 10µl of furfural using a magnetic bead for 30 minutes, followed by sonication with a probe sonicator. Initial FTIR spectroscopy shows that 10µl is insufficient, prompting an increase in furfural concentrations to 1ml, 10ml, and 20ml, with the outcomes depicted in Figures B.2. and B.3. The furfural, sourced from Sigma Aldrich, matches the FTIR patterns provided by the National Institute of Standards and Technology (NIST), U.S. Department of Commerce [3] and [4].

Upon detecting furfural, the DCBDV of the samples is tested using VDE electrodes, following ASTM D1816 standards, which require a minimum of five breakdowns to determine the mean DCBDV. Six breakdown tests are conducted for each sample to ensure consistency with previous experiments documented in the manuscript. According to the results in Figures B.2. and B.3., there is a negligible difference in IR with additions of 10µl and 1ml of furfural. Higher concentrations were deemed impractical; hence, the highest feasible concentration is used further for only comparison purpose. The tests included samples with no added furfural, 10µl/L, and 20ml/L. The results, depicted in Figure B.4., show the average DCBDV in positive polarity and negative polarity for six breakdowns using VDE configurations. The analysis indicates that adding 10µl of furfural for MO leads to a DCBDV change of approximately 1-1.5 kV. With 20ml of furfural, the BDV increases by a similar margin. FR3 displays a consistent pattern with both 10µl and 20ml additions. In negative DCBDV, both oils show changes within the range of 0.5-1 kV when considering error bars.

Despite observing an average difference of about 1kV in DCBDV between positive and negative polarities for the 10 µl furfural concentration. It is important to contextualize these findings with international furfural standards. The concentration used, approximately 10-15 mg/L, significantly exceeds the typical formation rate of 0.1 mg/L during the first 1-5 years of a transformer's life without faults—this standard amount is substantially lower than what was tested, suggesting that the impact of such small furfural amounts on BDV would be almost negligible.

This research focuses mainly on the effects of electrode geometries in fresh oils, not on aged or faulty conditions. Given the minor changes observed in DCBDV, the authors continue using the same experimental values in the manuscript, as any potential deviations from furfural content are likely within the standard error range. Additionally, it should be noted that even after pre-treatment, the oil samples still retained some moisture content, further affecting the study conditions since the oils were not completely moisture-free.

[1] D. Feng, G. Chen, X. Yan, X. Fu and R. Liao, "Furfural Analysis on Aging State Assessment of Oil-Immersed Transformers: A Review," in ***IEEE Transactions on Dielectrics and Electrical Insulation***, vol. 30, no. 6, pp. 2758-2768, Dec. 2023.

[2] W. Chen, Z. Gu, J. Zou, F. Wan and Y. Xiang, "Analysis of furfural dissolved in transformer oil based on confocal laser Raman spectroscopy," in ***IEEE Transactions on Dielectrics and Electrical Insulation***, vol. 23, no. 2, pp. 915-921, April 2016.

[3] Data from NIST Standard Reference Database 69: ***NIST Chemistry WebBook***

[4] R. S. Purbowatiningrum, M. Hapsari, F. H. Rafi'ah, and M. S. Haq. "Synthesis of furfural from water hyacinth (Eichornia croassipes)." ***In IOP Conference series: materials science and engineering***, vol. 172, no. 1, p. 012027. IOP Publishing, 2017.

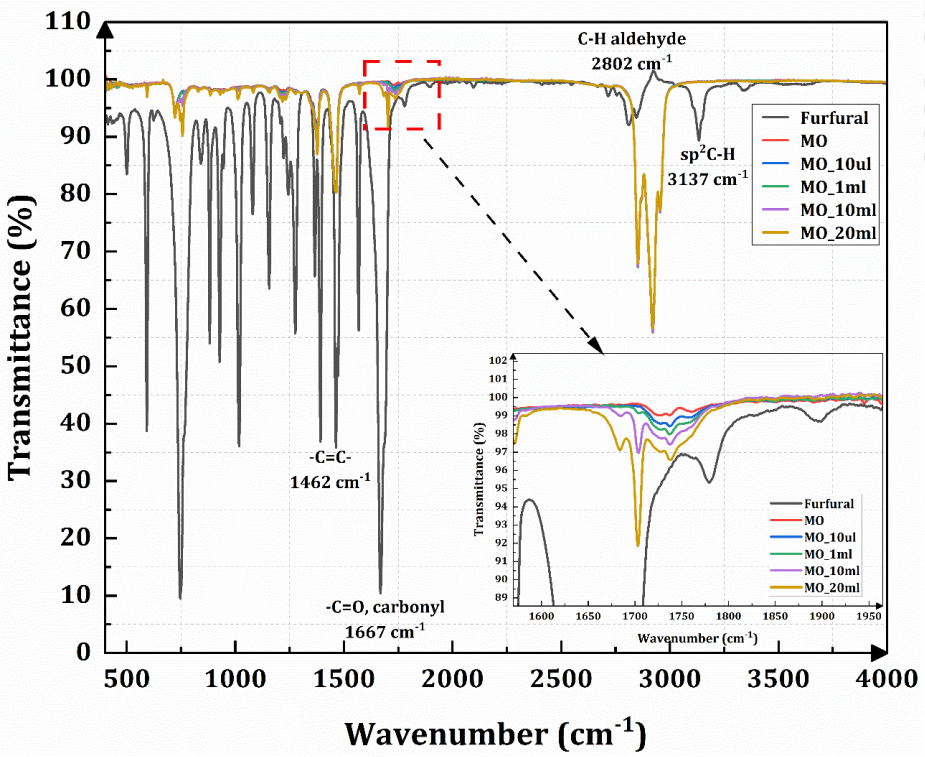

Fig. B.2. FTIR analysis of furfural and furural mixed in MO at various concentrations

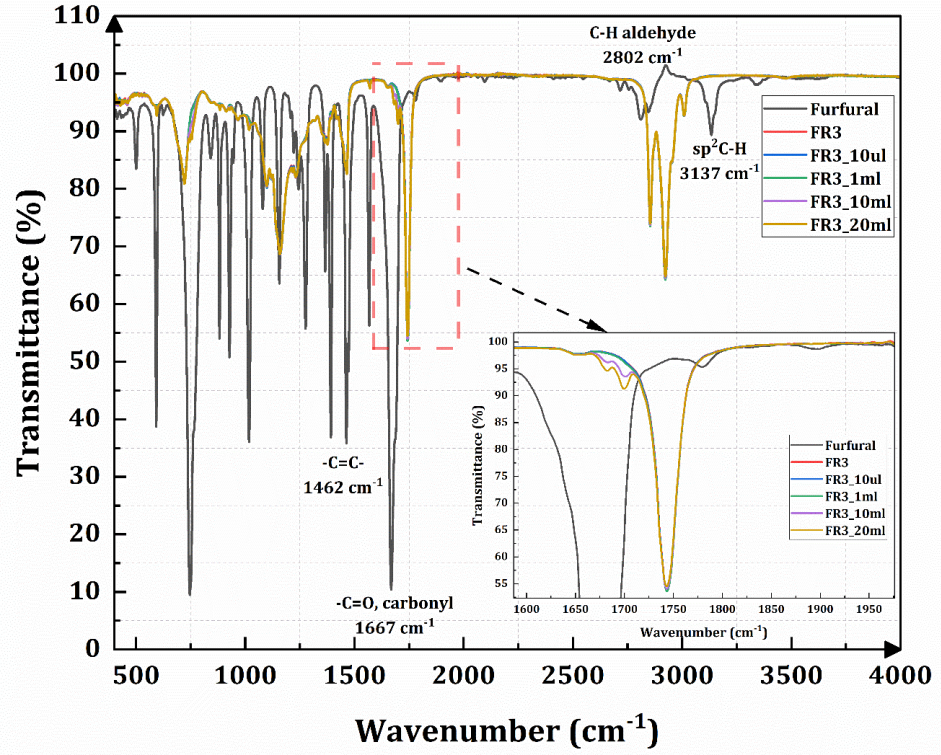

Fig. B.3. FTIR analysis of furfural and furural mixed in FR3 at various concentrations

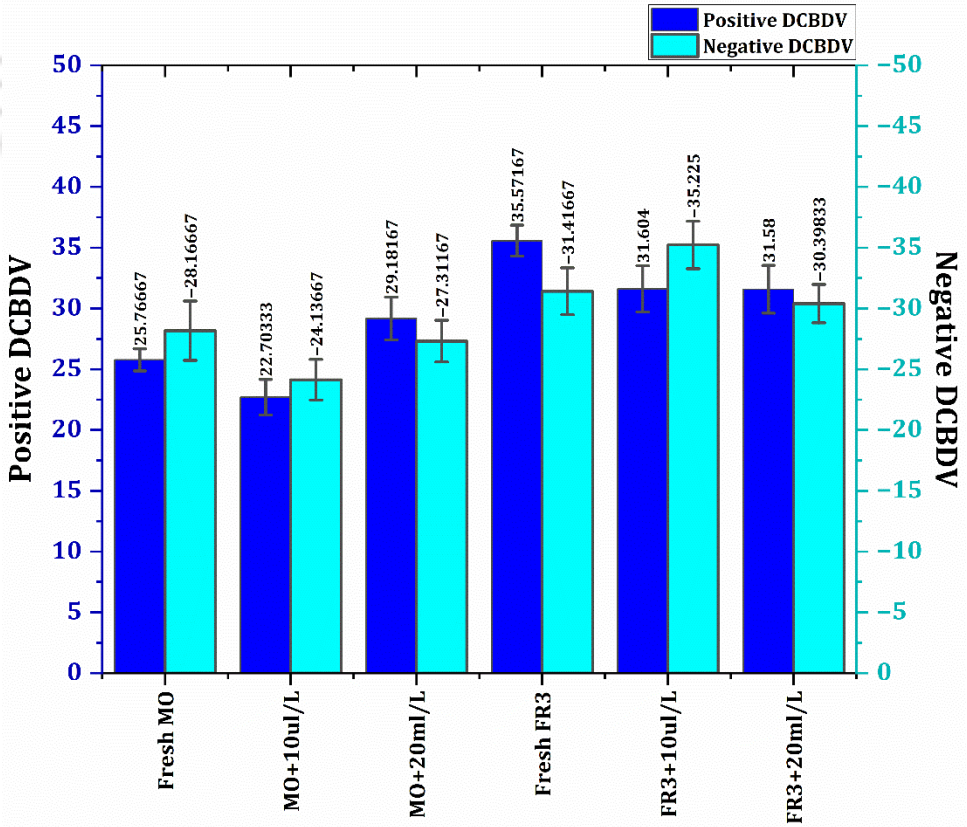

Fig. B.4. Average DCBDV (kV) of fresh and furfural mixed MO and NEO